Hell is other polypeptides

- Studying the role of β-hairpins in amyloid formation

Inaugural Dissertation

for the attainment of the title of doctor
in the Faculty of Mathematics and Natural Sciences
at the Heinrich Heine University Düsseldorf

Presented by

Emil Dandanell Agerschou

from Solbjerg, Morsø, Denmark

Düsseldorf, July, 2020

From the Institut für Physikalische Biologie
of Heinrich Heine University Düsseldorf

Printed by permission of the
Faculty of Mathematics and Natural Sciences at
Heinrich Heine University Düsseldorf

Examiners:

Supervisor: Jun. Prof. Wolfgang Hoyer
co-supervisor: Prof. Alexander Kai Büll

Date of the oral defence:
07.12.2020

I declare under oath that I have produced my thesis independently and without any undue assistance by third parties under consideration of the "Principles for the Safeguarding of Good Scientific Practice at Heinrich Heine University Düsseldorf"

Date	Signature

ACKNOWLEDGEMENT

Throughout my work on this dissertation I have received a substantial amount support without which its completion would not have been possible.

First and foremost I would like to extended my gratitude to Jun. Prof. Wolfgang Hoyer for giving me this opportunity and for helpful supervision. His tremendous insight in the amyloid literature and creative mind have been of utmost importance. Besides his purely academical support, his friendly and tolerant leadership style has been admirable.

I would like to thank Prof. Alexander Kai Büll for getting me in touch with Wolfgang but also for the many discussions and ideas, especially when working on the AS69 manuscript. His high intellect and ability to form clear ideas have been sources of inspiration.

I would like to extend my gratitude to Dr. Michael M.W. Wördehoff for sharing his technical expertise as well as many fruitful discussions. His attention to details, curiosity, and easy-going nature have been of large value and I am happy to have had the opportunity to work with him. Furthermore, he prepared or supervised the preparations of most of the CC and dimer variants.

The contributions of the the many collaborations on the AS69 manuscript cannot be overstated as they not only made it possible to explore the *in vivo* efficacy, they had also made a substantial amount of the ground work before I entered the project. Additionally, Dr. Hamed Shaykhalishahi and Nikolas Hochheimer cloned the β-turn variants prior to my arrival, making that particular project possible.

Vera Borgmann as part of her Master's Projects have been of enormous technical help in generating most of the dimer data for the CC48 manuscript as well as helping with the monomer dependency. Her bright and sceptical mind coupled to a hard-working and pleasant personality made it a delightful experience to supervise her. Luzie Kruse as part of her project internship helped to establish a more safe elongation assay through optimising seed preparation. Her hard-working and curious spirit made it a joy to supervise her, however brief it was. Fabin Schmitz as part of his Master's Project helped me purify the CC variants, and verified the correctness of their sequence. His work furthermore helped change the direction the CC project went.

The local environment within AG Hoyer in particular but also in the broader sense the entire IPB / IBI-7 have made for a stimulating work environment.

Heidi Redmond and Celina Schulz did not contribute directly to the work in this thesis, but are thanked for their work in further optimising the secondary nucleation and continuing the work on understanding how the AS69:α-synuclein complex accomplishes secondary nucleation respectively.

Lastly on more personal notes, the Monday-night-out gang has been pivotal in keeping up my spirit over the years. Hannah kept me fit through many tough running sessions. Nicola's contributions as a source of support and friendship over the years cannot be overstated. Najoua's support and patience with me while writing this thesis has been nothing short of herculean.

SUMMARY

Amyloid fibrils are highly ordered insoluble protein aggregates wherein the protein adopts the cross-β conformation. Very dissimilar sequences can adopt this conformation and aggregate, which is often seen in neurodegenerative diseases. In Parkinson's disease, amyloid fibrils of α-synuclein (αS) accumulate. In this thesis, the mechanisms of amyloid formation and inhibition of αS are studied. This is done mainly by elucidating the inhibition mechanisms of previously identified inhibitors.

The region of αS composed of residues 37-54 has previously been shown to adopt a β-hairpin when bound to an engineered binding protein known as AS69. Many of the known disease associated mutations are found within this region. Furthermore, binding of AS69 inhibits conversion of soluble αS into amyloid fibril in a highly substoichiometric manner, however, the mechanism was not understood. Here, the mechanism of inhibition was investigated by selectively favouring specific amyloid-forming pathways by tuning the solution conditions. It was found that AS69 only had a stoichiometric effect on elongation, compatible with sequestration of textalpha S monomers by AS69. Secondary nucleation was found to be highly substoichiometrically inhibited. By linking AS69 to αS, it was shown that inhibition of secondary nucleation likely was caused by the complex of AS69 and αS rather than by AS69 alone.

Earlier, favouring the β-hairpin conformation of αS was done by introducing a disulphide bond between residue 41 and 48 using cysteine mutations (CC48). CC48 did not form amyloids unless the disulphide bond was reduced. Furthermore, CC48 inhibited elongation of wild-type (WT) fibrils. Here, the position dependency of the disulphide bond was studied by mutations. A large variation in inhibition strength was seen among these mutants, but, CC48 was the strongest inhibitor. Applying the theoretical framework from reversible enzyme inhibition, it was established that CC48 caused inhibition by competing with WT for binding to the fibril-end. However, an increase in efficiency of inhibition at high WT concentrations was observed. Modelling of this unusual behaviour where the substrate, WT, cooperated with the inhibitor, CC48, to accomplish inhibition revealed that two additional WT monomers could bind to fibril-ends where CC48 was already bound. The proposed mechanism was corroborated by constructing linked dimers of WT and CC48 which exhibited substantially higher inhibition efficiency than monomeric CC48.

An alternative to stabilisation of the β-hairpin conformation by disulphide bonds, was stabilising it by increased turn-formation propensity. αS mutants with increased β-hairpin propensity, through stabilised β-turn propensity, were prepared. Here, the ability of these mutants to form amyloid was evaluated and, surprisingly, the mutants tended to have increased aggregation kinetics compared to the WT. Lastly, cross-elongation experiments revealed a large asymmetry between ability to elongate non-self fibrils, and ability to be elongated by non-self monomers.

β-Hairpin formation upon binding to inhibitors has been observed for several amyloidogenic proteins in addition to αS. A single wrapin, AS10, binds, induces a β-hairpin, and inhibits three different amyloidogenic proteins. Here, the human proteome was analysed to locate potentially amyloidogenic sequences that would bind AS10. The TANGO algorithm was used as the first

filter, and to increase specificity, biophysical characteristics of known AS10 binders were used as the second filter. A surprisingly large number of sequences were located.

Interactions of proteins, either among identical species to form amyloid or between different species causing inhibition, was the core subject of this thesis. The behaviour of individual polypeptides, like people, was dominated by the presences of others. It thus seems that Sarte's concept of "Hell is other people" might apply to polypeptides as well.

CONTENTS

List of Figures

LIST OF TABLES

List of Abbreviations

αS α-synuclein

AD Alzheimer's Disease

AFM Atomic Force Microscopy

AS69fusASN AS69 C-terminally joined to αS by a flexible linker

ANOVA ANalysis Of VAriance

BBB Blood-Brain Barrier

BiFC Bimolecular Fluorescence Complementation

CC Cysteine-Cysteine

CC48 αS with mutations G41C and V48C

CC49 αS with mutations G41C and V49C

CC50 αS with mutations G41C and H50C

CC52 αS with mutations G41C and V52C

CC48-CC48 Dimeric construct where two CC48 are joined by a flexible linker

CC48-WT Dimeric construct where CC48 is joined C-terminally to WT αS by a flexible linker

CD Circular Dichroism

CryoEM Cryogenic Electron Microscopy

DGC Density Gradient Centrifugation

DTT Dithiothreitol

DMPS 1,2-Dimyristoyl-sn-glycero-3-phospho-*L*-serine

EGFP Enhanced Green Fluorescent Protein

IEC Ion Exchange Chromatography

L-DOPA 3,4-Dihydroxyphenylalanine

MOPS 3-(*N*-MOrpholino)PropaneSulfonic acid

NAC Non-Amyloid-β Component

NMR Nuclear Magnetic Resonance

PAGE Poly-Acrylamide Gel Electrophoresis

PD Parkinson's Disease

pI Isoelectronic point

SDS Sodium dodecyl sulphate

SEC Size Exclusion Chromatography

SEM Standard Error of the Mean

Tht Thioflavin T

TIRF Total Internal Reflection Fluorescence

VC C-terminal part of the venus protein

VN N-terminal part of the venus protein

WT Wild Type

WT-CC48 Dimeric construct where WT αS is joined C-terminally to CC48 by a flexible linker

WT-WT Dimeric construct where two WT αS are joined by a flexible linker

1

INTRODUCTION

1.1. Amyloids

> Amyloid fibrils are just one of the types of aggregate that can be formed by proteins, although a significant feature of this particular species is that its highly organized hydrogen-bonded structure is likely to give it unique kinetic stability. Thus, once formed, such aggregates can persist for long periods, allowing a progressive build-up of deposits in tissue, and indeed enabling seeding of the subsequent conversion of additional quantities of the same protein into amyloid fibrils.
>
> Dobson, 2003

A growing number of proteins have been shown to aggregate into tightly packed and highly ordered polymer arrays known as amyloid fibrils. These fibrils tend to have a remarkably high aspect ratio with thickness in nm range but lengths in the μm range. They have been shown to occur in such diverse places as protein heat denaturation [1], neurodegenerative diseases [2, 3, 4], Type-2 diabetes [5, 6], systemic deposits [7], deposits as side effect deposits of B-cell type cancer [8], storage of hormones in cells [9], and finally as a vital part of biofilms [10]. The diversity is not only in where amyloid fibrils are found, but also in which protein sequences and starting conformations can give rise to them. This makes it all the more remarkable that all amyloids share a similar final conformation as well as specific staining properties. Their formation has received considerable scientific attention not only as they are associated with several diseases, but also because they might represent a generic property of polypeptides thereby being of interest from a more basic perspective. However, much still remains to be understood about them. In this introduction I will provide an overview of what is known about these interesting structures before turning my attention to Parkinson's Disease and α-synuclein amyloid formation.

1.1.1 Historical overview of amyloids

Virchow's paper from 1854 is often cited as the first observation of amyloid in abnormal looking human brain samples [11]. He observed that small bodies in the brain stained with iodine led to a blueish colouration that turned purple upon addition of sulphuric acid (cellulose/starch positive), while at the same time not giving rise to the yellowish brown colour (nitrogen negative), he conclude that they were cellulose-like. Paradoxically, even though the *corpora amylacea* in the central nervous system Virchow studied was believed to be predominately composed of polysaccharides, the terms amyloid and *corpora amylacea*[1] quickly became associated with nitrogenous bodies elsewhere in the body. This was partly due to Virchow's own work on staining other organs that had waxy or lardaceous deposits [13, 14] . The notion of amyloid being composed of proteins (not fat, nor cellulose) was recognised as early as 1859 where Friedreich and Kekulé thoroughly investigated the properties of amyloid deposits obtained from a human spleen [15].

Even though the cellulose-like conclusion reached by Virchow was falling out of favour, the iodine staining technique for amyloid deposits remained in use even though it was a somewhat difficult technique. This was about to change as advancements in synthetic chemistry led to new dyes being created, some of which turned out in 1875 to be relative specific for amyloid [16, 17]. The use of dyes was further advanced in 1922 when Bennhold showed specific and long lasting staining of amyloid using the dye Congo red [18]. The following year he suggested that Congo red could be used to diagnose amyloidosis by measuring the retention of the dye in the blood, as abnormally fast reduction was seen as a sign that the dye was being depleted by binding to amyloid, something that was confirmed by *post mortem* examination [19, 20]. The specificity and possibility for long lasting samples allowing scientist and clinicians to share stained material with each other made Congo red an improved method to study amyloid deposits.

Four years later in 1927 it was shown that amyloid stained with Congo red exhibited birefringence under polarised light [21]. The birefringence increased the specificity of Congo red even further, but more so, it suggested something that had not been noted before, namely that amyloid might have internal structure [22, 23]. This led Cohen and Calkins to investigate amyloid deposits using electron microcopy, where they indeed found abundant unbranched fibrils in samples from different sources [24].

Over the next decade, the connection between Alzheimer's Disease (AD) and amyloid (also noted by Divry in 1934) became more well established [25], and the first indications that fibrillar material was present in Parkinson's Disease (PD) also became available [26]. Towards the end of the decade, the finer details of amyloid fibrils became apparent as negative staining electron microscope revealed that they tended to be composed of smaller filaments that twisted around each other [27]. Shortly hereafter, it was shown with X-ray fibre diffraction [28, 29] that amyloid obtained from different organs and organisms all exhibited a characteristic diffraction pattern. Unaligned fibrils had two diffraction rings corresponding to 4.7 Å and 10 Å respectively. When aligned, the rings separated into arcs with the 4.7 Å arcs became perpendicular to the 10 Å arcs. Interestingly, this pattern had already been observed more than 30 years earlier, in the context of denatured proteins [1], a connection that resonates to this day.

The next leap forward came from a rather unexpected side in the early 1980s. Research into understanding the nature of the pathogen(s) causing a particular class of fatal neurological

[1] To make the confusion complete, *corpora amylacea* was observed early on to be more numerous in the brains of people with neurodegenerative diseases, and are still believed to be so, however their role is unclear [12].

diseases known as Transmissible Spongiform Encephalopathies. In sheep it was known as Scrapie, Bovine Spongiform Encephalopathy in cattle, Chronic wasting disease in deer, and in humans as Kuru, Creutzfeldt-Jakob's Disease, and Gerstmann–Sträussler–Scheinker syndrome. In particular, Prusiner, whilst working on Scrapie, discovered that one of the sheep's own proteins (named Prion protein, PrP) could become infectious (prions) and undergo a conformational change. The change was between its usual globular and membrane bound form (PrP^{C}), to a proteases resistant one that turned out to show birefringence when stained with Congo red (PrP^{Sc}) [2, 30, 31]. Later research have shown that misfolding of PrP is the likely cause of all the above mentioned Transmissible Spongiform Encephalopathies [32]. This showed that proteins, in their normal environment, were able to convert into amyloid-like filaments in a templated fashion. This raised the question whether conversion in to amyloid was the cause of other amyloid diseases (a debate that remains open to this, see subsection 1.3.2). Furthermore, what prevented normally functioning PrP^{C} to spontaneously undergo PrP^{C} to PrP^{Sc} conversion? The latter question was partly answered during 1992-1993 where kinetic studies on smaller peptides derived from amyloidogenic proteins (including PrP) showed the presence of a clear lag time and a subsequent sigmoidal curve [33, 34]. This led the authors to propose a model where, analogous to crystallisation, the rate determining step of *de novo* formation of amyloid (and prion) was the formation of an unfavourable nucleus, after which growth of this nucleus would readily occur. This was offered as an explanation of the rare occurrence but comparably fast spreading of prions and potentially amyloids as well.

1.1.2 Characteristics of amyloids

Amyloids are fibres of poly-peptides that are stacked tightly together in a cross-β conformation, *i.e.* where the peptide backbone is arranged to form β-sheets parallel to the fibre axis, with the β-strands (and side-chains) running perpendicular to the fibre axis (see Figure 1.1). The dimensions of the amyloid fibres (fibrils) are characterised by a rather narrow distribution of widths (thicknesses) in the range 5–25 nm, where on the contrary the lengths ranges from being as short as 100 nm to longer than 15 µm [35, 36, 37]. Although, to get fibrils as short as 100 nm usually require mechanical perturbation such as extensive stirring or sonication [38]. Small periodical variations in thickness along the fibril axis are commonly observed, and are attributed to several strands of amyloids (usually two) wrapped around each other. It is not understood whether strands grow individually, or if the entire fibril grow as one with monomer addition occurring in an alternating fashion to each strand. Indications of both types of elongation has been observed [39, 40, 41] and might be system specific.

Spreading of prions and amyloids was considered a somewhat controversial topic as their ability to spread within and between individuals without the use of DNA or RNA was difficult to grasp as this had never been observed before. And to make matters worse, if a state (amyloid) can be reached without input of additional energy it is heavily implied that this state is more stable than the state that preceded it (the native conformation). This seemed to contradict a treasured doctrine in protein folding originally stated by Anfinsen namely that, at physiological conditions, the native conformation is the lowest energy conformation (stability condition) [43]. And to add insult to injury, amyloids have been shown to be polymorphic, where the specific structures are not just given by differences in "packaging" of strands, but also by the individual fibrils having different conformations (see Figure 1.3). This contradicts the uniqueness of translating a sequence into a specific structure. It is noteworthy that the uniqueness condition was early on deemed unlikely by Levinthal [44]. In order to adapt our understanding of protein folding to these observations, two related lines of ideas have been proposed to overcome the stability violation: i)

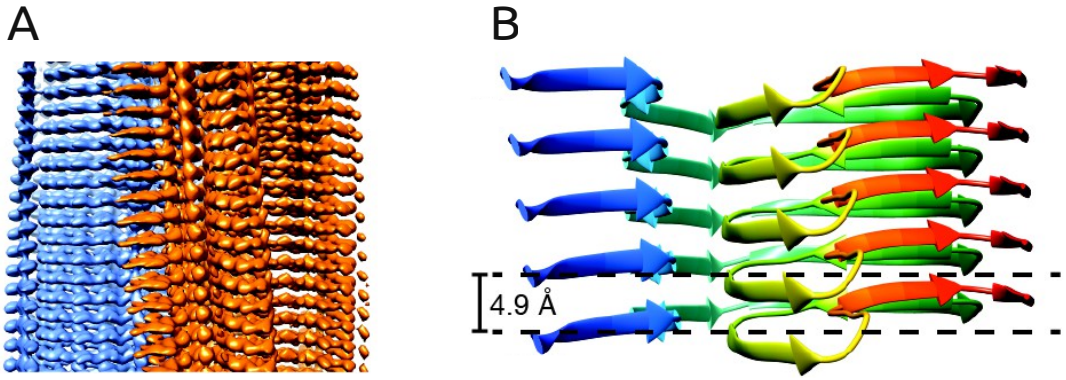

Figure 1.1: Amyloid structure, (A) High resolution structure of an amyloid fibril (α-synuclein 1-121), obtained using Cryogenic electron microscopy(CryoEM). **(B)** A zoom-in on of one of the strands from the structure shown in (A) as a cartoon representation, note how the β-sheets run parallel to the axis and the strands that form them stack perpendicular to the axis. Figure was adopted from [42]

to treat Anfinsen's doctrine as a special case for very dilute systems where interactions between different peptide molecules can be neglected ii) that the doctrine is not quite valid, and amyloid instead represents the generic thermodynamically most stable state [45, 46, 47]. Experimental support for the concentration dependency of stability comes from the observations that fibrils does not form (or dissolves if already formed) below as certain system specific concentration [48, 49]. Evidence for the generic view is that a large number of different proteins can adopt an amyloid conformation independent of their initial conformation (reviewed in [50, 51]).

The thermodynamic stability of amyloids is still a subject of active research, which is somewhat complicated by the fact that different types of stabilities are frequently discussed in connection with amyloids. Amyloid stabilities include ability to resist degradations by unspecific proteases [2, 52, 53, 54], as well as resistance toward denaturing surfactants such as as Sodium Dodecyl Sulphate (SDS) and in particular sarkosyl [55, 56]. This is sometimes used as an argument for the extraordinary stability of the amyloid conformation over globular ones. However, unspecific protease eventually degrades amyloids[2, 52, 53, 54] , which seen in the light of the tightly packed peptide backbones in cross-β conformation could be interpreted merely as a kinetic stability towards degradation rather than a large thermodynamic stability as such. Although the resistance of amyloids towards SDS (which readily denatures many globular proteins) is a bit puzzling, they are susceptible to denaturation by solvent denaturation using Guanidinium Chloride and in particular Urea [57, 58]. This is analogous to solvent denaturation of globular states, *i.e.* stability is solvent depended and not an absolute parameter. Not only is this in line with the some of Anfinsen's ideas, it might also at some point bring "amyloid folding" closer to the more familiar subject of protein folding.

1.1.3 Mechanism of amyloid formation

Even though the amyloid represents a stable state, and therefore act as an attractor in conformational space, the conversion from free peptide to amyloid is not a straightforward phenomenon to model. A large part of our theoretical understanding of the self-assembly of proteins into filaments (not just of the amyloid variety) can be traced back to the seminal work of Oosawa

and Asakura in the early 1960'ies [59, 60, 61]. Working on modelling the self-assembly of actin, they derived several models to rationalise the behaviour they observed, all of which starts from the following framework that centres around monomer addition [62]:

$$\begin{aligned}
M + M &\underset{k_{2-}}{\overset{k_{2+}}{\rightleftharpoons}} M_2 & K_2 &= \frac{k_{2+}}{k_{2-}} = \frac{[M_2]}{[M]\,[M]} \\
M + M_2 &\underset{k_{3-}}{\overset{k_{3+}}{\rightleftharpoons}} M_3 & K_3 &= \frac{k_{3+}}{k_{3-}} = \frac{[M_3]}{[M_2]\,[M]} \\
&\vdots & &\vdots \\
M + M_{i-1} &\underset{k_{(i-1)-}}{\overset{k_{(i+1)+}}{\rightleftharpoons}} M_i & K_i &= \frac{k_{i+}}{k_{i-}} = \frac{[M_i]}{\left[M_{(i-1)r}\right]\,[M]} \\
&\vdots & &\vdots \\
[M]_{\mathrm{Tot}} &= \sum_{i=1}^{\infty} i\,[M_i] & &
\end{aligned} \tag{1.1}$$

Where M is the monomeric building block, M_i is the filament of size i; k_{i+}, k_{i-}, and K_i are the association rate constant, dissociation rate constant, and association constant of M_i respectively; and finally, $[M]_{\mathrm{Tot}}$ is the total concentration of the monomeric building block.

The simplest model to describe filamentous growth is the so-called isodesmic model where addition of a monomer has the same association constant K_e independent of the length of the underlying filament *i. e.*:

$$K_e = K_2 = K_3 = \ldots = K_i = \ldots \tag{1.2}$$

The implications of Equation 1.2 on Equation 1.1 are:

$$\begin{aligned}
[M_2] &= K_e[M]^2 \\
[M_3] &= K_e\,[M_2]\,[M] = K_e^2[M]^3 \\
&\vdots \\
[M_i] &= K_e\left[M_{(i-1)}\right][M] = K_e^{(i-1)}[M]^n = K_e^{-1}\left(K_e[M]\right)^i \\
&\vdots \\
[M]_{\mathrm{Tot}} &= \sum_{i=1}^{\infty} iK_e^{-1}\left(K_e[M]\right)^i
\end{aligned} \tag{1.3}$$

(1.4)

Where the series can be found to be convergent if:

$$K_e[M] < 1 \tag{1.5}$$

And furthermore that it converges to:

$$[M]_{\text{Tot}} = \frac{[M]}{(1-K_e[M])^2} \tag{1.6}$$

$$K_e[M] = 1 + \frac{1}{2K_e\,[M]_{\text{Tot}}} - \sqrt{\frac{1}{K_e\,[M]_{\text{Tot}}} + \frac{1}{4\,(K_e\,[M]_{\text{Tot}})^2}} \tag{1.7}$$

For a large total concentration (using Equation 1.7), C_{Tot} the equilibrium monomer concentration $[M]$ will tend towards K_e^{-1}. It has indeed been shown that the concentration of monomer tends towards a specific value for an increasing monomer concentration [48, 49]. Furthermore, relating K_e to change in energy/stability is straight forward using:

$$\Delta G = RTln(K_e^{-1}) \tag{1.8}$$

This ΔG has indeed been used as a measure for stability [57, 58], and the isodesmic model has been used to model amyloid stability [48, 57]. However, the isodesmic model (using Equation 1.3 and Equation 1.6) suggests that the monomer will be the species with the highest concentration, and any length hereafter will be exponentially rarer. This proposed size distribution is not observed [35, 36, 37] (see *e.g.* Figure 2.5 and Figure 2.7). Furthermore the isodesmic model is also unlikely to be able to explain the observation that adding preformed fibrils greatly enhances the rate with which fibrils form. Instead, this hints towards the presence of an unfavourable intermediate, a nucleus, that upon further addition becomes favourable. Although this extension to account for a nucleus can be formulated in several ways, a version that has been shown to successfully describe filamentous growth of small peptide analogues as well as amyloids is [58, 63]:

$$K_2 = K_3 = \ldots = K_n < K_e = K_{n+1} = K_{n+2} = \ldots = K_i = \ldots \tag{1.9}$$

Where K_n is the association constant up to the aggregate reaches its nucleus size n. Following the same procedure as for the isodesmic model, the implications of Equation 1.9 on Equation 1.1 are evaluated:

For $i \leq n$:

$$
\begin{aligned}
[M_2] &= K_n[M]^2 \\
[M_3] &= K_n\,[M_2]\,[M] = K_n^2[M]^3 \\
&\vdots \\
[M_n] &= K_n\left[M_{(n-1)}\right][M] = K_n^{(n-1)}[M]^n
\end{aligned}
$$

For $i > n$:

$$
\begin{aligned}
\left[M_{(n+1)}\right] &= K_e\,[M_n]\,[M] = K_e K_n^{(n-1)}[M]^{(n+1)} \\
\left[M_{(n+2)}\right] &= K_e\left[M_{(n+1)}\right][M] = K_e^2 K_n^{(n-1)}[M]^{(n+2)} \\
&\vdots \\
[M_i] &= K_e\left[M_{(i-1)}\right][M] = K_e^{(i-n)} K_n^{(n-1)}[M]^i \\
&\vdots \\
[M]_{\mathrm{Tot}} &= \sum_{i=1}^{\infty} i\,[M_i] = K_n^{-1}\sum_{i=1}^{i=n} i(K_n[M])^i + \left(\frac{K_n}{K_e}\right)^{(n-1)} \sum_{i=n+1}^{\infty} iK_e^{-1}(K_e[M])^i
\end{aligned}
\tag{1.10}
$$

To generalise and simplify Equation 1.10, a dimensionless unit of $[M]$ is introduced along the ratio of the association constants σ:

$$
\begin{aligned}
x &= K_e[M] \\
x_{\mathrm{Tot}} &= K_e\,[M]_{\mathrm{Tot}} \\
\sigma &= \frac{K_n}{K_e}
\end{aligned}
$$

This leads to the following equation, that can be solved using techniques similar to the ones used for solving the isodesmic model [63]:

$$
\begin{aligned}
x_{\mathrm{Tot}} &= \sigma^{-1}\sum_{i=1}^{i=n} i(\sigma x)^i + \sigma^{(n-1)} \sum_{i=n+1}^{\infty} ix^i \\
&= \sigma^{-1}\left(\frac{(\sigma x)^{(n+1)}(n\sigma x - n - 1) + \sigma x}{(\sigma x - 1)^2}\right) - \sigma^{(n-1)}\left(\frac{x^{n+1}(nx - n - 1)}{(x-1)^2}\right)
\end{aligned}
\tag{1.11}
$$

Although Equation 1.11 is not a closed form solution, it can be numerically solved, and has a more well defined equilibrium monomer concentration than the isodesmic model. As soon as the total concentration $[M]_{\mathrm{Tot}}$ concentration exceeds K_n^{-1}, the monomer concentration remains constant. Another implication of this nucleation model is that it predicts a very different size distribution than the isodesmic model. In particular, much larger aggregates are would be observed at the same $[M]_{\mathrm{Tot}}$ as long is it is even marginally above K_n^{-1} [62]. Finally, this model sits better with the observation that addition of preformed fibrils substantially increases the rate of

fibril formation [33, 34], as these fibrils have already exceeded the kinetic barrier, namely nucleus formation. As such, amyloid formation is considered a nucleation-elongation phenomenon where an unstable nucleus must form before the favourable elongation reaction can take place.

In the framework above, species of the same size were all placed in one term and they all represented either amyloid fibrils of different sizes, or nuclei of different sizes. This implicitly stated that the only reactions occurring were those leading to amyloid formation. However, this is not the only reactions that can occur in conditions that favour amyloid formation. For several amyloid systems, is has turned out that the same conditions that lead peptides to form amyloids, can also lead them to form a class of so-called off-pathway aggregates (*i.e.* not leading directly to amyloids) that are collectivity known as oligomers. Some of these off-pathway oligomers even inhibit amyloid formation. However, as the term oligomer is being used to describe more or less every species bigger than a monomer that does not have a cross-β conformation (*i.e.* also on-pathway assemblies), the topic will not be discussed in general terms as it is not clear that it is meaningful to discuss this wide class of species under one term. For some specific details of oligomer formation of one system, namely α-synuclein, see subsection 1.3.3.

1.1.4 Kinetics and pathways of amyloid formation

Even though Congo red is still being used for staining histological samples, the most commonly used dye when experiments are conducted *in vitro* is the fluorescence dye Thioflavin T (Tht). Apart from being more specific [64, 65], it has the advantage of changing its fluorescence intensity at 482 nm (when excited at 450 nm) drastically upon binding to amyloid [66]. This makes it sensitive, but also more suitable for kinetic studies as the increase in fluorescence can be measured in real-time *in situ* [67]. Although, it is important to note that fluorescence in general is sensitive to the local environment of the fluorophore and Tht is no exception. This can lead to differences in intensity due to differences in *e.g.* pH [66] and binding affinities [68]. Due to these complications, Tht assays needs to be adapted, optimised, and validated for each type of experiment performed [69]. After this optimisation has been performed, the intensity readout of Tht as a function of time is the standard way of measuring the kinetics of fibril formation.

Although the nucleation-elongation model, as argued above, is sufficient to describe the overall thermodynamics of amyloid formation, a somewhat more complicated analysis is needed to describe the kinetics due to the multitude of possible reactions. However, regardless of mechanism, the concentration of amyloid mass, in monomer equivalents, $[A]$, is thought to be overwhelmingly derived from monomer addition to and from growth-competent ends $[F]$, which is a collective term for nuclei and growth competent fibril ends:

$$\frac{d[A]}{dt} = k_+[F][M] - k_-[F] \tag{1.12}$$

Where k_+ and k_- denotes the rate constants of growth and shrinkage respectively. Depending on the model being used, $-k_-[F]$ is usually neglected in kinetic analysis. This is a particular if a large amount of seeds or a low monomer concentration are employed, and Equation 1.12 can be integrated to yield the familiar first order reaction:

$$[A](t) = [M](0)(1 - e^{-k_+[F]t}) + [A](0) \tag{1.13}$$

It is important to note that what is observed is growth from ends, and therefore methods to generate more ends by fragmentation, such as sonication or vigorous shaking/stirring, are commonly employed before starting an elongation type assay in order to speed it up. At low monomer concentrations (or equivalently, high seed concentrations) Equation 1.12 is usually sufficient, but it has been noted that at high monomer concentrations, the rate of amyloid formation is not linear in monomer concentration [70]. Instead, the rate of formation tends towards a constant value in a hyperbolic fashion. This can be attributed, in analogy to enzyme kinetics, to a two-step mechanism where the monomer first binds to the fibril end, and then subsequently reorganises to its final state as a new fibril end [71]:

$$F + M \underset{k_-}{\overset{k_+}{\rightleftharpoons}} FM \xrightarrow{k_{\text{cat}}} A + F \tag{1.14}$$

With associated rate equations:

$$\frac{d[M]}{dt} = -k_+[F][M] + k_-[FM] \tag{1.15}$$
$$\frac{d[FM]}{dt} = k_+[F][M] - k_-[FM] - k_{\text{cat}}[FM] \tag{1.16}$$
$$\frac{d[F]}{dt} = -k_+[F][M] + k_-[FM] + k_{\text{cat}}[FM] \tag{1.17}$$
$$\frac{d[A]}{dt} = k_{\text{cat}}[FM] \tag{1.18}$$

Of special interest is Equation 1.16 and Equation 1.18 which when applying the pseudo steady-state assumption, $\frac{d[FM]}{dt} = 0$, yields:

$$K_M = \frac{k_- + k_{\text{cat}}}{k_+} = \frac{[F][M]}{[FM]} \tag{1.19}$$

which when inserted in Equation 1.18 and normalised to the total concentration of fibrils yields the familiar equation Michealis-Menten:

$$\begin{aligned} \frac{\frac{d[A]}{dt}}{[F]_{\text{Tot}}} &= k_{\text{cat}} \frac{\frac{[F][M]}{K_M}}{[F] + \frac{[F][M]}{K_M}} \\ v &= k_{\text{cat}}[F]_{\text{Tot}} \frac{[M]}{K_M + [M]} \end{aligned} \tag{1.20}$$

For $[M] \ll K_M$ Equation 1.20 tends toward:

$$\begin{aligned} v &= k_{\text{cat}}[F]_{\text{Tot}}\frac{[M]}{K_M} \\ &= \frac{k_{\text{cat}}[F]_{\text{Tot}}}{K_M}[M] \\ &= k_{\text{app}}[M] \end{aligned} \tag{1.21}$$

Which is linear in monomer concentration and is identical to Equation 1.12 with negligible dissociation.

For $[M] \gg K_M$ Equation 1.20 tends toward:

$$\begin{aligned} v &= k_{\text{cat}}[F]_{\text{Tot}}\frac{[M]}{[M]} \\ &= k_{\text{cat}}[F]_{\text{Tot}} \\ &= k_{\text{app}} \end{aligned} \tag{1.22}$$

Which does not have any monomer dependency, *i.e*, the elongation rate has saturated.

Thus far, it has been assumed that the concentration of growth-competent ends remained constant throughout the measurement. This obviously cannot be true for all cases as the growth competent ends themselves must have been the result of a reaction where more growth competent ends were created. And indeed in socalled *de novo* type experiments a sigmiodal curve, *i.e.* accelerating aggregation, is observed. Fitting of raw Tht fluorescence intensity using a generic sigmoidal curve is one approach, and it captures both the acceleration of growth as well as the limiting amount of monomer that would eventually be available for incorporation into nuclei and fibrils [69]:

$$y = y_i + m_i t + \frac{y_f + m_f t}{1 + exp\left[\left(t_{1/2} - t\right) k_{\text{app}}\right]} \tag{1.23}$$

Where y_i and y_f are the initial and final intensity values respectively, m_i and m_f are the initial and final (linear) slopes respectively, $t_{1/2}$ is the time at which the half-maximal value has been reached, and k_{app} is the apparent elongation rate. Either $t_{1/2}$, or the lag-time $t_{\text{lag}} = t_{1/2} - \frac{2}{k_{\text{app}}}$ is used as an indicator of the nucleation rate. However, there are many ways whereby sigmoidal traces can be observed, each variation can give hints as to which underlying mechanism that gave rise to a sigmoidal curve if data is fitted more carefully rather than with the above generic equation.

The first descriptive model is the direct implementation of the nucleation reaction from the elongation-nucleation model, which is known as primary nucleation and can be written as is:

$$\frac{d[A]}{dt} = [M][F]k_+ - k_-[F]$$
$$\frac{d[F]}{dt} = k_n[M]^n \tag{1.24}$$

Where $\frac{d[F]}{dt}$ is the change of growth competent ends over time, k_n, is the rate of nucleus formation, and n is the effective nucleus size. For a negligible k_-, it has be shown [60, 72, 73] to have an analytical solution. It is however surprisingly complicated but is shown here order to get an idea of the type of problems that are tackled:

$$\frac{[A]}{[M]_{\text{Tot}}} = 1 - \frac{[M]_0}{[M]_{\text{Tot}}}\left[\frac{1}{\mu}\cosh\left(\sqrt{\frac{n}{2}}\mu\lambda t + \rho\right)\right]^{-\frac{2}{n}} \tag{1.25}$$

$$\tag{1.26}$$

Where

$$\lambda = \sqrt{k_+ k_n [M]_0^n}$$
$$\alpha = \sqrt{\frac{k_+ n}{k_n [M]_0^n}}[F]_0$$
$$\mu = \sqrt{1+\alpha^2}$$
$$\rho = \log(\alpha + \mu)$$

The primary nucleation model is sufficient to describe the polymerisation reaction of actin [61], flagellin [74] and some functional amyloids from bacterial biofilm [75]. It is, however, insufficient in describing the kinetic behaviour of many of the disease related amyloids. In particular, the positive curvature is not strongest at the beginning of the kinetic curve (*i.e.* where $[M]$ is largest) as predicated by Equation 1.24.

Two additional models have been proposed to account for the acceleration of amyloid formation. The first one is inspired by the observation that fibrils can break, and it was believed that breakage could occur even in the absence of vigorous mechanical perturbation. This is easy to suggest, whereas the implication of such a statement in terms of modelling is exceedingly challenging as the following model reveals. The goal is to keep track of how many growing ends there are at any given time. The longer a fibril gets, the more ways it can break and make new growing ends. One way to solve this is to use the Master Equation approach and keep track of how fibrils (f) enters, or move away from a state having a given length j at time t:

$$\frac{\partial[f(t,j)]}{\partial t} = 2[M](t)k_+[f(t,j-1)] \tag{1.27}$$
$$-2[M](t)k_+[f(t,j)] - k_-(j-1)f(t,j) \tag{1.28}$$
$$+2k_- \sum_{l=j+1}^{\infty} [f(t,j)] \tag{1.29}$$

This describes how fibrils can grow into having length j by addition of a monomer to fibrils of length $j+1$ Equation 1.27. Alternatively, fibrils can move away from being j long by either growing to be of length $j+1$ by monomer addition, or by breaking at one of the $j-1$ internal bonds Equation 1.28. Finally, fibrils longer than j can break into pieces that ends up being j long Equation 1.29. Unsurprisingly, adding this additional layer of complexity to Equation 1.24 does not make it easier to integrate and requires more sophisticated mathematics than lies within scope of this thesis, however, solutions do exists [76] and data can be fitted to this model using the dedicated software Amylofit [73]. Breakage has successfully described some data that was recorded using vigorous shaking [76], most cases still could not be described by this model, especially in the absence of vigorous shaking.

The last idea was, analogous to crystallisation and the aggregation of sickle haemoglobin aggregation, that secondary nucleation could be taking place:

$$\begin{aligned} \frac{d[A]}{dt} &= [M][F]k_+ \\ \frac{d[F]}{dt} &= k_n[M]^n + k_{n_2}[A][M]^{n_2} \end{aligned} \tag{1.30}$$

Here the amyloid is directly involved in creating new growth-competent ends, not by breakage, but rather by acting as a site for new nucleations. The main difference between fragmentation and secondary nucleation lies in the monomer dependency where fragmentation depends weaker on monomer concentration than secondary nucleation. The reason is that secondary nucleation (like primary nucleation) depends polynomially on monomer concentration as nucleation still represent a meeting of individual molecules. On the other hand, fragmentation is only mildly increased with monomer concentration as it makes the fibrils grow faster and therefore faster have more ways to break. The amplification through secondary nucleation is the model that fits best for the disease related proteins aβ [77] and α-synuclein [78].

Using a combination of the models shown in this section, often assisted by the use of the dedicated software Amylofit [73], it is possible to distinguish between which mechanisms are the dominating ones for a particular experimental setup which is then recorded at different monomer concentrations. However, it is only feasible if done using global fitting of parameters and very high quality of kinetic data which for some systems are very challenging to achieve. None the less, the use of these techniques has significant improved our ability to model amyloid formation and understand which pathways are dominating. Understanding what is dominating allows for a more targeted approach to interfere with amyloid formation, hopefully alleviating the diseases they are associated with. However, even though our understanding of amyloid formation has been

advancing, the very large number of failed drug trials against in particular Alzheimer's Disease (reviewed in [79]) has taught us that the role of amyloid in disease is not well understood.

Even though we have the mathematical toolkit to describe how amyloids form, the molecular details of how proteins come together and form highly ordered growth-competent nuclei rather than a amorphous blobs, and how incorporation of monomers at the fibril end is achieved, are lacking. It is, however, outside the scope of this thesis to tackle this problem for all proteins, and the focus will be on getting closer to answers regarding α-synuclein that has been implicated in the debilitating Parkinson's Disease.

1.2. Parkinson's Disease

> Involuntary tremulous motion, with lessened muscular power, in parts not in action and even when supported; with a propensity to bend the trunk forwards, and to pass from a walking to a running pace: the senses and intellects being uninjured.
>
> Parkinson, 1817

1.2.1 Historical overview of Parkinson's Disease and treatment

In 1817 Parkinson published an essay which included six medical case studies (although he only saw one of them from afar) alongside a definition of what had up to that point more vaguely been described as the Shaking Palsy [80]. In his essay, he described many of the symptoms as well as the progressive character of the disease that should later come to bear his name. Although the disease was now recognised, a larger extension of the hallmarks of the disease did not occur until Charcot continued to expand on the description of the disease from the 1860's to the 1880's by thoroughly reviewing the literature, using larger sets of patients, and how to distinguish it from similar diseases [81, 82, 83, 84]. It was also around this time that consensus on naming of the disease after Parkinson arose. Although the symptoms and progression of the disease was at this point in time rather well established, understanding of the origin of the disease had not progressed significantly. In 1895 Brissuad (a prominent student of Charcot) hypothesised that PD was related to ischaemia in the brain region known as *substantia nigra* [84, 85], this however was based on one or two clinical cases. Soon hereafter in 1912, Lewy, working out of the lab of Alzheimer, dissected brains from PD patients and noticed, likely proteinaceous, intracellular inclusion bodies [86, 87]. Just a few years later in 1919 Tretiakoff, also through dissection, described the degeneration of the *substantia nigra* and confirmed and expanded on Lewy's observations by finding inclusion bodies in other parts of the brain as well [87, 88]. Somewhat later in 1938, Hassler confirmed Tretiakoff's results and added a more detailed view of the distribution Lewy body pathology in particular that degeneration of *pars compacta* in the *substantia nigra* led to PD [87, 89].

Although a region of the brain had now been shown to degenerate during PD, it did not offer hints toward how to treat the disease or its symptoms. This was about to change due to the rapid development and understanding of neurotransmitters in the late 1950s early 1960s, leading to an equally rapid development in understanding of PD. It was shown that a tranquilliser used in psychiatry, reserpine, occasionally produced PD-like symptoms in patients, something that was shown in a large study by Kline and Stanley in 1955 [90]. During a somewhat frantic year, 1957, it was shown that reserpine lowered serotonin levels in the brain, however it was at that point unclear if that was the central effect of reserpine [91]. Just five months later Montagu discovered and measured the amount of dopamine in the brain of humans [92]. And an additional three months later, 3,4-Dihydroxyphenylalanine (L-DOPA), a precursor to dopamine, was shown to be a antagonist of reserpine but 5-Hydroxy-tryptophan, a precursor to serotonin was not [93]. Shortly hereafter it was shown that reserpine resulted in lowered dopamine levels in the brains [94] of mammals. Collectively, this suggested that dopamine was intimately linked with PD.

This became even more tantalising when dopamine was shown to be predominately localised in the brain region known as the *striatum* in various animals [95, 96], an area which was believed to be involved in movement. A breakthrough came in 1960 when Ehringer and Hornykiewicz measured the dopamine level in the brain of recently deceased patients. The patients that had been diagnosed with PD had a lower dopamine level in the *striatum* (a region which is connected to the *substantia nigra*) as compared to patients that had been neurologically healthy [97]. Shortly hereafter Birkmayer and Hornykiewicz (same as above) showed that a precursor of dopamine (L-DOPA, also known as levodopa), was capable of crossing the blood-brain barrier (BBB) and become decarboxylated into active dopamine, alleviated several of the symptoms of PD patients (even though side effects were observed) [98, 99]. A clinical trial using L-DOPA was commenced which gave very promising results [100]. The same year, a stringent clinical description of PD was also published [101].

Although a treatment was now available, the causal link between the early recognised degeneration of the *substantia nigra* and the more recently discovered lowered dopamine level was still missing. The next leap in the understanding came when drug addicts intravenously injected the compound 1-Methyl-4-phenyl-1,2,3,6-tetrahydropyridin, sold to them as "synthetic heroin" which was however a by-product of a poor synthesis of 1-methyl-4-phenyl-4-propionoxypiperidine which is indeed a form of synthetic heroin. Within two weeks, these addicts developed a chronic disease very similar to PD that furthermore could be treated with L-DOPA [102]. The same year 1-Methyl-4-phenyl-1,2,3,6-tetrahydropyridin was used to generate an animal model of PD. Using this model, it was shown that indeed, the dopamine level in the striatum was lowered, and furthermore that is was due to death of dopaminogenic neurons in the *pars compacta* of the *substantia nigra* which would explain the lowered dopamine level in the *striatum* [103] (this type of animal model is still being used for PD research, especially in drug testing).

1.2.2 Symptoms of Parkinson's Disease

PD is a progressive disease where more symptoms become present and more severe as the loss of dopaminergic neurons becomes more widespread. It is thought that most of the symptoms does not arise until reduction of striatal dopamine by 70–80 % has occurred [104, 105]. This reduction is accompanied by the death of ~ 30 % of the dopaminergenic neurons in the *pars compacta* of the *substantia nigra* [104, 106]. Clinically, the diagnosis of PD (technically Parkinsonism, of which ~ 80 % is PD [107]) is made if patients exhibit atleast two of the four following physical symptoms [108, 109]:

Tremor Tremors affecting one side of the body while it is at rest with a frequency of 4–6 Hz is one of the standard symptoms of PD. Hands and feet are most commonly affected, but other muscle groups including legs, lips, chin, jaw can be involved. The tremor usually recedes during movement or sleep. Apart from the resting tremor, some patients also exhibit postural tremor, *i.e.*, tremors while holding a posture against gravity such as outstretched arms [110].

Rigidity Rigidity of muscles resisting movement. This is often observed as the "cogwheel phenomenon" where jerks that resist movement are observed when the limb is moved passively. The latter phenomenon is usually more prevalent in arms than legs [111].

Bradykinesis/hypokinesis/akinesis Akinesis is the slowness of movement as well as reaction times. It is often observed when shifting between different motoric tasks. It includes the loss of facial expression, loss of spontaneous gesturing, decreased blinking, as well as

problems swallowing. It is noteworthy that akinesis can be related to the emotional state of the patient, *e.g.* an immobile PD patient might be able to run if somebody shouts fire [108].

Postural instability Postural instability due to loss of postural reflexes. It is the main reason that PD patients are likely to fall as they might not be able to recover if they lose their balance. It can be tested by pulling the patient backward by the shoulders and the severity can be judged (from taking a few steps but recovering unaided, over not being able to recover unassisted to an inability to stand unassisted) [112].

In addition to the four socalled cardinal or primary physical symptoms mentioned above other physical symptoms are occasionally observed as well. These include postural deformities, where the most common appearances are the torso bend forward and the elbows bend outwards while walking [108] or a constantly bend neck. So-called freezing can also occur, where for shorter periods (< 10 s) the patient freezes and is unable to move. This can occur both at the beginning of a movement, or during specific movements such as turning corner or crossing busy streets; it is another common cause of falls [113].

In addition to physical symptoms related to the motoric system, various other physical symptoms might be observed, some even occur before motor symptoms begins to appear. These include low blood pressure [114], gastrointestinal dysfunctions [115], urinary complications [116], and a loss of the sense of smell [117].

lastly, several non-physical symptoms have been shown to occur such as fractioned sleep [118] and dementia are among the more common symptoms, although dementia tends to develop late in disease progression [119].

1.2.3 Treatment of Parkinson's Disease

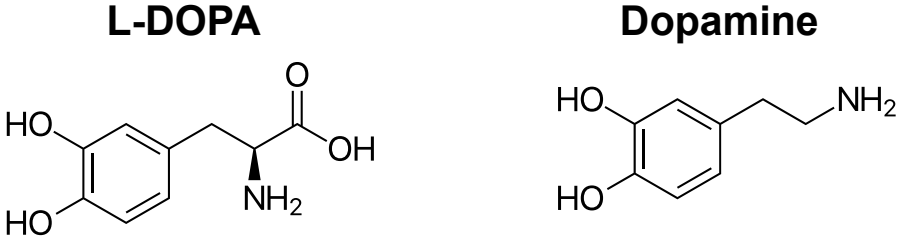

Figure 1.2: Chemical structure of L-DOPA and dopamine, L-DOPA is the most commonly used drug to treat PD. Unlike dopamine L-DOPA is capable of crossing the BBB and enter the brain, where it will become decaboxylated into dopamine.

Parkinson's Disease is the second most common neurodegenerative disease after Alzheimer's. It is rare in people aged 50 and below, but affects up to 3.5–4 % of people aged 80 and above, and as such is expected to increase in prevalence over the next decades due to ageing populations [120, 121]. Initially, the motor symptoms of the disease can be controlled well with medication, however, due to the progressive nature of the disease patients require larger and larger doses of medication due to the continued loss of neurons. Eventually, it may not be possible treat it satisfactory with medications [122]. The non-motor symptoms vary more among patients and are treated as one would for non-PD patients, (*e.g.* constipation are dealt with using laxatives, sleep

disorders with sedatives *etc.*), hence in the following I will restrict myself to the description of the treatment of the motor symptoms of PD. It should be noted that a combination of drugs tailored to the patient is usually given rather than stand-alone treatments of individual medications, especially at later stages.

Although the efficacy of L-DOPA towards treating PD was shown already in the 1960s (see above) it remains the dominant way of treating PD to this day. However, a peripheral decarboxylase (aromatic-L-amino-acid decarboxylase) will turn L-DOPA into dopamine rendering it unavailable to the brain as dopamine does not cross the BBB. One of the improvements to L-DOPA treatments has been to administer it together with compounds (Carbidopa and Benserazide) that inhibits the peripheral decarboxylation, such that a larger amount of the administered L-DOPA makes it into the brain [123]. Although L-DOPA is usually effective in managing the symptoms of PD, it does however have many side effects, especially if taken over many years and in large doses. One of the more problematic side effects is dyskinesias (jerky movements the patient does not have control over) [124].

An alternative/supplement to L-DOPA is dopamine agonists (*e.g* Ropinirole) that have the same effect as L-DOPA. The difference is that they do not need to be activated by decarboxylation and they readily cross the BBB. The dopamine agonists tend to lead to fewer side effects, although their effectiveness tends to be lower as well [125].

Another possibility is to prevent degradation of dopamine in the brain by administering inhibitors (*e.g* selegiline) of the enzyme that degrades dopamine namely Monoamine oxidase B. However, using this treatment requires that dopamine is present in the brain in relatively large amounts, *i.e.* early in disease progression where most dopaminergic neurons are still alive, or given together with L-DOPA [126].

A similar strategy is used when administering inhibitors of Catechol-O-methyltransferase as this enzyme also breaks down dopamine. Furthermore, this enzyme breaks down L-DOPA directly and, atleast at later stages of PD, inhibition of degradation might be necessary to achieve high enough L-DOPA concentrations as well as reducing the fluctuations in L-DOPA concentration in the brain over time [127].

Lastly, a treatment that does not rely on drugs is occasionally used namely deep brain stimulation. It is performed by implanting an electrode in the subthalimic region of the brain to counter the disturbances from the degenerated *substantia nigra*. It is, however, a rather complicated procedure with significant risks to introduce objects deep inside the brain. As such, it is usually only performed on patients that have been in medical treatments for many years and are experiencing large side effects (especially long term L-DOPA related dyskinesias) [128].

It should be noted that non of the treatments listed above provides a cure for PD nor do they slow down the progression of the disease. The reason they do not provide a cure is that they are not attacking the root cause of PD, namely the dying-off of neurons. Our lack of a cure is not due to a sinister conspiracy of clinicians, it is due to the fact that the underlying reason why the neurons are dying is poorly understood. The root cause of PD remains a matter of controversy and is the subject of active research, of which this thesis is a small part.

1.3. α-Synuclein

> Since it is unclear how α-synuclein, a very soluble protein, ends up in cellular inclusions, we carried out studies to determine whether wild type (WT) and/or mutants of α-synuclein can self-aggregate *in vitro*.
>
> Giasson *et al.*, 1999

1.3.1 α-Synuclein and Parkinson's Disease

A seminal study from 1997 for the first time implicated α-synuclein directly in PD. The hint came from observing of an Italian family that had an unusually high incidence rate of early-onset PD 46 ± 13 years. It was shown that all the members that had early onset PD (except one) had a mutation that caused a substitution of alanine to threonine at position 53 in a protein termed α-synuclein [129]. Intriguingly, they found the same mutation in a Greek family with several cases of early onset PD. Subsequently, several mutations in α-synuclein has been shown to lead to PD (*i.e.* autosomal dominate inheritance) including A30P [130], E46K [131], G51D [132], and A53E [133]. Additionally point mutations have been found in individual patients including, A18T and A29S [134], and H50Q [135], which have not been found in healthy individuals, but it has not been directly shown to lead to inheritable PD. Although, it is noteworthy that the vast majority of PD cases (estimates lie in the range of $\sim$ 85–95 % [136, 137]) are thought to occur sporadically (*i.e.* not hereditary) and even among hereditary ones, mutations in α-synuclein have turned out not to be common [136, 138]. However, Two further lines of evidence points towards the protein α-synuclein being central in understanding PD namely that duplications [139] and triplications of the gene also leads to PD [140]. Furthermore, triplication usually leads to earlier onset than duplication. These observations have been very important as they hint towards the wild-type leading to PD, albeit if present in higher concentration. This lends some credit to the notion that α-synuclein under the wrong circumstance becomes toxic. In fact, a very large body of research is still being conducted under the assumption that PD is caused by the misbehaviour of α-synuclein.

1.3.2 Aggregation of α-synulein and Parkinson's Disease

Just a few months after it was shown that A53T led to familial PD, it was shown that Lewy bodies from patients with sporadic PD could be stained with polyclonal antibodies against α-synuclein [141]. Although Lewy bodies (and neurites) has long been known to be a hallmark of PD (see subsection 1.2.1), and conclusive diagnosis of PD cannot be made without finding them *post mortem*, their role in the disease remains obscure. Even though almost all people diagnosed with PD (or related diseased) indeed have Lewy bodies [142], they have also been found in a substantial percentage of neurologically healthy patient in increasing proportions with age [143]. Some argue that this is a sign of preclinical PD rather than a normal part of ageing [144]. Even though the exact role of Lewy bodies in PD is not well understood, it is attractive to investigate what they are composed of, and how they form. Shortly after Lewy bodies were found to stain positive for α-synuclein, they were also found to contain large amounts of amyloids [4, 145] and both the A53T mutant as well as WT was able to form amyloid. Although more recent work has shown that not all Lewy bodies contain amyloid, and the ones that do, also contain large

amounts of lipids and even organelles [146]. Intriguingly, A53T formed amyloids much faster than the WT *in vitro* [147], which suggested that amyloid was the cytotoxic species, the faster it formed and proliferated, the worse.

However, as mentioned in the subsection 1.1.3, amyloid formation is an exceedingly complicated phenomenon with many intermediates representing both on and off pathway species, something that holds true for α-synuclein as well (review in [148]). It is therefore a complicated task to pinpoint which parts of the complicated mixture of α-synuclein species is the cytotoxic one(s). A dominant line of thought is that oligomeric species are the ones predominately responsible for cytotoxicity [149, 150], where the amyloids themselves only play an indirect role direct as a source of new oligomers [151].

Another line of research focus on the amyloids themselves being the primary toxic species which has also been shown [152], and especially shorter fibrils seem to be toxic [35]. However, as more mutants have been investigated *in vitro*, it became clear that faster aggregation of the known disease causing mutant forms is not the rule, and neither do they all exhibit faster or more complete oligomer formation [153, 154, 155].

Regardless of which species are believed to be the toxic one, spreading of pathology in terms of Lewy bodies is thought to be a central feature (reminiscent prion research, see subsection 1.1.1). That spreading occurred in a particular order was proposed in a very influential paper from 2003 [156]. In this work, the brains from several groups of patient were dissected and categorised in stages based on how many of the investigated section had PD pathological hallmarks. These included Lewy neurites, Lewy bodies / α-synuclein positive intracellular aggregates. In addition to evaluation of the presence of pathological hallmarks, how many there were in each section was also done, and in some regions the total number of neurons was also evaluated. Collectively, these measures were termed "PD related lesions" [156]. From this investigation it seemed clear that patients with later stages of PD tended to have more widespread pathology, a spreading that followed a pattern. In mostly symptomless patients, the earliest signs of PD occurred in the dorsal motor nucleus of vagal nerves (note that the brains was investigated *post mortem*, *i.e.* spreading was inferred not shown).

Trying to understand the pathways of spreading of PD pathology became a field of research in its own rights. This led to the discovery that injecting preformed amyloid fibrils of α-synuclein into the brain of mice, caused them to develop a PD-like disease [157]. Although, whether it was the fibrils themselves or oligomeric species that causes pathology and spreading, is a source of debate, especially as thorough characterisation of the preformed fibrils [158] that are used for injection are often lacking. More recently it was shown that injecting preformed fibrils in the gutwall of mice was enough to cause them to develop PD [56]. It was already known that the neurons of the gut was affected in patients with PD, but it was shown that if the vagus nerve, which connects the gut to the brain, was severed, injection of amyloid in the gut wall had no effect [159]. Not only is this in good agreement with the observation and subsequent hypothesis by Braak *et al.* that PD started in the gut [160], it is also in agreement with cohort studies finding a reduced PD incident rate of people who had undergone truncal vagotomy *i.e.* have had their vagus nerve severed [161, 162]. Building on this, it has been shown that even oral administered fibrillar material can lead to PD-like pathology in mice, although the link was less robust compared to brain or gut wall injection [163]. Remarkably, it was shown that even injection of amyloid material in the muscle of the leg of mice could lead to PD-like pathology in the brain of mice, again highlighting the capability of α-synuclein amyloid to spread and cause pathology [164]. Although it is not necessarily believed that all cases of PD starts in the periphery

in general or the gut in particular, it highlights that spreading from brain to gut, and gut to brain can be amyloid depend. Furthermore, the presence of seeding competent (Tht positive) material from both brain cerebrospinal fluid, was found to correlate with PD (and related diseases) in independent setups [165, 166]. Thus, understanding how to prevent the growth and spreading of amyloid fibrils still provide potential targets for halting the relentless progression of PD or at the very least understanding important biomarkers.

1.3.3 Biophysically properties of α-synuclein

Human α-synuclein is a 140 aa residue long, 14.5 kDa, acidic protein (pI of 4.67), the biological function of which is not fully understood. It is found predominantly in presynaptic neurons at termini [167, 168], with a concentration reported to be $\sim 40\,\mu M$ [169], even though, estimates as high as 1 % of total protein content in certain brain regions also exist [168]. It is thought to be involved in vesicle fusion to membranes together with the SNARE proteins [170, 171]. Indeed, one of the generally agreed upon features is binding to negatively charged lipids [172, 173] both micelle-forming lipids like SDS [173] or vesicle forming ones like 1,2-Dimyristoyl-sn-glycero-3-phospho-L-serine (DMPS) [174], with a general preference for membranes with high curvature [175]. This is also underpinned by the primary sequence which harbours seven imperfect repeats of eleven residues with the consensus motif XKTKEGVXXXX, showing similarities to the lipid binding proteins in the apolipoproteins, in particular the A2 type [176, 177, 178]. Furthermore, α-synuclein has been shown to bind metal ions in particular divalents ones including copper, calcium, iron, manganese, cobalt, nickel, and zinc [179, 180, 181]. It is usually said to consist of three regions that differ in roles when the protein adopts its membrane bound or amyloid conformation:

The Amphiphatic N-terminal region spanning residues 1-60 is critical for the ability of α-synuclein to bind to lipids [182]. Upon binding to lipids, it adopts an α-helical conformation where the hydrophobic residues cluster predominately on one side and hydrophilic ones on the other. The residues from ~ 30 onwards are thought to be at part of the fibril together with the NAC region [183, 184].

NAC The Non amyloid-β component (NAC) from 61-95 harbours hydrophobic residues and is believed to form the core of the fibril when the protein is in amyloids. The reason for the rather peculiar name is that it was found as an amyloid in the brain of some Alzheimer's patients, the dominant amyloid forming protein known as Amyloid-β [185]. Together with the N-terminal region, NAC, adopts an α-helical conformation when the protein is bound to lipids, however the conformation varies depending on the exact type of the lipid [173].

The Acidic C-terminal region from 96-140 (sometimes referred to as the acidic tail) is most noted for the large amount of negative charges, 14, it harbours. It is here the putative binding sites for metal ions reside, except copper which binds to the N-terminus [180]. Besides binding, the many negative charges increases the solubility of the protein as well as inhibiting aggregation due to repulsion of like-charges. Indeed, C-terminally truncated forms are found in the Lewy bodies and Lewy neurites [186], and aggregation of C-terminally truncated forms are more aggregation prone [187, 188].

1.3.4 Oligomeric species

α-Synuclein is said to be a so-called natively unfolded protein as it dose not adopt any well defined tertiary structure at physiologically relevant conditions [189], and even in cells it seems to

lack any [190]. Evidence has been put forth that α-synuclein adopts a stable tetramer that should be the dominant species *in vivo* [191, 192]. This, however, has not been possible to reproduce by groups not directly associated with the original proponents [190, 193, 194, 195, 196].

That α-synuclein forms various oligomeric species ranging from dimers formed by dityrosine formation [197, 198, 199] to several hundred kilodaltons ones are on the other hand well established. There are almost as many methods to prepare oligomers as there are groups studying them, but the predominately studied oligomers are made using high α-synuclein concentrations $\sim$ 500–2000 µM at 25–37 °C for anywhere between 5–20 h quiescently or with shaking (900–1250 RPM). This tends to be followed by an isolation/fractionation step using one or more of the following methods: centrifugation, filtration, and Size Exclusion Chromatography (SEC) [150, 200, 201, 202, 203]. Note that all of these rely on lyophilised protein, which was noted to be critical for the procedure [202].

An alternative class of oligomers are prepared incubating α-synuclein with organic compounds such as Epigallocatechin gallate [150, 204] or Baicalein [205]. Lastly, addition of divalent metal ions have also been shown to cause oligomerisation especially when copper or iron is added [206, 207].

Unsurprisingly, the large variation in methods employed in the creation of oligomers lead to large variation in toxicity spanning from none to severe in terms of cell survival and stress [200, 202, 207]. Generally, oligomers tend to show some secondary structure and β-strand formation in particular is commonly observed [150, 201, 202] compared with monomeric α-synuclein which exhibits random coil.

1.3.5 Amyloid formation

Most infamously though is the ability of α-synuclein to form amyloid fibrils. Somewhat more surprising is how reluctantly α-synuclein forms amyloids, and how difficult it is to reproduce the kinetic parameters of its aggregation. Various methods have been employed to accelerate and/or improve reproducibility, including agitation with stir bars [208], shaking ± beads of glass or plastics [209, 210, 211]; addition of various lipids in various assemblies including micelles [209], vesicles [174], and nanodiscs ± shaking [212], α-synuclein derived lipoparticles [213]; increasing temperature [214], high salt concentrations [215], and lowering of pH [188, 211, 214]. From these studies, it is thought that primary nucleation likely needs to occur at an interface [216] such as an air-water or lipid-water one (accelerating effect from certain lipids, surfactants, or shaking). Furthermore, fibrils can be mechanically broken creating new growth-competent ends (stirring or shaking with beads). And finally that primary and secondary nucleation as well as elongation is inhibited by the many negative charges in the C-terminus of α-synuclein that can be overcome by bringing the effective charge closer to zero by lowering the pH, shielding them with salt, or truncating the C-terminus.

The emergent view then is that the rates associated with different amyloid formation pathways are differentially altered by specific conditions. Hence, employing different conditions, one can begin to investigate the effect of disease related mutants to try and understand which pathways might be most problematic in terms of PD. Indeed, several studies attempted to do just this [153, 155, 217]. It is noteworthy that no single unifying theme was found in terms of oligomer formation, primary nucleation, secondary nucleation, elongation rate, and lipid binding. Whether this implies a multitude of ways in which α-synuclein can misbehave to give rise to PD, or whether these parameters are not of direct relevance to PD remains an open question.

Furthermore, the conditions does not only change the rates of fibril (and oligomer) formation, they also change morphology of the resulting fibrils [215]. Interestingly, fibrils prepared at different conditions gave rise to different disease profiles when injected into rat brains [54]. This promising result lends hope to the notion that *in vitro* differences can be translated into *in vivo* behaviour. Central to this notion is structural investigations of α-synuclein amyloids. The earlier structural investigation at molecular level were performed using solid state Nuclear Magnetic Resonance (NMR). It was noted that α-synuclein was polymorphic within each fibril preparation, as well as between different preparations [218]. Eventually, a structure of the amyloid fibril was obtained which suggested the socalled greek key motif being composed of single filaments [219]. Soon after, the rapid development of Cryogenic Electron Microscopy (CryoEM) allowed several groups to obtain high resolution structures of α-synuclein where better long-range constrains are available compared to NMR. Shared for all of them is that they are composed of two filaments twisted around each other [42, 220, 221, 222, 223]. Although at first glance the new structures appeared to be similar to the NMR morph[2], closer inspection reveals that this is not the case [148]. The NAC region is always found in the fibril and residues down to residue 46 are commonly observed in the CryoEM, in a few case as far down as residue 14 are seen in forming a β-strand [222]. The C-terminus is also never found inside the fibril. What differs between these structures is which residue belong to which β-strand, and how the β-strands are arranged with respect to each other. In on case the filaments are nearly identical but arranged differently with respect to each other [222] (morphs 2a and 2b in Figure 1.3). In several of the structures [42, 220, 222] though, several of the residues in the region composed of residues 44-55 are in, or at the interface between filaments (see Figure 1.3). However, counterexamples exist where this region is not part of the interface but simply a part of β-strands [219, 220] (see morph 1b in Figure 1.3). It is noteworthy that all of the known disease-causing mutants lie in the N-terminal region, however in very close proximity to, and often inside the fibril. Understanding this critical region's influence on amyloid formation is therefore of interest.

1.3.6 β-wrapins and hairpins

One of the more straightforward ways of inhibiting amyloid formation could be to sequester the monomer, rendering them unable to enter fibrils. Such an approach was developed for the amyloid forming Alzheimer's disease associated peptide aβ. It was based on finding binding-partners of monomeric aβ using directed evolution via phage-display with the Z-domain from the IgG binding domain of *Stapylococcus aureus* as the starting point [224, 225]. Indeed, two high affinity binders were found and named $Za\beta_1$ and $Za\beta_3$. In the initial characterisation of $Za\beta_1$ and $Za\beta_3$ it was suggested that multimeric species of them, minimally dimers, were needed on order for them to bind aβ. Subsequent work showed that $Za\beta_3$, indeed, binds aβ as a cysteine linked homodimer with high affinity (20 nM) [226, 227]. The same studies revealed that it did indeed sequester monomeric aβ, thereby inhibiting amyloid formation, and was later shown to have a protecting effect of flies co-transfected with dimeric $Za\beta_3$ and the toxic aβ [228]. The structure of the complex revealed aβ adopted a β-hairpin conformation that $Za\beta_3$ wrapped around [226, 227]. To explore the capacity of small proteins to interfere with amyloid formation, $Za\beta_3$ was used as a starting point for different phage display experiments with monomeric α-synuclein, tau, and amylin, as targets [229, 230, 231]. In all cases binding partners were found, shown to be

[2] Literature tends refer to them as polymorphs, this however is a peculiar choice of nomenclature considering that polymorph means "many shape", and labelling a specific structure *e.g* "many shape" 1a seems like a self-contradiction or that one is talking about a single species that is polymorphic. Neither case is meant and morph 1 and morph 2 would be more easily understood and is therefore used here.

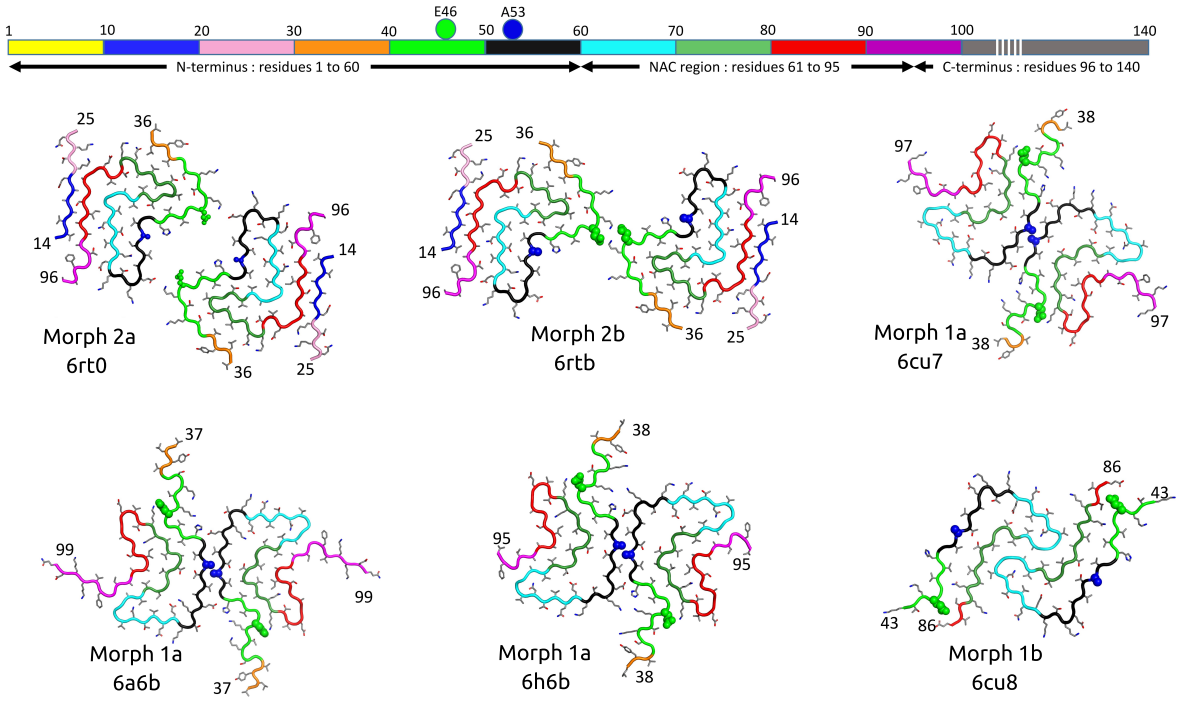

Figure 1.3: Polymorphism of α-synuclein from Cryo EM, Where one of the morphs (1a) have been observed and published in three different publications, however three more has been observed. Note that 2a and 2b are almost identically except from how the strands pack together. The PDB codes of the individual structures are shown. The figure was adopted from [222].

inhibitory, and the targets all adopted a β-hairpin with the binding partner wrapped around them, hence the binding proteins were named wrapins. One of the generated binding partners, termed AS69, had four substitutions with respect to Zaβ$_3$, showed relatively high affinity (240 nM) for α-synuclein, and as the other wrapins it bound to its target as a cysteine linked homodimer [229]. Surprisingly, it was shown that AS69 was able to inhibit α-synuclein in a highly substoichiometric manner, something that was not expected of a monomer binder (see chapter 2 which is an attempt to shed light on this very conundrum). As in the Zaβ$_3$:aβ complex, a region of α-synuclein adopted β-hairpin with AS69 wrapped around it. More precisely, the β-hairpin was formed by one strand from residues 37-43, then a turn consisting of residues 44-47, and finally the second strand from 48-54. It is highly interesting that AS69 would bind to this exact region, not only as this region a part of the fibril core, but it also harbours several of the known disease associated mutants in particular E46K, H50Q, G51D, A53E, A53T. Furthermore, the β-strands were known to interact transiently in solution [232], and to be involved in strain determination of fibrils [233]. The first investigation of how this part of α-synuclein was contributing to amyloid formation was done by introducing a Cysteine-Cysteine (CC) bridge by mutations G41C and V48C (CC48) in the attempt to lock α-synuclein in the β-hairpin conformation [234]. Although α-synuclein nor CC48 adopted a stable β-hairpin in solution, CC48 did not readily aggregate, except when the CC bridge was reduced. Somewhat more surprising, CC48 was shown to be inhibitory of WT aggregation. The assays performed at this earlier state did not fully reveal the mechanism whereby inhibition occurred (see chapter 3 for an attempt to shed more light on this aspect). Locking the 37-54 region of α-synuclein in a β-hairpins conformation by linking the β-strands is not the only way of favouring a β-hairpin. The turn connecting the two β-strands can also

be optimised in order to favour β-hairpin formation. Such optimised versions with optimised turns might, analogous to CC48, yield inhibitors that could be used to better understand amyloid formation (see chapter 4 for an investigation of this hypothesis). Although it is perhaps not too surprising that several proteins are able to form a β-hairpin considering that they all form the similar cross-β structure amyloid. It was, however, rather surprising that one of binding partners generated for α-synuclein, AS10, was able to bind and inhibit amyloid formation of aβ, α-synuclein, and amylin, although with severely reduced affinity compared to their specific wrapins [235]. The existence of such a generic ability to bind to amyloidogenic proteins, might suggest a general amyloidogenic role of the type of β-hairpins found in aβ, α-synuclein, and amylin (see chapter 5 for development of a method to investigate this hypothesis).

1.4. Aims

This thesis is centred around the topic of gaining insights into the role of β-hairpins in amyloid formation and inhibition, in particular, the following questions will be addressed:

1. By which mechanim(s) does the α-synuclein specific wrapin AS69 achieve substoichiometric inhibition by binding to the β-hairpin forming part of α-synuclein?
2. How does locking the β-hairpin region of α-synuclein with disulphide bridges affect its aggregation?
3. Does stabilising the β-hairpin through increased turn formation propensity lead to an altered amyloid forming potential?
4. Are the presences of β-hairpins in the human proteome associated with aggregation prone peptides that can be inhibited by AS10?

2

AN ENGINEERED MONOMER BINDING-PROTEIN FOR α-SYNUCLEIN EFFICIENTLY INHIBITS THE PROLIFERATION OF AMYLOID FIBRILS

2.1. Article information

Title of paper: An engineered monomer binding-protein for α-synuclein efficiently inhibits the proliferation of amyloid fibrils

Authors: Emil D. Agerschou [1,§], Patrick Flagmeier [2,3,§], Theodora Saridaki [4], Céline Galvagnion [5,6], Daniel Komnig [4], Laetitia Heid [1], Vibha Prasad [4], Hamed Shaykhalishahi [1], Dieter Willbold [1,7], Christopher M. Dobson [2,3], Aaron Voigt [4], Björn H. Falkenburger [4,8,9,*], Wolfgang Hoyer [1,7,*], Alexander K. Buell [1,10,*]

[1] Institute of Physical Biology, Heinrich Heine University Düsseldorf, Universitätsstraße 1, 40225 Düsseldorf, Germany

[2] Department of Chemistry, University of Cambridge, Lensfield Road, Cambridge CB2 1EW, UK

[3] Centre for Misfolding Diseases, University of Cambridge, Lensfield Road, Cambridge CB2 1EW, UK

[4] Department of Neurology, RWTH Aachen University, Aachen, Germany

[5] German Centre for Neurodegenerative Diseases (DZNE), Siegmund-Freud-Strasse 27, 53127 Bonn, Germany

[6] Department of Pharmacology and Drug Design, University of Copenhagen, Copenhagen, Denmark

[7] Institute of Complex Systems (ICS-6), Structural Biochemistry, Research Centre Jülich, Germany

[8] Department of Neurology, Dresden University Medical Center, Dresden, Germany

[9] JARA BRAIN Institute II, Julich and Aachen, Germany

[10] Department of Biotechnology and Biomedicine, Technical University of Denmark, Søltofts Plads, 2800 Kgs. Lyngby, Denmark

[§] Authors contributed equally

[*] To whom correspondence should be addressed

Journal: eLIFE

DOI: 10.7554/eLife.46112

2.2. Declaration of Article Contributions

2.2.1 Experimental

Secondary nucleation experiments, density gradient centrifugation (DGC), elongation in the presence of Zaβ_3W, AFM at pH 5, and Circular dichroism (CD) melting curves were performed by me.

2.2.2 Data analysis

Data analysis of elongation data, secondary nucleation data, DGC, CD melting curves was performed by me in collaboration with Alexander Kai Büll.

2.2.3 Manuscript preparation

All main figures for the *in vitro* section was prepared by me in collaboration with Alexander Kai Büll. I wrote the parts for the main manuscript where I been directly involved in the experimental work preceding it in collaboration with Alexander Kai Büll. Furthermore, I wrote the supplementary information regarding data analysis of aggregation kinetics in collaboration Alexander Kai Büll.

2.3. Abstract

Removing or preventing the formation of α-synuclein aggregates is a plausible strategy against Parkinson's disease. To this end we have engineered the β-wrapin AS69 to bind monomeric α-synuclein with high affinity. In cultured cells, AS69 reduced the self-interaction of α-synuclein and the formation of visible α- synuclein aggregates. In flies, AS69 reduced α-synuclein aggregates and the locomotor deficit resulting from α-synuclein expression in neuronal cells. In biophysical experiments *in vitro*, AS69 highly sub-stoichiometrically inhibited both primary and autocatalytic secondary nucleation processes, even in the presence of a large excess of monomer. We present evidence that the AS69-α-synuclein complex, rather than the free AS69, is the inhibitory species responsible for sub-stoichiometric inhibition of secondary nucleation. These results represent a new paradigm that high affinity monomer binders can lead to strongly sub-stoichiometric inhibition of nucleation processes.

2.4. Introduction

Cytoplasmic aggregates of the protein α-synuclein are the pathological hallmark of Parkinson's disease (PD) and other synucleinopathies [141]. Point mutations in the α-synuclein gene or triplication of the α-synuclein locus are associated with familial forms of PD, and the α-synuclein locus is a genetic risk factor for sporadic PD [236]. Targeting α-synuclein pathology is therefore a plausible strategy to stop disease progression in PD. Since α-synuclein aggregate pathology was demonstrated to propagate from neuron to neuron [237], recent work has focused on understanding the cellular and molecular events in this process. From a therapeutic perspective, α-synuclein aggregation is thought to be the underlying cause of PD and remains the focus of causal therapeutic strategies. The link between α-synuclein aggregation and PD has been known for two decades [141, 238]; however, the translation of this scientific discovery into a therapy has proven challenging. Since the first description of small molecules that inhibit α-synuclein aggregation [239], the search for promising compounds continues [240, 241, 242, 243, 244]. While the first small molecules also inhibited the aggregation of tau and amyloid-β, more recent compounds bind α-synuclein more selectively and showed reduced α-synuclein toxicity in mouse models of PD [242].
We have taken a different strategy by engineering a protein, the β-wrapin AS69, to induce the formation of a β-hairpin in monomeric α-synuclein upon binding (Figure 2.1 a) [229]. AS69 was selected by phage display [229] from protein libraries based on ZAβ3, an affibody against the amyloid-βpeptide [226, 227, 228]. AS69 thus not only binds α-synuclein with high and approximately constant affinity throughout the pH range most relevant for α-synuclein aggregation [211] (Figure 2.1 b,c) , but induces a specific conformational change - akin to molecular chaperones [245].

AS69 induces local folding of the region comprising residues 37-54 into a β-hairpin conformation in the otherwise intrinsically disordered, monomeric α-synuclein (Figure 2.1 a). The critical role of this region for α-synuclein aggregation is indicated by the cluster of disease-related mutation sites (Figure 2.1 a). Accordingly, modification of the local conformation by, e.g., introduction of a disulfide bond strongly modulates aggregation [234]. Sequestration of residues 37-54 of monomeric α-synuclein by AS69 inhibits the amyloid fibril formation of α-synuclein under conditions of vigorous shaking of the solution even at highly substoichiometric ratios [229]. Amyloid fibril formation, however, is not a one-step process but can be decomposed into different individual steps, including primary and secondary nucleation and fibril elongation. With vigorous

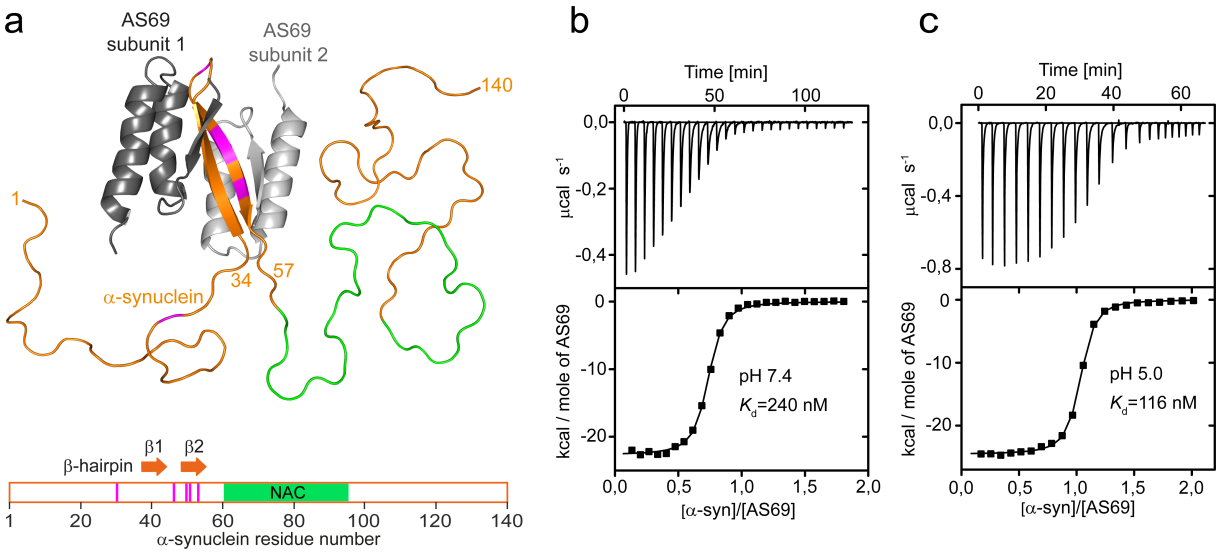

Figure 2.1: AS69 binds to monomeric α-synuclein, inducing local folding of the region comprising residues 37 to 54 into a β-hairpin conformation. **(a)** Structural model of the AS69:α-synuclein complex based on NMR (pdb entry 4BXL) [229], generated with PyMOL (The PyMOL Molecular Graphics System, 1.2; Schrödinger, LLC.). AS69 (grey) is a disulfide-linked homodimer. α-Synuclein (orange) locally adopts β-hairpin conformation, while the remainder of the molecule, including the hydrophobic NAC segment (green), remains intrinsically disordered [229] . Positions at which disease-related mutations have been identified are given in magenta. **(b,c)** The affinity of AS69 to α-synuclein at pH 7.4 **(b)** and pH 5.0 **(c)** analyzed by isothermal titration calorimetry (ITC) experiments. Titration of 420 µM α-synuclein into 47 µM AS69 in 20 mM sodium phosphate, 50 mM NaCl, pH 7.4 (b), or 320 µM α-synuclein into 32 µM AS69 in 20 mM sodium acetate, pH 5.0 (c), at 30 °C. The upper panels show the baseline-corrected instrumental response. The lower panels show the integrated data (filled squares) and the fit to a 1:1 binding model (continuous line).

shaking, for instance, primary nucleation can occur readily at the air-water interface [216] and fibril fragmentation induced by the shaking amplifies the number of growth-competent fibril ends [35]. In order to validate AS69 as a potential therapeutic agent we therefore tested its biological effects in cellular and animal models, and we found it to be a highly efficient inhibitor of α-synuclein aggregation and associated toxicity. In addition, we designed a set of experimental conditions to measure selectively the effect of AS69 on specific steps of α-synuclein aggregation. We found that AS69 is able to efficiently interfere with both the lipid-induced formation and the auto-catalytic amplification of α-synuclein amyloid fibril formation. These inhibitory effects on nucleation are observed even in the presence of a large excess of α-synuclein monomer, which is expected to sequester AS69 into inhibitor-monomer complexes. We show evidence that the secondary nucleation of α-synuclein can be inhibited by the α-synuclein-AS69 complex and that therefore the inhibitory effect of AS69 on this crucial step of aggregate amplification is unaffected by even large excess concentrations of free α-synuclein monomer.

2.5. Results

2.5.1 Coexpression of AS69 reduces visible α-synuclein aggregates in cell culture

First, we explored the effect of the expression of AS69 on the viability of living cells and the association of α-synuclein in a cellular environment. In these model systems we not only expressed WT α-synuclein but also the A53T variant, which has been associated with familial PD and which produces aggregates more quickly than the WT protein [153, 238]. We first used bimolecular fluorescence complementation (BiFC) to probe whether AS69 can interfere with the formation of oligomeric α-synuclein species in living HEK293T cells [246]. Constructs of WT and A53T α-synuclein were tagged with the C-terminal segment of the fluorescent protein Venus (synuclein-VC) or with the complementary N-terminal segment of this protein (VN-synuclein) (Figure 2.2 a). Neither of the two Venus fragments shows significant fluorescence by itself, but together they can generate a functional fluorescent protein [247] and hence function as a reporter for protein-protein interaction. We then transfected HEK293T cells with both synuclein-VC and VN-synuclein, in addition to AS69 (or LacZ as a control) and determined by flow cytometry the fraction of cells that displayed Venus fluorescence (Figure 2.2 b, the raw data can be found in the table in Table 2.2. In the absence of AS69, the fraction of fluorescent cells was larger with the expression of A53T-α-synuclein than WT-α-synuclein (Figure 2.2 b, $p<0.05$, two-way ANOVA). Coexpression of AS69 with both variants reduced the number and fraction of fluorescent cells (Figure 2.2 b, $p<0.05$ for WT and $p<0.01$ for A53T, two-way ANOVA). AS69 did not, however, significantly affect the total quantity of α-synuclein in the cells, as determined from immunoblots (Figure 2.2 c and d). This finding is consistent with the hypothesis that the effects of AS69 in this cellular model system result from the inhibition of a direct interaction between α-synuclein molecules, and not from an enhanced clearance of α-synuclein. Despite the enhanced affinity for self-interaction which the fluorescence complementation tag might convey to α-synuclein compared to the untagged protein, the affinity for AS69 is high enough to sequester a significant proportion of the α-synuclein in living cells.

Having established that α-synuclein and AS69 can interact in cells, we next probed its effects on the formation of larger, optically visible aggregates of α-synuclein by transfecting HEK293T cells with A53T-α-synuclein tagged with enhanced green fluorescent protein (EGFP) as previously described [248, 249, 250] (Figure 2.2 e). The distribution of EGFP within transfected cells was classified as ”homogenous”, ”containing particles” or ”unhealthy” (rounded cells that in time-lapse microscopy were observed to subsequently undergo apoptosis). Co-expression of AS69 with A53T α-synuclein led to an increase in the fraction of cells with a ”homogenous” distribution of EGFP and fewer cells showed α-synuclein particles relative to those cells without AS69 (Figure 2.2 f). These findings indicate that the co-expression of AS69 reduces the formation of visible aggregates in cultured human cells.

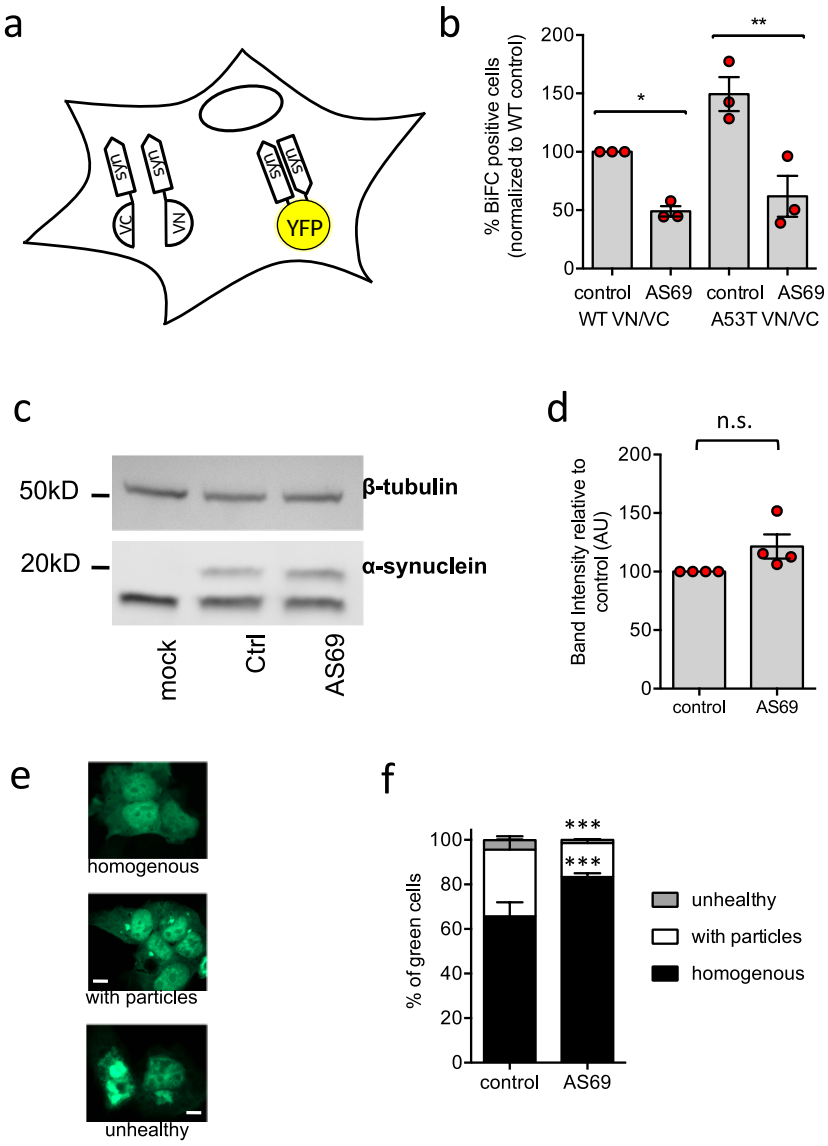

Figure 2.2: AS69 reduces the aggregation of α-synuclein in cellular models. **(a)** Schematic representation of bimolecular fluorescence complementation where α-synuclein is tagged by either the C-terminal (VC) or the N-terminal (VN) fragment of the Venus protein. In dimers or larger oligomers of α-synuclein, the two Venus fragments can form a functional fluorescent protein. **(b)** The percentage of cells with BiFC fluorescence as determined by flow cytometry. HEK293T cells were transfected with α-synuclein (WT or A53T), fused to the VN or VC fragment and either LacZ (control) or AS69. Displayed are the results of n=3 independent experiments and mean ± SEM. In each experiment, 75,000 cells were analyzed per group. Results were compared by one-way ANOVA, results of Sidak's posthoc test depicted. **(c)** Immunoblot of lysates of cells transfected with EGFP-tagged α-synuclein and in addition AS69 or LacZ (control), developed with antibodies against α-synuclein (band just below 20 kDa, note that only the upper band reports α-synuclein [250] and β-tubulin (band just below 50 kDa), the latter as a loading control. **(d)** Quantification of n=4 independent blots as described in **(c)**. Results were compared by t-test. **(e)** HEK293T cells were transfected with EGFP-tagged α-synuclein and the distribution of fluorescence was classified into the depicted groups. **(f)** Summarized results of n=3 independent experiments with n=300 cells classified per group in each experiment (mean ± SEM). Results were compared by two-way ANOVA and Sidak's posthoc test.

2.5.2 Coexpression of AS69 rescues A53T α-synuclein dependent phenotype in Drosophila melanogaster

Subsequently we tested the effects AS69 has in *Drosophila melanogaster* (fruit flies) expressing untagged A53T-α-synuclein in neurons (Figure 2.3). In the absence of AS69, these flies show a progressive reduction in the spontaneous climbing (*i.e.* neuronal impairment) between 15 and 25 days of age [250, 251] (illustrated in Figure 2.3 a). We then generated flies co-expressing either AS69 or GFP (as a control) with A53T α-synuclein in neurons. Flies expressing AS69 and A53T α-synuclein showed preserved climbing behaviour (Figure 2.3 b, two-way ANOVA), demonstrating that neuronal expression of AS69 reduces the phenotype in this fly model of A53T α-synuclein toxicity. We further went on to determine whether or not the observed effect of AS69 on climbing behaviour could result from a reduction in the number of α-synuclein aggregates and used flies expressing in all neurons one copy of A53T-α-synuclein fused to VC, one copy of A53T-α-synuclein fused VN [252], and in addition AS69 or "always early RNAi" (see Methods section) as a control. Aggregates of α-synuclein were quantified by a filter trap assay in which urea treated lysates of fly heads were passed through a membrane and the quantity of α-synuclein aggregates retained in the membrane was detected by antibodies raised against α-synuclein (illustrated in Figure 2.3 c). We found that the quantity of aggregates retained in the filter was significantly smaller in lysates from flies coexpressing AS69 and A53T-α-synuclein than in lysates from flies only expressing VN- and VC-tagged A53T-α-synuclein (Figure 2.3 d and e). These findings confirm that AS69 reduces high molecular weight aggregates of α-synuclein in neuronal cells of *Drosophila melanogaster*.

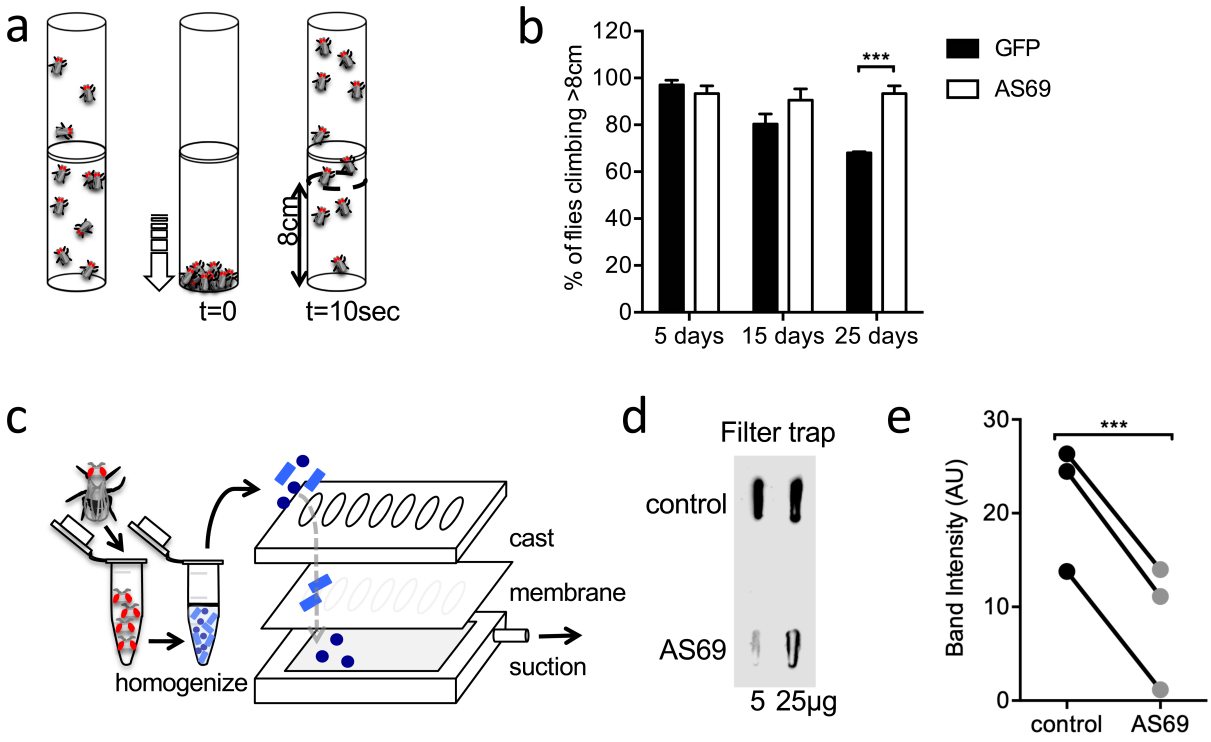

Figure 2.3: AS69 rescues the motor phenotype and reduces α-synuclein aggregation in *Drosophila melanogaster* **(a)** Schematic representation of the climbing assay. The vials are tapped to move the flies to the base of the vial, and thereafter the flies climb towards the top of the vial; in this experiment the number of flies climbing 8 cm in 10 s was determined. **(b)** Performance in the climbing assay of Drosophila melanogaster expressing A53T-α-synuclein and either AS69 or GFP in neurons. At each time point, n = 30 flies were assayed per genotype; similar findings were observed for 8 different lines expressing AS69. Results were compared by two-way ANOVA and Sidak's posthoc test. **(c)** Schematic representation of the filter trap assay in which aggregates in the protein lysate are retained by a membrane, which is subsequently developed in the same manner as an immunoblot. **(d)** Results of the filter trap assay from lysates of control flies and flies expressing AS69 in addition to A53T-α-synuclein in all neurons. Two different quantities of the protein lysate were applied in each case, 5 and 25 µg. **(e)** Summary of the quantification of n=3 dot blots as in **(d)**. Only the 25 µg band was quantified. Results were compared by t-test.

2.5.3 AS69 stoichiometrically inhibits the elongation of α-synuclein fibrils

We next set out to elucidate the origin of the remarkable ability of AS69 to inhibit α-synuclein aggregate formation in cells and *in vivo* (Figure 2.2, Figure 2.3) and amyloid fibril formation *in vitro* [229]. To this end, we performed a detailed mechanistic analysis, where we examined the effect of AS69 on the growth [211], autocatalytic amplification [153, 211] and lipid-induced formation [174] of α-synuclein amyloid fibrils. We first carried out experiments in the presence of micromolar concentrations (in monomer equivalents) of pre-formed seed fibrils of α-synuclein at neutral pH under quiescent conditions (Figure 2.4 a,b). We have shown previously that under these conditions only fibril elongation through the addition of monomeric α-synuclein to fibril ends occurs at detectable rates [211] and that the rate of *de novo* formation of fibrils is negligible. We therefore examined the effects of AS69 on fibril elongation and analyzed these data by fitting

linear functions to the early stages of the aggregation time courses (see subsection 2.9.1 for details of the analysis). The results indicate that fibril elongation is indeed inhibited by AS69 in a stoichiometric concentration-dependent manner (Figure 2.4 c). In this experiment, both the seed fibrils and the AS69 compete for the monomeric α-synuclein and the relative affinities determine the kinetics and thermodynamics of the system.

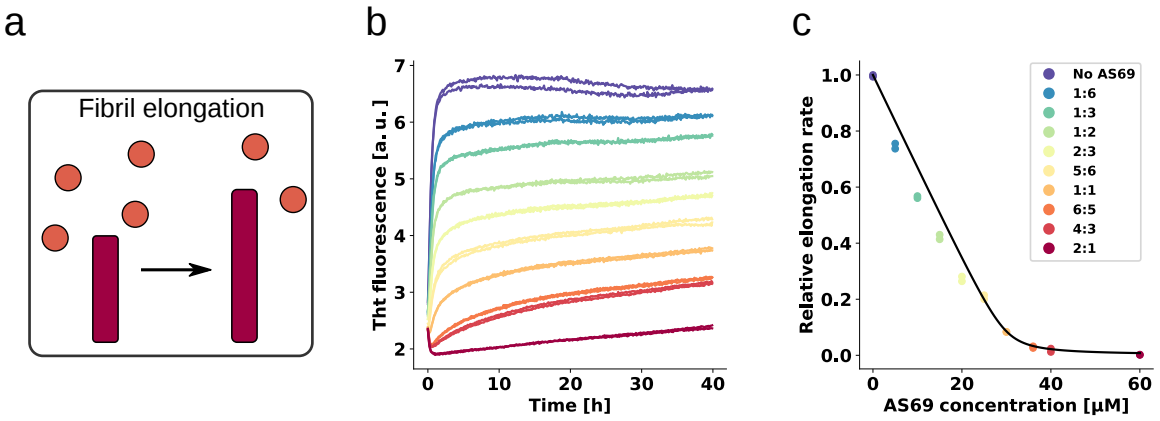

Figure 2.4: AS69 inhibits α- synuclein fibril elongation. **(a)** Schematic representations of fibril elongation. **(b)** Change in ThT fluorescence when a 30 µM solution of monomeric α-synuclein was incubated in the presence of 5 µM pre-formed fibrils under quiescent conditions with increasing concentrations of AS69. **(c)** Relative rates of fibril elongation with increasing concentrations of AS69. The solid line corresponds to a prediction based on the affinity of AS69 for monomeric α-synuclein (240 nM, Figure 2.1 b [229], see subsection 2.9.1 for details).

In order to obtain an estimate of the affinity of monomeric α-synuclein for the ends of fibrils, we performed elongation experiments at low monomer concentrations in the absence of AS69. We found evidence that the fibrils are able to elongate in the presence of 0.5 µM monomeric α-synuclein (see subsection 2.9.1), providing an upper bound of the critical concentration (which is formally equivalent to a dissociation constant, see subsection 2.9.1). Despite the similar affinity of monomeric α-synuclein for both fibril ends and AS69, the time scales of the two types of interactions are very different; monomeric α-synuclein was found to interact on a timescale of seconds with AS69, as seen by isothermal titration calorimetry (ITC) experiments ([229] and Figure 2.1 b and c), but to incorporate on a timescale of minutes to hours into free fibril ends (see Figure 2.4 b and [211, 253]). The slow kinetics of the latter process is partly due to the fact that the number of fibril ends is much smaller than the number of monomers [211], such that each fibril sequentially recruits many α-synuclein molecules. Therefore, the equilibrium between AS69 and α-synuclein should be rapidly established and perturbed only very slowly by the presence of the fibrils.

2.5.4 The inhibition of fibril elongation is due to monomer sequestration

The initial fibril elongation rate as a function of AS69 concentration was found to follow closely the predicted concentration of unbound α-synuclein across the entire range of concentrations of AS69 used in this study, as shown in Figure 2.4 c, where the solid line corresponds to the predicted elongation rate, assuming fibrils can only be elongated by unbound α-synuclein. The inhibition of fibril elongation can therefore be explained quantitatively by the sequestration

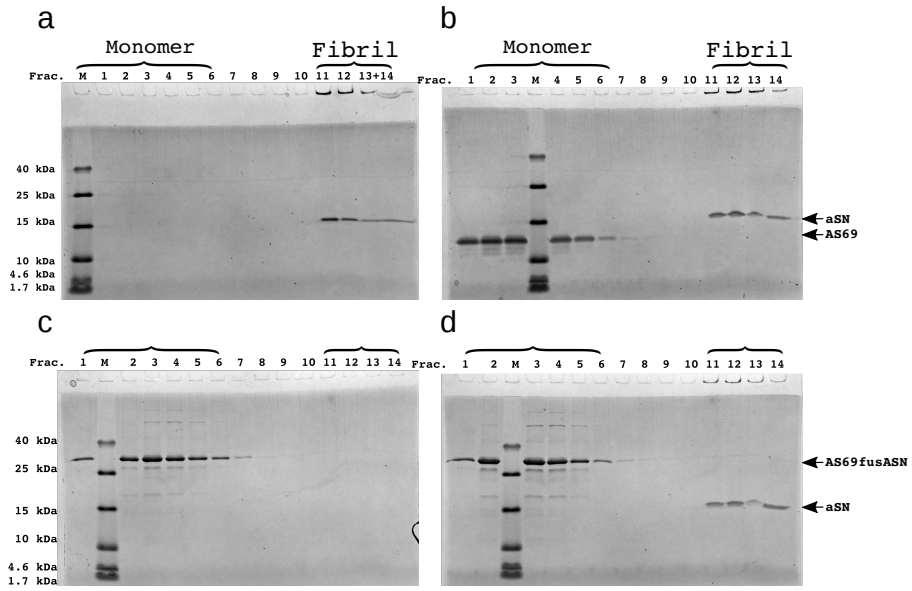

Figure 2.5: SDS-PAGE of Density Gradient Centrifugation (DGC) experiments to probe the binding of AS69 to α-synulein fibrils at pH 7.4 after elongation experiments. (a) 25 µM seeds, **(b)** 25 µM AS69 and 25 µM seeds **(c)** 16.7 µM AS69fusASN, **(d)** 25 µM AS69fusASN and 25 µM seeds.

of monomeric α-synuclein by AS69 and the assumption that the AS69:α-synuclein complex cannot be incorporated into the growing fibril. This conclusion is supported by the finding that the fibrils formed in the presence of increasing concentrations of AS69 are morphologically indistinguishable from the fibrils formed in the absence of AS69 (as judged from AFM images, see Figure 2.15). Our kinetic analysis of fibril elongation in the presence of AS69 does not, however, suggest a preferential interaction with fibril ends, as such an interaction can be expected to lead to a sub-stoichiometric inhibition of fibril elongation, which is not observed in our experiments. Indeed, the finding that the effect on elongation can be quantitatively described by considering only the interaction of AS69 with monomeric α-synuclein (subsection 2.9.1) suggests a weak, if any, interaction of AS69 with fibrils. Furthermore, density gradient centrifugation (DGC) of samples containing only seeds and AS69 (Figure 2.5 a and b) did not show AS69 to co-migrate with large species to any significant extent under conditions that favour elongation. In agreement with inhibition of fibril elongation by monomer sequestration, ZAβ_3W, a binding protein for amyloid-βpeptide [254] that is a significantly weaker α-synuclein binder than AS69, correspondingly showed a considerably weaker inhibitory effect on α-synuclein fibril elongation (Figure 2.14).

2.5.5 AS69 sub-stoichiometrically inhibits the amplification of α-synuclein fibrils

These findings clearly demonstrate that AS69 inhibits fibril elongation in a stoichiometric manner through monomer sequestration. Consequently, inhibition of fibril elongation cannot explain the previously observed substoichiometric inhibition of α-synuclein fibril formation by AS69 [229]. We therefore performed seeded experiments under mildly acidic solution conditions in the presence of very low concentrations of pre-formed fibrils (nM monomer equivalents)

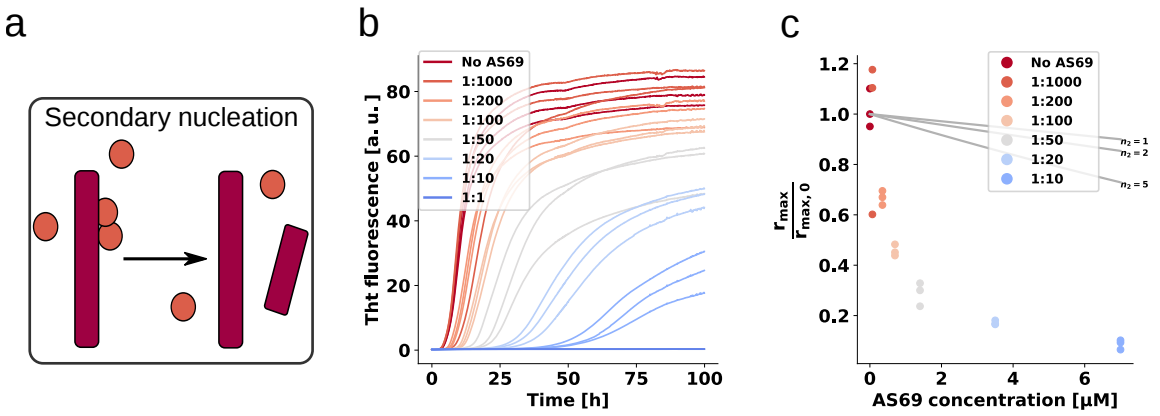

Figure 2.6: AS69 inhibits α-synuclein fibril amplification. **(a)** Schematic representation of fibril amplification through secondary nucleation [211]. **(b)** Change in ThT fluorescence intensity when a 70 μM solution of monomeric α-synuclein was incubated with increasing concentrations of AS69 in acetate buffer (pH 5.0) under quiescent conditions and weak seeding. **(c)** Relative rate of fibril amplification as a function of the concentration of AS69. The solid lines correspond to simulations based on the assumption that AS69 acts only through monomer sequestration, for different values of the monomer dependence (reaction order) of secondary nucleation (see subsection 2.9.2 for details)

under quiescent conditions (Figure 2.6 a,b) [78, 211]. Under those solution conditions, seeded aggregation has been shown to consist of two processes in addition to fibril elongation, namely secondary nucleation, which increases the number of growth competent fibril ends, and higher order assembly (”flocculation“, Figure 2.16 b,c), which decreases the overall aggregation rate by reducing the number of accessible fibrils through their burial within higher order aggregates [211]. The *de novo* formation of amyloid fibrils through primary nucleation is suppressed if the solution is not agitated and if non-binding surfaces are used Figure 2.16 a). We find that under these solution conditions, where only growth and secondary nucleation contribute to the increase in fibril mass and number, respectively, the seeded aggregation is inhibited in a strongly sub-stoichiometric manner (Figure 2.6 b,c). We analysed these data to determine the maximum rate of aggregation (see subsection 2.9.2 for details) using the framework from [72] (Figure 2.6 c). Based on recent results on the concentration-dependence of autocatalytic secondary nucleation of α-synuclein amyloid fibrils [78], we have calculated the predicted inhibitory effect due to monomer sequestration by AS69 in Figure 2.6 c) Figure 2.17 and subsection 2.9.2 for details). We find that, unlike the case of fibril elongation, monomer sequestration cannot explain the extent of inhibition, even by assuming a very high reaction order of 5 (*i.e* a dependence of the rate of secondary nucleation on the 5th power of the free monomer concentration; $\frac{dP(t)}{dt} \propto m(t)^5$) which is not compatible with recent results, showing that secondary nucleation of α-synuclein amylid fibrils depends only weakly on the concentration of free monomer [78]. However, even in this unlikely scenario, the very strong inhibitory effect of low AS69 concentrations cannot be explained by monomer depletion.

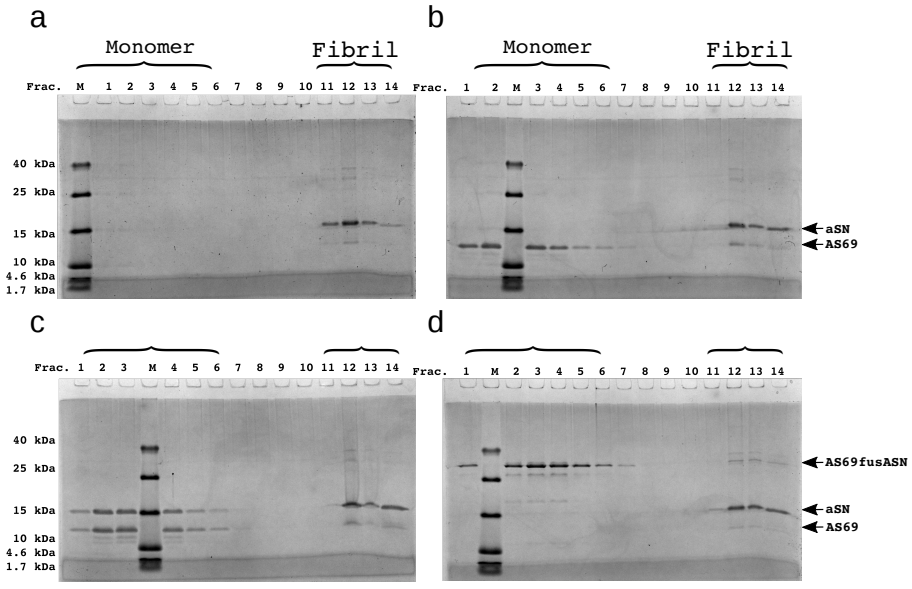

Figure 2.7: SDS-PAGE of Density gradient centrifugation of binding to fibril at pH 5.0. **(a)** 12.5 µM, **(b)** 12.5 µM AS69 and 12.5 µM seeds, **(c)** 12.5 µM AS69, 12.5 µM seeds, and 12.5 µM monomer, and **(d)** 12.5 µM AS69fusASN and 12.5 µM seeds.

2.5.6 The sub-stoichiometric inhibition of fibril amplification is not due to interaction with the fibril surface

We have previously been able to rationalise the inhibition of the secondary nucleation of α-synuclein by the homologous protein β-synuclein through a competition for binding sites on the surface of the fibrils [255]. Here we find that AS69 is a significantly more efficient inhibitor of the autocatalytic amplification of α-synuclein amyloid fibrils than β-synuclein (a similar degree of inhibition is achieved with a ten fold lower concentration ratio). This result is particularly interesting in the light of the fact that AS69 binds efficiently to monomeric α-synuclein under both neutral and mildly acidic solution conditions (Figure 2.1 b,c), whereas we found no evidence for a relevant direct interaction between the monomeric forms of α- and β-synuclein, given the complete absence of any inhibitory effect of β-synuclein on the elongation of α-synuclein fibrils [255]. Therefore, despite the fact that the vast majority of the AS69 is bound within a complex with monomeric α-synuclein, AS69 is an efficient sub-stoichiometric inhibitor of the secondary nucleation of α-synuclein. This finding suggests that in addition to inhibiting through competition for nucleation sites on the fibril surface, AS69 or its complex with α-synuclein could interact directly with intermediates of the secondary nucleation process. To investigate whether AS69 binds to the fibril surface under these secondary nucleation-inducing solution conditions, we performed additional DGC experiments. Co-migration in the density gradient of AS69 with fibrils, which would imply direct interactions between these species, was undetectable (Figure 2.7 a-c). If AS69 were able to inhibit secondary nucleation through binding to the fibril surface in the presence of a large excess of monomer, its affinity to fibril surfaces would need to be much higher than to monomeric α-synuclein. This implies that under the conditions of the DGC experiments which were performed in the absence of monomeric α-synuclein, all binding sites on the fibrils should be occupied. Therefore, the absence of detectable binding implies

either a weak affinity for fibrils or a very low stoichiometry, i.e. a very low density of binding sites for AS69 on the fibril surface.

2.5.7 AS69 binds to stable α-synuclein oligomers with comparable affinity as to monomers

We next tested whether binding of AS69 to oligomeric states of α-synuclein could explain the efficient inhibition of secondary nucleation. The heterogeneous and often transient nature of oligomeric intermediates on the pathway to the formation of amyloid fibrils makes any interaction between such species and AS69 difficult to probe. However, monomeric α-synuclein can be converted into kinetically stable oligomers that can be studied in isolation, because they do not readily convert into amyloid fibrils [201]. Despite the fact that these species are not likely to be fibril precursors, they are intermediate in size and structure between monomeric and fibrillar α-synuclein and hence can serve as a model for AS69 binding to α-synuclein oligomers. Using microscale thermophoresis (MST [203]) at neutral pH, we were able to confirm the binding of AS69 to both monomeric (Figure 2.18 a) and oligomeric α-synuclein (Figure 2.18 b) and provide estimates of the respective binding affinities (ca. 300 nM for monomeric and ca. 30 nM for oligomeric α-synuclein). The former value is in good agreement with results from ITC experiments under the same solution conditions (Figure 2.1 b and [229]), whereas the affinity of AS69 to oligomeric α-synuclein has not previously been determined. The finding that AS69 is able to inhibit secondary nucleation in a highly sub-stoichiometric manner in the presence of a large excess of free monomer, to which it binds with high affinity, necessitates that the interactions of AS69 with aggregation intermediates must be of significantly higher affinity, if they are to explain the inhibition. Otherwise the monomer would out-compete the aggregation intermediate for AS69 binding, due to the much lower concentration of the latter. An estimate (see subsection 2.9.2 for details) suggests that the affinity of AS69 for aggregation intermediates would need to be several orders of magnitude higher than to α-synuclein monomer in order to explain an inhibitory effect of the observed magnitude. This required affinity is indeed much higher than the affinity we have determined here for an oligomeric state of α-synuclein.

2.5.8 The covalent complex of AS69 and α-synuclein efficiently inhibits secondary nucleation

The analysis described in the previous section suggests, therefore, that the α-synuclein:AS69 complex itself could be the inhibitory species. The population of this complex is sufficiently high, even at low ratios of AS69:α-synuclein, to interact with a considerable fraction of aggregation intermediates. It is possible, therefore, that while the AS69:α-synuclein complex is unable to incorporate into a fibril end (see section above on the stoichiometric inhibition of fibril elongation), it can interact with oligomeric fibril precursors and block their conversion into fibrils.
We tested this hypothesis by producing a molecular construct whereby α-synuclein and AS69 are linked together with a flexible glycine tether that allows the formation of an intramolecular complex (AS69fusASN). The formation of the intramolecular complex was verified by performing CD spectroscopy at 222 nm over the temperature range from 10–90 °C and fitting the data to a two-state model [256] (see Figure 2.20). Both at neutral and mildly acidic pH, the fusion construct AS69fusASN has a higher thermal stability than the free AS69 and, indeed, as the stoichiometric mixture of AS69 and α-synuclein (Table 2.1). The difference in melting temperatures between the covalent and non-covalent complex can be explained by the differences

Table 2.1: The melting temperatures , T_m, obtained from fitting of CD melting curves in Figure 2.20 *Data from [257] was refitted to obtain the numerical values listed in the table.

Construct	T_M [°C] at pH 7.4	T_M [°C] at pH 5
AS69	37.5(±1.6)*	36.5(±1.8)
AS69 + α-synuclein	51.0(±0.6)*	55.8(±0.2)
AS69fusASN	66.5(±0.3)	66.1 (±0.2)

in the entropy of binding, which is more unfavourable in the case of the non-covalent complex, given the loss of three degrees of freedom of translational motion upon binding.

We performed weakly seeded aggregation experiments under conditions where secondary nucleation leads to the amplification of the added seed fibrils (see above) at different concentrations of AS69 (Figure 2.8 a) as well as AS69-α-syn complex (Figure 2.8 b). We found that the pre-formed complex is a similarly efficient inhibitor as the free AS69 under secondary nucleation conditions (Figure 2.8 e). These results provide strong support of our hypothesis that the AS69-α-synuclein complex, covalent or non-covalent, is the species that is responsible for the sub-stoichiometric inhibition of secondary nucleation. Therefore, we propose a model whereby rather than requiring the binding of free AS69 to an aggregation intermediate, the AS69:α-synuclein complex is able to incorporate into a fibril precursor and efficiently prevent it from undergoing the structural rearrangement required to transform into a growth-competent amyloid fibril.

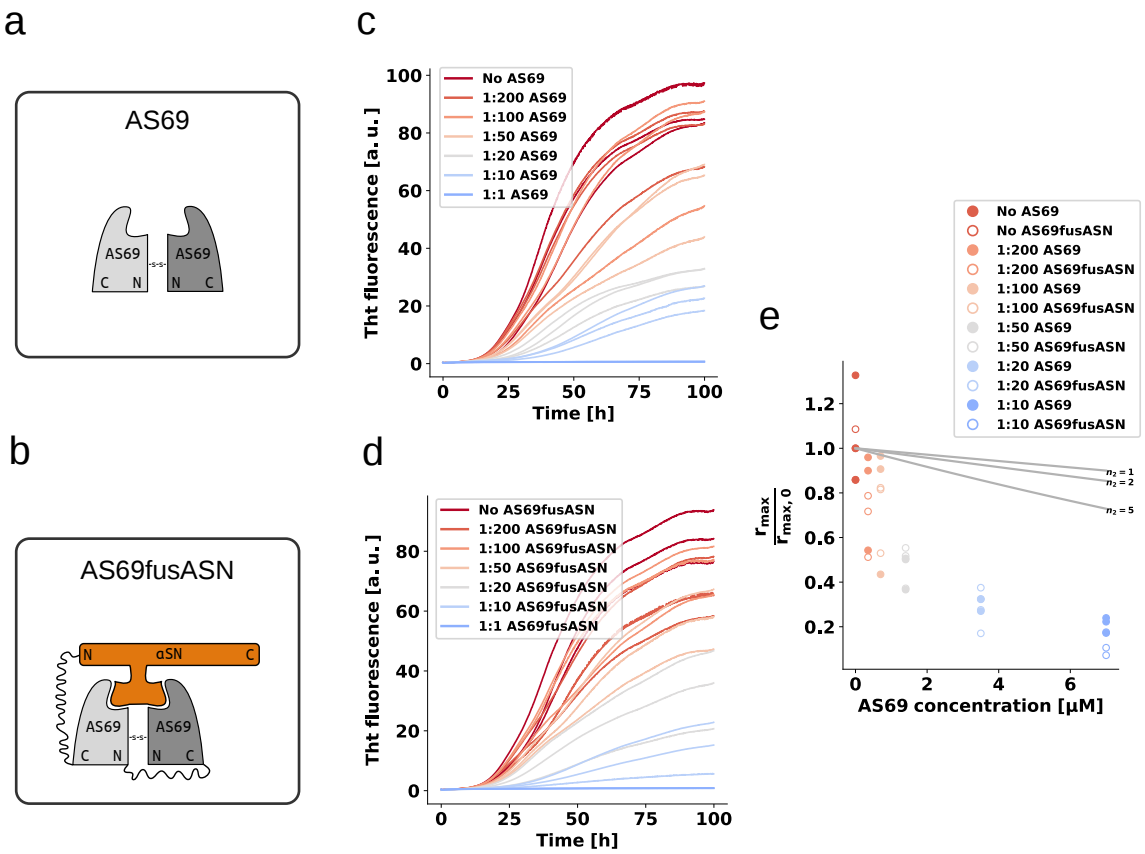

Figure 2.8: AS69 and AS69fusASN inhibit α-synuclein fibril amplification to similar extent. **(a)** and **(b)** Schematic representation of AS69 and AS69fusASN respectively. **(c)**, **(d)** Change in ThT fluorescence when a 70 μM solution of monomeric α-synuclein was incubated with increasing concentrations of AS69 or AS69fusASN respectively in sodium acetate buffer (pH 5.0) under quiescent conditions. **(e)** Relative maximum rate of elongation as a function of the concentration of AS69 (closed circles) and AS69fusASN (open circles). The solid lines correspond to simulations based on the assumption that AS69 acts only through monomer sequestration, for different values of the monomer dependence (reaction order) of secondary nucleation (see subsection 2.9.2 for details

2.5.9 AS69 inhibits the lipid-induced aggregation of α-synuclein

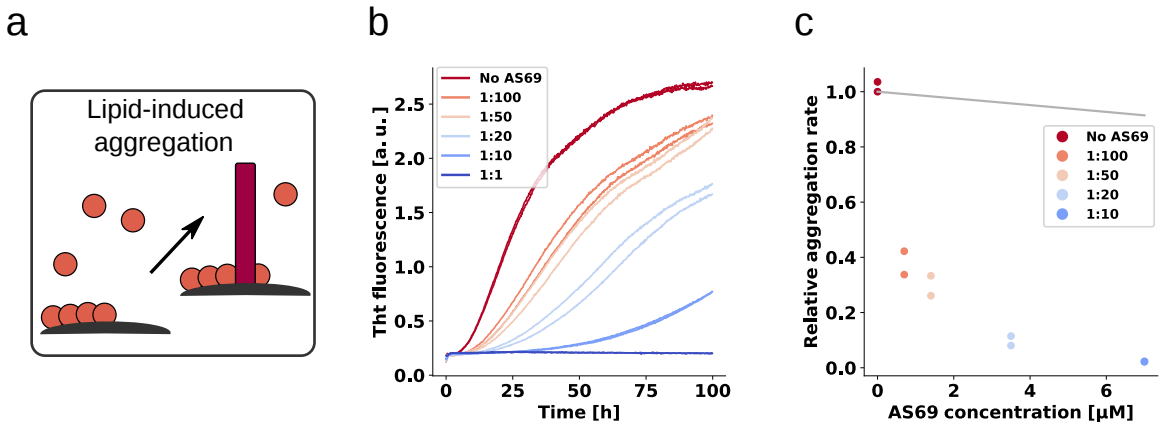

Figure 2.9: AS69 inhibits lipid-induced aggregation of α-synuclein. **(a)** Schematic representation of lipid induced aggregation [174]. **(b)** Change in ThT fluorescence intensity when a 70 μM solution of monomeric α-synuclein was incubated with 100 μM DMPS SUVs and increasing concentrations of AS69 in 20 mM phosphate buffer (pH 6.5) under quiescent conditions. **(c)** Relative rate of lipid-induced formation of α-synuclein amyloid fibrils as a function of the concentration of AS69. The solid line corresponds to a simulation based on the assumption that AS69 acts only through monomer sequestration (see subsection 2.9.3 for details).

Having established and rationalised the high efficiency of AS69 to inhibit autocatalytic amplification of α-synuclein amyloid fibrils through secondary nucleation, we next investigated whether the *de novo* formation of α-synuclein amyloid fibrils is also efficiently inhibited. As experimental setup, we chose a recently developed paradigm of lipid-induced aggregation [174], which allows to analyse the resulting kinetic data in a more quantitative manner compared to the widely employed conditions of strong mechanical agitation and high affinity multiwell plate surfaces. In the latter conditions, the dominant role of the air-water interface [216] as well as of fragmentation have rendered quantitative analysis of the resulting data challenging. In the lipid-induced aggregation, under quiescent conditions and in non-binding plates, the nucleation on the lipid vesicles is the dominant source of new of α-synuclein amyloid fibrils. We therefore probed the inhibitory effect of AS69 on lipid vesicle (DMPS-SUV)-induced aggregation of α-synuclein (Figure 2.9 a,b). We then analysed the early times of the kinetic traces using a single-step nucleation model (Figure 2.9 c) that includes only primary nucleation and fibril elongation (see subsection 2.9.3). The results reveal that AS69 inhibits lipid-induced aggregation at substoichiometric concentrations to α-synuclein in a concentration dependent manner (Figure 2.9 c). In order to characterise the system α-synuclein-AS69-DMPS-SUV in more detail, we performed titration experiments where we varied the concentration of SUVs at constant α-synuclein:AS69 ratios of 10:1 and 1:1. We monitored the formation of α-helical structure, induced by the binding of α-synuclein to the DMPS-SUV by circular dichroism (CD) spectroscopy (Figure 2.22 a-c). We find that the system is well-described as a competition between the AS69 and the lipid vesicles for the monomeric α-synuclein (Figure 2.22 d and see Methods section for details on the mathematical analysis). We simulated the effects that AS69 has on the aggregation process of α-synuclein in the presence of lipids, assuming that the sequestration of free monomer is the only mechanism

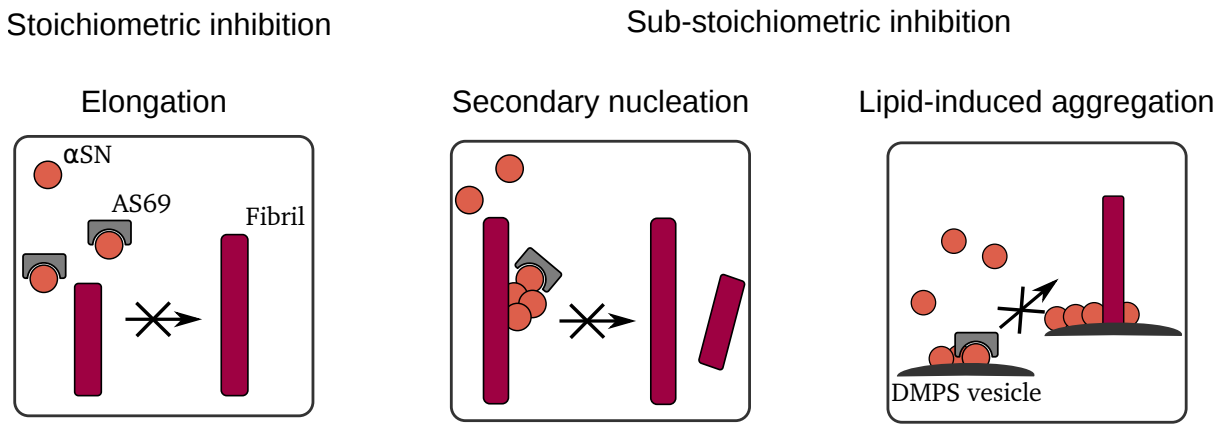

Figure 2.10: summary of mechanisms by which AS69 inhibits amyloid fibril formation of α-synuclein *in vitro*.

through which AS69 inhibits the aggregation reaction (Figure 2.9 c). The results show that the lipid-induced aggregation of α-synuclein is inhibited by AS69 significantly more strongly than predicted by monomer sequestration alone. However, before being able to conclude that AS69 inhibits the lipid-induced aggregation of α-synuclein through a mechanism similar to that defined above for secondary nucleation, it needs to be established whether or not AS69 can directly interact with the lipid vesicles and exert an inhibitory effect through this interaction. We have previously reported that this type of inhibition is displayed by β-synuclein, a homologous protein which directly competes with α-synuclein for binding sites on the lipid vesicles [255]. In order to test for a direct interaction between AS69 and the DMPS-SUV, we performed both isothermal titration and differential scanning calorimetry (ITC and DSC, Figure 2.23). We find that the melting temperature of DMPS vesicles is decreased in the presence of AS69 (Figure 2.23 a,b) and furthermore, titration of AS69 into DMPS-SUV reveals a complex signature of heat release and consumption (Figure 2.23 c,d). While a detailed analysis of this interaction behaviour is beyond the scope of the present study, taken together these calorimetric experiments suggest indeed a direct interaction between AS69 and DMPS-SUV. Therefore, despite the fact that AS69 appears to be a more potent inhibitor of lipid-induced aggregation than β-synuclein, with similar inhibitory effects for very different ratios of inhibitor to α-synuclein of 5:1 (β-synuclein) and 1:10 (AS69), it cannot be excluded that the same mechanism of inhibition contributes significantly to the overall inhibitory effect in lipid-induced aggregation.

2.6. Discussion

The β-wrapin AS69 is a small engineered monomer binding protein that upon coupled folding-binding induces a local β-hairpin conformation in the region comprising amino acid residues 37-54 of otherwise intrinsically disordered monomeric α-synuclein (Figure 2.1). AS69 shows strongly substoichiometric inhibition of α-synuclein aggregation *in vitro*, which is remarkable for a monomer binding-protein [229]. Here, we show that potent aggregation inhibition of AS69 can be recapitulated in cell culture as well as an animal model. In cell culture, AS69 interfered with the interaction between tagged α-synculein molecules as judged by a fluorescence complementation assay and reduced the formation of visible aggregate particles of GFP-tagged

α-synuclein (Figure 2.2). In fruit flies, co-expression of AS69 led to reduced abundance of large molecular weight aggregates of tagged α-synuclein and rescue of the motor phenotype resulting from neuronal expression of untagged A53T-α-synuclein (Figure 2.3). While the nature of the α-synuclein aggregates formed inside the cells and fly neurons remains elusive, these results show that AS69 is able to interact with different constructs and forms of α-synuclein *in vivo* and hence its inhibition of α-synuclein amyloid fibril formation observed *in vitro* [229] warrants further in depth analysis.

Our detailed biophysical *in vitro* aggregation experiments under well-defined conditions enabled us to reveal several distinct modes of inhibition of α-synuclein amyloid fibril formation by AS69, summarised in Figure 2.10. First, as expected for a monomer-binding species, AS69 inhibits fibril growth in a strictly stoichiometric manner, suggesting that the non-covalent AS69-α-synuclein complex is unable to add onto a fibril end and elongate the fibril. This is consistent with our results from density gradient centrifugation of the lack of a detectable interaction between AS69 and fibrils. Second, AS69 is found to be a very efficient inhibitor of secondary nucleation at highly sub-stoichiometric ratios. The overall result of our experimental and theoretical analysis is that this inhibitory effect is unlikely to stem from a direct interaction between the AS69 and either fibril surfaces or secondary nucleation intermediates. Such an interaction would need to be of an unrealistically higher affinity than the interaction between AS69 and α-synuclein monomer. A possible solution to this conundrum is presented by the hypothesis that the AS69-α-synuclein complex is the inhibitory species. This hypothesis gains strong support from our finding that a covalently linked complex is an equally efficient inhibitor of secondary nucleation as the free AS69 molecule. It is important to note here that this proposed mode of action is very distinct from other types of inhibitory behavior reported previously. For example in the case of nanobodies raised against monomeric α-synuclein, at least stoichiometric amounts of the nanobodies are needed in order to interfere significantly with unseeded aggregation [258]. In the case of molecular chaperones, on the other hand, sub-stoichiometric inhibitory behaviour has been reported previously [259, 260], but it is usually found that these molecules do not interact significantly with the monomer, but rather bind specifically to aggregated states of the protein. Therefore, the AS69 affibody represents a new paradigm in the inhibition of amyloid fibril formation: strongly sub-stoichiometric inhibition by a tight monomer-binding species. In this scenario, not the inhibitor itself plays the role of a molecular chaperone, *i.e.* interaction with an on-pathway species and interfering with its further evolution, but rather the monomer-inhibitor complex acts as a chaperone. This mode of action represents a range of significant advantages over the other previously described modes of action (*i.e.* monomer sequestration and direct interaction with aggregation intermediates). First, it is rather straightforward to develop further molecules that bind to the monomeric forms of proteins, given that the latter are well-defined, reproducible and easy to handle. This simplicity is in contrast to the difficulty presented by targeting on-pathway aggregation intermediates which are difficult to isolate for the development of inhibitors. Second, binders of oligomeric aggregation intermediates can be expected to be less specific compared to binders of a well-defined monomeric state, as suggested by the existence of antibodies that interact with protofibrillar species independently of the protein from which they have formed [261]. This lack of specificity can potentially lead to cross-reactivity and side effects. And third, the mode of inhibition presented here avoids the need for stoichiometric amounts of inhibitors that are usually required in the case of monomer sequestering species, resulting in a more efficient inhibition. Interestingly, we find that AS69 is a similarly potent inhibitor also in a lipid-induced aggregation paradigm, whereby heterogeneous primary, rather than secondary nucleation is the dominant source of new aggregates. However, we found that the inhibitory effect in this case to possibly also stem from a direct interaction between AS69 and

the lipid vesicles. It is therefore not straightforward to decide whether the dominant mechanism of inhibition by AS69 in heterogeneous primary and secondary nucleation is closely related.
An inhibitor functioning according to this dual mode, i.e. being active both as free molecule and as a complex with monomeric α-synuclein, is expected to efficiently reduce α-synuclein aggregation *in vivo*. This is in agreement with the cell culture and fly data we present in this manuscript. Further steps will be to test the effects of AS69 in cell-based fibril seeding assays, in mammalian dopaminergic neurons, and in PD models where synuclein aggregates are formed from endogenous α-synuclein.
In conclusion, high affinity monomer binders displaying strong sub-stoichiometric inhibition of fibril formation represent attractive agents to interfere with pathological protein aggregation, due to their multiple inhibitory action.

2.7. Methods and Materials

2.7.1 Reagents

Thioflavin T UltraPure Grade (ThT > 95%) was purchased from Eurogentec Ltd (Belgium). Sodium phosphate monobasic (NaH_2PO_4, BioPerformance Certified > 99.0%), sodium phosphate dibasic (Na_2HPO_4, ReagentPlus, > 99.0%) and sodium azide (NaN_3), ReagentPlus, > 99.5%) were purchased from Sigma Aldrich, UK. 1,2-Dimyristoyl-sn-glycero-3-phospho-L-serine, sodium salt (DMPS) was purchased from Avanti Polar Lipids, Inc, USA.

2.7.2 Protein preparation

α-synuclein was expressed and purified as described previously [211, 215]. To determine the concentrations in solution we used the absorbance value of the protein measured at 275 nm and an extinction coefficient of 5600 $M^{-1}\,cm^{-1}$. The protein solutions were divided into aliquots, flash frozen in liquid N_2 and stored at −80 °C, until used. A pET302/NT-His plasmid carrying AS69 with a N-terminal hexahistag (on each monomer) was expressed and purified as previously described [229] in *E. coli* JM109(DE3) with small modifications. Briefly, 20 µl cell culture from a glycerol stock was used to inoculate 50 ml 2YT (PanReac AppliChem) with 100 $\mu g\,ml^{-1}$ ampicillin overnight culture, from which 5 ml was added per 500 ml 2YT medium with 100 $\mu g\,ml^{-1}$ ampicillin. Expression was induced when OD_{600} reached 0.6, using IPTG to a final concentration of 1 mM, after which the cells were grown for an additional 4 h; the temperature of growth and expression was 37 °C and shaking was 100 RPM. Cells were harvested by centrifugation at 5000 g for 20 min at 4 °C after which the cell pellets were resuspended in 50 mM Tris:Cl pH 8, 500 mM NaCl, 20 mM imidazole, and one protease inhibitor cocktail tablet (Roche) before being placed at −20 °C. Cells were thawn and lysed using a probe sonicator (Bandelin, Sonopuls UW 3200, Berlin, Germany) with a MS72 sonotrode with pulses of 3 s with pauses of 5 s in between for a total of 5 min using 35 % maximum power. Cell debris was removed by centrifugation at 13 500 g for 20 min, before the supernatant was loaded on a 5 ml Histrap FF (GE Healtcare). A 50 mM imidazole containing buffer (as opposed to 20 mM see above) was loaded to remove unspecifically bound material before elution was performed using 250 mM imidazole. The eluate was placed on ice overnight before it was concentrated to a volume < 2.5 ml and then loaded onto a Hiload 16/600 Superdex 75 pg column, that had been equilibrated in 20 mM NaPi, pH 7.4, 50 mM NaCl, for collection of the dimer peak. Protein concentration was measured at 275 nm with an extinction coefficient of 2800 $M^{-1}\,cm^{-1}$, protein solutions were aliquoted, flash frozen in in liquid N_2 and stored at −80 °C. AS69fusASN with a C-terminal hexahistag was expressed

from a pET302/CT-His plasmid and purified identically to AS69 with the only exception that an anion exchange chromatography step was included (identical to the one used for α-synuclein). Protein concentration was measured at 275 nm with an extinction coefficient of 8400 $M^{-1}\,cm^{-1}$, protein solutions were aliquoted, flash frozen in in liquid N_2 and stored at −80 °C.

2.7.3 Seed fibril formation

Seed fibrils were produced under different solution conditions, depending for which type of experiments they were needed (see section on ThT experiments below).

Elongation assays: Seed fibrils were produced as described previously [211]. 500 µl samples of α-synuclein at concentrations from 500–800 µM were incubated in 20 mM phosphate buffer (pH 6.5) for 48–72 h at ca. 40 °C and stirred at 1500 RPM with a Teflon bar on an RCT Basic Heat Plate (IKA, Staufen, Germany). Fibrils were diluted to a monomer equivalent concentration of 200 µM, divided into aliquots, flash frozen in liquid N_2 and stored at −80 °C. For experiments at pH 6.5 and 5 µM fibril concentrations the 200 µM fibril stock was sonicated between 30–60 s using a probe sonicator (Bandelin, Sonopuls HD 2070, Berlin, Germany), using 10 % maximum power and a 50 % cycle.

Secondary nucleation assays: Seed fibrils were produced in 10 mM acetate buffer at pH 5.0. 1.2 ml sample of α-synuclein at a concentration of 25 µM was prepared and aliquoted into 12 wells of a 96-well Half Area Black Flat Bottom Polystyrene NBS Microplate, Corning, where a single glass bead of 2.85–3.45 mm diameter (Carl Roth) had been added. Plate was incubated at 37 °C for 48–72 h at 500 RPM. Sonication was performed using a probe sonicator (Bandelin, Sonopuls UW 3200, Berlin, Germany) with a MS72 sonotrode 5 times for 1 s using 10 % maximum power.

2.7.4 Lipid vesicle preparation

DMPS lipid powder was dissolved in 20 mM phosphate buffer (NaH_2PO_4/ Na_2HPO_4), pH 6.5, 0.01 % NaN_3 and stirred at 45 °C for at least 2 h. The solutions were then frozen and thawed five times using dry ice and a water bath at 45 °C . Lipid vesicles were prepared by sonication (Bandelin, Sonopuls HD 2070, 3 x 5 min, 50 % cycle, 10 % maximum power) and centrifuged at 15 000 RPM for 30 min at 25 °C. The average size of the vesicles was verified by dynamic light scattering (Zetasizer Nano ZSP, Malvern Instruments, Malvern, UK) to ensure a distribution centred at a diameter of 20 nm

2.7.5 Circular dichroism (CD) measurements and data analysis of α-synuclein - lipid interactions in the presence of AS69

Samples were prepared as described before [174] by incubating 20 µM α-synuclein with 2 or 20 µM AS69 and DMPS concentrations ranging from 0–1.2 mM in 20 mM phosphate buffer, pH 6.5, 0.01 % NaN_3. Far-UV CD spectra were recorded on a JASCO J-810 instrument (Tokyo, Japan) equipped with a Peltier thermally controlled cuvette holder at 30 °C. Quartz cuvettes with path lengths of 1 mm were used, and the CD signal was measured at 222 nm by averaging 60 individual measurements with a bandwidth of 1 nm, a data pitch of 0.2 nm, a scanning speed of 50 $nm\,min^{-1}$ and a response time of 1 s. The signal of the buffer containing DMPS and different concentrations of AS69 was subtracted from that of the protein. The data were then analysed as described previously [174, 255]. First the fraction of protein bound to DMPS for

the different [α-synuclein], [DMPS] and [AS69] used in our study was determined using the following equation:

$$x_b = \frac{CD_{mes} - CD_{free}}{CD_{bound} - CD_{free}} \tag{2.1}$$

where CD_{free} is the signal of α-synuclein measured in the absence of both DMPS and AS69, CD_{bound} is the signal of the α-synuclein measured in the presence of DMPS only under saturating conditions and CD_{mes} is the signal of the α-synuclein measured at a given [DMPS] and [AS69]. The values of x_b obtained from our CD measurements were then compared to those estimated from a competitive binding model where both AS69 and DMPS compete for the binding to α-synuclein molecules using the binding constants of the systems AS69:α-synuclein and DMPS:α-synuclein, determined from previous studies [174, 229]. We considered the following two equilibria:

$$\alpha\text{+ (DMPS)}_L \rightleftharpoons \alpha(DMPS)_L$$
$$\alpha\text{+ AS69} \rightleftharpoons \alpha\text{AS69}$$

that are described by the following equations:

$$K_{D,\alpha-DMPS} = \frac{[\text{DMPS}_f][\alpha_f]}{L_\alpha[\alpha_b]} \tag{2.2}$$

$$K_{D,\alpha-AS69} = \frac{[\alpha_f][\text{AS69}_f]}{[\text{AS69}_b]} \tag{2.3}$$

with

$$[\alpha] = [\alpha_f] + [\alpha_b] + [\text{AS69}_b] \tag{2.4}$$

$$[\text{DMPS}] = [\text{DMPS}_f] + L_\alpha[\alpha_b] \tag{2.5}$$

$$[\text{AS69}] = [\text{AS69}_f] + [\text{AS69}_b] \tag{2.6}$$

where $K_{D,\alpha-DMPS}$, $K_{D,\alpha-AS69}$ are the binding constants of the system DMPS:α-synuclein and AS69:α-synuclein, respectively; L_α is the stoichiometry in which DMPS binds to α-synuclein, i.e., the number of DMPS molecules interacting with one molecule of α-synuclein; [α],[α_f], [α_b] are the concentrations of total, free and DMPS-bound α-synuclein; [AS69], [$AS69_f$], [$AS69_b$] are the concentrations of total, free and α-synuclein-bound AS69 and [DMPS] and [$DMPS_f$] are the concentrations of total and free α-synuclein. The change in the fraction of protein bound with increasing concentration of DMPS can be described using the standard solution of the cubic equation:

$$K_{D,\alpha-DMPS} = \frac{([DMPS] - L_\alpha[\alpha_b])([\alpha] - [\alpha_b] - [AS69_b])}{[\alpha_b]L_\alpha} \tag{2.7}$$

$$
\begin{aligned}
[AS69_b] &= \frac{-b-\sqrt{b^2-4ac}}{2a} \\
a &= [\alpha] \\
b &= -[AS69]+[\alpha_b]-[\alpha]-K_{D,\alpha-AS69} \\
c &= -\frac{[\alpha_b]}{[\alpha]}[AS69]+[AS69]
\end{aligned} \tag{2.8}
$$

Its solution is not shown here due to its length. For each data point, the concentrations $[\alpha_b]$, [AS] and [DMPS] are known and the equilibrium constants and stoichiometry for the α-synuclein:DMPS and α-synuclein:AS69 systems were set to the values determined previously [174, 229].

2.7.6 Differential scanning calorimetry (DSC) and isothermal titration calorimetry (ITC) measurements

DSC experiments with lipid vesicles, α-synuclein and AS69 (Figure 2.23 a and b) were performed as described previously [262]. We used a VP-DSC calorimeter (Malvern Instruments, Malvern, UK) at a scan rate of $1\,^{\circ}\mathrm{C\,min^{-1}}$. The lipid concentration was 1 mM and the protein concentrations are indicated in the figure legend.
ITC binding experiments between AS69 and α-synuclein were performed on a Microcal iTC200 calorimeter (GE Healthcare) at 30 °C. The buffer was either 20 mM sodium phosphate, 50 mM NaCl, pH 7.4, or 20 mM sodium acetate, pH 5.0. AS69 was used as titrant in the cell at a concentration of 40 µM, and α-synuclein at approximately 10-fold higher concentration as titrant in the syringe. The heat of post-saturation injections was averaged and subtracted from each injection to correct for heats of dilution and mixing. Data were processed using MicroCal Origin software provided with the calorimeter. Dissociation constants were obtained from a nonlinear least-squares fit to a 1:1 binding model.
ITC binding experiments between SUVs made from DMPS and AS69 (Figure 2.23 c and d) were performed using an ITC200 instrument (Malvern Instruments, Malvern, UK). A solution of 0.47 mM AS69 was titrated into 0.5 mM DMPS in 20 mM phosphate buffer pH 6.5 at 30 °C, corresponding to the conditions under which the lipid-induced aggregation of α-synuclein had been studied. An interaction between AS69 and DMPS vesicles can be clearly detected, and the binding behaviour is complex, with an initially exothermic interaction at low protein to lipid ratios, followed by an endothermic interaction at molar ratios higher than 0.05. Due to the complex binding signature, it is not straightforward to fit the data and extract a binding affinity but it can be estimated that the binding affinity is in the sub-micromolar range, comparable to that of α-synuclein to the same lipid vesicles [174].

2.7.7 Thioflavin-T (ThT) fluorescence assays of amyloid formation kinetics

The ThT experiments were performed under two distinct sets of solution conditions. Firstly, we used phosphate buffer (PB) at pH 6.5, where we have previously shown that highly quantitative kinetic data of amyloid fibril growth can be obtained, and where under strongly seeded and quiescent conditions, all nucleation processes can be neglected [211]. Furthermore, we also employed mildly acidic solution conditions (acetate buffer at pH 5.0), where secondary nucleation is strongly enhanced and can be conveniently studied [78, 211].

In most of the ThT experiments, samples of 100 µl were loaded into a 96-well Half Area Black Flat Bottom Polystyrene NBS Microplate (Corning, product number 3881). 150 µl water was added into the wells directly surrounding the wells containing sample, and the outer most wells were not used for experimental measurements. These measures minimise sample evaporation during prolonged kinetic experiments. The plate was sealed using clear sealing tape (Polyolefin Acrylate, Thermo Scientific) and placed inside a platereader (CLARIOStar or FLUOStar Omega, BMG LABTECH, Germany) that had been equilibrated to 37 °C. Data points were obtained every 120–360 s, depending on the duration of the experiment. In some experiments, the fluorescence was read by averaging 12–20 points, measured in a ring with a diameter of 3 mm (orbital averaging mode). Excitation and emission in the CLARIOStar (monochromator) was 440 nm (15 nm bandwidth) and 485 nm (20 nm nm bandwidth), respectively. Excitation and emission in the FLUOStar Omega (filter) was 448 nm (10 nm bandwidth) and 482 nm (10 nm nm bandwidth) respectively. In addition to the proteins of interest and buffer, all samples contained 0.04 % NaN_3 and 40 or 50 µM Thioflavin-T.

2.7.8 Preparation of fluorescently labelled oligomers

Fluorescently labeled α-synuclein oligomers were prepared as described previously [203, 263]. In brief, we produced fluorescently labelled α-synuclein monomer by expressing and purifying the N122C cystein variant of α-synuclein, which was then labelled through an incubation with a 10 fold excess of Alexa 647 malimide (Thermo Fisher Scientific, Loughborough, UK), followed by removal of the excess dye with a Superdex 200 10/300 Increase gel filtration column (GE Healthcare, Amersham, UK). Wild type and fluorescently labeled N122C variant α-synuclein were combined at a ratio of 30:1, corresponding approximately to the stoichiometry of the oligomers [201], at a total concentration of ca. 200 µM, dialysed against distilled water for 24 h and lyophilised. The dry protein was redissolved in PBS at concentrations between 500–800 µM and incubated at RT over night under quiescent conditions. The oligomers were then separated from the monomeric protein and larger aggregates by using a Superdex 200 10/300 Increase column that had been equilibrated with 20 mM phosphate buffer pH 7.4 and 50 mM NaCl, collecting fractions of 500 µl. The exact concentration of the oligomer fractions are difficult to determine, due to the weak absorption signal. However, based on the absorptions at 275 nm and 647 nm, we estimated the oligomer concentration to be 3–6 µM in monomer equivalents, corresponding to an oligomer number concentration of 100–200 nM, which also corresponds roughly to the concentration of Alexa label.

2.7.9 AFM images

pH 6.5: Atomic force microscopy images were taken with a Nanowizard II atomic force microscope (JPK, Berlin, Germany) using tapping mode in air. Solutions containing fibrils were diluted to a concentration of 1 µM (in monomer equivalents) in water and 10 µl samples of the diluted solution were deposited on freshly cleaved mica and left to dry for at least 30 min. The samples were carefully washed with ∼50 µl of water and then dried again before imaging.

pH 5: Atomic force microscopy images were taken with a Bruker Mulitmode 8 (Billerica, Massachusetts, USA) using ScanAsyst-Air cantilvers (Camarillo,California,USA) using the ScanAsyst PeakForce tapping in air. 15 µlof a 0.7 µM fibril containing solution was deposited on freshly cleaved mica and incubated for 10 min before the sample was carefully rinsed by

applying an removing 100 µl water three times before the sample was dried under a gentle stream of nitrogen.

2.7.10 Density Gradient Centrifugation (DGC)

The DGC experiments were performed as previously described [264]. We performed DGC experiments both under conditions of neutral pH (pH 7.4), where the reaction is elongation dominated and under mildly acidic conditions (pH 5.0) where secondary nucleation strongly contributes to the reaction. We find that under both sets of conditions there is no detectable binding between amyloid fibrils and AS69.

2.7.11 Thermophoresis experiments

The thermophoresis experiments with fluorescently labeled monomeric and oligomeric α-synuclein were performed as described previously [203], using a Monolith instrument (Nanotemper, Munich, Germany) and glass capillaries (Nanotemper, Munich, Germany) with hydrophobic coating (oligomeric α-synuclein) or uncoated (monomeric α-synuclein). A two-fold dilution series of AS69 in 20 mM phosphate buffer pH 7.4 with 50 mM NaCl was prepared and then either 10 µl of 5x diluted oligomers (corresponding to 0.6–1.2 µM) or 1 µM labelled monomer was added to each sample of the dilution series. We performed the binding experiments under this buffer conditions for optimal comparability with previous ITC experiments of AS69 binding to monomeric α-synuclein [229].
MST experiments were performed at 40 % laser power and 75 % LED power (oligomers) or 60 % laser power and 20 % LED power (monomers). For the calculation of the relative change in fluorescence due to thermophoresis, the cursors were set before the temperature jump followed by 5 s after the temperature jump (oligomers) and 45 s after the temperature jump (monomers).

2.7.12 CD melting curves

CD melting curves were obtained as described in [257], with the exceptions that slightly higher concentrations of protein were used, and the samples were heated to 90 °C rather than 80 °C. The CD data was fitted directly using a two-state model in order to obtain the melting temperature, T_m, as described in ([256]):

$$y = \frac{\left(y_f + m_f T\right) + \left(y_u + m_u T\right) \cdot \exp\left(\frac{\Delta H_m}{RT} \cdot \frac{T - T_m}{T_m}\right)}{1 + \exp\left(\frac{\Delta H_m}{RT} \cdot \frac{T - T_m}{T_m}\right)} \tag{2.9}$$

using least-square fitting from the Python packages `scipy.optimize.curve_fit`. y is the CD signal in mdeg, $y_f + m_f T$ and $y_u + m_u T$ describes linear change in CD signal of the folded and unfolded state with respect to temperature respectively, T is the temperature in Kelvin, R is the ideal constant constant, and ΔH_m is the change in enthalpy at T_m.

2.7.13 Cell culture and transfections

HEK293 cells (RRID CVCL0063) were obtained from the Department of Biochemistry, RWTH Aachen University, Aachen, Germany, and were cultured and transfected using Metafectene as previously described [250]. Cell line authentication was performed by Eurofins Forensik, using PCR-single-locus-technology. Cell lines were tested for mycoplasma contamination. HEK293T cells were used because they are the established cell line for our protocol. A53T-α-synuclein

flexibly tagged with EGFP by the interaction of a PDZ domain with its binding motif was previously described [248, 250]. WT and A53T-α-synuclein tagged by the C-terminal and N-terminal half of venus was obtained from Prof. Tiago Outeiro (University of Goettingen, Germany).

2.7.14 Immunoblots

Immunoblots were carried out 24 h after transfection as previously described [250] using NP40 lysis buffer containing protease inhibitors (Pierce, Thermo Fisher Scientific) and the following primary antibodies: rabbit anti-α-synuclein (1:500, No. 2642, Cell Signalling Technology, Danvers, USA), mouse anti-beta-tubulin (1:1000, E7, Developmental Studies Hybridoma Bank, Iowa, USA). Secondary antibodies were anti-mouse IgG (NXA931) and anti-rabbit IgG (NA934V) from GE Healthcare Life Sciences (1:10000). These antibodies produce several nonspecific bands that are also visible in cells not expressing α-synuclein. Among the bands around 20 kDa observed with the α-synuclein antibody, only the upper band is considered specific and was used for quantification (see [250] for details).

2.7.15 Flow cytometry

Cells were grown in 6-well plates and used 24 h after transfection. Adherent cells were washed with phosphate buffer saline (PBS) 3 times and detached with trypsin. Subsequently cells were collected in FACS tubes, centrifuged for 5 min at 2000 RPM and washed again with PBS. Cell pellets were finally resuspended in 200 µl of PBS. Flow cytometry was carried out by a FACSCalibur (BD Biosciences) using forward and sideward scatter to gate cells and a fluorescence threshold of 300 AFU to detect cells with venus (YFP) fluorescence. This threshold was determined from measurements with untransfected cells and cells expressing either the N-terminal or the C-terminal half of venus only.

2.7.16 Microscopy

For classification of EGFP distribution patterns, cells were grown on coverslips and fixed 24 h after transfection. The distribution of EGFP fluorescence was classified manually by a blinded observer into the categories "homogenous distribution", "containing particles" and "unhealthy" (round, condensed cells) using an Olympus IX81 fluorescence microscope (60x oil objective, NA 1.35). At least 100 cells per coverslip were classified. In each experiment, 3 coverslips were evaluated per group and the results averaged.

2.7.17 Drosophila stocks

Flies expressing A53T-α-synuclein in neurons, $w[*];;P\{w[+mC] = GAL4-elav.L\}$, $P\{w[+mC] = UAS-HsapSNCA.A53T\}$ and flies expressing GFP under control of GAL4 $w[*];P(acman)\{w[+] = UAS-GFP\}5$ were previously described [250]. Flies expressing AS69 under control of GAL4, $w[118];;P\{w[+] = UAS-AS69\}$, were generated using standard P-element transformation (BestGene Inc). Expression of A53T-α-synuclein fused to VN and VC in neurons was achieved by genetically crossing and recombining flies carrying GAL4 under the elav promoter and VN and VC tagged A53T-α-synuclein under the UAS promoter. The resulting genotype of these flies is $P\{w[+mW.hs] = GawB\}elav[C155];P[w[+] = UAS-Hsap\ SNCA[A53T]:VC]$, $PBac\{attB[+mC] = UAS-VN:Hsap\ SNCA[A53T]\}/Cyo$. Flies expressing "always early RNAi", w[1118]; P$\{GD4261\}$v13673, were used as control in experiments conducted with the A53T-α-synuclein VN/VC expressing flies. These flies have

been shown to have no effect in genetic screens for modifiers in neurodegenerative disease models. Flies were raised and maintained at 25 °C under a 12 h dark/light cycle.

2.7.18 Climbing assay and fly head immunoblot

Virgins of the stock $w[*];;P\{w[+mC] = GAL4 - elav.L\}$, $P\{w[+mC] = UAS - Hsap\ SNCA.A53T\}$ were either crossed to males $w[118];;P\{w[+] = UAS - AS69\}$, or $w[*];P(acman)]\{w[+] = UAS - GFP\}5$ (control). In the F1-progeny we selected for males with pan neural [A53T]α-synuclein and either AS69 or GFP concomitant expression. Climbing analysis was performed 5, 15 and 25 days post eclosion as previously described [250]. For each time point and per genotype 10 flies were analyzed in 10 tapping experiments with 60 s resting interval and the results averaged. The crosses where repeated n=3 times.
In parallel 10 fly heads from the F1-progeny and also from male w[*]; P(acman)w[+]=UAS-GFP flies were homogenized in 100 µl RIPA buffer using the Speedmil P12 (Analytik Jena AG). The lysates were centrifuged at 12 000 RPM for 10 min and the supernatant collected and used for immunoblot analysis. The following primary antibodies were used: mouse anti-α-synuclein (1:500, syn204, ab3309, Abcam) and mouse anti-syntaxin (1:500, 8C3, Developmental Studies Hybridoma Bank, Iowa, USA. Secondary anibodiy was anti-mouse IgG (NXA931) from GE Healthcare Life Sciences (1:5000).

2.7.19 Fly head filter trap assay

Virgins of the stock $P\{w[+mW.hs] = GawB\}elav[C155]; P[w[+] = UAS - Hsap\ SNCA[A53T] : VC]$, PBac$\{attB[+mC] = UAS - VN : Hsap\ SNCA[A53T]\}/Cyo$ were either crossed to $w[118];;P\{w[+] = UAS - AS69\}$ or $w[1118];P\{GD4261\}v13673$ (control) males. In the F1-progeny we selected for males with pan neural [A53T]α-synuclein and either AS69 or "always early RNAi" concomitant expression. 10 fly heads were homogenized in 100 µl RIPA buffer using the Speedmill P12. The lysates were centrifuged at 12 000 RPM for 10 min at 4 °C and the supernatant collected. For the filter trap assay equal protein amounts of RIPA fly head lysates (30 µg) were adjusted to equal volumes. An equal volume of Urea buffer (8 M) was subsequently added, samples were incubated rolling at 4 °C for 1 h and sonicated in a water bath for 10 min. SDS and DTT were added to a final concentration of 2 % and 50 mM. Using a dot blot filtration unit, the resulting solutions were filtered through a 0.2 µm nitrocellulose membrane (Whatman) previously equilibrated with 0.1 % in TBS and afterwards washed in TBS-T. Membranes were further treated as an immunoblot described previously.

2.8. Acknowledgments

AKB thanks the Leverhulme Trust and the Parkinson's and Movement Disorder Foundation (PMDF) for funding and the Novo Nordisk Foundation for support through a Novo Nordisk Foundation professorship. PF thanks the Böhringer Ingelheim Fonds and the Studienstiftung des Deutschen Volkes for support. CG thanks the Alexander von Humboldt Foundation and the European Commission (H2020-MSCA grant agreement No 706551) for support. This project has received funding from the European Research Council under the European Union's Horizon 2020 research and innovation program, grant agreement No. 726368 (to WH). We thank Nadine Rösener for help with the density gradient centrifugation and Sabine Hamm for excellent technical assistance.

2.9. Supplemental Information

Table 2.2: Raw cell counts of cells from the three independent experiments shown in Figure 2.2 b. The data can be found under the following link: `https://osf.io/qs2yf/`

	Number of BiFC positive cells			Number of BiFC negative cells			Total number of cells			Percentage of BiFC positive cells		
Independent experiment	1	2	3	1	2	3	1	2	3	1	2	3
a-syn wt VNVC/ control	1590	3615	862.5	73410	71385	74137.5	75000	75000	75000	2.12	4.82	1.15
a-syn wt VNVC/ AS69	712.5	2092.5	382.5	74287.5	72907.5	74617.5	75000	75000	75000	0.95	2.79	0.51
a-syn A53T VNVC/ control	2820	4642.5	1230	72180	70357.5	73770	75000	75000	75000	3.76	6.19	1.64
a-syn A53T VNVC/ AS69	802.5	3480	337.5	74197.5	71520	74662.5	75000	75000	75000	1.07	4.64	0.45

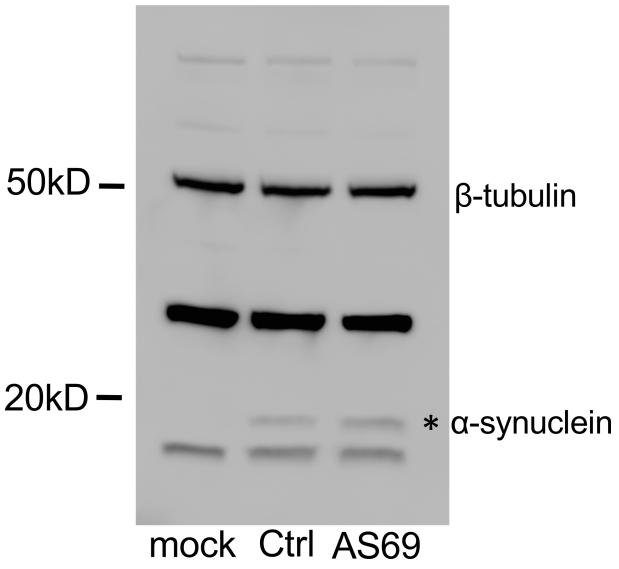

Figure 2.11: Complete Western blot Figure 2.2 c) from cell culture lysates showing the loading control with β-tubulin at 50 kD, two nonspecific bands visible also in mock transfected cells,i.e. without α-synuclein expression, and one specific band just below 20 kD (*).

2.9.1 Analysis of strongly seeded aggregation data at neutral pH

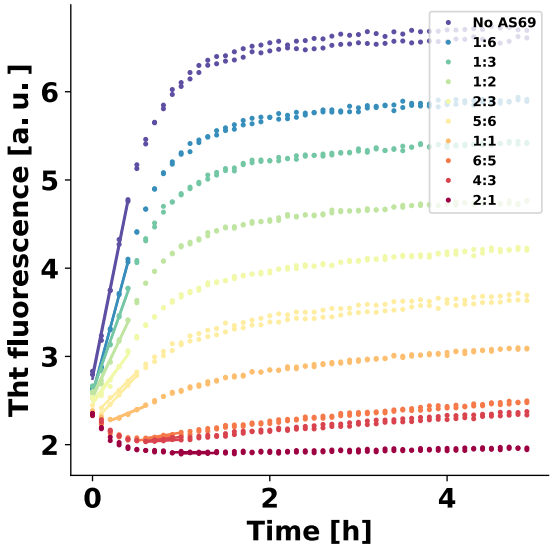

Figure 2.12: Linear fitting of the early times of strongly seeded aggregation kinetics. Solid lines show the fits. These data were used to produce the plot in Figure 2.4 c. At the highest inhibitor concentrations, the rates were so low that the temperature increase upon introduction of the plate into the platereader led to an initial decrease in fluorescence intensity. Therefore, the data was fitted once the fluorescence intensity had started to increase.

In the case of aggregation experiments at high concentrations (μM) of pre-formed seeds under quiescent conditions, primary nucleation and fragmentation of α-synuclein amyloid fibrils can be neglected [211]. The aggregation kinetics were analysed as previously reported by fitting a linear function to the early times of the kinetic traces [211], with the exception that fitting was only performed after the initial decrease in fluorescence intensity, which is due to the temperature dependence of ThT fluorescence and a consequence of the thermal equilibration of the multiwell-plate prepared at room temperature. The fit was performed through 5 time points starting from the point of minimal fluorescence intensity (see Figure 2.12). The temperature-induced decrease in fluorescence intensity is superimposed to the increase in fluorescence due to fibril elongation. Therefore, using the initial growth rates likely leads to a small but systematic underestimation of the elongation rates. This fitting procedure was performed to obtain the values of $2k_+P(0)m(0)$, where k_+ is the fibril elongation rate constant, $m(0)$ the initial monomer concentration and $P(0)$ the initial number concentration of fibrils. For the comparison of the rates at different concentrations of AS69, we then calculate the ratios r:fig:AS69:4:1

$$r = \frac{\left(\frac{dM(t)}{dt}\right)_{AS69}\Big|_{t\approx 0}}{\left(\frac{dM(t)}{dt}\right)\Big|_{t\approx 0}} = \frac{k_+P(0)m(0,[AS69])}{k_+P(0)m(0)} \tag{2.10}$$

r is the ratio of the initial gradient fitted to the kinetic trace for monomer elongating fibrils in the presence of AS69 and the initial gradient fitted to the kinetic trace for monomer elongating fibrils

in the absence of AS69. $P(0)$ is the initial number concentration of fibrils, which is constant, as the same stock solution of seeds was used, and $m(0)$ is the initial monomer concentrations. For the prediction in Figure 2.4 c of the main manuscript, we calculated the equilibrium concentrations of unbound α-synuclein, $m(0,[AS69]) = [m]_{\text{free}}$ as:

$$[m]_{\text{free}} = \frac{-([AS69]_{\text{tot}} + K_D - [m]_{\text{tot}}) + \sqrt{([AS69]_{\text{tot}} + K_D - [m]_{\text{tot}})^2 + 4K_D[m]_{\text{tot}}}}{2} \tag{2.11}$$

where the values obtained at different $[AS69]_{\text{tot}}$ were then used for $m(0,[AS69])$ in Equation 2.10. This procedure corresponds to the assumption that the only effect of the AS69 is to sequester soluble α-synuclein.

Seeded aggregation experiments at very low monomer concentrations (0.75 µM seeds) were performed in order to test whether a concentration could be determined at which no net elongation is observed Figure 2.13). The concentration of free monomer at which the rates of fibril elongation and dissociation are equal corresponds to the equilibrium concentration [265]:

$$k_+[m]_{\text{eq}}[P] = k_-[P] \tag{2.12}$$

where k_+ is the elongation rate constant and k_- is the dissociation rate constant. The equilibrium constant of monomer addition to fibril ends therefore corresponds to the inverse of the monomer concentration at equilibrium:

$$K_{\text{eq}} = \frac{k_-[P]}{k_+[m]_{\text{eq}}[P]} = \frac{1}{[m]_{\text{eq}}} \tag{2.13}$$

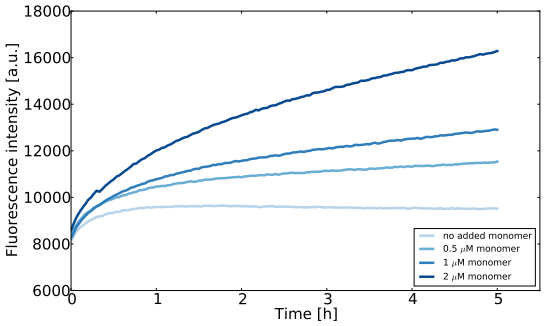

Figure 2.13: Seeded aggregation experiments at low monomer concentrations designed to estimate the concentration of monomeric α-synuclein in equilibrium with fibrils. The seed concentration is in all cases 0.75 µM and the ThT concentration is 10 µM. The experiment was performed at room temperature in order to slow the reaction down and avoid temperature effects on the fluorescence upon introduction of the multiwell plate into the fluorescence platereader.

The results of these experiments are shown in Figure 2.13. We find that even at a concentration as low as 0.5 µM, the slight increase over time of Thioflavin-T fluorescence suggests that the

fibril mass increases. This result is significant, given that the ThT fluorescence in a sample that contains only fibrils decreases over time. The fact that all samples, including that measured in the absence of added α-synuclein monomer, show an increase in ThT fluorescence during the first hour could be explained through sedimentation processes. We have shown previously that the sedimentation of fibrils can lead to an increase in detected ThT signal if the fluorescence is read from the bottom of the multiwell plate [211]. However, the subsequent increase in fluorescence intensity over several hours at concentrations of 0.5 µM or higher suggests an increase in fibril mass, and hence that the critical concentration under these conditions is lower than 0.5 0.5 µM.

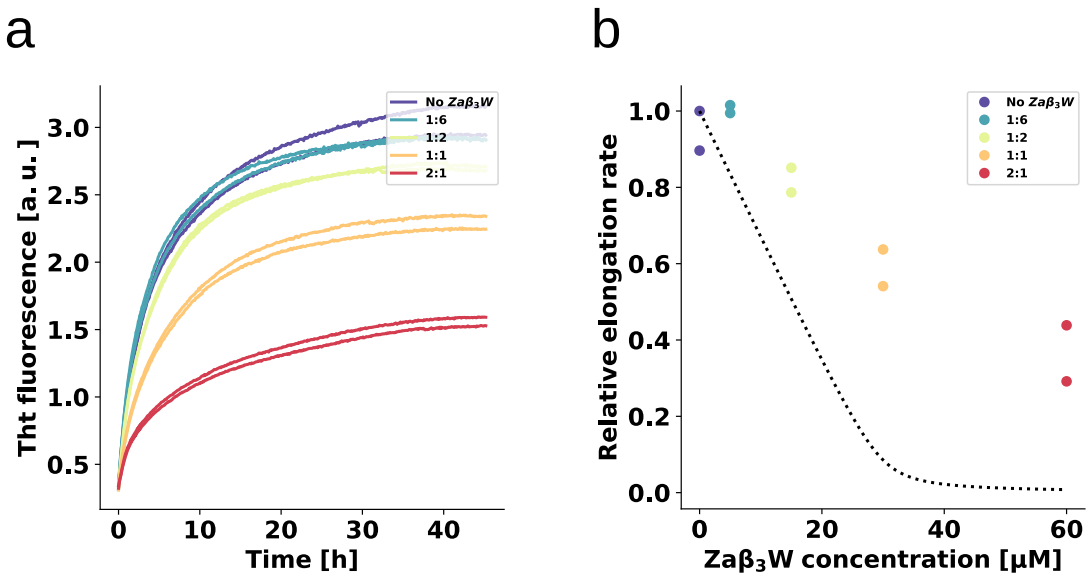

Figure 2.14: Binding specificity determines the inhibitory activity. The fibril elongation assay was repeated for ZAβ$_3$W, a binding protein for amyloid-βpeptide ([254]) that is a significantly weaker α-synuclein binder than AS69. The absence of detectable heat of binding in ITC allows only an estimate to be made for a minimal Kd of the ZAβ$_3$W-α-synuclein interaction on the order of 10 µM [229]. **(a)** Change in ThT fluorescence when a 30 µM solution of monomeric α-synuclein was incubated in the presence of 5 µM pre-formed fibrils under quiescent conditions with increasing concentrations of ZAβ$_3$W. **(b)** Relative rates of fibril elongation with increasing concentrations of ZAβ$_3$W. For comparison to AS69, the dotted line corresponds to the solid line in Figure 2.4 c.

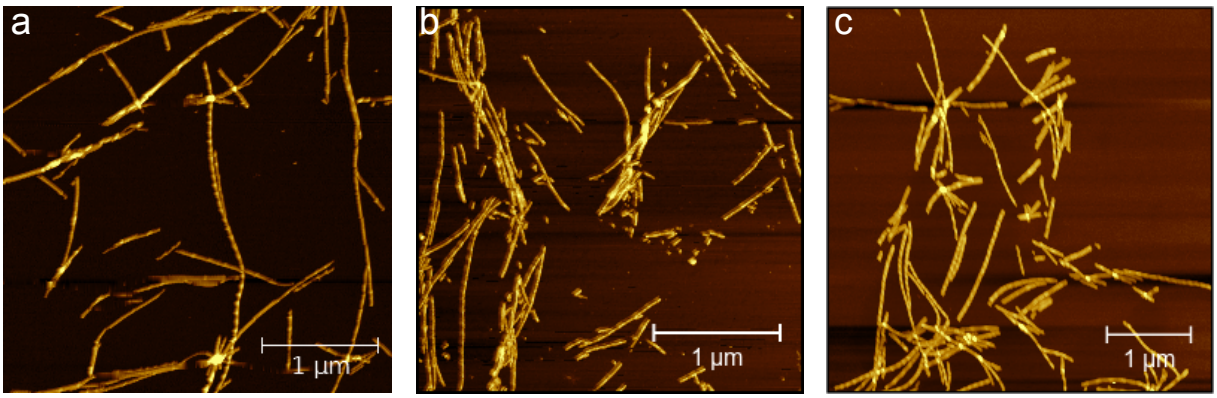

Figure 2.15: Characterisation of α-synuclein fibrils formed in the presence and absence of AS69 by AFM. AFM images of 30 µM monomeric α-synuclein that was incubated with 5 µM pre-formed fibrils, **(a)** in the absence, **(b)** the presence of 3 µM AS69, or **(c)** 30 µM AS69 in 20 mM phosphate buffer at pH 6.5 under quiescent conditions at 37 °C for 24 h.

2.9.2 Analysis of weakly seeded aggregation data at mildly acidic pH

Aggregation experiments were also performed at very low (nM) seed concentrations at mildly acidic pH and under quiescent conditions, where it has been shown that autocatalytic secondary nucleation of α-synuclein amyloid fibrils plays an important role [211]. In the present study, we performed these aggregation experiments in 20 mM sodium acetate buffer at pH 5.0, well below the threshold for secondary nucleation [211].
In order to quantitatively analyse the effects that AS69 and AS69fusASN exert on secondary nucleation, we started with the following equation describing the maximum aggregation rate in the presence of autocatalytic secondary nucleation [72]:

$$r_{\max} = \frac{M(\infty)\kappa}{e} \qquad \kappa = \sqrt{2m(0)^{n_2}[m(0)k_+ - k_{\text{off}}]k_2} \tag{2.14}$$

Where $M(\infty)$ is the long time limit of the fibrillar mass concentration, $m(0)$ is the starting concentration of monomeric α-synuclein, n_2 is the effective nucleus size of secondary nucleation, k_+ and k_{off} are the rate constants of elongation and de-polymerisation respectively, and k_2 is the rate constant of secondary nucleation. For our analysis, we assumed the rate of de-polymerisation to be negligible and that $M(\infty)$ was not altered by the presence of AS69. Furthermore we use the upper limit of how much monomer the AS69 could possibly sequester, which is equal to the AS69 concentration. Under these assumptions, the maximum rates relative to the case where no inhibitor was present can be described as:

$$\frac{r_{\max,I}}{r_{\max,0}} = \left(1 - \frac{I}{m(0)}\right)^{\frac{n_2+1}{2}} \tag{2.15}$$

Where $r_{\max,0}$ is the maximal aggregation rate in the absence of inhibitor, $r_{\max,I}$ is the maximal aggregation rate at inhibitor concentration I . The values of $r_{\max,I}$ for each kinetic trace were

found by applying the gradient function from numpy and smoothing the resulting curves using a ten-point sliding average. The maxima of the resulting curves were taken to be $r_{\mathrm{max},I}$. For the simulations, n_2 was varied in order to test whether the sequestration of monomer in conjunction with a higher reaction order of secondary nucleation can explain the observed strong inhibitory effect. However, even a value of n_2 as high as 5 was not able to explain the strong decrease in aggregation rate as a function of increasing inhibitor concentration. Therefore, we conclude that monomer sequestration cannot explain the highly efficient inhibition of secondary nucleation by AS69.

In the main manuscript, we discuss that the efficient inhibition of secondary nucleation by AS69 is likely to stem either from an interaction of AS69 alone or of the AS69:α-synuclein complex with an oligomeric aggregation intermediate. Given the low population of nuclei/oligomers compared to monomers during the aggregation time course, as well as the high affinity of the AS69 for monomeric α-synuclein, its affinity for such intermediate species would have to be significantly higher than that to monomers. This can be illustrated with a simple argument. At the end of an aggregation experiment, the fibrils typically are up to several micrometers in length, corresponding to thousands of protein molecules per fibril. Therefore, the total number of 'on pathway' oligomers that has formed during the aggregation process is three to four orders of magnitude smaller than the initial monomer concentration. In order to trap a significant fraction of these intermediates in the presence of a large excess of monomer, the affinity of AS69 to these intermediates would therefore have to be at least three orders of magnitude higher than that for monomer and hence be in the picomolar regime.

The alternative explanation, the binding of the AS69:α-synuclein complex to the aggregation intermediate, is more plausible. A clear inhibitory effect is still observed at a ratio α-synuclein:AS69 of 100:1, which according to the estimate above corresponds to at least one order of magnitude more AS69:α-synuclein complex than 'on pathway'-intermediate, rendering an efficient interference with the nucleation process plausible.

Therefore, we propose a model whereby rather than requiring the binding of free AS69 to an aggregation intermediate, the AS69:α-synuclein complex is able to incorporate into a fibril precursor and efficiently prevent it from undergoing the structural rearrangement required to transform into a growth-competent amyloid fibril.

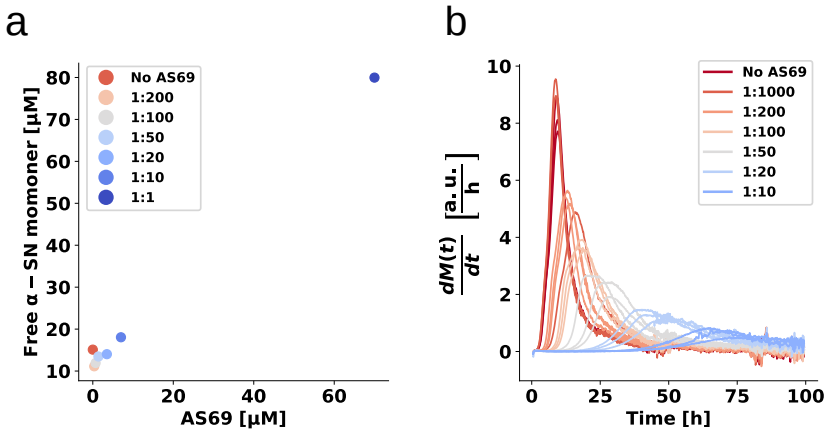

Figure 2.16: Weakly seeded aggregation experiments at pH 5.0 (a) The concentration of monomer left in solution after the weakly seeded experiments, as determined by the method described in [174]. **(b)** the numerically computed first derivatives (using a ten point rolling average) of the weakly seeded kinetic time courses shown in Figure 2.6.

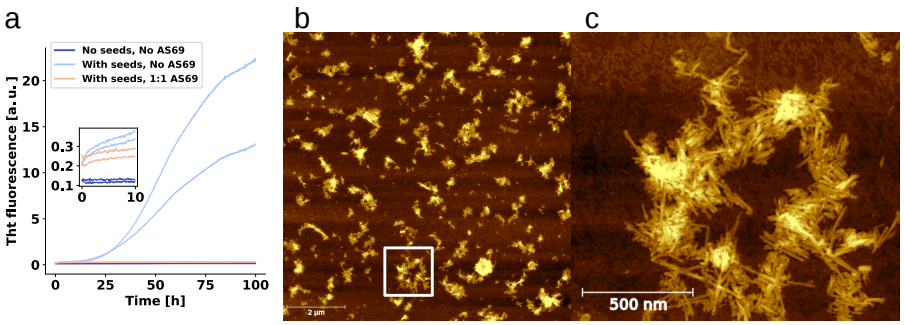

Figure 2.17: Seeds are required for aggregation under quiescent conditions. (a) Change in ThT fluorescence intensity when a 70 μM solution of monomeric α-synuclein was incubated either with or without pre-formed seeds, and with or without AS69 in acetate buffer (pH 5.0) under quiescent conditions. The inset shows the initial fluorescence intensity values. **(b)** AFM image of the seeds that were used for the experiment shown in **(a)**, note the inhomogeneity in the dispersion of the fibrils, due to the solution conditions that favour higher order assembly. The white square shows the approximate area of the zoom-in shown in **(c)**.

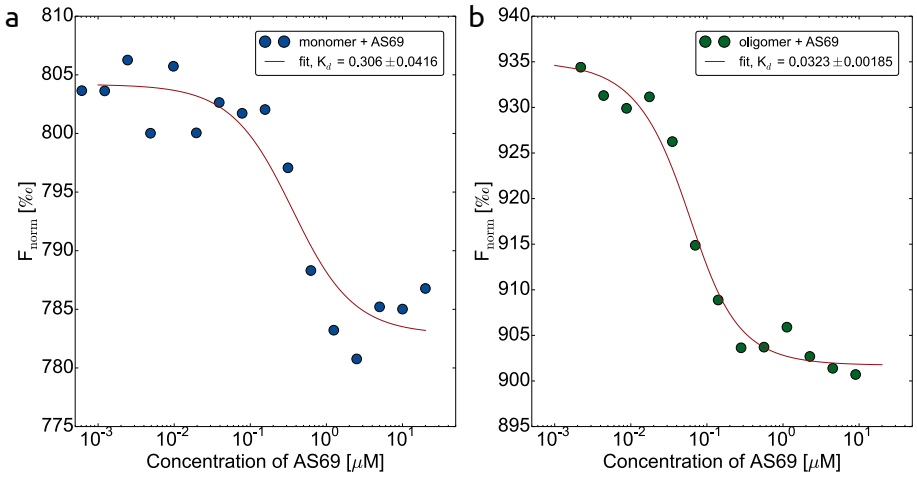

Figure 2.18: AS69 interacts with two distinct α-synuclein species. The binding of AS69 to monomeric **(a)** and oligomerc [201] **(b)** α-synuclein was quantified by microscale thermophoresis (MST) measurements [203] in 20 mM phosphate buffer pH 7.4 and 50 mM NaCl. The oligomers used in this assay are kinetically stable and can be purified and studied in isolation [201, 203]. The preparation of labelled monomeric and oligomeric α-synuclein is described in detail in the Methods section.

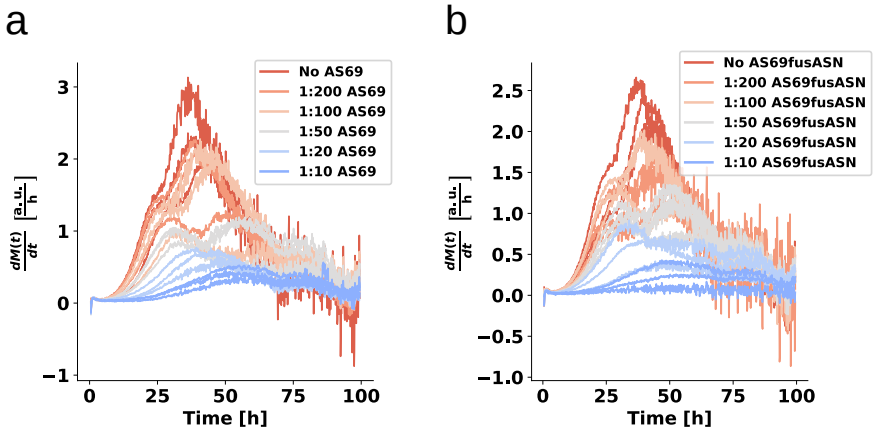

Figure 2.19: Weakly seeded aggregation experiments at mildly acidic pH 5. (a) the numerically computed first derivatives (using a ten point rolling average) of the weakly seeded kinetic time courses shown in Figure 2.8 **(c)**. **(b)** the numerically computed first derivatives (using a ten point rolling average) of the weakly seeded kinetic time courses shown in Figure 2.8 **(d)**.

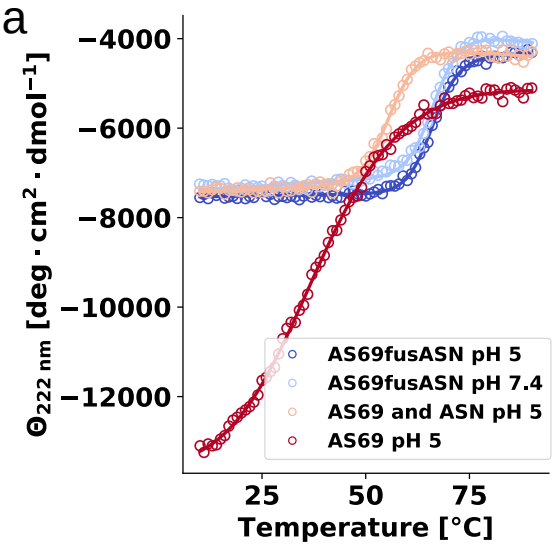

Figure 2.20: Melting curves **(a)** 25 µM AS69, 25 µM AS69 + 25 µM α-synuclein in 20 mM sodium acetate pH 5.0, and 25 µM AS69fusASN 20 mM sodium acetate pH 5.0, 17.5 µM AS69fusASN 20 mM phosphate buffer 50 mM NaCl pH 7.4. Solid lines represents fit to the equation described in [256].

2.9.3 Determination of the lipid-induced aggregation rate

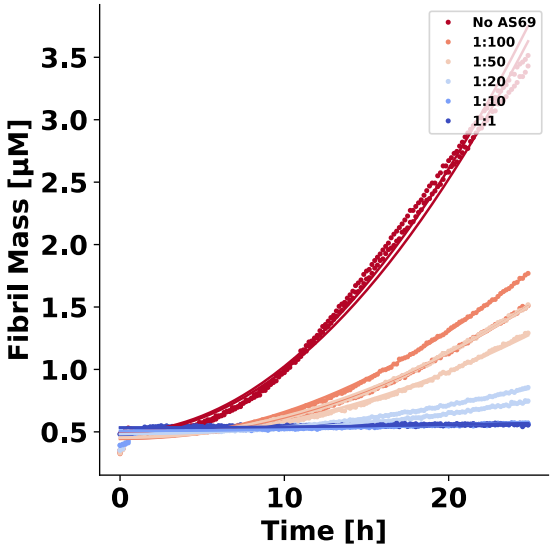

Figure 2.21: Early time points of lipid-induced aggregation.

The change in mass concentration of fibrils with time $M(t)$ during the early time points of the lipid-induced aggregation of α-synuclein aggregation was fitted using the single-step nucleation model described previously [174] and the following equation [73]:

$$M(t) = \frac{K_M k_+ m(0)^{n+1} k_n b t^2}{2(K_M + m(0))} \tag{2.16}$$

where k_+ is the elongation rate constant of fibrils from lipid vesicles, k_n is the heterogeneous primary nucleation rate constant, n is the reaction order of the heterogeneous primary nucleation reaction relative to the free monomer m, b is the total mass concentration of the protein bound to the lipid at 100% coverage ($b = \frac{[\text{DMPS}]}{L}$, with L the stoichiometry) and K_M is the Michaelis constant which defines the concentration of soluble protein above which the elongation rate no longer increases linearly (fixed at 125 µM [174]). The data was normalised such that the final amount of fibril mass was set to $2b$ for the traces where no AS69 was present as it was previously shown that the fibril mass is proportional to the concentration of DMPS [174].
A quadratic equation of the form $M(t) = at^2$, was fitted to the early time points of the normalised aggregation data (see Figure 2.21) where $a = \frac{(K_M k_+ k_n)_{\text{AS69}} b m(0,[AS69])^{n_{\text{AS69}}+1}}{2(K_{M,AS69} + m(0,[As69]))}$. The aggregation rate, $\frac{dM(t)}{dt}$ in the presence of AS69 normalised by the rate in the absence of AS69, for the same initial concentrations of free monomer and monomer bound to the lipid, can be computed according to:

$$r = \frac{\left(\frac{dM(t)}{dt}\right)_{\text{AS69}}}{\left(\frac{dM(t)}{dt}\right)} = \left(\frac{(K_M k_n k_+)_{\text{AS69}} m(0,[AS69])^{n_{\text{AS69}}+1}}{K_{M,AS69} + m(0,[AS69])}\right) \times \left(\frac{K_M + m(0)}{K_M k_n k_+ m(0)^{n+1}}\right) \tag{2.17}$$

In order to test whether the lipid vesicle induced aggregation of α-synuclein in the presence of AS69 can be explained by monomer sequestration alone, we simulated the ratio r for different concentrations of AS69. Starting from Equation 2.16 and assuming values of $k_n k_+$, K_M, b and n independent of AS69 (which amounts to the assumption that the presence of AS69 does not change the mechanism of aggregation, but merely inhibits through depleting the free monomer) and using $n + 1 = 1.2$ (see [174] for justification of $n = 0.2$) it can be shown that r takes the form:

$$r = \left(\frac{m(0,[AS69])^{1.2}}{m(0)^{1.2}}\right) \times \left(\frac{K_M + m(0)}{K_M + m(0,[AS69])}\right) \tag{2.18}$$

Where $m(0,[AS69])$ was calculated using Equation 2.11. The result of this simulation is shown in Figure 2.9 c.

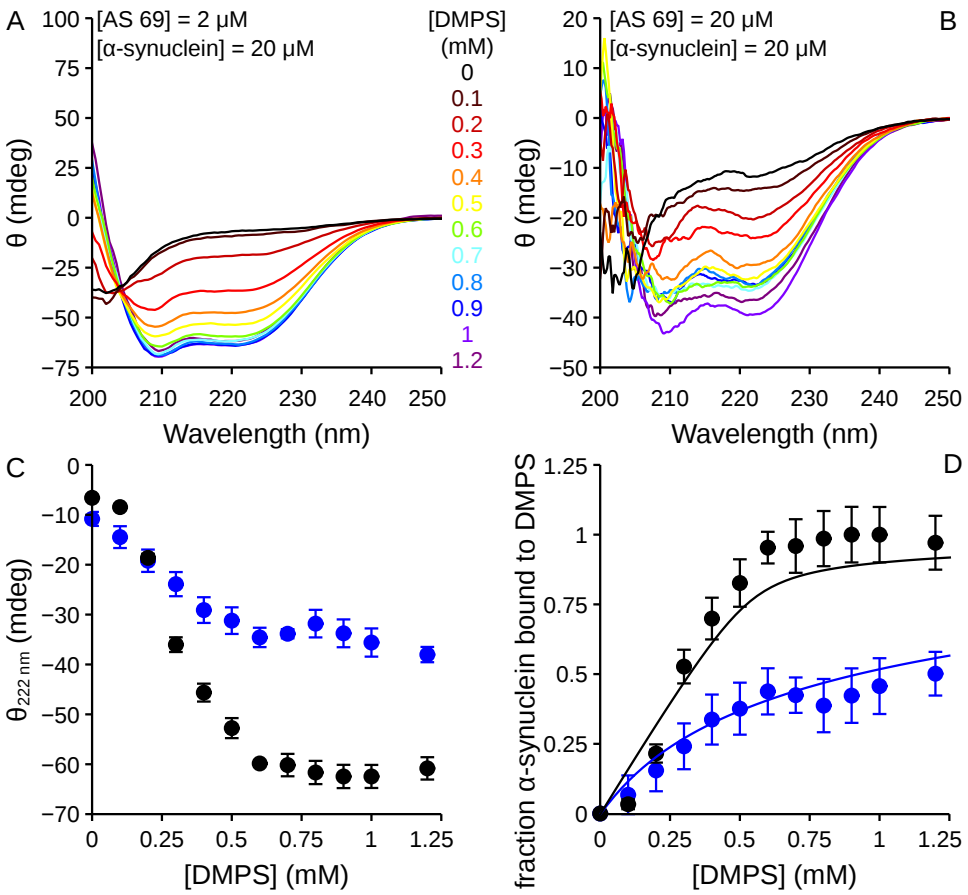

Figure 2.22: Influence of AS69 on the lipid-binding of α-synuclein monitored using circular dichroism (a),(b) CD spectra of α-synuclein (20 μM) in the presence of increasing concentrations of DMPS and 2 **(a)** or 20 **(b)** μM AS69. **(c)** Change in the CD signal of α-synuclein measured at 222 nm 222 nm when the protein was incubated in the presence of 2 (black dots) or 20 (blue dots) μM AS69 and increasing concentration of DMPS. **(d)** Change in the fraction of α-synuclein bound to DMPS vesicles in the presence of 2 (black dots) or 20 (blue dots) μM AS69. The solid lines correspond to predictions of the fraction of bound protein calculated using a competitive binding model using the binding constants previously determined for the systems DMPS:α-synuclein [174] and AS69:α-synuclein [229].

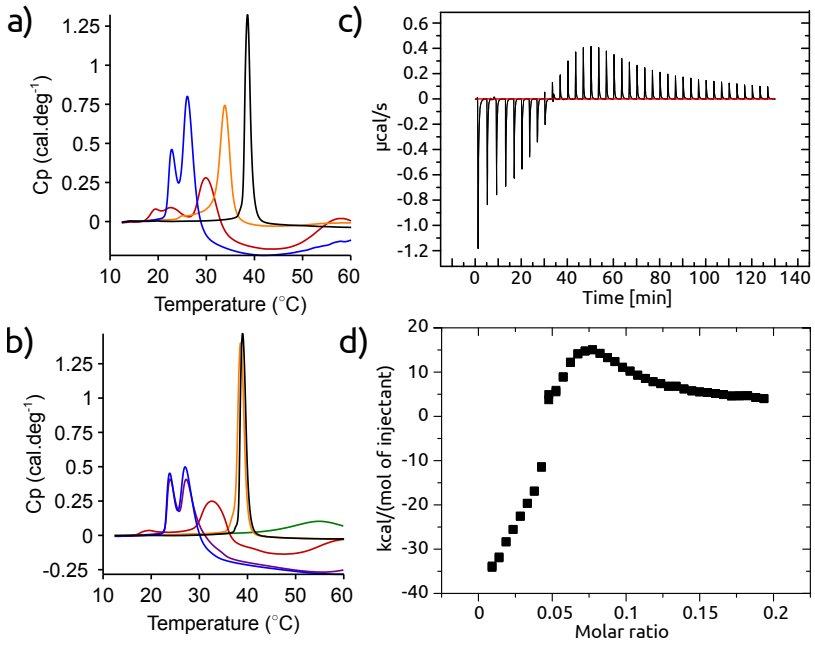

Figure 2.23: Calorimetric experiments designed to elucidate the molecular mechanism of inhibition of lipid-induced aggregation of α-synuclein by AS69. **(a)** DSC thermographs of 1 mM DMPS incubated in the absence (black) and the presence of 50 µM α-synuclein (blue), 50 µM AS69 (orange) or 50 µM α-synuclein and 50 µM AS69 (red). **(b)** Differential scanning calorimetry (DSC) thermographs of 1 mM DMPS incubated in the absence (black) or the presence of 33 µM α-synuclein (blue), 33 µM α-synuclein and 3.3 µM AS69 (purple), 33 µM α-synuclein and 33 µM AS69 (red) or 3.3 µM AS69 (orange). The green curve corresponds to the DSC thermograph of the mixture 33 µM α-synuclein and 33 µM AS69 (red). **(c),(d)** Isothermal titration calorimetry (ITC) experiments, in which a solution of 0.47 mM AS69 was titrated into 0.5 mM DMPS in 20 mM phosphate buffer pH 6.5 at 30 °C, corresponding to the conditions under which the lipid-induced aggregation of α-synuclein had been studied. These ITC experiments provide a direct confirmation of the binding of AS69 to lipid vesicles. The binding behaviour is complex and corresponds to more than one type of interaction. Therefore it is not straightforward to determine the binding affinity from these data.

3

INHIBITOR AND SUBSTRATE COOPERATE TO INHIBIT AMYLOID FIBRIL ELONGATION OF α-SYNUCLEIN

3.1. Article information

Title of paper: Inhibitor and substrate cooperate to inhibit amyloid fibril elongation of α-synuclein

Authors: Emil D. Agerschou [1], Vera Borgmann [1], Michael M. Wördehoff [1], and Wolfgang Hoyer [1,2,*]

[1] Institute of Physical Biology, Heinrich Heine University Düsseldorf, Universitätsstraße 1, 40225 Düsseldorf, Germany

[2] Institute of Biological Information Processing, Structural Biochemistry (IBI-7) and JuStruct: Jülich Center for Structural Biology, Forschungszentrum Jülich, 52425 Jülich, Germany.

[*] To whom correspondence should be addressed: wolfgang.hoyer@hhu.de

Journal: Chemical Science

DOI: 10.1039/D0SC04051G

3.2. Declaration of Article Contributions

3.2.1 Experimental

All protein experiments not involving WT-WT, WT-CC48, CC48-WT were planed and performed by me. Furthermore, all the protein based experiments that were not carried out by me was carried out under my supervison by Vera Borgmann.

3.2.2 Data analysis

With the exception of the development of the inhibition models, which was carried out by Wolfgang Hoyer, all the data analysis in this paper was performed by me.

3.2.3 Manuscript preparation

I wrote the first draft of the main manuscript and supplementary information, including all figures and text. The final manuscript and supplementary information was prepared by me in close collaboration with Wolfgang Hoyer.

3.3. Abstract

In amyloid fibril elongation, soluble growth substrate binds to the fibril-end and converts into the fibril conformation. This process is targeted by inhibitors that block fibril-ends. Here, we investigated how the elongation of α-synuclein (αS) fibrils, which are associated with Parkinson's disease, is inhibited by αS variants with a preformed hairpin in the critical N-terminal region comprising residues 36-57. The inhibitory efficiency is strongly dependent on the specific position of the hairpin. We find that the inhibitor and substrate concentration dependencies can be analyzed with models of competitive enzyme inhibition. Remarkably, the growth substrate, *i.e.*, wild-type αS, supports inhibition by stabilizing the elongation-incompetent blocked state. This observation allowed us to create inhibitor-substrate fusions that achieved inhibition at low nanomolar concentration. We conclude that inhibitor-substrate cooperativity can be exploited for the design of fibril growth inhibitors.

3.4. Introduction

A growing number of proteins have been shown to undergo an autocatalytic aggregation reaction where soluble polypeptide chains convert to insoluble 1D quasi-crystals exhibiting cross-β conformation.[28, 47, 266] When proteins are found in this state they are referred to as amyloid fibrils. The amyloid state is thought to be a generic state that all proteins can adopt and is associated with several diseases, especially neurodegenerative ones.[45, 46, 47, 266]

In this paper we focus on the protein α-synuclein (αS) which is believed to play a central role in the pathology of Parkinson's Disease (PD). In PD, αS is found in insoluble inclusions, termed Lewy bodies, where it is thought to predominantly inhabit the amyloid state.[129, 141, 145, 147]

Amyloid fibril formation is a multi-step reaction that minimally includes primary nucleation and elongation, but commonly involves additional reactions including secondary nucleation, fragmentation, and competition from so-called off-pathway reactions.[73, 267, 268, 269] This complexity can make interpretation of experimental data exceedingly complicated.[73, 148] However, all of these reaction steps are amenable to modulation by ligands, affording a range of therapeutic opportunities that target different sites on distinct species on the aggregation pathway.[270] Importantly, molecules that are able to interact with specific sites/species can also provide insight into the mechanism of amyloid formation.[271]

Here we will focus on elongation of fibrils which is the most frequent process in amyloid formation. Elongation of αS fibrils can be studied in isolation using specific solution conditions.[211] During elongation, a free αS monomer, which in its free state is intrinsically disordered,[190] i) absorbs onto the fibril-end and ii) converts into the specific structure of the templating fibril.[268] This is reminiscent of enzyme kinetics, and elongation can be treated as a two-step enzymatic reaction, in which fibril-end and monomer serve as catalyst and substrate, respectively.[70, 71, 272]

Proteins and peptides have been designed to specifically inhibit the elongation of αS fibrils,[39, 41, 273, 274] *e.g.*, by aiming to dock complementary β-strands onto the open β-sheets at the fibril-ends, to prevent the catalytic site from guiding the conformational conversion of further monomers. However, understanding how monomers and inhibitors get incorporated at fibril-ends is still a subject of active research.[268] We have previously reported that a double cysteine αS mutant containing the amino acid exchanges G41C and V48C, here denoted CC48, inhibits the elongation of wild-type (WT) αS fibrils.[234] This double exchange introduces an intramolecular disulfide bond that is important for inhibitory activity of CC48. The positions of the two cysteines

were chosen to promote the formation of a β-hairpin motif in the region spanning residues 36-57, a region we previously observed to be in complex with an αS monomer-binding protein, the β-wrapin AS69 (Figure 3.1a,b).[229, 275]

The strong inhibitory effects of both CC48 and AS69 on αS fibril formation highlight the importance of this region, which contains several of the disease associated mutations (E46K, H50Q, G51D, A53E, and A53T).[131, 132, 133, 135, 141] This was corroborated recently when an αS deletion mutant lacking residues 36-42 and 45-57 was shown not to aggregate.[276] In the present work, we investigated sequence requirements and mechanism of the inhibition of αS fibril elongation achieved by CC48 and related constructs. We observe inhibitor-substrate cooperativity, which provides insight into blocked fibril-end states and supports the design of improved inhibitors.

3.5. Results and Discussion

Our first experimental goal was to gauge the dependency of the inhibitory activity of CC48 on the precise position of the disulfide bond. In addition to CC48, we therefore generated a set of double cysteine αS variants by systematically mutating residues 49 through 52 into cysteines while keeping the other end of the disulfide fixed at position 41 (Figure 3.1b). All mutants except CC51, which only resulted in low yield and many impurities, were obtained in monomeric form. We performed elongation assays by incubating 2.5 μM preformed and sonicated fibrils (seeds) with WT monomer. Our specific choice of elongation reaction conditions were tested by measuring the rate of elongation using Thioflavin T (Tht) fluorescence over time (Figure 3.1c), as Tht is an amyloid specific dye that drastically increases its fluorescence when binding to amyloid fibrils.[66] As elongation is a bimolecular reaction, the initial rates, r, should be directly proportional to available fibril-ends and initial WT αS monomer concentration. The initial rates were extracted by fitting linear curves to the initial slopes as shown in Figure 3.1c (see SI for the theoretical considerations). To further validate that elongation was the only reaction occurring, atomic force microscopy (AFM) was conducted on seeds before (**??**d) and after (Figure 3.1e) elongation. While indeed only short fibrils could be found initially, much longer fibrils were dominating after the Tht time course measurement. Lastly, SDS-PAGE of selected samples from kinetic experiments was performed. The overwhelming amount of protein was found in the insoluble pellet fractions, and the final Tht values correlated with protein amount found in pellet (Figure 3.5). Based on AFM and the non-sigmoidal shape of the Tht time course measurements, it could safely be assumed that elongation was the only amyloid-generating reaction occurring in our setup.

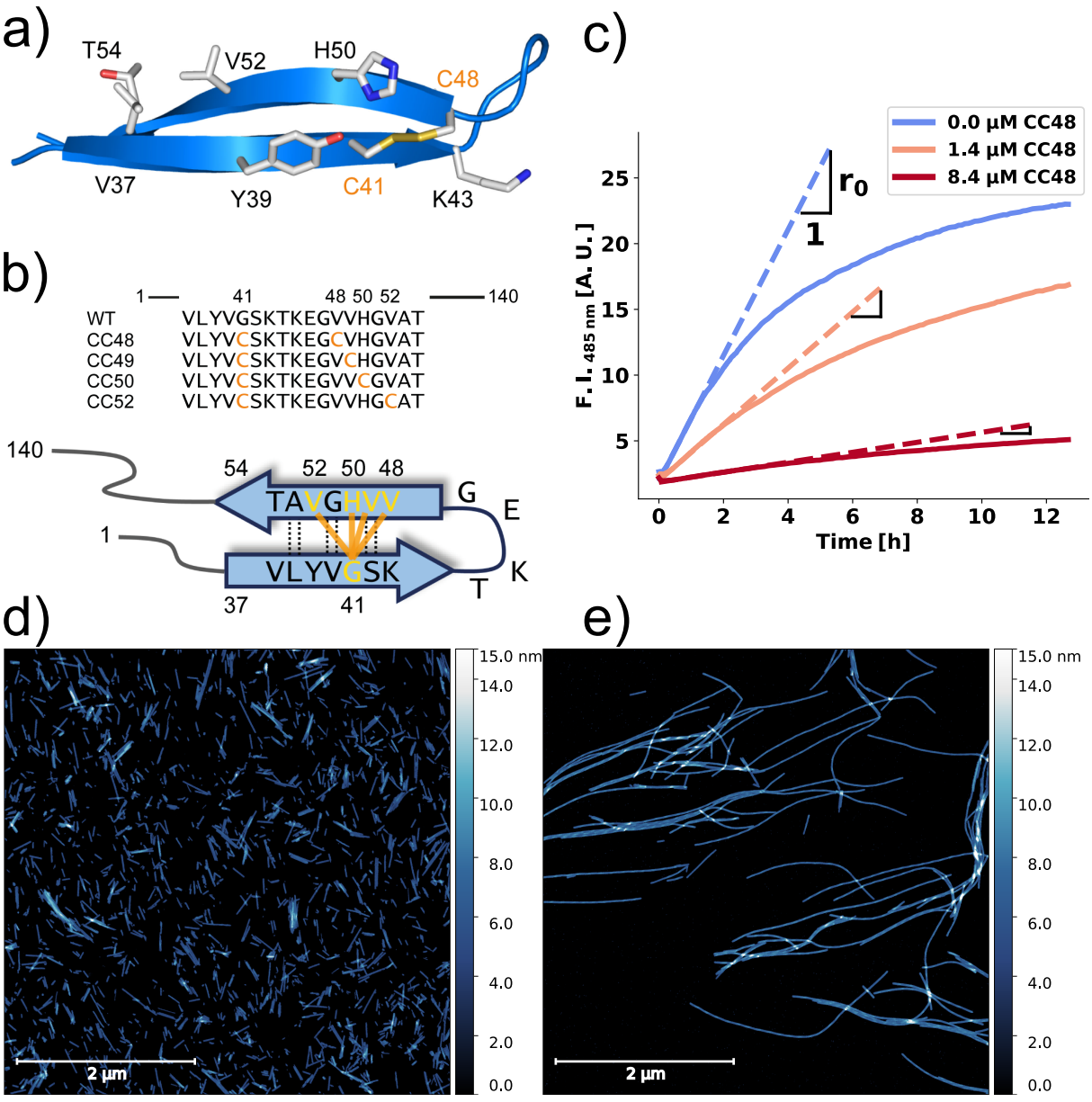

Figure 3.1: αS variants containing disulfide-stabilized hairpins inhibit elongation of WT αS fibrils. αS variants containing disulfide-stabilized hairpins inhibit elongation of WT αS fibrils. **a)** Model of a β-hairpin conformation of CC48 based on the NMR structure of αS bound to β-wrapin AS69 (PDB: 4bxl). **b)** Overview of investigated CC mutants, including a scheme of the disulfide bond positions (orange lines) with respect to the β-sheet registry of the hairpin shown in a). Dashed lines indicate hydrogen bonding across the strands. **c)** Exemplary time courses of Tht fluorescence where 25 µM WT monomer was mixed with 10 % seeds and allowed to elongate in absence or presence of the inhibitor CC48. The initial slopes, r, are extracted by fits to a linear equation (discontinuous lines), where r_0 is the slope when no inhibitor was present. **d, e)** AFM imaging of seeds before elongation (d), and after elongation (e) in the presence of 25 µM WT monomer and 0.472 µM CC48-CC48 dimer.

The effect of CC48 on WT elongation was determined in the presence of 25 µM WT monomer and increasing concentrations of CC48 (Figure 3.2a and 3.6). The initial rates, r, were extracted and divided by the initial rate when no CC48 was present r_0 (Figure 3.2b). A clear inhibition

profile curve could be observed where the relative initial rate, $\frac{r}{r_0}$, was halved at a [CC48]/[WT] ratio of $0.054 \pm 0.008 \sim {}^{1}/_{20}$. It should be noted that CC48 on its own does not elongate WT fibrils unless the elongation is carried out under reducing conditions, here done using the reducing agent dithiothreitol (DTT) (Figure 3.11). This is in line with the incompatibility of the disulfide-induced hairpin with all near-atomic-resolution αS fibril structures reported to date [42, 220, 221, 222, 223, 277]. Adding DTT also severely reduces the inhibitory potential of CC48 (Figure 3.12).

The same type of experiment and data analysis was performed on the newly created CC mutants (Figure 3.2c, 3.7, 3.8, and 3.9). Although all mutants were inhibitory to some degree, only CC48 and CC50 inhibited sub-stoichiometrically in terms of the [CCX]/[WT] ratio, indicating specific inhibition, where the latter achieved a halving of $\frac{r}{r_0}$ at a [CC50]/[WT] ratio of $0.43 \pm 0.05 \sim {}^{1}/_{2}$, an effect that also strongly depended on DTT (Figure 3.12).

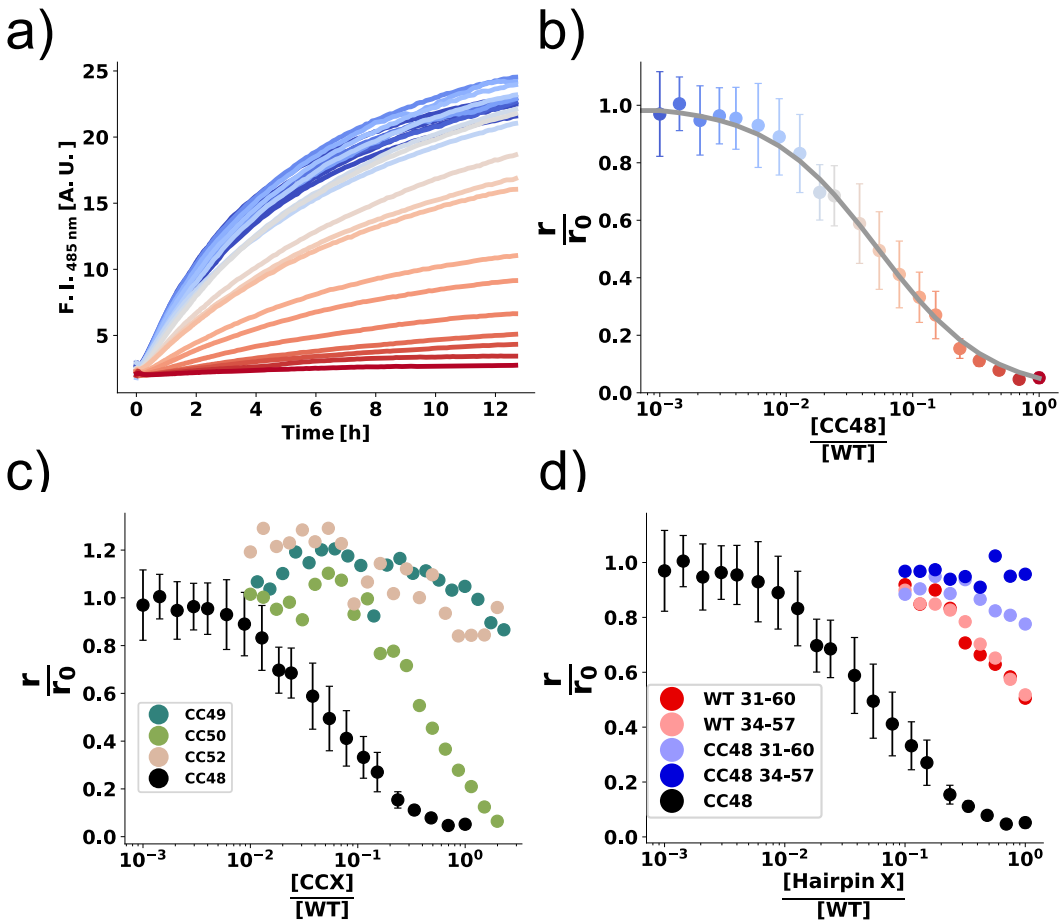

Figure 3.2: The inhibition efficiency is strongly dependent on the position of the disulfide bond. a) Elongation experiment performed in the presence of increasing concentrations of CC48 and **b)** the mean relative initial slopes, $\frac{r}{r_0}$, extracted from four independent experiments. The solid line shows a fit to the competitive inhibitor (FI) model. Error bars correspond to the standard deviations (SD). **c)** Relative initial slopes of WT elongation in the presence of the different CC variants and **d)** WT and CC48 hairpin peptides. Note that the concentration axis in (b), (c), and (d) is logarithmic and given as the ratio between the inhibitor and the 25 µM WT monomer that was present. For comparison, the CC48 data is also shown in (c) and (d).

On the other hand, neither CC52 nor CC49 were particular inhibitory. This position dependency of inhibitory activity is remarkable, especially for the low inhibitory variant CC49 where the variable cysteine is located exactly in between its positions in the highly inhibitory variants CC48 and CC50. Furthermore, the variable exchange is valine to cysteine in CC49, just as in CC48. This argues for a structure-specific origin of the inhibitory activity, perhaps related to formation of a specific β-hairpin. β-Hairpins are stabilized by cross-strand disulfide bonds between directly opposed cysteine residues at non-hydrogen-bonding positions in the N- and C-terminal β-strands.[278, 279, 280] For the β-hairpin registry shown in Figure 3.1b, residues 41 and 50 lie at such directly opposed non-hydrogen-bonding positions n and c. Apart from interactions between n and c, diagonal side chain-side chain interactions especially between residues n and c-2 can also stabilize β-hairpins.[281] These positions correspond to residues 41 and 48 in the

β-hairpin registry in Figure 3.1b. Thus, the disulfide bonds in the two variants CC48 and CC50 may promote the formation of a common β-hairpin conformer. The disulfide in CC49, on the other hand, would not support the same β-hairpin as the side chains of cysteines 41 and 49 would lie on opposite faces. Involvement of a β-hairpin conformer according to the registry displayed in Figure 3.1b could therefore explain the position dependency of the inhibitory activity. Promotion of an individual peptide β-hairpin through introduction of favourable cross-strand interactions enhances the population of the β-hairpin conformer, but is usually not sufficient to fully stabilize a defined β-hairpin structure.[281, 282] In line with this, CC48 does not form a stable β-hairpin but remains disordered also in the region spanning residues 36-57.[234] Nevertheless, the disulfide bond will alter the ensemble of β-hairpin conformers that are populated in this region,[283] with potential consequences for the interaction with fibril-ends and for the inhibition of fibril elongation.

CC48 was by far the strongest inhibitor and was therefore chosen for further mechanistic studies. It was earlier observed that subtly modified fragments of an amyloidogenic protein can be highly inhibitory.[284, 285] CC48, as well as αS, is intrinsically disordered in solution and as such the β-hairpin region is available for potential binding and interfering with fibril-ends.[234] To test if the observed inhibition could be explained solely by the β-hairpin region of CC48, we performed elongation experiments in the presence of synthetic peptides composed of the β-hairpin region of CC48 as well as the WT sequence (Figure 3.2d and 3.10). Two different lengths of CC48 β-hairpin peptides were tested, comprising residues 31-60 or 34-57 (pI = 9.14 or 6.74, respectively) and compared to WT peptides (pI = 9.60 or 6.76, respectively). The CC48 hairpin peptides were far less inhibitory than the full-length CC48, meaning that the β-hairpin region alone was not enough to accomplish the observed inhibition. This indicates that (WT) sequence segments beyond the β-hairpin region of CC48 are required for efficient inhibition. As CC48 substoichiometrically inhibits fibril elongation, it most likely acts on fibril-ends,[270] the sites where WT monomers dock and convert into the fibril structure. While the CC48 β-hairpin region is required for inhibition, WT sequence segments are obviously essential for binding to the fibril-end.

Using ideas from enzymology, which has a long tradition of investigating inhibition mechanisms, we postulate that the mechanism of elongation inhibition by CC48 is analogous to competitive inhibition of enzyme catalysis. Specifically we suggest that CC48 is similar enough to WT monomer to compete for attachment to the fibril-end, where it forms a tight complex, possibly supported by the structural modification in the β-hairpin region. In contrast to WT, however, CC48 bound to the fibril-end cannot serve as a template for incorporation of further monomers to extend the fibril structure. Thus, CC48 suspends the catalytic activity of the fibril-end. The observed inhibition curve was compatible with competitive inhibition with a ∼20-fold higher affinity of CC48 for the WT fibril-end than WT monomer (Figure 3.2b). However, the inhibition curve obtained at a varying inhibitor (CC48) concentration and constant substrate (WT) concentration is not sufficient to determine the inhibition mechanism and affinities, as its shape is compatible with a wealth of different mechanisms. When both the substrate and the inhibitor concentrations are varied, a drastic increase in features for identifying the precise mechanism becomes available.[39] Such experiments revealed a remarkable dependence of the initial rate, r, on both the WT and CC48 concentrations (Figure 3.3a and 3.13). In the absence of CC48, r increased almost linearly with WT concentration, in line with fibril elongation by monomer addition to non-saturated fibril-ends. When CC48 was present, r initially increased with increasing WT concentration, indicating competitive inhibition (see SI theoretical section). But rather than continuing this trend, r reached a maximum and began declining. This rather

surprising observation indicates that the substrate of the reaction, *i.e.* WT monomer, joined forces with the inhibitor, CC48, to increase the efficacy of the inhibitor.

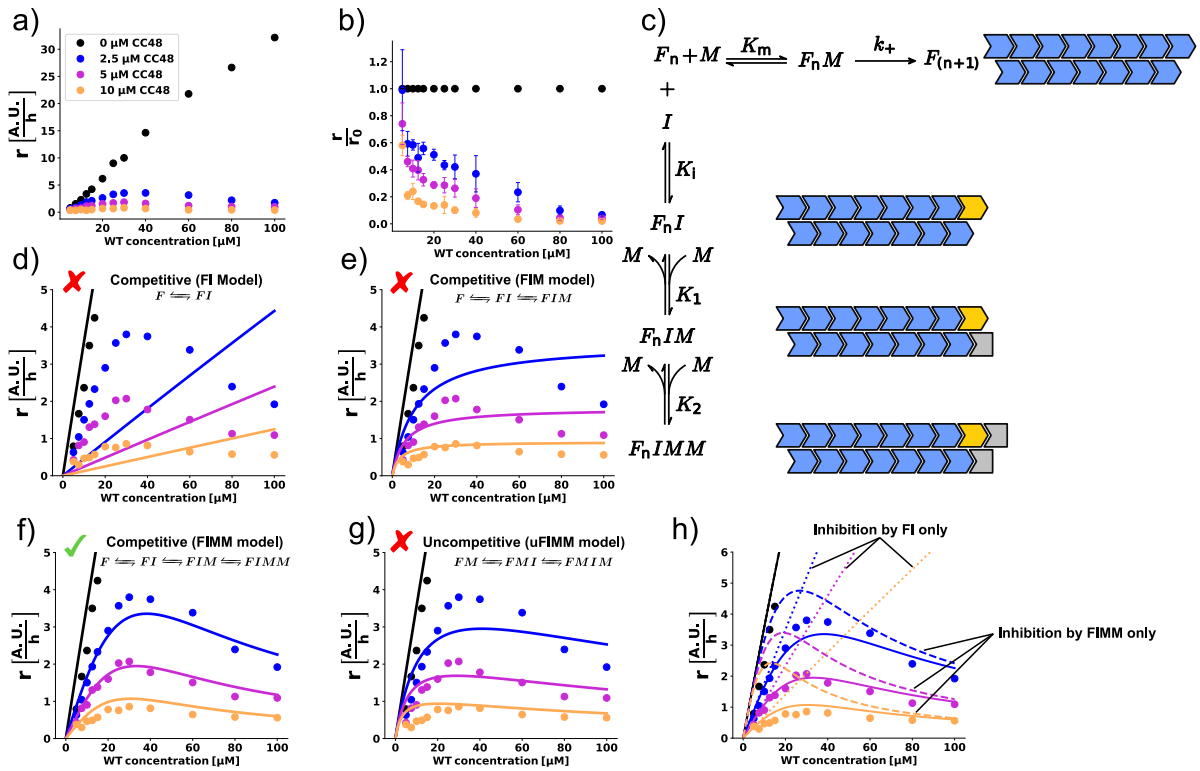

Figure 3.3: WT monomer cooperates with CC48 in inhibition of WT fibril elongation. **a)** WT monomer concentration dependence of the initial slopes, r, in the presence of different concentrations of CC48. **b)** Mean relative initial slopes, $\frac{r}{r_0}$, extracted from three independent experiments, error bars correspond to the SD. **c)** Reaction mechanism where the horizontal reaction is elongation and the vertical one describes inhibition. M is a WT monomer, I is a CC48 monomer, and F is a fibril-end. **d-f)** Zoom-in of the data shown in a) fitted (solid lines) to competitive inhibitor models where the inhibitory species are **d)** FI **e)** FI and FIM, **f)** FI, FIM, and $FIMM$. **g)** Fit to an uncompetitive model where the inhibitor does not bind until a monomer has docked onto the fibril-end, resulting in inhibitory complexes FMI and $FMIM$. **h)** Simulation using the parameters obtained from f) of how inhibition would appear if only FI or $FIMM$ were inhibitory.

This WT monomer concentration effect was clearly captured by the relative initial slopes, where a constant decline with respect to the uninhibited sample at the same WT monomer concentration was observed (Figure 3.3b). The unusual WT monomer dependency cannot be explained by the standard competitive inhibition model that attributes inhibitory activity only to the complex FI formed from fibril-end (F) and inhibitor CC48 (I) (Figure 3.3c,d). The cooperation of WT and CC48 in inhibition suggests that FI can recruit further WT monomer (M), which stabilizes the elongation-incompetent blocked state (Figure 3.3c). .

A model including the formation of the species FIM can account for a deviation from the linear increase but can still not explain the reduction of r with WT monomer concentration (Figure 3.3c,e). However, when a second WT monomer can stabilize the blocked state by

forming the $FIMM$ species, reduction of r with WT monomer concentration can be accounted for (Figure 3.3c,f). Global fits to a competitive model including the formation of FIM and $FIMM$ species showed good agreement with the data (Figure 3.3f).

In enzyme kinetics, an alternative to competitive inhibition is uncompetitive inhibition, where the inhibitor binds to the enzyme-substrate complex. In inhibition of fibril elongation this would correspond to preferential binding of the inhibitor to a fibril-end with docked but unconverted WT monomer, resulting in the FMI species. If such a species is stabilized by forming the $FMIM$ species with a WT monomer, a reduction of r with WT monomer concentration can be achieved. However, a global fit to an uncompetitive model with formation of a $FMIM$ species was not in agreement with the data (Figure 3.3g).

Global fits to the competitive $FIMM$ model yielded equilibrium constants that followed the order $K_1 > K_m > K_i > K_2$ (Figure 3.3c and Table 3.1). To gain intuition into the role played by the different inhibiting species, we simulated, using the obtained fitting parameters, how r would depend on WT monomer concentration if either FI or $FIMM$ were the only inhibitory species (Figure 3.3h). FIM was not considered due to its high dissociation constant, K_1, which results in a negligible population of FIM. According to the simulations, the FI species accounts for the WT monomer concentration dependence at low monomer concentration but does not account for the maximum nor for the decline in elongation rate (Figure 3.3h). The $FIMM$ species, on the other hand, does not capture the efficient and CC48 concentration-dependent inhibition at low WT monomer concentrations but accounts for the peak and decline of r at high WT monomer concentrations.

According to the obtained equilibrium constants, binding of WT monomer to FIM is much more favourable than to FI (K1 $\gg$ K2). Rationalisation of this observations has to take into consideration that αS fibrils consist of two protofilaments, in which αS subunits are staggered with respect to their neighbours in the other subunit (schematically depicted in Figure 3.3c). Binding of CC48 to the fibril-end might alter the protofilament interface, disfavouring addition of another WT monomer. Once a WT monomer attaches to FI nonetheless, a structurally different binding site with high affinity for an additional WT monomer is created. While the kinetic data does not provide structural information on the different fibril-end complexes, it indicates that at least two WT monomers cooperate with the CC48 inhibitor to form a stabilized blocked state that is incompatible with fibril elongation. The cooperation of CC48 with WT monomers in inhibition suggests that an improved inhibitor could be designed by combining CC48 and WT in fusion constructs. As formation of the FIM complex from FI and M was the least favoured step on the inhibition path, IM fusion constructs consisting of one CC48 and one WT unit might show increased inhibitory activity by bypassing this step. We recombinantly expressed dimeric constructs of WT and CC48 separated by flexible linkers as shown schematically in Figure 3.4a.

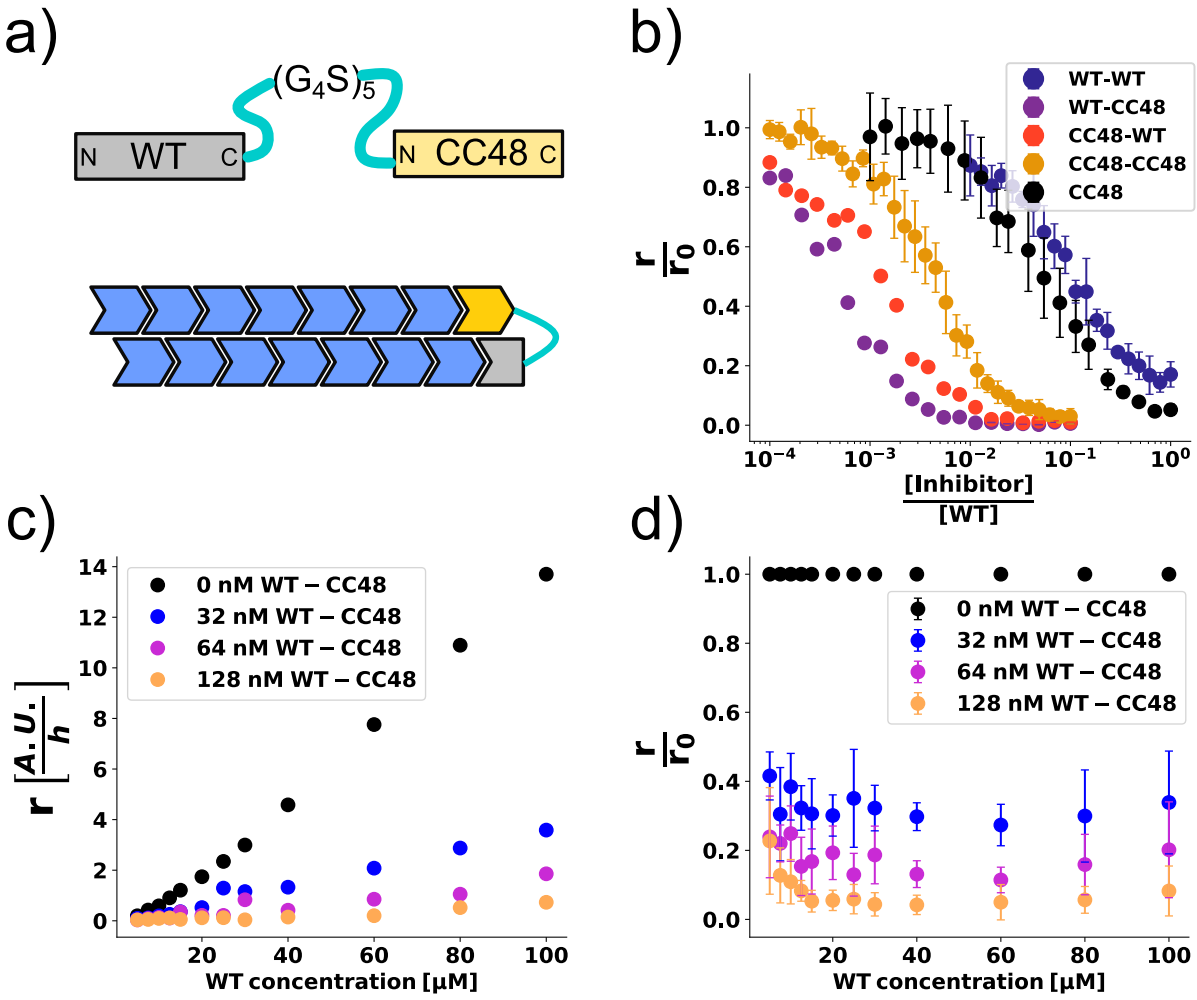

Figure 3.4: CC48-WT fusion inhibits elongation of WT αS fibrils at low nanomolar concentrations. **a)** Schematic overview of the dimer constructs of combinations with zero, one, or two CC48 and WT with a flexible $(G_4S)_5$ linker in between, here exemplified by WT-CC48 dimer. **b)** Relative initial rates, $\frac{r}{r_0}$, of elongation assays with increasing concentrations of the dimer constructs at constant WT concentration. The CC48 data is the same as shown in Figure 3.2b. **c)** WT monomer concentration dependence of the initial slopes, r, in presence of different concentrations of WT-CC48. **d)** The average $\frac{r}{r_0}$ of the WT-CC48 monomer dependency investigations. Error bars, where present, correspond to the SD.

In addition to two heterodimeric constructs WT-CC48 and CC48-WT that differ by the order of WT and CC48 with respect to the linker, we also constructed two homodimers WT-WT and CC48-CC48. The relative initial rates of elongation assays in the presence of these dimers are shown in Figure 3.4b, 3.17, 3.18, 3.19, and 3.20. In agreement with the design concept, the heterodimeric species were far more inhibitory than CC48 as the concentration needed to achieve half relative initial rate corresponded to an [Inhibitor]/[WT] ratio of $0.00048 \pm 0.00005 \sim {}^{1}/_{2000}$, *i.e.*, two orders of magnitude less than what was needed for CC48 alone. The heterodimeric constructs were also more inhibitory than the homodimeric ones, showing that it is in fact the particular combination of CC48 and WT that blocks fibril elongation most efficiently. The WT-WT dimer was almost as inhibitory as the CC48 alone, a result that is in agreement with

what has been observed for similar constructs.[41, 199] The CC48-CC48 dimer also exhibited strongly increased inhibition compared to CC48, which could be an avidity effect. As expected, the heterodimeric construct exhibited much less monomer dependency than what was observed for CC48 alone (Figure 3.4c,d, 3.22, 3.23, 3.24, and 3.25). This is in line with a notion of *FIM* being the least favoured species on the inhibition path, whose formation is promoted as the inhibitor, *i.e.* CC48, now carries its own co-inhibitor, *i.e.* the WT, in the heterodimeric fusion constructs. At a WT monomer concentration of 25 µM, the WT-CC48 fusion showed an IC_{50} of 11 ± 1 nM. This compares favourably to previously reported elongation inhibitors based on αS fusions. These inhibitors were based on different design principles, namely transport of steric bulk to the fibril-end or direct linkage of two αS subunits at different positions within the αS sequence, and reached IC_{50} values of 300 nM,[39, 286] or 22 nM.[41] In one of these approaches, the function of a fused WT monomer is to serve as a fibril-end-binding domain that brings the fused inhibitor domain close to the second protofilament, with the inhibitor acting as steric bulk that impedes incorporation of further WT monomers.[39, 286] While this approach is related to the current study with regard to the fusion of a WT monomer domain to an inhibitor domain, there are crucial differences: First, CC48 forms an inhibiting FI complex without requiring fusion to a WT monomer. Second, WT monomer,*i.e.*, the unmodified substrate of the elongation reaction, stabilizes the CC48-FI state without requiring fusion to an inhibitor domain. Third, the WT monomer concentration dependency of the steric bulk fusions is different from those of CC48 and the CC48-WT dimers,[39] indicating a different mechanism of inhibition. Nevertheless, all these approaches show that modified versions of αS can block fibril-ends, with the potency determined by the nature of the fused proteins as well as the type of linkage. Binding of CC48 to the fibril-end creates a templating-incompetent state with an efficiency that is highly dependent on the specific disulfide fusion (Figure 3.2c). Can WT monomer also dock to the fibril-end in such templating-incompetent conformations? Real-time observation by AFM or TIRF microscopy of αS fibril elongation in the presence of WT monomers revealed the existence of long-lived stop states,[253, 287] which were subsequently also reported for several other amyloid proteins.[288, 289, 290, 291] These stop states were suggested to be due to docking of the WT monomer on the fibril-end in a templating-incompetent conformation.[253, 289, 291] Thus, the inhibitory efficiency of CC48 might be an enhanced representation of a property that is already inherent to WT monomers. Possibly in a similar vein, certain types of post-translational modified αS might inhibit fibril elongation by establishing templating-incompetent fibril-ends, which could for example explain the inhibitory activity reported for dityrosine-modified αS.[199]

3.6. Conclusion

Exploitation of the principle of self-recognition has proven fruitful for the design of amyloid formation inhibitors [284, 285]. Here, we showed that modification of αS by introduction of a hairpin in a critical N-terminal region results in an inhibitor of fibril elongation, whose efficiency is strongly dependent on the precise position of the hairpin. Our data demonstrates that the efficiency of such fibril-end blocking inhibitors may be dramatically enhanced by linkage to WT monomer, as WT monomer is capable of stabilizing the blocked fibril-end state. As a consequence of the catalytic nature of fibril formation,[71] we find that inhibition of fibril elongation can be analysed along the lines of enzyme inhibition. However, the specific architecture of the fibril-end can lead to atypical inhibitor properties. We observed here that the substrate of the fibril elongation reaction can contribute to inhibition by stabilizing the enzyme-inhibitor complex.

3.7. Acknowledgement

This project has received funding from the European Research Council under the European Union's Horizon 2020 research and innovation program, grant agreement No. 726368. We thank Fabian Schmitz for technical assistance in validating and purifying some of the CC variants and Hamed Shaykhalishahi and Walfried Schneider for technical assistance in obtaining the CC variants.

3.8. Supplemental Information

3.8.1 Materials and Methods

αsynuclein variants plasmid preparation: CC48 and CC52 were generated by site directed mutagenesis.[234] To generate the CC49, CC50, WT-CC48, CC48-WT, and WT-WT constructs, the respective DNA sequences were obtained from Life Technologies. CC49 and CC50 were cloned into the pT7-7 vector using NdeI and HindIII restriction sites, whereas the remaining constructs were obtained using AQUA cloning.[292] The sequence for CC48-CC48 already cloned into pT7-7 was obtained from Genscript.

Preparation and transformation of chemically competent *E. coli* BL21(DE3): 20 ml 2YT medium (PanReac AppliChem ITW reagents, Darmstadt, Germany), with antibiotics if appropriate, was inoculated and grown overnight at 37 °C and 180 RPM. 1 ml of the overnight culture was used to inoculate 100 ml 2YT medium, which was then incubated at conditions identical to the overnight culture. When the 100 ml culture reached an OD_{600} of 0.4-0.5, the culture was divided into two and centrifuged at 2000 g for 20 min at 4 °C, after which the supernatant was discarded. The cell pellets were carefully resuspended in 10 ml containing 30 mM potassium acetate pH 5.8, 100 mM RbCl, 50 mM $MnCl_2$, 15 (v/v)% glycerol and incubated on ice for 5 min. Cells were centrifuged at 2000 g for 5 min at 4 °C, and the supernatant was discarded. The pellets were carefully resuspended in 1 ml 10 mM MOPS pH 6.5, 75 mM $CaCl_2$, 100 mM RbCl, 15 (v/v)% glycerol before the cells were pooled and incubated on ice for 30 min. Aliqouts of 50 µl were made, flashfrozen in liquid nitrogen, and placed at −80 °C.

Transformation of chemically competent cells: 50 µl chemically competent cells (see above) were thawed on ice, for 10 min before 10–100 ng plasmid was added to the cells, and the sample was mixed by gently flicking the tubes. Sample was incubated on ice for 10 min before the sample was mixed again by gently flicking the tube. The sample was placed at 42 °C for 60 s and then immediately transferred to ice for 2 min. 450 µl SOC medium (2 (w/v)%, tryptone, 0.5 (w/v)% yeast extract, 10 mM NaCl, 2.5 mM KCl, 10 mM $MgCl_2$, 10 mM $MgSO_4$, 20 mM glucose) was added to the sample, that was then placed at 37 °C and 800 RPM for 1 h. 100 µl sample was spread on a LB medium (PanReac AppliChem ITW reagents, Darmstadt, Germany) with 1.5 % agar plate inside a Petri dish.

Preparation of expression system: pT7-7 plasmids encoding the α-synuclein variants were used to transform chemically competent *E. coli* BL21(DE3) cells, that had previously been transformed with the pNatB vector. The pNatB vector encodes for the NatB complex [293] which acetylates amino termini of eukaryotic proteins having the N-terminal amino acid sequence MD. Transformation of chemically competent cells was performed (see above). Glycerol stocks were prepared of all variants by thoroughly mixing 500 µl of overnight culture with 500 µl 60 % glycerol.

Protein expression and purification:

Expression of α-synuclein variants: Expression was performed similar to a previously established protocol.[215, 294] 50 ml autoclaved 2YT medium, supplemented with 100 µg ml^{-1} ampicillin and 35 µg ml^{-1} chloramphenicol, was inoculated with 20 µl *E. coli* BL21(DE3) glycerol stock. The 50 ml culture was left overnight at 37 °C and 160 RPM. 5 ml of the overnight culture was used to inoculate 0.5 L culture of identical composition as the overnight culture and placed at 37 °C at 110 RPM. Cultures were grown until OD_{600} reached 1 before IPTG was added to a final concentration of 1 mM to induce expression, that was carried out for 4 h without changing incubation conditions. Cells were pelleted by centrifugation at 5000 g for 20 min at 4 °C after which the supernatant was removed. Cells from 0.5 L were resuspended in 7.5–10 ml MilliQ water before being placed at −20 °C for storage.

Purification of α-synuclein variants: Purification was performed similar to previously established protocols. [215, 294] The resuspended cell pellet was thawed at ∼ 50 °C before lysis was performed by sonication using a Sonopuls UW 3200 (Bandelin, Berlin, Germany) sonicator with a MS72 probe for 10 min at 35 % maximal amplitude in pulses of 5 s on, 3 s off. The cell lysate was placed at 99 °C for 5 min with frequent vortexing. The lysate was cleared by centrifugation at 13 600 g for 30 min at 4 °C before transferring the supernatant to a clean 50 ml tube. Precipitation was done by dropwise addition of a 4 M solution of $(NH_4)_2SO_4$ to a final concentration of 1.75 M while gently stirring the sample; stirring was done for an additional 3 min before sample was placed on ice for ∼ 10 min. Pelleting was performed by centrifugation at 13 600 g for 20 min at 4 °C before the supernatant was discarded and the pellet was placed at −20 °C. The pellet was resuspended in 3 ml of 25 mM Tris:Cl pH 8 placed inside a Slide-a-lyzer dialysis cassette with a capacity of 3–12 ml and molecular weight cutoff of 3.5 kDa (Thermo Scientific, Rockford IL, USA) and dialysed against 1.4 L of the same buffer for at least 1.5 h. The dialysed sample was loaded onto a 5 ml HiTrap Q HP anion exhange chromatography column (GE Healthcare, Uppsala, Sweden), connected to an Äkta Purifier (GE Healthcare, Uppsala, Sweden). In case of the dimeric constructs, 10 M Urea in 50 mM Tris:Cl pH 8 was loaded onto the column and incubated for 0.5 h. The bound protein was eluted using a linear gradient of NaCl from 0–500 mM (using a buffer containing 25 mM Tris:Cl pH 8, 0.8 M NaCl) where the protein usually began eluting when the conductivity was in the 30–40 mS cm^{-1} range and fractions were collected until the ratio of absorbance at 280 nm and 260 nm reached ∼ 1. The fractions that corresponded to the peak from the anion exchange chromatography was pooled and $(NH_4)_2SO_4$ was added to a final concentration of 1.75 M and the sample was left on ice for 10 min before being centrifuged at 13 600 g for 20 min at 4 °C. The supernatant was discarded and the pellet was resuspended in up to 2.5 ml 20 mM MOPS pH 7.4, 50 mM NaCl depending on the size of the pellet. Size exclusion chromatography of the sample was performed by loading the samples onto a Superdex 75 increase 10/300 or a Hiload Superdex 75 16/600 pg. 1.5 ml centred at an elution volume of 12 ml or 8 ml centred at 58 ml was collected for Superdex 75 increase 10/300 and Hiload Superdex 75 16/600 pg respectively.

α-synuclein concentration determination: Absorbance in the 340–240 nm range was measured with an UV-VIS Spectrophotometer V-650 (JASCO, Pfungstadt, Germany) on a 1:4 dilution of the samples. Concentration was determined using an extinction coefficient defined by the number tyrosine residues times 1400 M^{-1} cm^{-1} at 275 nm (*i.e.* 1400 M^{-1} cm^{-1} for the hairpin peptides, 5600 M^{-1} cm^{-1} for the monomeric constructs, and 11 200 M^{-1} cm^{-1} for dimeric constructs) subtracting the signal at 320 nm.

Elongation assays using Tht fluorescences: All experiments were performed in 96-well half area assay plates, non-binding surface, black with clear bottom, polystyrene, (REF 3881), from Corning (Kennebunk ME, USA). Furthermore, the outermost wells were never used for samples. Water was added to the empty wells in the immediate vicinity of samples, and the plate was sealed with sealing tape, clear polyolefin (232701) from Thermo Scientific (Rochester NY, USA). Assays were performed on a FLUOstar Omega or Clariostar (BMG Labtech, Ortenberg, Germany) using 12-point orbital averaging with at diameter of 3 mm using bottom optics and a settling time of 1.0 s between measuring each well. Measurements were done every 100 s for the first 100 cycles, subsequent measurements were done every 360 s. For the FLUOstar Omega, a Thioflavin T filter with excitation at 448 nm (10 nm bandwidth) and emission at 482 nm (10 nm bandwidth) was used, and a gain of 800 employed. For the Clariostar, the monochromator was set to excitation at 440 nm (15 nm bandwidth) and emission at 485 nm (20 nm bandwidth), and a gain of 750 was employed.

All assays were performed using 25 µM Thioflavin T UltraPure Grade (Anaspec Inc., Fremont CA, USA) and the reaction buffer was 20 mM MOPS, 50 mM NaCl pH 7.4, and 0.04 % NaN_3. Unless otherwise stated, the samples were prepared at room temperature without seeds to a volume of 90 µl and placed onto the plate. The plate was then sealed and placed at 37 °C inside the plate reader for 10–20 min for temperature equilibration. The seal was removed and seeds injected by manually pipetting 10 µl seed solution (see below) into the relevant wells. The final seed concentration was then 2.5 µM in monomer equivalents. The plate was resealed placed in the plate reader again and measurements carried out. The injection procedure took less than five minutes.

Seed preparation: Seeds were prepared in the same reaction buffer as in Tht fluorescences experiments (see above). Seeds were prepared either by incubating 25 µM WT monomer in a 1.5 ml Eppendorf tube at 37 °C with an added glass bead of 2.85–3.45 mm at 800 RPM for at least 3 days. Alternatively, fibrils from previous elongation experiments were diluted to 25 µM in monomer equivalents. The fibrils were sonicated twice using a UP200St sonicater with a VialTweeter (Hielscher Ultrasound Technology, Teltow, Germany) at 20 s at 70 % maximum amplitude. The VialTweeter did not lead to a high degree of reproducibility of the absolute rates even when fibrils were prepared identically (data not shown), however, it has the advantage of working with closed and sealed tubes, thereby minimising formation of aerosols.

Gel electrophoresis of monomer and fibrils: Samples of 80 µl were spun at 16 100 g for 30 min using a tabletop centrifuge. 70 µl was removed without disturbing the pellet and the remaining 10 µl was mixed with 70 µl 9 M urea to dissolve the pellet. The pellet samples were then diluted fivefold by additional 9 M urea. 10 µl sample (diluted pellet or undiluted supernatant) was mixed with reducing SDS loading buffer (2 mM dithiothreitol, 2 % SDS, 8 % glycerol, 0.05 % bromophenol blue, 0.05 M Tris:Cl pH 6.8), and incubated for 1 h at room temperature. Samples were loaded onto a Tris/glycine/SDS buffer (Bio-Rad, Feldkirchen, Germany) 15 % polyacrylamide gel made from Rothiphorese 30 (37.5:1) (Carl Roth) and cast on. Gel electrophoresis was performed on a Mini-PROTEAN Tetra System (Bio-Rad, Feldkirchen, Germany), and the gels were stained using SERVA Blue R (equivalent to Coomassie brilliant blue R-250) (SERVA, Heidelberg, Germany). Transilluminated images of the gels were recorded on a ChemiDoc MP* (Bio-Rad, Feldkirchen, Germany), using the standard coomassie filter. The images were exported as 16-bit images (export for analysis feature), lanes were marked and plotted using the Gel Analyzer tool from ImageJ, and the baseline subtracted area of the peaks corresponding to $\sim$ 15 kDa bands were extract from each lane excluding the marker lane.

Atomic force microscopy (AFM): Endpoint samples of several kinetic experiments where inhibitor dependency was investigated were prepared for AFM by first transferring the entire content of the wells into clean 1.5 ml Eppendorf tubes. From these tubes, 10 µl (25 µM in WT monomer equivalents in reaction buffer) was placed on freshly cleaved mica and incubated for 10–20 min. Samples were then washed by careful addition of 100 µl dH_2O that was immediately removed, a procedure that was repeated five times. Samples were dried under a gentle stream of nitrogen. AFM was performed on a Bruker Mulitmode 8 (Billerica, Massachusetts, USA) using ScanAsyst-Air cantilevers (Camarillo, California, USA) using the ScanAsyst PeakForce tapping mode in air. The data was imported into Gwyddion and background correction was performed by aligning rows using the median.

3.8.2 Determination of IC_{50} and the ratio that halves the relative initial rate

The IC_{50} values were done by fitting, using the package scipy.optimize, the normalised (and averaged if applicable) initial slopes, y, with the known inhibitor concentration, x, to the function:

$$y = \frac{y_{\max} - y_{\min}}{1 + \left(\frac{x}{\mathrm{IC}_{50}}\right)^{n}} + y_{\min} \tag{3.1}$$

Where $y_{\max}$ and $y_{\min}$ are the initial and final plateau values, respectively, and n is the slope factor. Of the four obtained values, only the IC_{50} values are reported. The reported errors are obtained by the taking the square-root of the diagonal elements of the covariance matrix returned by the fitting procedure. To obtain ratios (and errors), the IC_{50} values were divided with the WT monomer concentration (25 µM).

3.8.3 Modelling of the mechanisms of inhibition

In order to understand which chemical mechanism would be able to explain the observed inhibition of CC mutants, we tested different models of amyloid growth. Regardless of the exact inhibition model, it was assumed that:

- The total concentration of fibril-ends does not change during the initial elongation (or indeed throughout the growth reaction).
- The total concentration of fibril ends is much smaller than WT monomer concentration.
- The free WT monomer concentration remains constant and equal to the total monomer concentration during the initial elongation.
- The free inhibitor concentration remains constant and equal to the total inhibitor concentration during the initial elongation.

What follows is a description of how the models of growth and inhibition can de derived and which assumptions are used in doing so.

Competitive inhibition (FI) model: Tentative similarities between fibril elongation kinetics and enzyme kinetics have previously been suggested. In particular, non-linear dependency of the elongation rate at the high concentration monomer regime have been observed for several amyloidogenic including α-synuclein and a dock-lock models have been proposed for others.[70, 71, 211, 272, 295, 296] As noted earlier, this could potentially be explained by a

Michaelis–Menten like mechanism. Although linearity in monomer concentration was observed here (in the absence of inhibitor), the underling elongation mechanism could still be susceptible to Michaelis–Menten inhibition types known from enzyme kinetics. The CC mutants are almost identical to monomer, so it would not be too surprising if they could still bind to the fibril-end, but, due to their alteration in a region that is commonly found in the fibril core [42, 220, 221, 222, 223, 277], not be able to convert into a fibrillar conformation. This would block the end from growth until dissociation occurred. Such a mechanism would be equivalent to the Competitive Inhibition (CI) model from enzyme kinetics, more precisely:

$$\begin{array}{ccccc} F_n + M & \underset{}{\overset{K_m}{\rightleftharpoons}} & F_nM & \xrightarrow{k_+} & F_{(n+1)} \\ + & & & & \\ I & & & & \\ \Big\| K_i & & & & \\ F_nI & & & & \end{array}$$

F_n denotes a fibril-end of length n. however, it is assumed that all ends are equivalent, therefore the length will be omitted in the model derivations. M is free WT monomer, F_nM is the complex of a WT monomer bound to a fibril-end but not yet incorporated, K_m is the dissociation constant of WT monomer binding, k_+ is the reaction rate whereby a bound monomer gets incorporated, I is free inhibitor, FI is the unproductive complex between inhibitor and fibril-end, and K_i is the dissociation constant of inhibitor complex formation. Following the formalism from [297], the observed rate of fibril growth is given by conversion of F_nM:

$$r = k_+[FM] \tag{3.2}$$

It is assumed that both complexes are at equilibrium with dissociations constants given by:

$$K_m = \frac{[F][M]}{[FM]} \tag{3.3a}$$

$$K_i = \frac{[F][I]}{[FI]} \tag{3.3b}$$

Conservation of mass for the fibril-end is given by:

$$[F]_T = [F] + [FM] + [FI] \tag{3.4}$$

Deriving the observed elongation rate as function of total monomer, inhibitor, and fibril-end concentration is:

$$\begin{aligned}\frac{r}{[F]_T} &= \frac{k_+[FM]}{[F]+[FM]+[FI]} \\ &= \frac{k_+\frac{[F][M]}{K_m}}{[F]+\frac{[F][M]}{K_m}+\frac{[F][I]}{K_i}} \\ r &= \frac{R_{\max}[M]}{[M]+K_m\left(1+\frac{[I]}{K_i}\right)}, \quad R_{\max}=k_+[F]_T\end{aligned} \tag{3.5}$$

As it is possible to achieve the same total fibril-end concentration within one experiment but difficult to reproduce between different experiments, internal controls where no inhibitor is present can be used to normalise the data.

$$\begin{aligned}\frac{r}{r_0} &= \frac{\frac{R_{\max}[M]}{[M]+K_m\left(1+\frac{[I]}{K_i}\right)}}{\frac{R_{\max}[M]}{K_m+[M]}} \\ &= \frac{K_m+[M]}{[M]+K_m\left(1+\frac{[I]}{K_i}\right)}\end{aligned} \tag{3.6}$$

This model is enough to capture the decreasing relative rate when keeping the WT monomer concentration constant and increasing the inhibitor concentration. In order to understand if it can explain the monomer dependency as well, the limits of Equation 3.6 with respect to WT monomer concentration can be investigated:

$$\frac{r}{r_0} \to 1 \text{ as } [M] \to \infty \tag{3.7a}$$

$$\frac{r}{r_0} \to \frac{1}{1+\frac{[I]}{K_I}} \text{ as } [M] \to 0 \tag{3.7b}$$

From this it is clear that Equation 3.6 cannot explain the WT monomer dependency as Equation 3.6 would approach 1 at high WT monomer concentration, and not what is observed namely a monotonic decrease in relative rate with increasing WT monomer concentrations.

Cooperative inhibition (FIM) model: In order to be able to explain the increase in efficiency of the inhibitor as a function of monomer concentration, we modified the model from above by introducing a species where inhibitor, WT monomer, and fibril-end form a ternary inhibitory complex:

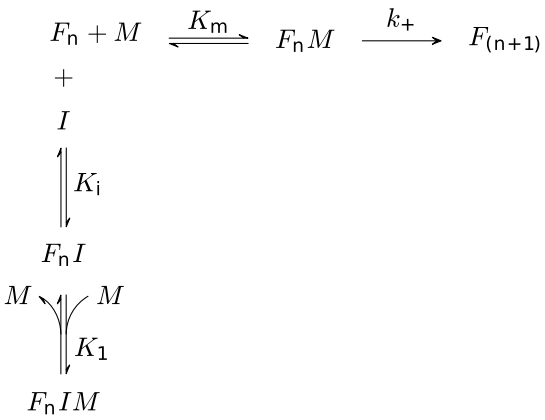

It is assumed that all species are at equilibrium and the dissociation constants and concentrations are given by:

$$K_m = \frac{[F][M]}{[FM]} \tag{3.8a}$$

$$K_i = \frac{[F][I]}{[FI]} \tag{3.8b}$$

$$K_1 = \frac{[FI][M]}{[FIM]} = \frac{[F][I][M]}{K_i[FIM]} \tag{3.8c}$$

Conservation of mass of the fibril-ends now reads:

$$[F]_T = [F] + [FM] + [FI] + [FIM] \tag{3.9}$$

As before, the growth rate is proportional $[FM]$:

$$r = k_+[FM] \tag{3.10}$$

Dividing r by the total concentration of fibril-ends and performing substitutions using Equation 3.9, Equation 3.8:

$$\begin{aligned}
\frac{r}{[F]_T} &= \frac{k_+[FM]}{[F] + [FM] + [FI] + [FIM]} \\
&= \frac{k_+ \frac{[F][M]}{K_m}}{[F] + \frac{[F][M]}{K_m} + \frac{[F][I]}{K_i} + \frac{[F][I][M]}{K_iK_1}} \\
r &= \frac{R_{\max}[M]}{K_m\left(1 + \frac{[I]}{K_i}\right) + [M]\left(1 + \frac{[I]K_m}{K_iK_1}\right)}, \quad R_{\max} = k_+[F]_T
\end{aligned} \tag{3.11}$$

Again, normalising to total fibril-end concentration:

$$\begin{aligned}\frac{r}{r_0} &= \frac{\frac{R_{\max}[M]}{K_m\left(1+\frac{[I]}{K_i}\right)+[M]\left(1+\frac{[I]K_m}{K_iK_1}\right)}}{\frac{R_{\max}[M]}{K_m+[M]}} \\ &= \frac{K_m+[M]}{K_m\left(1+\frac{[I]}{K_i}\right)+[M]\left(1+\frac{[I]K_m}{K_iK_1}\right)}\end{aligned} \tag{3.12}$$

Which has the limiting behaviour with respect to WT monomer concentration:

$$\frac{r}{r_0} \to \frac{1}{1+\frac{[I]K_m}{K_iK_1}} \text{ as } [M] \to \infty \tag{3.13a}$$

$$\frac{r}{r_0} \to \frac{1}{1+\frac{[I]}{K_i}} \text{ as } [M] \to 0 \tag{3.13b}$$

Which, contrary to Equation 3.6, is capable of capturing a decrease in relative rate with increasing WT monomer if $K_m > K_1$. This is however not the only requirement that needs to be satisfied. The non-relative (raw) rate first increases and then decreases at increasing WT monomer concentration in presence of inhibitor. Equation 3.11 is a monotonically increasing function with respect to monomer and therefore cannot capture this aspect.

Three-step inhibition (FIMM) model: In order to explain the increase in rate with WT monomer concentration followed by a decrease, we extended the FIM model by introducing an additional inhibitory species formed by binding of an additional WT monomer to the ternary (FIM) complex:

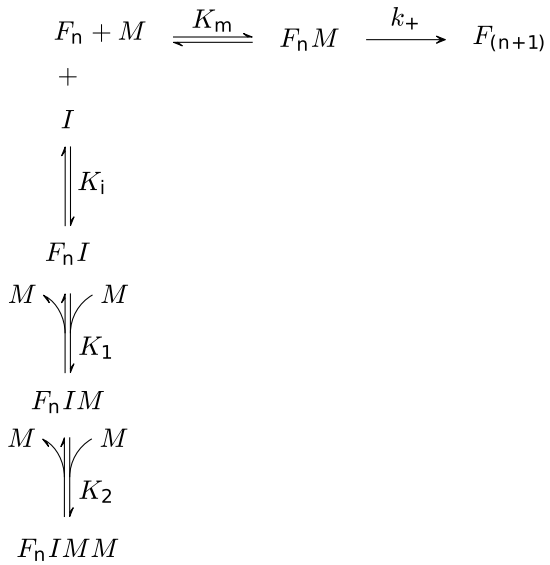

It is assumed that the binary $[FI]$, ternary $[FIM]$, as well as the quaternary complex $[FIMM]$ have reached equilibrium and the dissociation constants, K_1 and K_2 can be defined:

$$K_m = \frac{[F][M]}{[FM]} \tag{3.14a}$$

$$K_i = \frac{[F][I]}{[FI]} \tag{3.14b}$$

$$K_1 = \frac{[FI][M]}{[FIM]} = \frac{[F][I][M]}{K_i[FIM]} \tag{3.14c}$$

$$K_2 = \frac{[FIM][M]}{[FIMM]} = \frac{[F][I][M][M]}{K_i K_1[FIMM]} \tag{3.14d}$$

Conservation of mass of the fibril-ends now reads:

$$[F]_T = [F] + [FM] + [FI] + [FIM] + [FIMM] \tag{3.15}$$

As before, the growth rate is proportional to $[FM]$:

$$r = k_+[FM] \tag{3.16}$$

Dividing r by the total concentration of fibril-ends and performing substitutions using Equation 3.15 and Equation 3.14:

$$\begin{aligned}
\frac{r}{[F]_T} &= \frac{k_+[FM]}{[F] + [FM] + [FI] + [FIM] + [FIMM]} \\
&= \frac{k_+ \frac{[F][M]}{K_m}}{[F] + \frac{[F][M]}{K_m} + \frac{[F][I]}{K_i} + \frac{[F][I][M]}{K_i K_1} + \frac{[F][I][M][M]}{K_i K_1 K_2}} \\
r &= \frac{R_{\max}[M]}{K_m\left(1 + \frac{[I]}{K_i}\right) + [M]\left(1 + \frac{[I]K_m}{K_i K_1} + [M]\frac{[I]K_m}{K_i K_1 K_2}\right)}
\end{aligned} \tag{3.17}$$

Again, normalising to total fibril-end concentration:

$$\begin{aligned}
\frac{r}{r_0} &= \frac{\frac{R_{\max}[M]}{K_m\left(1 + \frac{[I]}{K_i}\right) + [M]\left(1 + \frac{[I]K_m}{K_i K_1} + [M]\frac{[I]K_m}{K_i K_1 K_2}\right)}}{\frac{R_{\max}[M]}{K_m + [M]}} \\
&= \frac{K_m + [M]}{K_m\left(1 + \frac{[I]}{K_i}\right) + [M]\left(1 + \frac{[I]K_m}{K_i K_1} + [M]\frac{[I]K_m}{K_i K_1 K_2}\right)}
\end{aligned} \tag{3.18}$$

The limiting behaviour is given by:

$$\frac{r}{r_0} \to 0 \text{ as } [M] \to \infty \tag{3.19}$$

$$\frac{r}{r_0} \to \frac{1}{1+\frac{[I]}{K_i}} \text{ as } [M] \to 0 \tag{3.20}$$

This limiting relative rate behaviour is similar to the FIM model (see Equation 3.13, and therefore is also able to describe the WT monomer dependency of inhibition. Additionally the growth rate given by the FIMM model (see Equation 3.17), contrary to the corresponding one in the FIM model(see Equation 3.11) potentially have extrema, which, if they exists, can be found where $\frac{\partial r}{\partial m} = r'([M]) = 0$ for constant $[I]$. In order to do this, the following substitutions are made:

$$\begin{aligned}
&x = [M] && a = R_{\max} && b = K_m\left(1+\frac{[I]}{[K_i]}\right)\\
&c = \frac{[I]K_m}{K_iK_1} && d = \frac{[I]K_m}{K_iK_1K_2}\\
&g = ax && h = b+x+xc+dx^2 && r([M]) = y
\end{aligned} \tag{3.21}$$

Which leads to:

$$\begin{aligned}
y &= \frac{g}{h}\\
y' &= \frac{g'h-gh'}{h^2}\\
y' &= \frac{a\left(b+x+cx+dx^2\right)-ax(1+c+2dx)}{h^2}\\
y' &= \frac{ab-adx^2}{h^2}\\
0 &= ab-adx^2\\
x &= \pm\sqrt{\frac{b}{d}}
\end{aligned} \tag{3.22}$$

This means that there exists an extremum in the positive WT monomer concentration range, which is located at:

$$\begin{aligned}
[M]_{\max} &= \sqrt{\frac{K_m\left(1+\frac{[I]}{[K_i]}\right)}{\frac{[I]K_m}{K_iK_1K_2}}}\\
&= \sqrt{K_1K_2\left(\frac{K_i}{[I]}+1\right)}
\end{aligned} \tag{3.23}$$

We're only interested in the positive solutions as x represents concentrations.

Three-step uncompetitive inhibition (uFIMM) model: An alternative to the FIMM model that has somewhat similar qualitative behaviour is an uncompetitive model where the inhibitor does not bind to the fibril-end before a fibril-end monomer complex has formed:

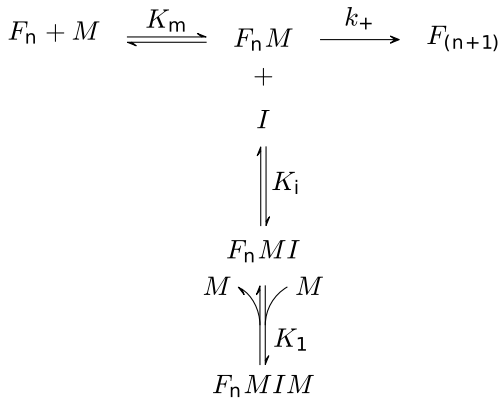

It is assumed that the binary $[FI]$, ternary $[FMI]$, as well the quaternary complex $[FMIM]$ have reached equilibrium and the dissociations K_i and K_1 can be defined:

$$K_m = \frac{[F][M]}{[FM]} \tag{3.24a}$$

$$K_i = \frac{[FM][I]}{[FMI]} = \frac{[F][M][I]}{K_m[FMI]} \tag{3.24b}$$

$$K_1 = \frac{[FMI][M]}{[FMIM]} = \frac{[F][M][I][M]}{K_i K_m[FMIM]} \tag{3.24c}$$

Conservation of mass of the fibril-ends now reads:

$$[F]_T = [F] + [FM] + [FMI] + [FMIM] \tag{3.25}$$

As before, the growth rate is proportional $[FM]$:

$$r = k_+[FM] \tag{3.26}$$

Dividing r by the total concentration of fibril-ends and performing substitutions using Equation 3.25 and Equation 3.24:

$$\begin{aligned}\frac{r}{[F]_T} &= \frac{k_+[FM]}{[F] + [FM] + [FMI] + [FMIM]} \\ &= \frac{k_+ \frac{[F][M]}{K_m}}{[F] + \frac{[F][M]}{K_m} + \frac{[F][M][I]}{K_m K_i} + \frac{[F][I][M]^2}{K_m K_i K_1}} \\ &= \frac{R_{\max}[M]}{K_m + [M]\left(1 + \frac{[I]}{K_i}\left(1 + \frac{[M]}{K_1}\right)\right)}\end{aligned} \tag{3.27}$$

Normalising to total fibril-end concentration:

$$\begin{aligned}\frac{r}{r_0} &= \frac{\dfrac{R_{\max}[M]}{K_m + [M]\left(1 + \frac{[I]}{K_i}\left(1 + \frac{[M]}{K_1}\right)\right)}}{\frac{R_{\max}[M]}{K_m + [M]}} \\ &= \frac{K_m + [M]}{K_m + [M]\left(1 + \frac{[I]}{K_i}\left(1 + \frac{[M]}{K_1}\right)\right)}\end{aligned} \tag{3.28}$$

The limiting behaviour is given by:

$$\frac{r}{r_0} \to 0 \text{ as } [M] \to \infty \tag{3.29}$$

$$\frac{r}{r_0} \to 1 \text{ as } [M] \to 0 \tag{3.30}$$

3.8.4 Supplementary figures and data

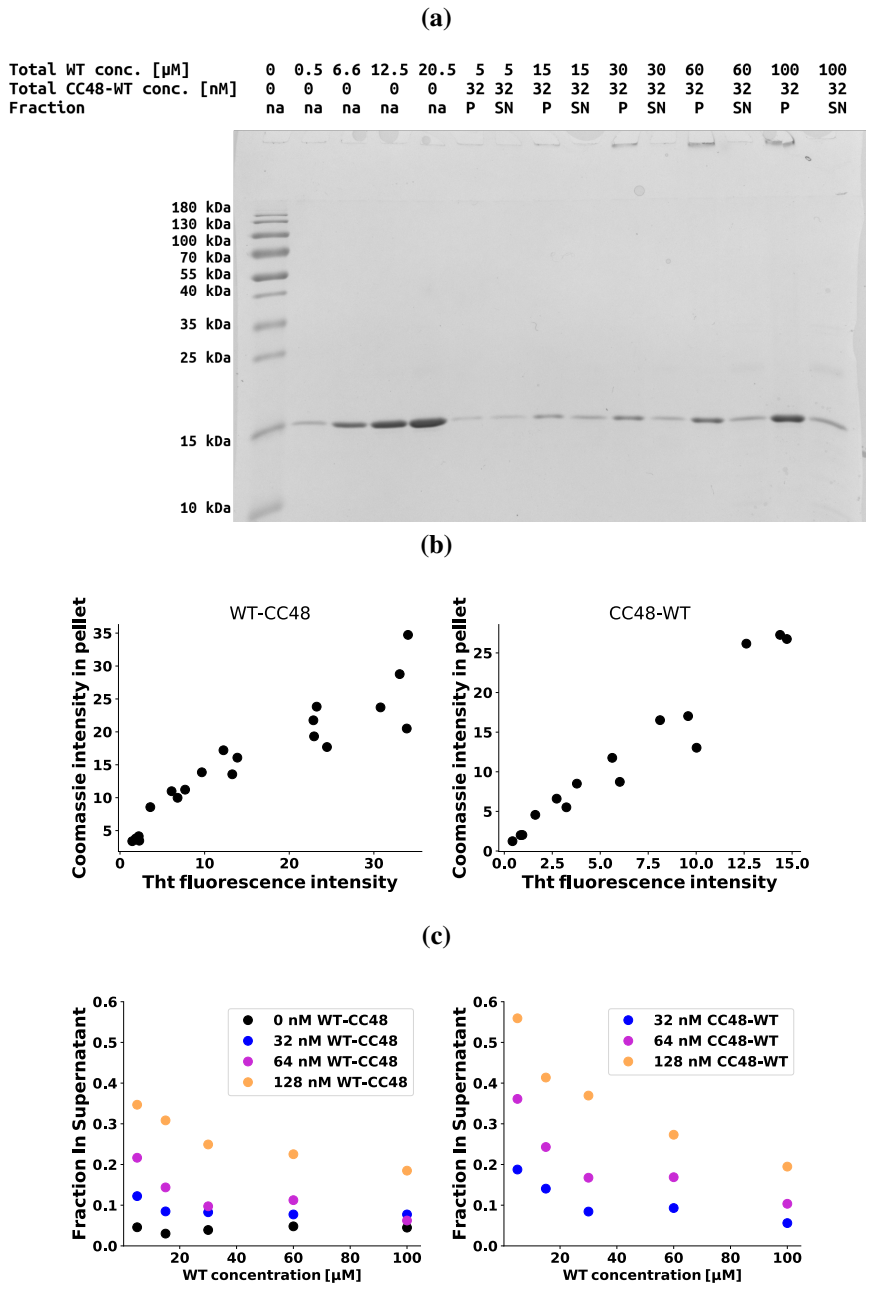

Figure 3.5: Validation of elongation conditions. (a) Example of a stained SDS-PAGE gel after a WT monomer dependency experiment in the presence of 32 nM CC48-WT. P and SN indicate pellet and supernatant fractions, respectively. Note that P was diluted five times with respect to the SN (see Materials and Methods above). (b) Correlation between band intensities corresponding to the pellet fractions of the coomassie stained gel vs. the average of the last ten measured points of the Tht fluorescence time traces shown in the last rows of Figure 3.22 and Figure 3.24 respectively. Note that the correlation is better at lower Tht signal/monomer concentrations. (c) The fraction $\frac{SN}{SN+5P}$,*i.e.*, monomer left in solution after aggregation of different concentrations of inhibitor and WT monomer.

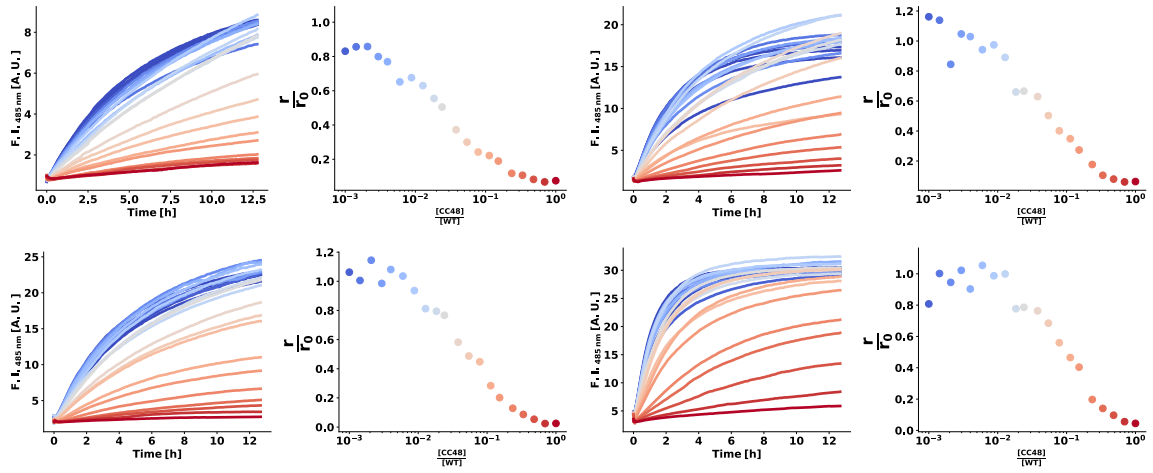

Figure 3.6: CC48 dependency of WT fibril elongation. Four independent experiments of Tht fluorescence over time of 25 µM WT monomer, 2.5 µM fibril seeds, with varying concentration of CC48, as well as the extracted relative elongation rates. Concentrations are plotted on a logarithmic x-axis, hence the 0 µM samples are not shown.

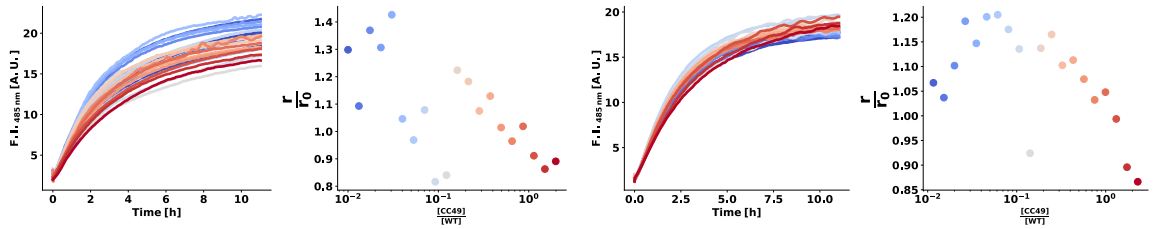

Figure 3.7: CC49 dependency of WT fibril elongation. Two independent experiments of Tht fluorescence over time of 25 µM WT monomer, 2.5 µM fibril seeds, with varying concentration of CC49, as well as the extracted relative elongation rates. Concentrations are plotted on a logarithmic x-axis, hence the 0 µM samples are not shown.

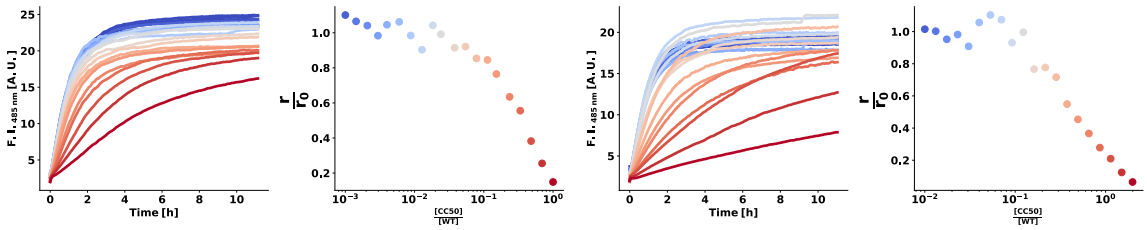

Figure 3.8: CC50 dependency of WT fibril elongation. Two independent experiments of Tht fluorescence over time of 25 µM WT monomer, 2.5 µM fibril seeds, with varying concentration of CC50, as well as the extracted relative elongation rates. Concentrations are plotted on a logarithmic x-axis, hence the 0 µM samples are not shown. Note that different concentrations of CC50 was used in the two repeats.

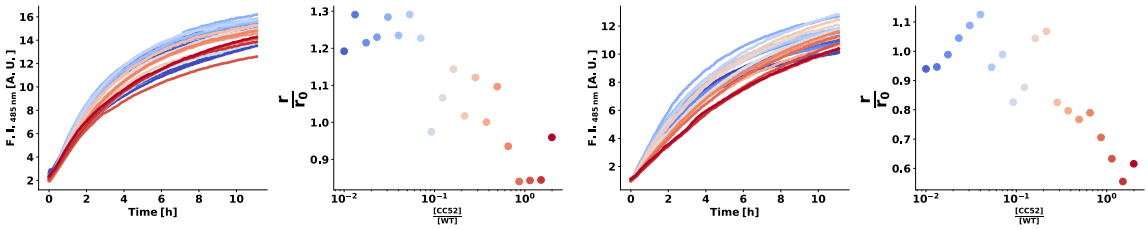

Figure 3.9: CC52 dependency of WT fibril elongation. Two independent experiments Tht fluorescence over time of 25 µM WT monomer, 2.5 µM fibril seeds, with varying concentration of CC52, as well as the extracted relative elongation rates. Concentrations are plotted on a logarithmic x-axis, hence the 0 µM samples are not shown.

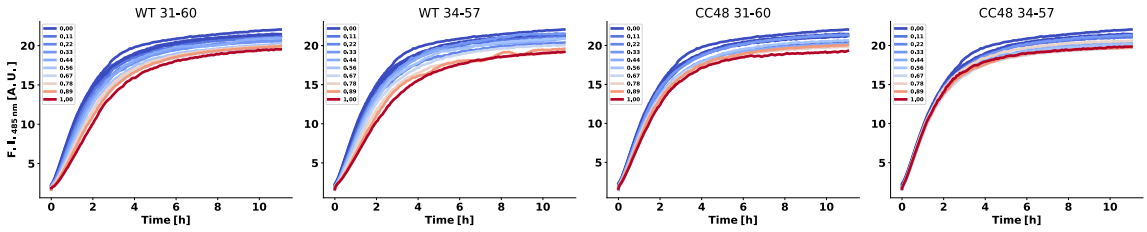

Figure 3.10: Hairpin peptide dependency of WT fibril elongation. Tht fluorescence over time of 25 µM WT monomer with varying concentration of peptide, the sequence of which is indicated above the plot using the numbering from the parent protein. The legend shows the concentrations as the ratio between hairpin peptide and the WT monomer concentration.

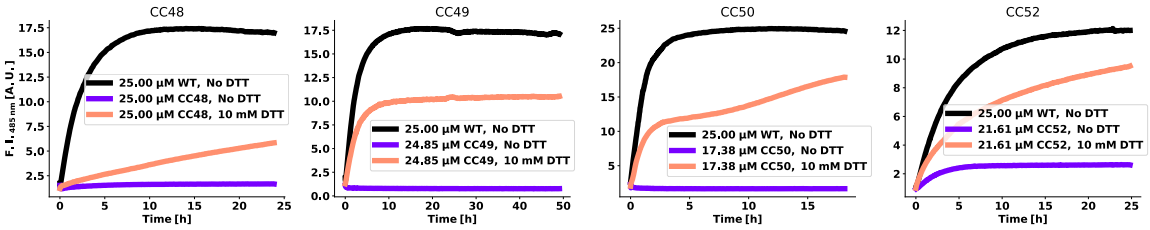

Figure 3.11: DTT dependent incorporation of CC variants. Tht fluorescence over time of seeds in the presence of: WT monomer, CC variant, or CC variant with the reducing agent DTT. The specific CC variant is indicated above each plot, and the concentrations used are indicated in the legends.

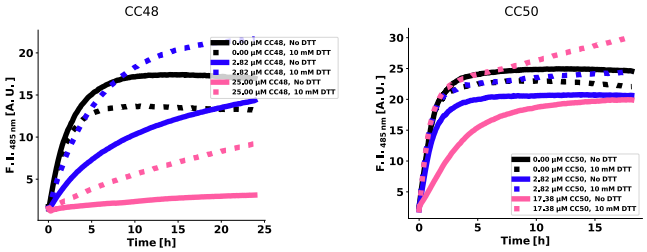

Figure 3.12: DTT dependency of inhibition of WT fibril elongation. Tht fluorescence over time of WT filbril seeds in the presence of WT monomer and CC variant, either with or without the reducing agent DTT. The specific CC variant is indicated above each plot, and the concentrations used are indicated in the legends.

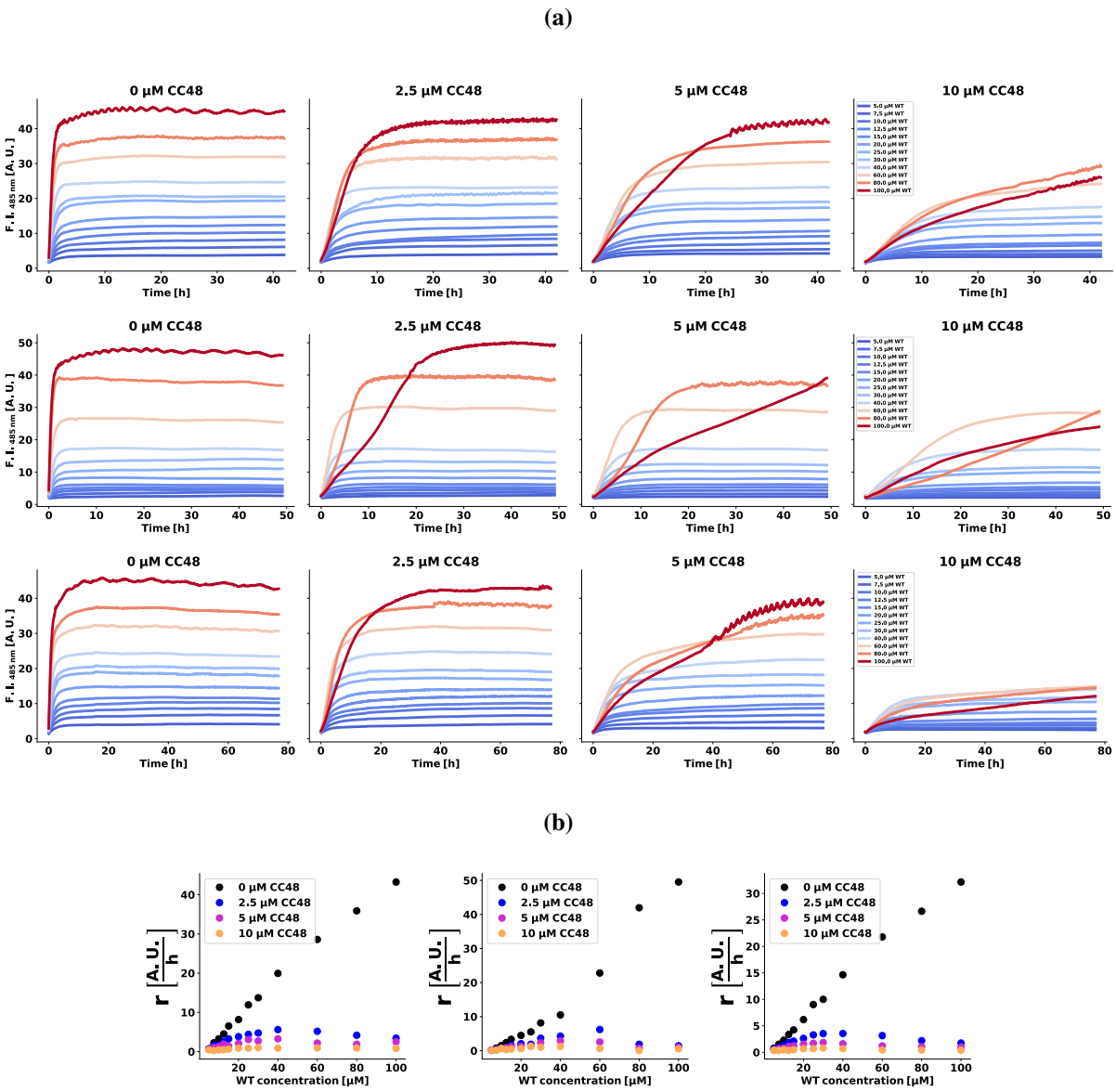

Figure 3.13: WT monomer dependency of the inhibitory activity of CC48 on WT fibril elongation. (a) Three independent experiments of Tht fluorescence of 2.5 µM WT fibril seeds over time in the presence of fixed CC48 concentrations with a varying concentration of WT monomer indicated in the panels on the right. (b) The initial rates extracted from (a), note that this figure is shown in the main manuscript as well, shown here for completeness.

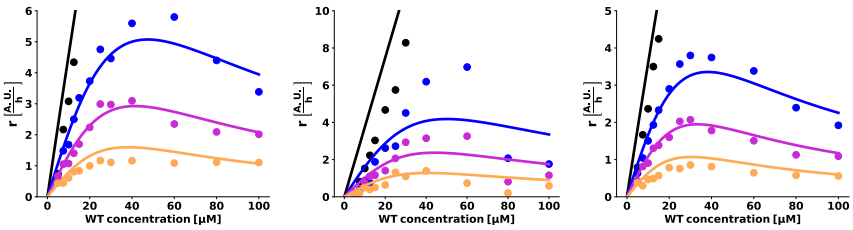

Figure 3.14: Fitting CC48 to FIMM model. Zoom-in and fit of the initial rates for the three independent experiments shown in Figure 3.13b. Note that left panel is also shown in the main manuscript.

Dataset #	K_m [10^{-4} M]	K_i [10^{-6} M]	K_1 [10^{-1} M]	K_2 [10^{-9} M]	$R_{\max}$ [10^{-4} M]
1	5.5 ± 1.9	2.2 ± 0.41	$8.8 \pm 1.8 * 10^{-13}$	1.4 ± 0.37	2.6 ± 0.75
2	$2.1 * 10^2 \pm 5.3 * 10^5$	2.0 ± 2.43	$3.7 \pm 9.6 * 10^4$	$3.7 \pm 9.6 * 10^4$	$7800 \pm 200 * 10^5$
3	4.0 ± 0.86	2.4 ± 0.44	$9.2 \pm 2.3 * 10^{-14}$	0.82 ± 0.22	1.5 ± 0.27

Table 3.1: CC48 FIMM fitting parameters. The parameters extracted from fitting using the package scipy.optimize with associated uncertainties in fitting. Note the large difference in the magnitude of parameters as well as the middle set being numerical very different from the other two sets.

3.8.5 Proxy initial slopes for dimeric constructs

For several of the dimeric constructs (see *e.g.* Figure 3.22, and Figure 3.24), a small kink in the initial growth phase was observed that became more prominent with increasing WT monomer concentration. Not only did it interfere with extraction of the initials slopes, it also raised the question if pure elongation was really what was seen in these experiments. It should be noted that the concentration of the dimeric constructs needed to induce inhibition was exceedingly low, in the nano molar range. Due to these low concentrations, it might take longer to establish the fibril-end-inhibitor equilibrium , giving rise to an initial burst growth phase. In order to test this, experiments were performed where the dimers and fibril-end were pre-incubated together before addition of WT (Figure 3.15). This pre-incubation led to disappearance of the initial kink. In order to get some "initial" slope, extraction of slopes were done after these kinks and compared to the initial slopes from the pre-incubation experiments performed at the same concentrations WT monomer, fibril seeds, and dimers (Figure 3.16). As the two kinds of slopes was in good agreement, the slopes extracted after the initial growth bursts was used as a proxy for initial slopes.

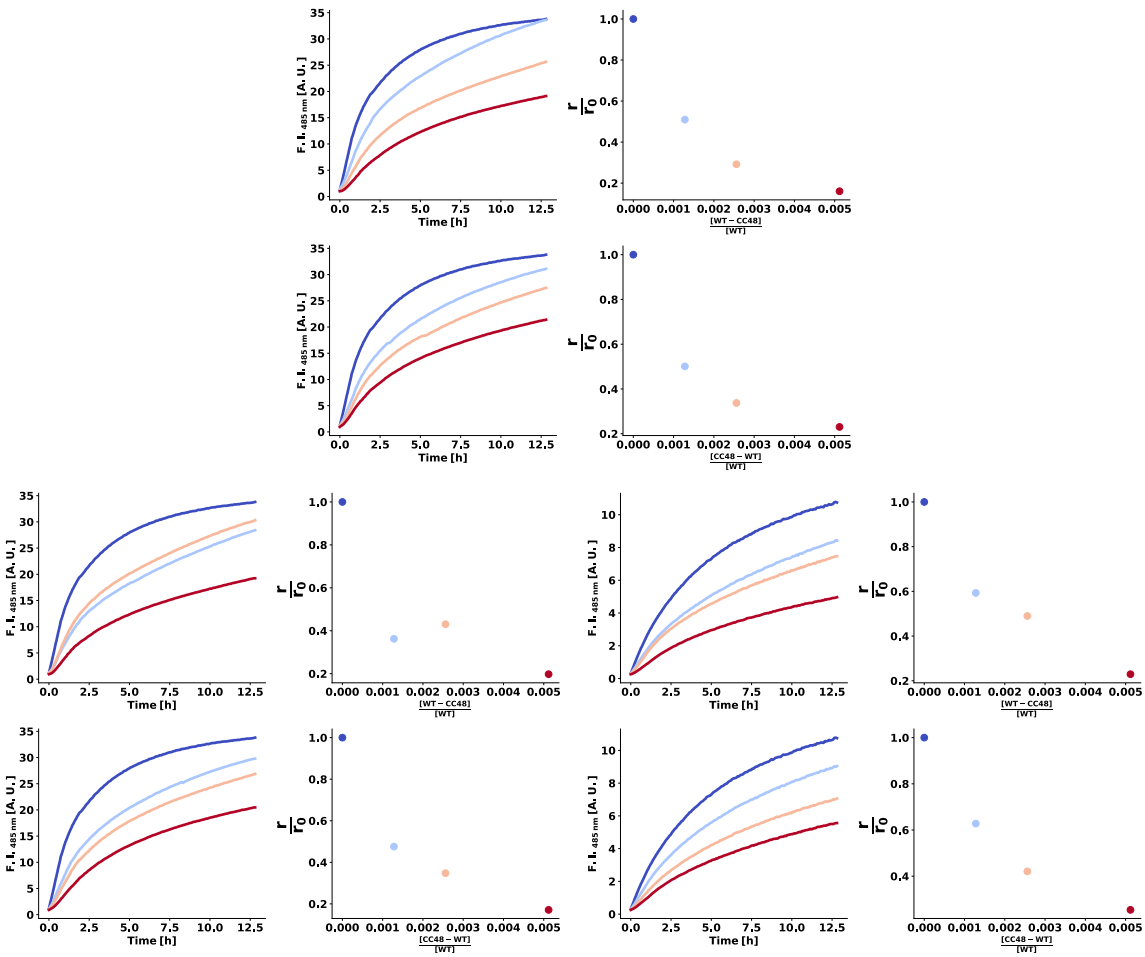

Figure 3.15: Pre-incubation of seeds and dimer. Three independent experiments of Tht fluorescence over time and relative initial rates using a fixed concentration of 100 µM WT monomer that was mixed with 2.5 µM seeds that had been pre-incubated with different concentrations of WT-CC48 and CC48-WT dimers.

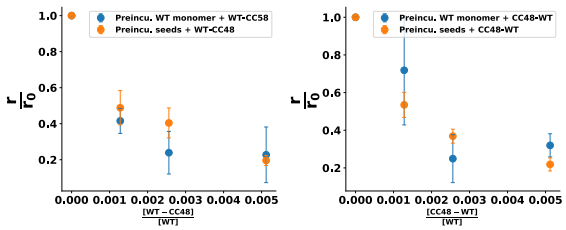

Figure 3.16: Direct initial slope *vs.* pre-incubation. Comparison between average initial rates from experiments where WT fibril seeds and inhibitor were pre-incubated (Figure 3.15), and where monomer and inhibitor were pre-incubated (Figure 3.23 and Figure 3.25).

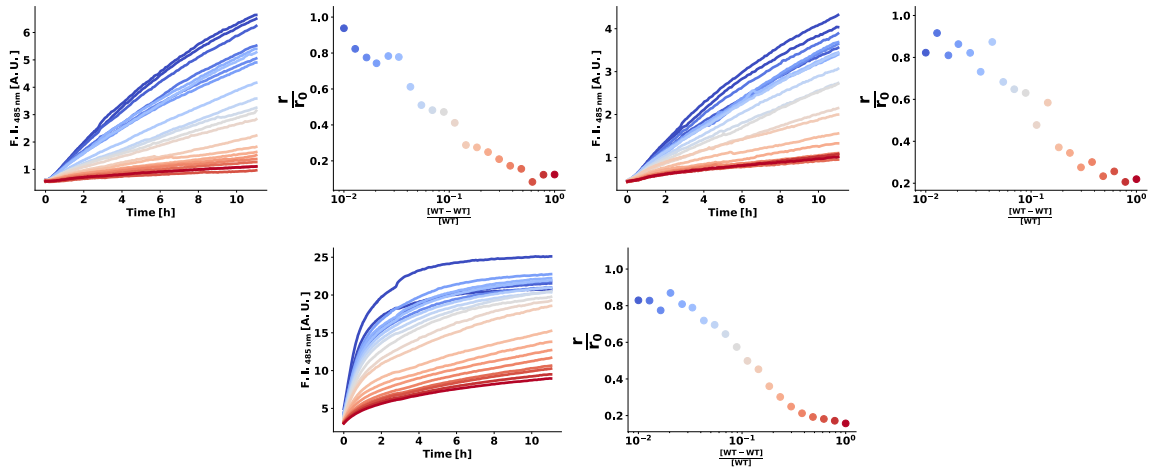

Figure 3.17: WT-WT dependency of WT fibril elongation. Three independent experiments of Tht fluorescence over time of 25 µM WT monomer, 2.5 µM fibril seeds, with varying concentration of WT-WT, as well as the extracted relative elongation rates. Concentrations are plotted on a logarithmic x-axis, hence the 0 µM samples are not shown.

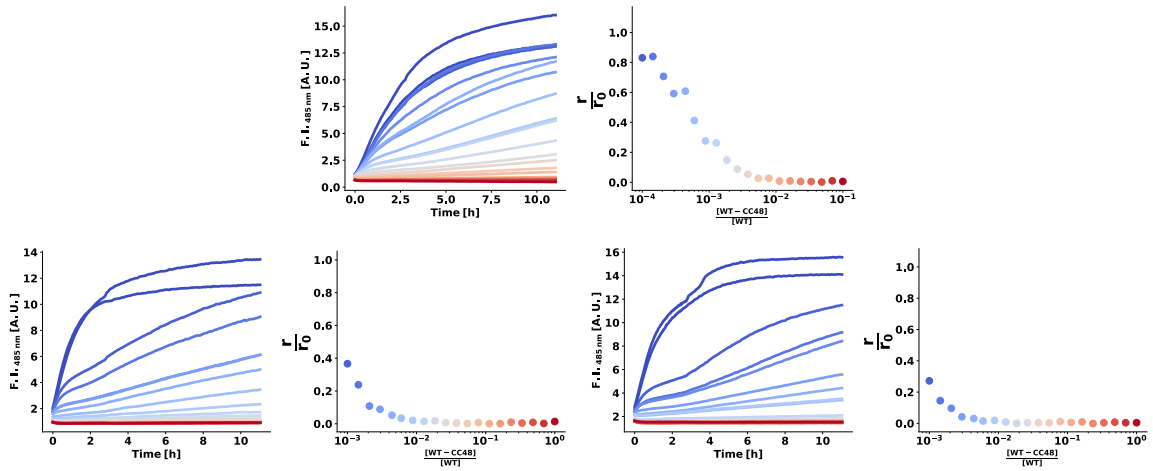

Figure 3.18: WT-CC48 dependency of WT fibril elongation. Three independent experiments of Tht fluorescence over time of 25 µM WT monomer, 2.5 µM fibril seeds, with varying concentration of WT-CC48, as well as the extracted relative elongation rates. Concentrations are plotted on a logarithmic x-axis, hence the 0 µM samples are not shown. Note that different concentrations of WT-CC48 was used in the different experiments.

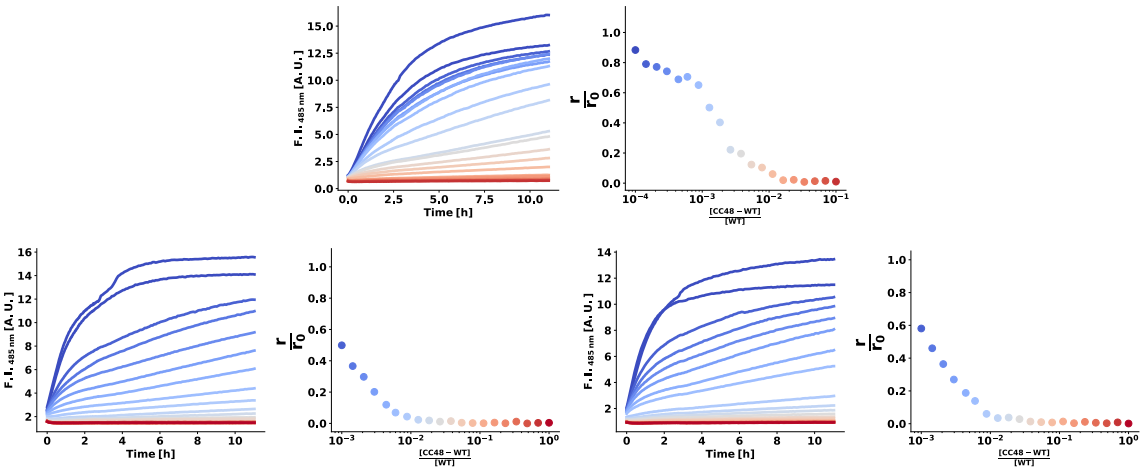

Figure 3.19: CC48-WT dependency of WT fibril elongation. Three independent experiments of Tht fluorescence over time of 25 µM WT monomer, 2.5 µM fibril seeds, with varying concentration of CC48-WT, as well as the extracted relative elongation rates. Concentrations are plotted on a logarithmic x-axis, hence the 0 µM samples are not shown. Not that different concentrations of CC48-WT was used in the different experiments.

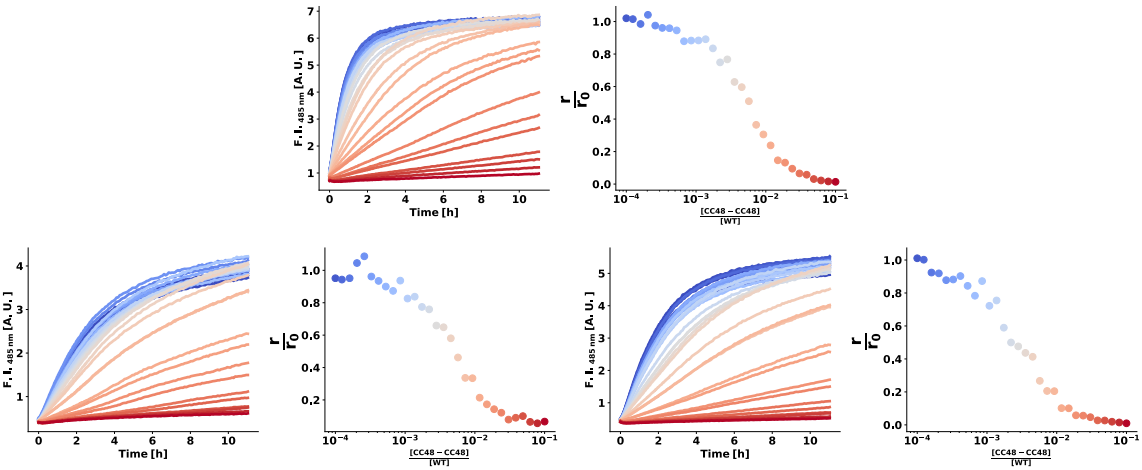

Figure 3.20: CC48-CC48 dependency of WT fibril elongation. hree independent experiments of Tht fluorescence over time of 25 µM WT monomer, 2.5 µM fibril seeds, with varying concentration of CC48-CC48, as well as the extracted relative elongation rates. Concentrations are plotted on a logarithmic x-axis, hence the 0 µM samples are not shown.

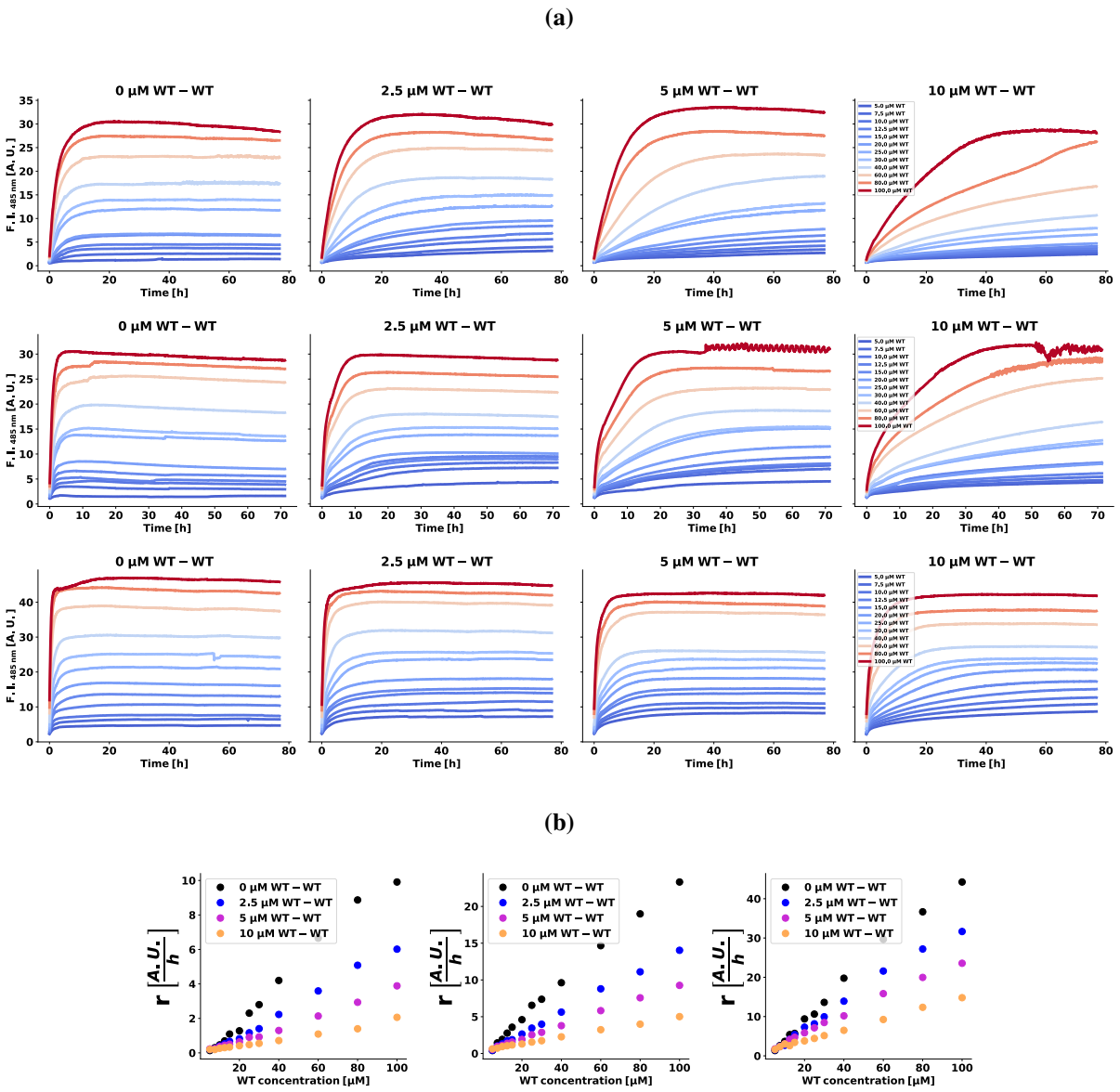

Figure 3.21: WT monomer dependency of the inhibitory activity of WT-WT inhibition on WT fibril elongation. (a) Three independent experiments of Tht fluorescence of 2.5 µM WT fibril seeds over time in the presence of fixed WT-WT concentrations with varying WT monomer concentrations indicated in the rightmost panels. (b) The initial rates extracted from (a).

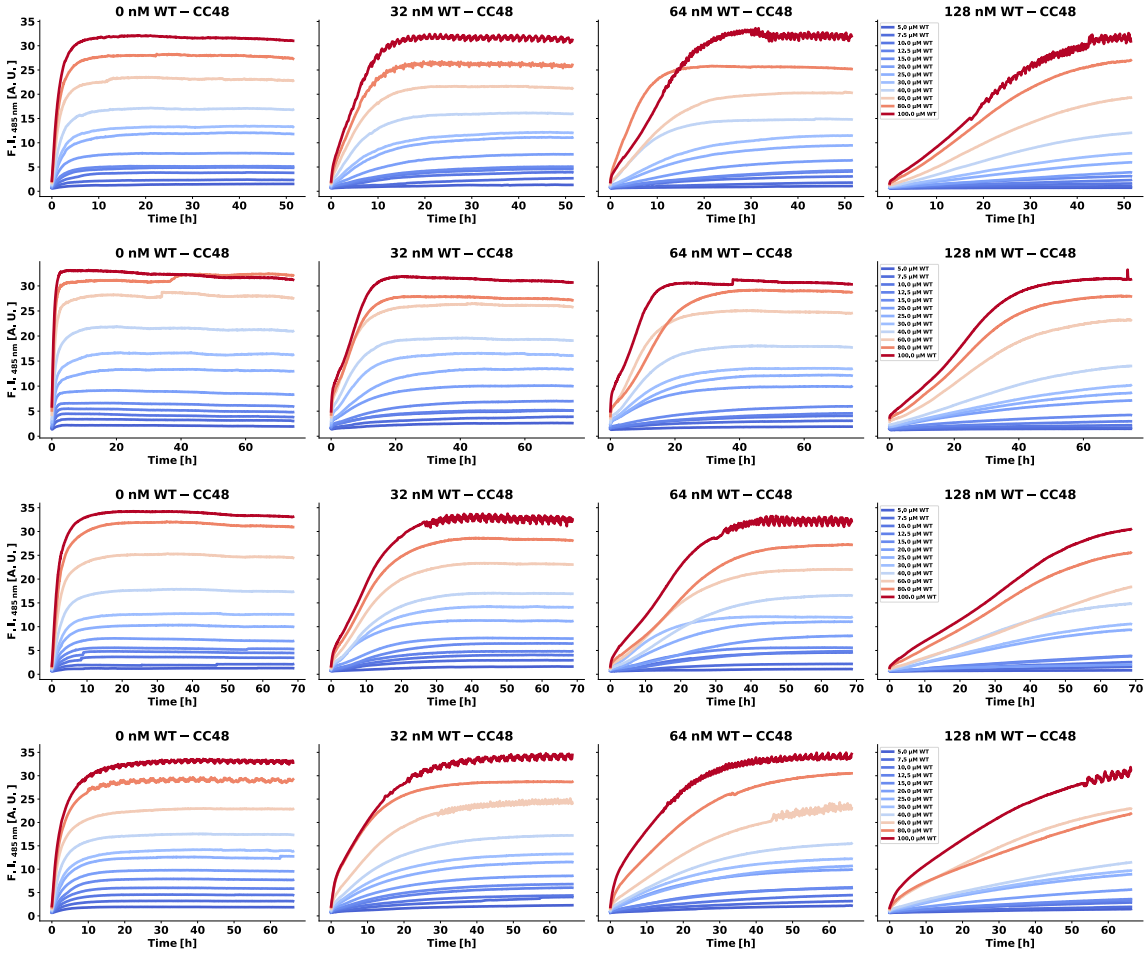

Figure 3.22: WT monomer dependency of the inhibitory activity of WT-CC48 inhibition on WT fibril elongation. our independent experiments of Tht fluorescence of 2.5 µM WT fibril seeds over time in the presence of fixed WT-CC48 concentrations with varying WT monomer concentrations indicated in the rightmost panels.

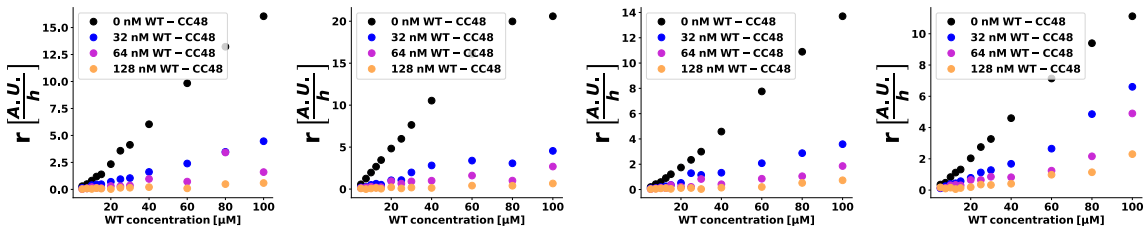

Figure 3.23: Initial rates of monomer dependency of WT-CC48 inhibition. The initial rates extracted from Figure 3.22.

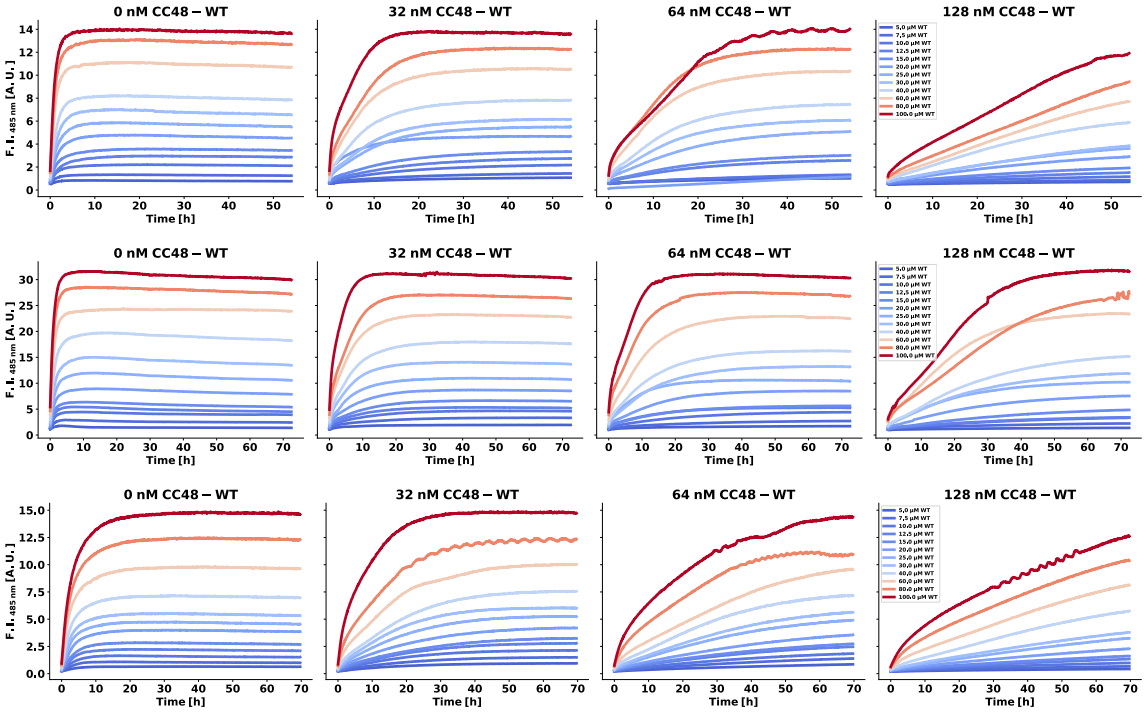

Figure 3.24: WT Monomer dependency of the inhibitory activity of CC48-WT inhibition on WT fibril elongation. Three independent experiments of Tht fluorescence of 2.5 µM WT fibril seeds over time in the presence of fixed CC48-WT concentrations with varying WT monomer concentrations indicated in the rightmost panels.

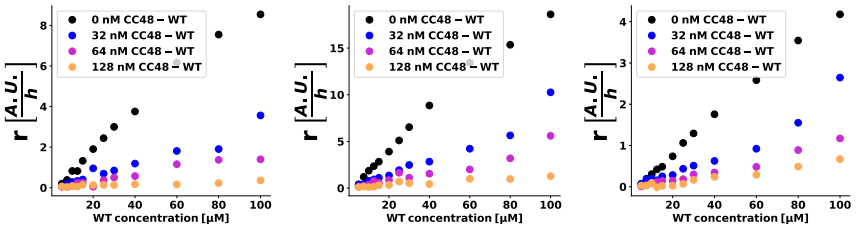

Figure 3.25: Initial rates of monomer dependency of CC48-WT inhibition. The initial rates extracted from Figure 3.24.

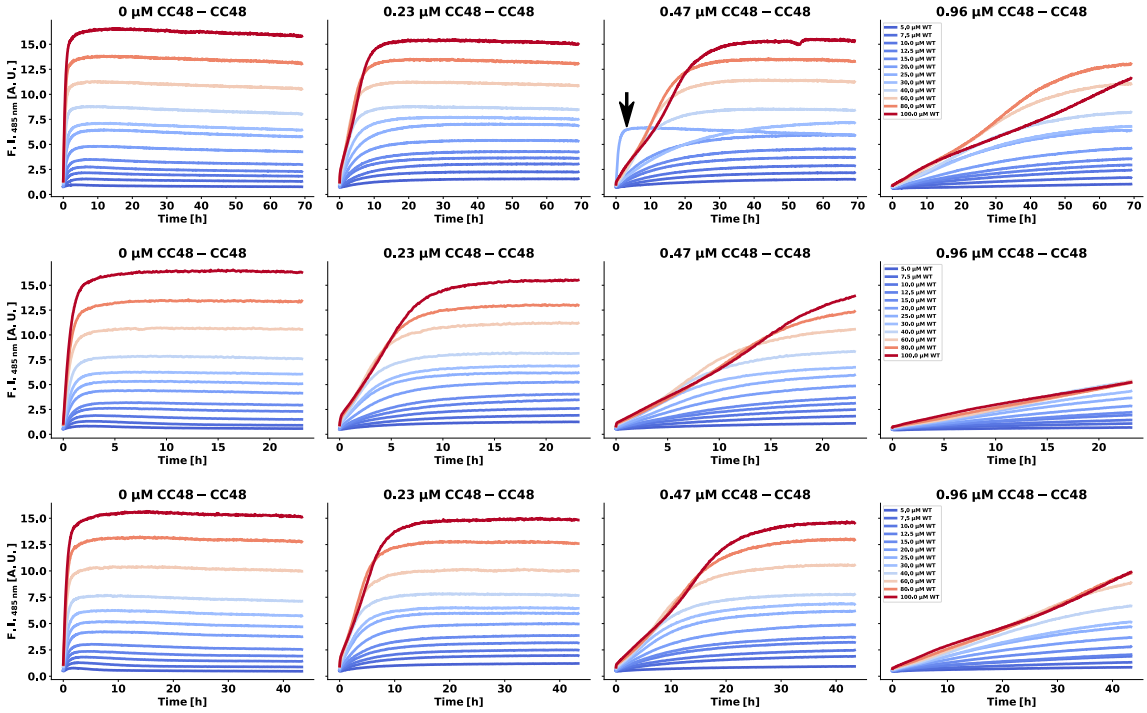

Figure 3.26: WT Monomer dependency of the inhibitory activity of CC48-CC48 inhibition on WT fibril elongation. Three independent experiments of Tht fluorescence of 2.5 µM WT fibril seeds over time in the presence of fixed CC48-CC48 concentrations with varying WT monomer concentrations indicated in the rightmost panels.

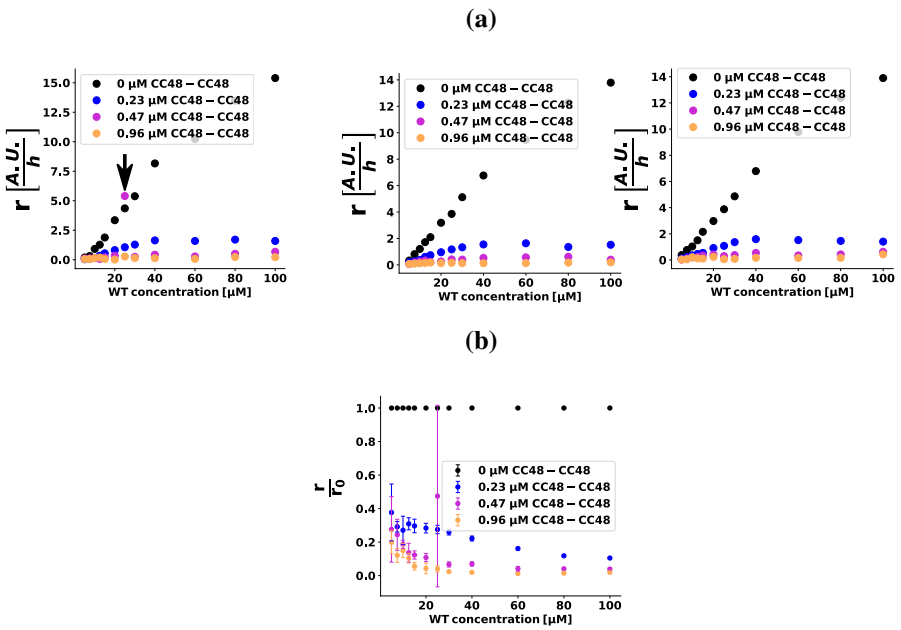

Figure 3.27: WT Monomer dependency of the inhibitory activity of CC48-CC48 inhibition on WT fibril elongation continued. (a) The initial rates extracted from Figure 3.26, where the black arrows points to an outlier. (b) Relative and averaged initial slope of the rates in (a).

4

STABILISING THE β-HAIRPIN OF α-SYNUCLEIN BY INCREASING β-TURN PROPENSITY

4.1. Introduction

The region of α-synuclein composed of residues 37-54 has been shown, as mentioned several time previously, to adopt a β-hairpin when bound to the inhibitor AS69. From a structural perspective, two β-strands connected by a short turn region is the simplest example of an antiparallel β-sheet. As mentioned earlier, CC48 was originally created to stabilise β-hairpin formation by forming a disulphide bridge. However, covalently linking the two strands might be considered a bit too invasive allow a claim that it is the transient β-hairpin conformation that is causing the difference between CC48 and WT. It could simply be that introducing a disulphide bridge prevents CC48 from adopting an amyloid structure as it places too severe constrains on a region that is commonly found in the fibril. This would be true in particular for the residues between the two cysteines. And indeed, all variants except CC52 did not elongate WT seeds unless a reducing agent was present (see chapter 3 for further details). However, the β-strands are not the only parts needed to form a β-hairpin, a turn is needed as well. In the AS69:WT complex, the part of the WT that forms a turn is residues 44-47 Figure 4.1.

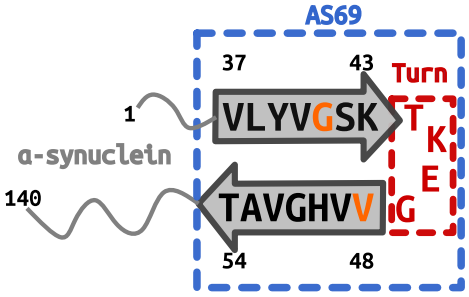

Figure 4.1: Schematic overview of α-synuclein β-hairpin. The β-hairpin that forms when α-synuclein (grey) is in complex with AS69 (blue rectangle). The β-strands (arrows) are connected by a turn (red rectangle). The sequence of the β-hairpin region is shown, and the residues that are changed to cysteines in CC48 are highlighted in orange.

β-turn type	φ(i+1)	ψ(i+1)	φ(i+2)	ψ(i+2)
1	-64	-27	-90	-7
1'	55	38	78	6
2'	60	-126	-91	1

Table 4.1: Overview β-turn types. The average dihedral angles of the β-turns most commonly observed in β-hairpins [299].

WT	β1	β1'	β2'	bad-turn
TKEG	TPDG	VNGK	SGNT	AAKP
	NPDG	YNGQ	YGNT	VAAM
	SPDT	TNGG	TGNG	VTMM
	SPNG	TYNG	TYGN	
		YNGK	SGDS	

Table 4.2: Overview of turn mutants. Sequence of residues 44-47 of the available constructs, and the β-turn class they should fall within. The mutants with in the bad-turn class should disfavour β-turn formation. The WT sequence is shown for comparison.

Although at least 11 types of turns occur naturally [298, 299], the turn connecting the two β-strands of naturally occurring β-hairpins in globular proteins are usually β-turns [280, 300]. β-Turns consist of four sequential residues (i, i+1, i+2, i+3) within hydrogen bonding distance of each other. They can be classified into nine different types depending on the dihedral angles (φ, ψ) of the residues (i+1) and (i+2) [298], *i.e.* the two residues in the middle of the turn. However, only three β-turn types are commonly observed in naturally occurring β-hairpins, namely type 1', 2' and to a lesser extent type 1 [280, 300]. The average dihedral angles of these three different β-turns are shown in Table 4.1.

The average dihedral angles observed in the turn region of the AS69 induced β-hairpin of WT α-synuclein at positions (i+1 = K45) and (i+2 = E46) are (-66, -43) and (-71, -35), respectively. These dihedral angles are not compatible with any of the most stabilising turn types. Rather than linking the regions forming β-strands together, as was the rational behind the CC48 mutant, the strategy here is to stabilise the β-hairpin by modifying the turn region, residues 44-47, to better stabilise β-hairpins. In particular the sequence of the turn region was changed to favour β-turns of the types 1, 1', 2', or low-turn forming propensity validated using the online software BEHAIRPRED [301] [1]. The mutants prepared are shown in Table 4.2.

[1] This software can be found at http://triton.rmn.iqfr.csic.es/software/behairpredv1.0/behairpred.htm, but citing it directly is not possible as a peer-reviewed article describing this software does not exist. It is therefore important to recognise that the correctness of this algorithm has not been properly validated and the classification is therefore at best tentative. The citation given is the article where it is first mentioned.

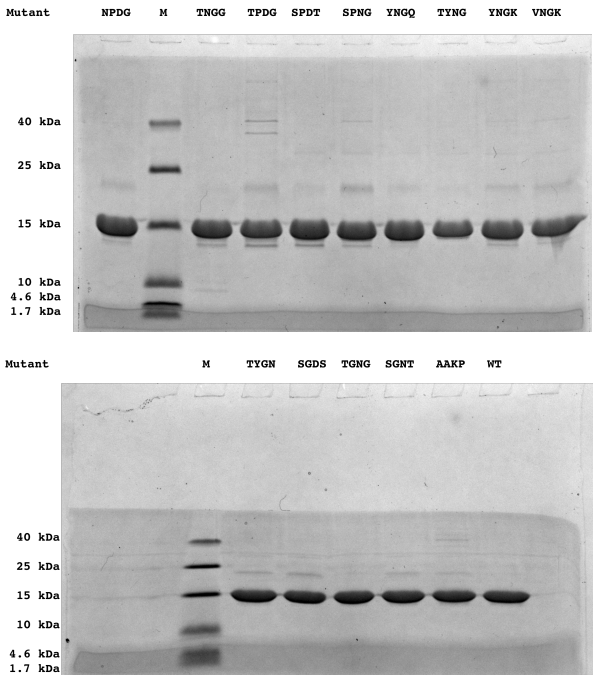

Figure 4.2: Testing the purity of β-turn variants. The obtainable β-hairpin variants run on a denaturing 15 % polyacrylamide gel in order to access their purity.

4.2. Results and discussion

4.2.1 Expression and purification considerations and issues

α-Synuclein have been shown to be N-acetylated *in vivo* [302]. In order to produce protein with as similar characteristics as possible, the β-hairpin mutants as well as WT was transformed into *E. coli* harbouring a plasmid with a version of N-acetyl transferase system (pNatB [293]) that should recognise the first two first amino acid residues of α-synuclein. Expression of most variants was possible, although repeated attempts to obtain VAAM and VTMM only resulted in a very small pellet after $(NH_4)_2SO_4$ precipitation, and further purification revealed that nothing in the expected size range could be obtained (data not shown). YGNT could be expressed, judging from the size of the $(NH_4)_2SO_4$ pellet, however, it repeatedly appeared to undergo gelation after resuspending the $(NH_4)_2SO_4$ precipitate and furthermore did not appear to be obtainable in monomeric form (data not shown). As a result, these three mutants were excluded from further analysis. SDS-PAGE was performed of the mutant after purification, on samples that had all been diluted to the same concentration, from where the purity was deemed acceptable Figure 4.2.

4.2.2 *De novo* aggregation suggested different classes

To understand if altering the turn region affected the aggregation propensity of the different mutants, a so-called *de novo* type aggregation experiment was performed. In this type of experiment, the mutants start out in monomeric form and amyloid formation was carried out under continuous shaking in the presence of a glass bead. These conditions, as mentioned in chapter 1, have the effect of enhancing fibrillation by disturbing the air-water interface, thereby increasing it and enhancing primary nucleation, but also by fragmentation due to mechanical

breaking of fibrils. The result of this experiment is shown Figure 4.3. It is noteworthy that all of the mutants were still able to aggregate, contrary to what was initially observed for CC48 [234]. However, especially the mutants that should adopt β1 namely TPDG, NPDG, SPDT, and SPNG all had a much longer lag-phase before aggregation began than the WT. This suggested that β-hairpin formation was occurring, with the β1 type turn might inhibit amyloid formation. However, it should be noted that a proline was introduced in the second position of all of them. All the naturally occurring prolines in α-synuclein is located in the non-aggregating C-terminus. This particular amino acid has a tendency to adopt both a cis and trans conformation in solution with almost equal probability. A large kinetic barrier slows down interconversion of these two conformations, a phenomenon that is known to be a limiting factor for protein folding [303]. In an amyloid, all incorporated monomers (on one filament) would be in the same conformation so it cannot be ruled out that this is not an example of the more well-known cis-trans isomerisation problem rather than β1-turn conformational dependent inhibition. All the remaining mutants that should adopt β1', β2', or not be able to form a turn, aggregated faster than the WT, which is in stark contrast to notion that stabilising a β-hairpins would inhibit aggregation directly. Although both β1', and β2' were faster than WT, a potential difference between the samples that should form β1' and β2' turns was that three out of five β2' forming mutants (SGNT, TGNG, TYGN) showed a rather prominent maximum that plateaued at a lower value. The faster aggregation of β1' and β2' suggests that the transient formation of these structures are not as inhibitory as the transient structures formed by the WT. Alternatively, both β1' and β2' might have higher nucleation rate as they potentially represent more direct on-pathway structures. As only one bad-turn mutant was available (AAKP), it is difficult to draw much from it being faster than the WT, although the difficulties in obtaining the other two (VAAM and VTMM) could be due to them being very aggregation prone. That the mutants unable to form β-turns (and therefore disfavour β-hairpins as well) might support the notion that WT might form transient inhibitory structures.

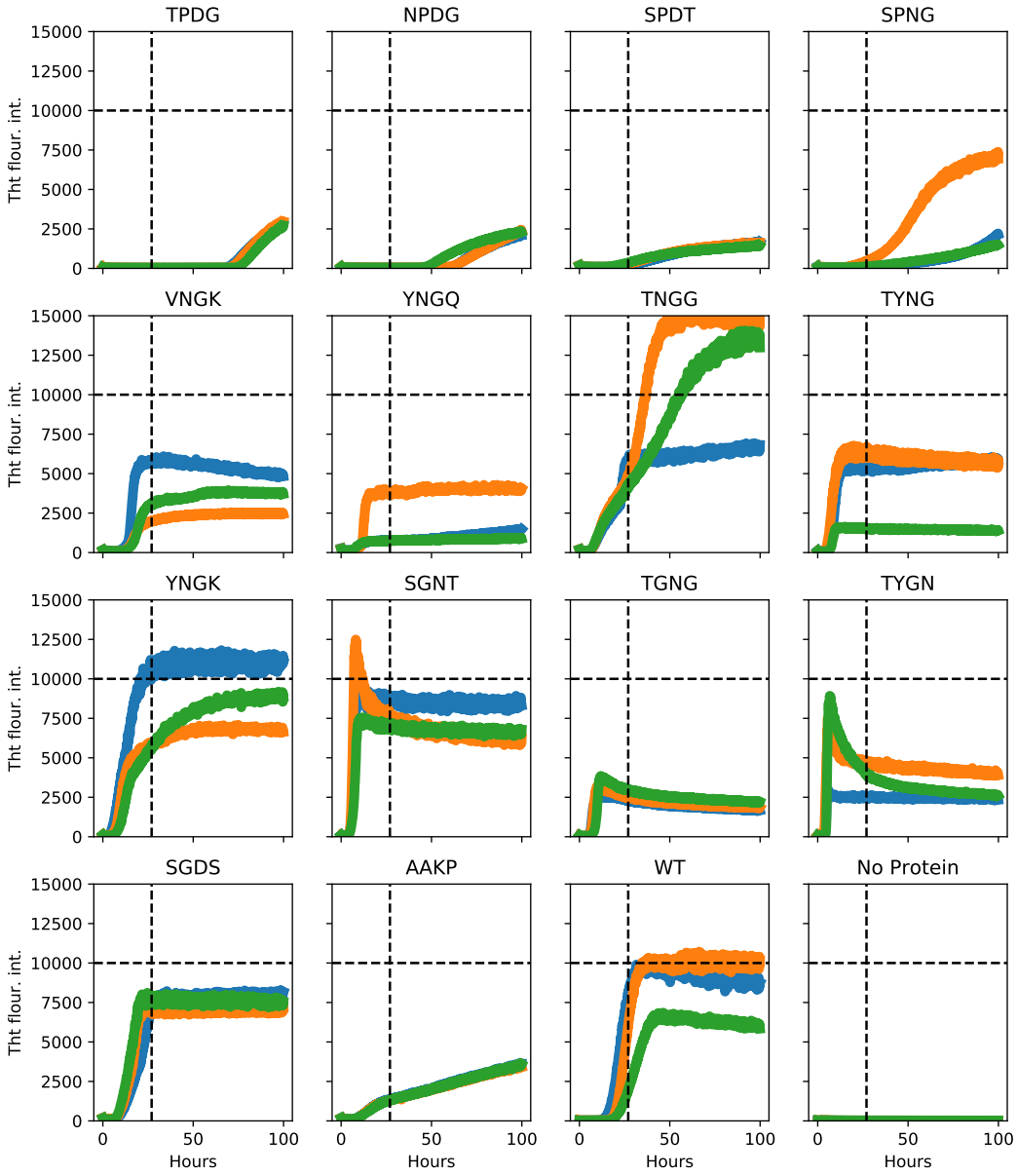

Figure 4.3: *De novo* aggregation of β-turn variants. Tht fluorescence as a function of time, where the mutant is indicated on top of each plot. The experiment was performed in triplicates for each mutant. The horizontal, and vertical lines are at the same x and y values in each plot and approximately corresponds to the final plateau value and time where final plateau value of the WT is reached, respectively.

4.2.3 β-turn variants exhibited large asymmetry in cross elongation with the WT

As mentioned in chapter 1, it can be difficult to obtain insights from *de novo* aggregation, especially when the shapes are as complicated as they are in Figure 4.3. Furthermore, performing *de novo* aggregation of each individual mutant on their own could potentially lead them to form their own particular fibril structures completely different from the WT, therefore making comparison to the WT, at best, challenging. In order to better understand if different fibril conformations of the different mutants, cross-seeding elongation type experiments were performed on β1, β1', β2', and WT. To account for any potential differences in elongation rates between different variants, self elongation of the mutants and WT was carried out as well. The results of the cross elongation experiment for the β1 variants are shown in Figure 4.4.

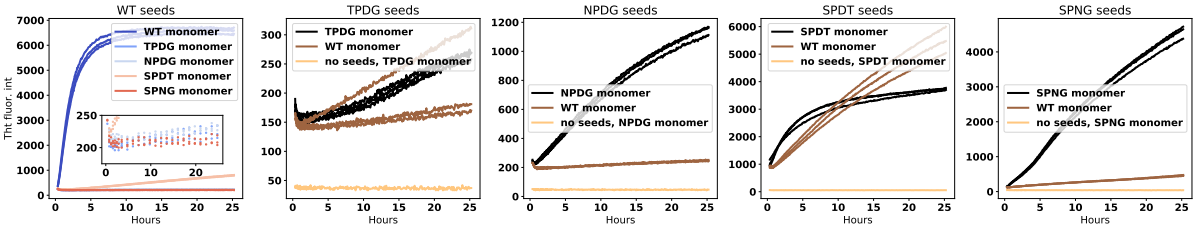

Figure 4.4: Cross-seeding experiment of β1. Tht fluorescence as a function of time, where the mutant from where the seeds were derived is indicated on top of each plot, and the legend indicates which mutant monomer was used.

Looking at the ability of the β1 mutants to elongate WT, only SPDT was able to elongate the WT seeds. On the hand, WT seemed capable of elongating all of the β1 mutant seeds, although at severely reduced rates, with the fastest elongation seen for SPDT seeds. This at least suggest that different amyloids are formed by the β1 mutants with respect the WT, perhaps with the exception of SPDT, but that the WT had greater flexibility to elongate these types of fibrils. Note the symmetry seen for β1 mutants where the fastest mutant to elongate WT seeds, SPDT, also gave rise to seeds that were fastest elongated by the WT. Performing this same type of experiment on the β1' mutants gave very different results as shown in Figure 4.4.

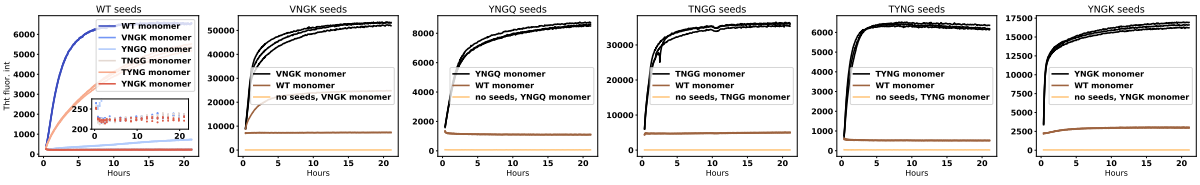

Figure 4.5: Cross-seeding experiment of β1'. Tht fluorescence as a function of time, where the mutant from where the seeds were derived is indicated on top of each plot, and the legend indicates which mutant monomer was used.

For the β1' mutants, TYNG and YNGQ were able to elongate the WT seeds. However, WT was only able to elongate YNGK seeds consistently (one of the WT triplicates was able to elongate VNGK). This seemed to suggest that the β1' formed different amyloid structures as compared with WT, and also different from the β1 mutants as well, as WT was able to elongate most β1 mutants but not most β1'. It is peculiar that there is no overlap between which β1' mutants can elongate WT seeds and which β1' mutants that can be elongated by WT monomer. This is in contrast to the symmetry seen for β1. This asymmetry became even more apparent when cross seeding experiments were performed on the β2' mutants as shown in Figure 4.6.

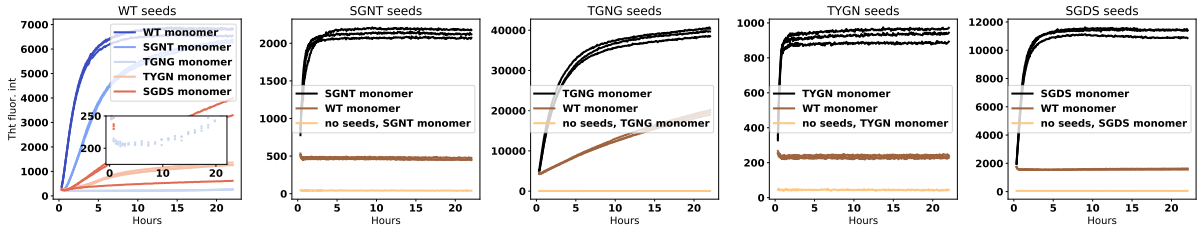

Figure 4.6: Cross-seeding experiment of β2'. Tht fluorescence as a function of time, where the mutant from where the seeds were derived is indicated on top of each plot, and the legend indicates which mutant monomer was used.

For the β2' mutants, all of them except TGNG were able to elongate the WT seeds as can be seen in Figure 4.6. TGNG seeds were, however, the only β2' mutant ones that could be elongated by the WT. This is as asymmetric as it can get in terms of cross elongation.

It should be noted that in all cases, self elongation of any mutant or WT was relatively speaking the fastest process compared to cross elongation. From a thermodynamic vantage-point it would not be too surprising to see a different equilibrium monomer concentration when performing cross elongation experiments. The reason being that the tight packing into amyloid of a particular protein sequence might not accommodate the side chains of even a slightly different sequence in the same conformation equally well. It is however not clear why the relative kinetics of cross elongations were all reduced compared to their self elongating counterparts.

An earlier cross elongation study on familial (point) mutations in the turn region (E46K), second β-strand region (H50Q,G51D,A53T) or outside the β-hairpin entirely (A30P) saw similar phenomena as observed here, although somewhat less prominent of an effect [153]. In their study, all of the mutants except G51D were able to elongate WT seeds at a similar rate to the WT. However that did not mean that WT elongated all the mutant seeds equally fast and especially elongation of H50Q, G51D, and to some degree, E46K were reduced. In a single instance though, namely WT on A30P mutant seeds, elongation was perhaps slightly higher than A30P on its own seeds, but otherwise similar to WT cross elongation. It should be noted that the mutants used in this thesis were atleast double mutants and furthermore the substitutions in each mutant were very close to each other within the sequence which might enhance mutational effects.

4.2.4 Non WT elongating mutants were not inhibitory of WT elongation

CC48 had been shown to have its *de novo* aggregation severely impaired if occurring at all as well as being strongly inhibitory of WT elongation. In particular the β1 mutants seemed to

atleast fall within the first category and it was tested if the non WT elongating ones would fall the inhibitor category as well. The three non WT elongating β1' (VNGK, TNGG, YNGK) mutants and the lone β2' (TGNG) was included as well as it would be interesting to see if they would be less inhibitory than the β1 mutants (TPDG, NPDG, SPNG). Performing elongation of WT seeds by WT monomer in the presences of the non WT elongating mutants was done, and the results is shown in Figure 4.7.

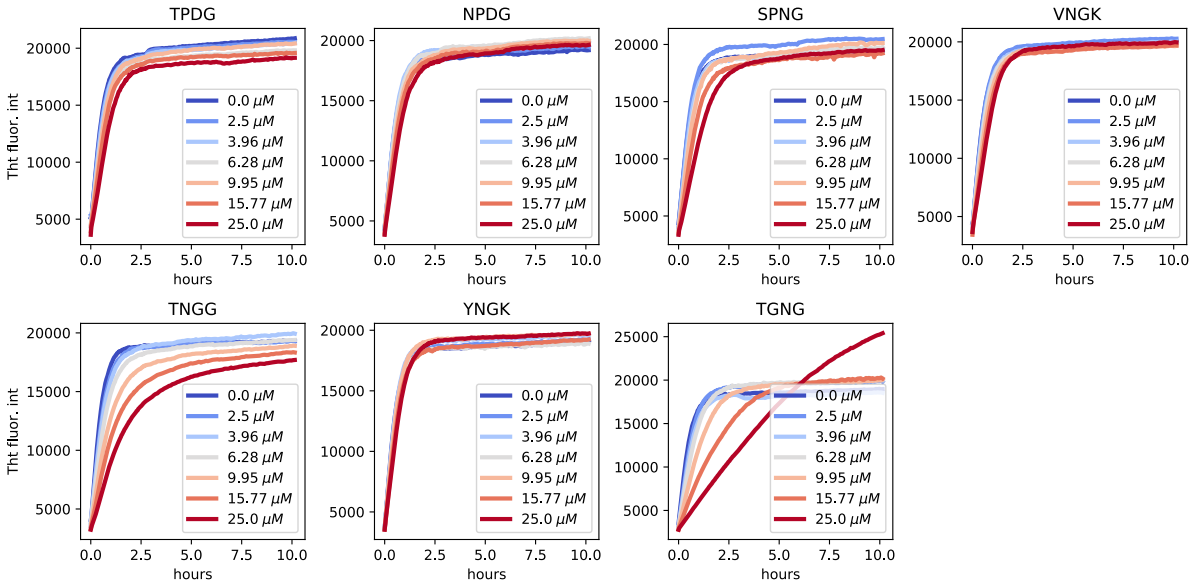

Figure 4.7: WT elongation in the presences of non-elongating turn mutants. Tht fluorescence as a function of time, elongation of WT monomer on WT seeds in the presence of the mutant monomer indicated on top of each plot, and the concentration of mutant indicated in the legend.

In the light of what was observed for CC48 and related mutants, it could perhaps be expected that some of the mutants that were not able to elongate WT seeds would inhibit WT elongation as well. As such, it was a little surprising to see how few of the mutants actually inhibited WT elongation. In particular, all of the non-elongation β1 mutants (TPDG, NPDG, and SPNG) hardly showed any inhibitory potential at all, and only one of the β1' (TNGG) and β2' (TGNG) mutants, respectively, showed partial inhibition. It is perhaps worth noting that both (TNGG) and (TGNG are "only" double-mutants where all others (except TPDG) had three or four mutations. And as mentioned above, the proline in TPDG might be quite invasive. However, why closeness of sequence would be important for inhibition of WT (TNGG and TGNG), but not for elongation of WT (*e.g.* SGNT), is not clear and it could be a coincidence that TNGG and TGNG were the most inhibitory mutants. It is, however, important to remember that even in the cases where inhibition occurred, the effects were substantivally less prominent than what was seen for CC48 and CC50 at the same concentrations.

4.3. Conclusions

Altering the aggregation behaviour of α-synuclein by stabilising the β-hairpin through enhanced β-turn formation propensity was somewhat successful. Contrary to what was expected, *de novo*

aggregation was not suppressed for the most common β-hairpins forming β-turns (1' and 2'), in fact, it was accelerated with respect to the WT. Although an increased lag-phase was observed for the β1 mutants, this could have been due to proline cis-trans isomerisation kinetics. The cross elongation revealed that the no clear symmetry existed between being able to elongate WT seeds and being able to be elongated by WT. Interestingly enough, it was rather rare for the WT to be able to elongate mutant seeds, and if it occurred, it was always at a slower rate than the mutant on itself. On the other hand, it was somewhat common for the mutants to be able to elongate the WT seeds, and especially the β2' mutants were elongating WT seeds. Again though, WT on WT seeds were faster than any mutant on WT seeds. The large asymmetry observed in the elongation potential might suggest that elongation as a phenomenon represents an intimate collaboration of both monomers free in solution as well as the fibril, rather than a process being completely dominated by either species. All in all, amyloid formation of α-synuclein seems to be quite sensitive to mutants in the region 44-47, hinting toward a prominent role for this region in the WT aggregation as well.

4.4. Methods and Materials

4.4.1 Protein Expression and Purification

Expression and purification was done identically to what was described above for the CC variants (see chapter 3 Protein expression and purification).

4.4.2 SDS-PAGE

10 µl sample was mixed with reducing SDS loading buffer (2 mM Dithiothreitol, 2 % SDS, 8 % glycerol, 0.05 % Bromophenol Blue, 0.05 M Tris:Cl pH 6.8), incubated 1 h at room temperature. Samples were loaded onto a Tris/glycine/SDS buffer (Biorad) 15 % polyacrylamide gel made from Rothiphorese 30 (37.5:1) (Carl Roth). Gels were cast and electrophoresis was performed using a Mini-PROTESAN Tetra System (Bio-Rad, Feldkirchen, Germany) system, and the gels were stained using SERVA Blue R (equivalent to Coomassie brilliant blue R-250) (SERVA, Heidelberg, Germany).

4.4.3 De novo aggregation

A single glass bead 2.85–3.45 mm (Carl Roth) stored in ethanol was blown dry under a stream of nitrogen and deposited in into a 96-well Half Area Black Flat Bottom Polystyrene NBS Microplate (Corning, product number 3881). 150 µl water was added into the wells directly surrounding the wells containing sample, and the outer most wells were not used for experimental measurements. These measures minimise sample evaporation during prolonged kinetic experiments. Samples of 100 µl were prepared at room temperature and transferred to the wells containing the glass beads. The plate was sealed using clear sealing tape (Polyolefin Acrylate, Thermo Scientific) and placed inside a platereader (CLARIOStar or FLUOStar Omega, BMG LABTECH, Germany) that had been equilibrated to 37 °C. Data points were obtained every 360 s with continuous orbital shaking of 500 RPM. Fluorescence was read by averaging 12 points, measured in a ring with a diameter of 3 mm (orbital averaging mode). Excitation and emission in the CLARIOStar (monochromator) was 440 nm (15 nm bandwidth) and 485 nm (20 nm nm bandwidth), respectively. Excitation and emission in the FLUOStar Omega (filter) was 448 nm (10 nm bandwidth) and 482 nm (10 nm nm bandwidth) respectively. In addition to

25 µM proteins of interest, all samples contained 20 mM MOPS pH 7.4, 50 mM NaCl, 0.04 % NaN_3 and 20 µM "Ultrapure" Thioflavin-T (Anaspec).

4.4.4 Seeded aggregation

The seeded aggregation was performed identically to what was described above to for the CC variants (see chapter 3 Elongation assays using Tht fluorescences).

5

LOCATING AMYLOIDOGENIC β-HAIRPINS IN THE HUMAN PROTEOME *in silico*

5.1. Introduction

The generic state hypothesis of amyloid suggests that all proteins not only are able to adopt the amyloid state, but, that it would also be favourable for them to do so. As such, there has likely been a strong evolutionary pressure towards allowing ways to escape this proverbial "hell is other polypeptides" amyloid state, where the presence of other proteins of the same kind ends up dominating the behaviour of the individual protein. It has been suggested that the folded state has to be assisted by high unfolding barriers or molecular chaperones in order for it to be stable enough to resist amyloid formation [46, 304, 305]. Even though an entire protein, *i.e.* whole and intact polypeptide sequence, might be stable enough to resist amyloid formation, the same might not hold true for all its individual components separately. A particular prominent cases of this includes the Alzheimer's disease associated aβ peptide, which is derived by cleavage of a longer protein [306]. As mentioned in chapter 1, tau, α-synuclein, aβ, and amylin can all be sequestered by their own specfic wrapin. Furthermore, all these amyloidogenic proteins adopted a β-hairpin conformation upon sequestration.

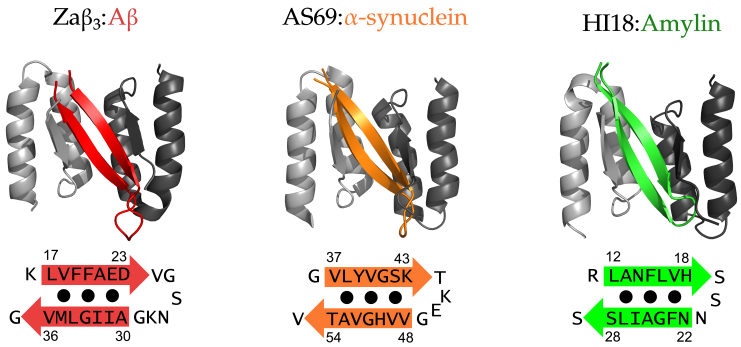

Figure 5.1: Overview of wrapin:amyloidogenic target complexes. The three complexes where the wrapin can be substituted with AS10. The three β-hairpins shown below form the basis for searching the human proteome for sequences that could potentially adopt similar amyloid related β-hairpins. Note that the numbering for aβ and amylin is after they have been cleaved from their parent proteins.

It is of course important to remember that all of the wrapins are derived from the same parent protein, Zaβ$_3$, and there might be limits to the differences in types of secondary structure elements this wrapin can be made to bind. Meaning, it might require a substantial number of mutations in the wrapin to allow it to wrap around an α-helix. None the less, it is still interesting that the β-hairpin conformation is available to all these amyloidogenic proteins and that forming the structure, shields them from forming amyloid. This is especially interesting in the light that a single wrapin, AS10, can bind to and inhibit amyloid formation of α-synuclein, aβ, and amylin. Although all proteins might be able to become amyloids, some might be more likely to do so within physiological relevant conditions than others. The presence of β-hairpin adopting potential might be worth locating in the human proteome to flag the proteins they occur in, or fragments thereof, as potentially amyloidogenic. To do this a search pattern needs to be established. The goal is to find sequences in the human proteome that have amyloid related β-hairpins similar to the ones found binding to wrapins. There are two main problems with structure searches in this context. Firstly, the β-hairpin are, to some extent, induced by the wrapin and the proteins are not predominately found as stable β-hairpins in solution. This means that searching for β-hairpins in *e.g.* crystal structures might not result in the transiently occurring ones we are interested in. Secondly, the structure is not known for a large fraction of the human proteome, and to make matters worse, some of members of it, including α-synuclein, does not appear to adopt any stable conformation even in the cellular environment. Here I present a method for locating, likely amyloidogenic, sequences that can bind to AS10 by adopting a β-hairpin conformation.

5.2. Results and Discussion

5.2.1 Too divergent to establish a consensus sequence

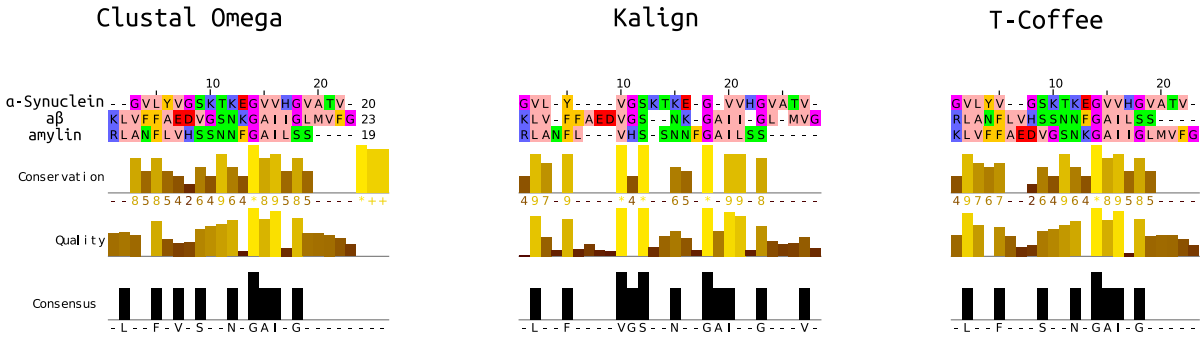

Figure 5.2: Alignment of β-hairpin sequences. Results of multiple sequence alignment using three different alignment tools Clustal Omega [307], Kalign [308], and T-Coffee [309].

A potential first approach towards creating such a search pattern would be to perform a multiple sequence alignment of the β-hairpin forming regions in the three polypeptides. From such a hypothetical alignment, a consensus sequence could be extracted and used to search the human proteome for matching sequences. The underling assumption being that similar sequences would have similar properties. However, when comparing the sequences directly, no obvious sequence similarity exist, and aligning these sequences and colouring them according to their biophysical

characteristics show no obvious pattern either Figure 5.2. Hence, a consensus sequence based search is not a viable strategy.

5.2.2 Secondary structure pattern was not present

Instead of comparing the sequences directly, one could do a second order approach and compare derived properties of the sequences. An example of this could be to compare which secondary structure the sequences would be predicted to form on their own. It was not important which particular type of secondary structure would be predicted, but rather if they all showed a similar pattern that could be used as a proxy for amyloid related β-hairpins. An algorithm to do just this is PSIPRED [310, 311], and using this, secondary strucure prediction was performed with the result shown in Figure 5.3. For the α-synuclein, β-strand propensity was lining up well with the β- strands in its β-hairpin, and even the turn region was exactly from 44-47 as in the wrapin complex (see above). However, secondary structure prediction did not reveal a common theme among the three sequences that could be used as a search pattern either.

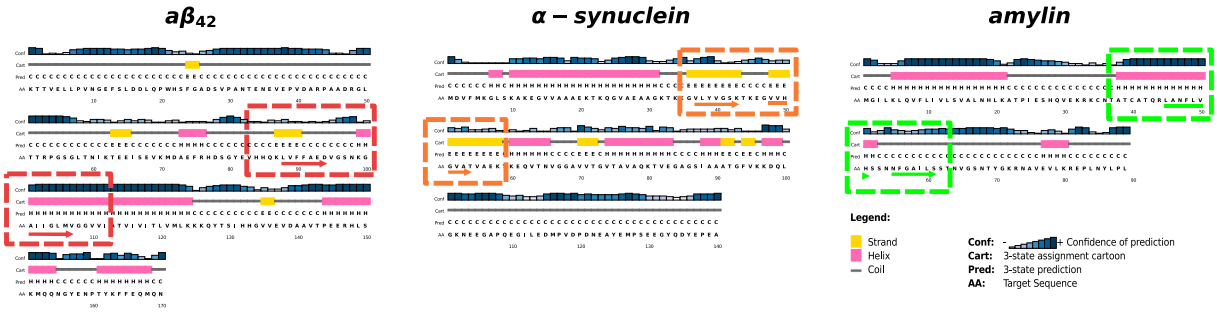

Figure 5.3: Secondary structure prediction. Result of predicting the secondary structure using PSIPRED. Boxes and arrows highlight the regions that adopts β-hairpins as shown in Figure 5.1. Note that only part of the C-terminus of the parent protein of aβ$_{42}$ is shown.

5.2.3 TANGO consensus pattern was found

As all of the β-hairpins where in amyloidogenic proteins, a differently derived quantity to be compared would be their amyloid forming propensity. The TANGO algorithm predicts secondary structure (partly using other tools) as well as having a specific way of calculating amyloid propensity, or β-aggregation as TANGO denotes it [312]. The β-aggregation is calculated as the propensity of forming a so-called fully buried β-strand *versus* forming other secondary structures. The result of applying TANGO to the proteins containing the β-hairpins and plotting the β-aggregation values (Tango aggregation score) is shown in Figure 5.4. A consistent pattern was observed where most of residues in the β-strands of the β-hairpins had high Tango scores and the part corresponding to the turn had a score of zero. Hence, two Tango-positive regions separated by a short of Tango-negative region was chosen as the first pattern to look for in the proteome.

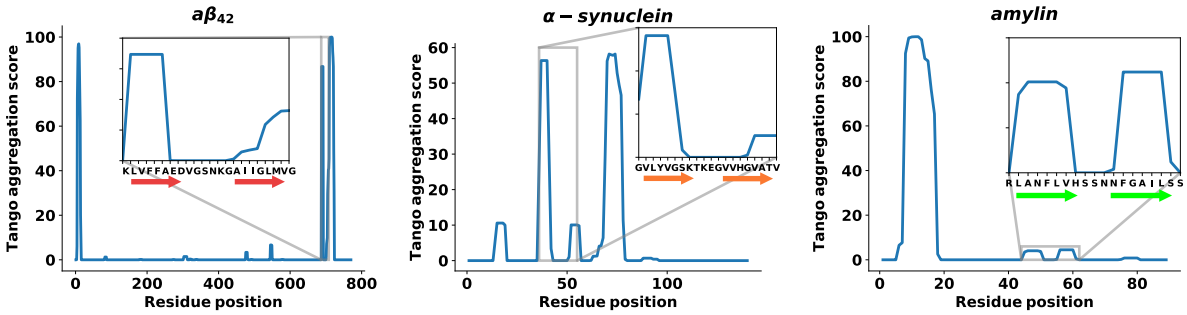

Figure 5.4: Tango scores of the β-hairpin forming proteins. The Tango scores along the full-length sequence, as found in the annotated human proteome, of β-hairpin forming proteins. The sequence corresponding to the β-hairpins are shown in the zoom-in along side arrows that mark the β-strands show in Figure 5.1.

The first step would be to run the TANGO algorithm on all sequences in the human proteome. Using the web interface this is not possible due to sequence length restrictions. Therefore processing was done locally using a pre-complied version [1] and running it in batch mode (see Methods and Materials and Code sections). 27 proteins had to be excluded at this point as they caused errors both when run locally or when using the online tool (see Methods and Materials for details).

As mentioned, sections of each protein might contain amyloidogenic stretches, and in the three polypeptides of interest that was also observed outside of the β-hairpin regions. However, the sheer prevalence of these sequences in the proteome was a little surprising. In fact as was published around the time this work was carried out, $\sim$ 80 % of proteins contained an averages of $\sim$4 stretches each when using a somewhat conservative cut-off Tango score of 10 per residues for minimally 6 residues in a row [313]. For the current study 10 % is too conservative a cut-off as the amylin β-hairpin region is below this value, meaning an even larger number of positive hits in order to capture amylin which we know should be among the hits. However, we are not only searching for single stretches, but for two consecutive (Tango positive) stretches with a short (Tango-negative) stretch in between which might mean a lower cut-off might not give too many false positive results.

The first pattern tested which found the three β-hairpin regions in the genome, was a Tango score cut-off of 1.06 per residue, a stretch between 5 and 23 consecutive (positive) residues, followed by maximally nine (negative) residues before the second stretch that had the same length requirements of (positive) residues. This resulted in 26715 potential β-hairpins forming amyloidogenic regions distributed on 10711 proteins. In other words 53 % of the sequences contained an average of $\sim$2.5 potential β-hairpin regions. Although this is reduction compared to only looking for Tango positive regions, it is not feasible to experimentally validate 26715 sequences.

[1] Obtained at http://tango.crg.es/

5.2.4 Increasing specificity using physiochemical characteristics

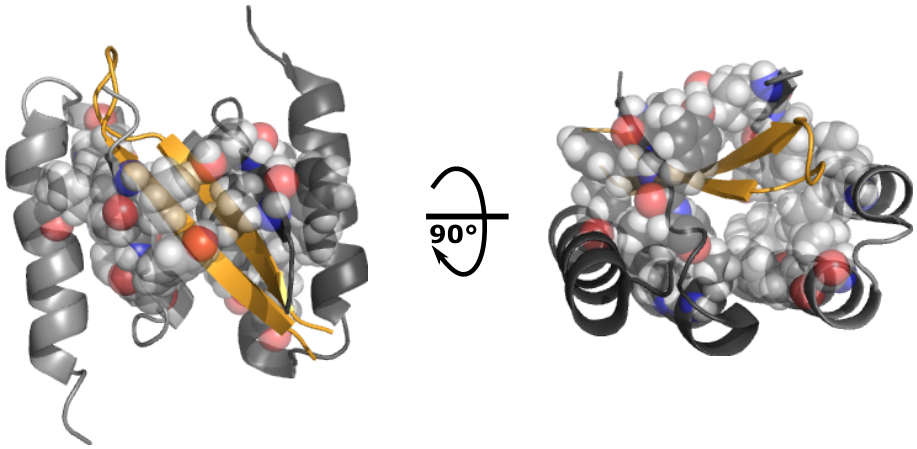

Figure 5.5: AS69:α-synuclein complex. The structure of the AS10 related complex of AS69 and α-synuclein, with AS69 in greys where the hydrophobic and aromatic resides are shown as space-filling and α-synuclein is shown in orange. Note that several phenylalanines present in the binding barrel of AS69 (that are also present in AS10) and the general high hydrophobicity.

A more stringent search pattern was build on top of the first pattern by adding requirements on the type of amino acids that could be find in the Tango-positive stretches. In particular hydrophobicity and the presences of aromatic amino acids was considered. Not only has these been implicated in amyloid formation directly [314, 315, 316], the binding pocket of the AS10 is rather hydrophobic [229, 235] as can also be seen in Figure 5.5. Slightly different requirements were placed on the first and second Tango-positive stretch to reflect the known properties of the three amyloid associated β-hairpins:

First Tango-positive stretch:

- At least one aromatic residue.
- A fractional content of the large aliphatic residues leucine, isoleucine, and valine between 0.32 and 0.5 of total residues.

Second Tango-positive stretch:

- Between 1 and 3 glycine residues.
- A fractional content of the large aliphatic residues leucine, isoleucine, and valine between 0.32 and 0.61 of total residues.

The use of these additional requirements resulted in a reduction of hits to 2505 potential β-hairpins distributed on 2098 proteins. In other words, ∼10 % of the sequences contained an average of 1.2 potential β-hairpins. Although this is still a relatively large number of sequences, it was deemed sufficiently low. This list of sequences became the starting point of a PhD project that I was only marginally involved in, and hence I will not claim involvement by mentioning the results here.

5.3. Methods and Materials

5.3.1 Human proteome

The entire annotated human proteome was obtained as a single fasta file on the 21. of February 2017 from Uniprot using the search pattern:

```
reviewed:yes AND organism:"Homo sapiens (Human) [9606]" AND proteome:up000005640
```

This resulted in a file containing 20162 protein sequences.

5.3.2 Preprocessing the proteome data and running the TANGO algorithm

TANGO can be run in so-called batch mode where files of maximally 1000 sequences (lines) can be present. Furthermore, parameters related to post translational modification and physiochemical conditions can be specified for each sequences. Here, parameters given to all sequences were (N)o modifications of N-terminus, (N)o modifications of C-terminus, pH (7), temperature of (298) kelvin, Ionic strength of (0.1) M. Which corresponds to the default parameter settings on the online versions. Hence, 21 batch files each of line of which having the form (see FASTA to TANGO batch file conversion for implementation details):
`"uniprotID" N N 7 298 0.1 "aa_sequence"`
The 27 proteins with the following uniprot identifiers were excluded due to unknown errors when run locally as well as online: Q8NHP1, P22352, P59796, P18283, P07203, Q9C0D9, P36969, Q8IZQ5, Q9BVL4, Q9BQE4, Q8WWX9, P49908, P62341, P59797, Q9NZV5, P63302, Q9Y6D0, O60613, Q99611, Q9NNW7, Q86VQ6, Q8WZ42, P49895, Q92813, P55073, Q9NZV6, Q16881 (see Removing error causing sequences for implementation details). The batch files were then supplied to TANGO one at a time and summary files (not the scores) were removed (see Running TANGO for implementation details).

5.4. Code

5.4.1 FASTA to TANGO batch file conversion

```
Seq_file = ('External_information/
             uniprot_swissprot_human_21022017.fasta')
Out_file_dic = 'Measurements/Tango_in/'
Max_seqs = 1000

def fasta2tango(raw_seqs):

    seqs = raw_seqs.split('\n>')
    seqs = [line.split('\n',1) for line in seqs]

    for seq in seqs:
        seq[0] = seq[0].split('|')
        seq[1] = seq[1].replace('\n','')

    seqs_len = len(seqs)
```

```
    tango_pattern = ' N N 7 298 0.1 '
    return ([seq[0][1]+tango_pattern+seq[1]+'\n'
         for seq in seqs],
            seqs_len)

def write_tango_file(tango_formated_list, file_name):

    with open(file_name,'a') as f_out:
        f_out.writelines(tango_formated_list)


with open(Seq_file,'r') as f_in:
        raw_seqs = f_in.read()
        form_seq, count = fasta2tango(raw_seqs)
        for i in range((count//Max_seqs )+1):
            write_tango_file(form_seq[i*Max_seqs:
              (i*Max_seqs)+Max_seqs],
              Out_file_dic+str(i)+'_Tango_seq'+'.txt')
```

5.4.2 Removing error causing sequences

```
Error_seqs = ['Q8NHP1','P22352','P59796','P18283','P07203',
              'Q9C0D9','P36969','Q8IZQ5','Q9BVL4','Q9BQE4',
              'Q8WWX9','P49908','P62341','P59797','Q9NZV5',
              'P63302','Q9Y6D0','O60613','Q99611','Q9NNW7',
              'Q86VQ6','Q8WZ42','P49895','Q92813','P55073',
              'Q9NZV6','Q16881']

from glob import glob

Non_error = []

for f in glob('Measurements/Tango_in/*.txt'):
    Non_error = []
    with open(f,'r') as current_read:
        l = current_read.readlines()
        for line in l:
            if line.split()[0] not in Error_seqs:
                Non_error.append(line)
    with open(f,'w') as current_write:
        for line in Non_error:
            current_write.write(line)
```

5.4.3 Running TANGO

```
cd Measurements/Tango_out/
for i in { ls ../Tango_in/*.txt }; do
    ./tango -inputfile=$i
```

```
done

rm Measurements/Tango_out/_aggregation*
rm Measurements/Tango_in/*_aggregation*
```

5.4.4 Filtering for potential β-hairpin

```
from glob import glob
import numpy as np
import pandas as pd

# Filtering parameters

# aa that are considered to be hydrofobic in this context
Hydrofob = ['I','L','V']

# aa that are considered to be aromatic in this context
Aromat = ['F','Y']

# The minimium Tango score for an aa
Min_agg_propen = 1.060

# The minimum and maximum stretch length
Min_agg = 5
Max_agg = 23

# The maximum turn lenght
Max_turn = 9

# The minimum fraction of hydrofob in a stretch
Min_hydro = 0.32

# The maximum fraction of hydrofob in the N and
# C terminal stretch respectively

Max_hydroN = 0.5
Max_hydroC = 0.61

def filter_tango(input_folder, output_folder,
                 min_agg_propen=Min_agg_propen,
                 min_agg=Min_agg,
                 max_agg=Max_agg,
                 max_turn=Max_turn,
                 min_hydro=Min_hydro,
                 max_hydroN=Max_hydroN,
                 max_hydroC=Max_hydroC):

    pos_hits = 0
```

```
    neg_hits = 0

    for tango_out in glob(input_folder + '*.txt'):
        input_df = pd.read_csv(tango_out,sep='\t',
            index_col='res')

        uni_id = tango_out.split('/')[-1][:-4]

        # finding where beta aggregation is bigger
        # than the defined threshold

        agg_seq = input_df['aa'][input_df
                        ['Aggregation'] >= min_agg_propen]

        # remove whitespaces

        agg_seq = agg_seq.str.strip()

        # finding consecutive stretches of high
        # beta aggregation

        agg_stretch = np.diff(agg_seq.index)
        strand = []
        ru = 0
        re = 0

        for i in range(len(agg_stretch)):
            ru += 1
            re += agg_stretch[i]
            if ru != re:
                strand.append((agg_seq.index[1+i-ru],ru))
                ru, re = (0,0)
            elif i == len(agg_stretch) -1:
                strand.append((agg_seq.index[1+i-ru],ru+1))

        # Filtering the data, beta strand longer than 5,
        # turn shorter than 9

        st_strand = [s for s in strand if s[1]
                     >= min_agg and s[1] <= max_agg]
        st_turn = [(s[0],s[1])
                   for s in zip(st_strand,st_strand[1:]) if (
                   (s[1][0] - (s[0][0] + s[0][1])) <= max_turn
                   and
                   (s[1][0] - (s[0][0] + s[0][1])) >= 4)]

        # Filtering for aromatic residue and overall
        # hydrofobicity in first strand
```

```
motif_first = [((a,b),(c,d)) for
    ((a,b),(c,d)) in st_turn
                if
                agg_seq.loc[a:a+b-1].isin(Aromat).sum()
                >= 1
                and
                (agg_seq.loc[a:a+b-1].isin(Hydrofob).sum()
                >= b*Min_hydro
                and
                agg_seq.loc[a:a+b-1].isin(Hydrofob).sum()
                <= b*Max_hydroN)]


# Filtering for glycine residue and overall hydrofobicity
# in second strand

motif_second = [((a,b),(c,d)) for
 ((a,b),(c,d)) in motif_first
                 if
                 (agg_seq.loc[c:c+d-1].isin(['G']).sum()
                 >= 1
                 and
                 agg_seq.loc[c:c+d-1].isin(['G']).sum()
                 <= 3)
                 and
                 (agg_seq.loc[c:c+d-1].isin(Hydrofob).sum()
                 >= d*Min_hydro
                 and
                 agg_seq.loc[c:c+d-1].isin(Hydrofob).sum()
                 <= d*Max_hydroC)]


if len(motif_second) == 0:
    neg_hits +=1
    next

else:
    # Sending the data to output file
    agg_potturn_agg = ''.join([',' + str(a) +
                               ','
                               + str(b) + ','
                               + str(c) + ','
                               + str(d)
                               for ((a,b),(c,d))
                               in
                               motif_second])
```

```
            out_line = uni_id + agg_potturn_agg + '\n'
            pos_hits +=1

            with open(output_folder + str(min_agg)+'_'
            +str(max_turn) + '_cap'
            +'_filter_tango.txt', 'a') as f:
                f.write(out_line)

        print('Passed ID: ' + uni_id)

    print('Positive proteins: ' + str(pos_hits) +
          '\nNegative proteins: '+ str(neg_hits))

filter_tango('Measurements/Tango_out/',
             'Measurements/Asymmetric_betaturn/')
```

5.5. Converting the hits to FASTA

```
def filter2seq(inputfile,outputfile):

    All_seqs = glob('Measurements/Tango_out/*.txt')
    with open(inputfile, 'r') as f:
        for line_terminated in f:
            line = line_terminated.rstrip('\n').split(',')
            uni_id = line[0]
            mot = [int(i) for i in line[1:]]

            # The begining and final aa residue spanned
            # by the motif is extracted

            motifs = [(mot[i],mot[i+2] + mot[i+3])
                      for i in range(0,len(mot),4)]
            df = pd.DataFrame()
            for fi in All_seqs:
                if fi.find(uni_id) > 0:
                    df = pd.read_csv(fi,sep='\t',
                                     index_col='res',
                                     usecols=['res','aa'])
                    df = df['aa'].str.strip()

                    # The sequence for each individual motif
                    # in the motif is extracted and send
                    # to outputfile

                    for i in range(len(motifs)):
                        out_name='\n>' + uni_id + '_'
                                 + str(i+1) + '\n'
                        out_seq = df[motifs[i][0]:
```

```
                                motifs[i][1]].str.cat()
                            with open (outputfile,'a') as out_f:
                                out_f.write(out_name + out_seq)

filter2seq('Measurements/Asymmetric_betaturn/filtered.txt',
'Measurements/Asymmetric_betaturn_seqs/filtered_seqs.txt')
```

6

CONCLUSIONS

Part of the experimental results and conclusions in this thesis was obtained by collaborators. Here, I will keep my focus on the parts I was directly involved in either by performing experiments or analysing data.

It was established before I began my work on AS69 that it substoichiometrically inhibited amyloid formation of α-synuclein. However, by which mechanism a monomer binder, AS69, was able to accomplish substoichiometric inhibition was not well understood. In chapter 2 it was shown that AS69 was able to inhibit all aggregation steps of α-synuclein namely elongation, low-pH-induced secondary nucleation, and lipid induced primary nucleation. Elongation was found to be stoichiometrically inhibited by AS69, an effect that could be attributed directly to monomeric α-synuclein being sequestered into the AS69:α-synuclein complex, thereby making it unavailable for elongation. Lipid-induced primary nucleation appeared to be inhibited substoichiometrically, but the exact mechanism remains somewhat unclear at this point. What is clear, however, is that the known monomer sequestration effect is not enough to explain this inhibition effect. The low-pH-induced secondary nucleation was highly substoichiometrically inhibited by AS69. Similar to inhibition of the lipid-induced aggregation, the inhibition effect on secondary nucleation also could not be explained by monomer sequestration, even when high effective nucleus sizes were assumed. Surprisingly, the effect on secondary nucleation appeared to depend on the AS69:α-synuclein complex rather than AS69 alone. Strangely, neither when alone nor when in complex with α-synuclein did AS69 appear to interact with the fibrils, the site where secondary nucleation occurs. This lack of interaction with fibrils was seen both at neutral pH where both AS69 and α-synulein are highly negatively charged, and at low pH (secondary nucleation regime) near the isoelectronic point of α-synulein and below the one for AS69. Even though the exact mechanism of how the AS69:α-synulein complex is achieving substoichiometric inhibition is unknown, it is worth pointing out that only the β-hairpin region of α-synuclein is sequestered within the complex. Hence, large regions of α-synuclein are still available for potential interactions. Finally, it is noteworthy that a protein, AS69, engineered to bind to monomeric α-synulein, was able to interfere with all amyloid generating pathways, seemingly through different mechanisms.

Building on the knowledge of the structure α-synuclein adopts when bound to AS69, a double cysteine mutant of α-synuclein, CC48, had been created to emulate, or at least favour, β-hairpin formation. As such, it was not too surprising that CC48 was shown not to be readily incorporated into fibrils. What was somewhat surprising though, was that it turned out to be inhibitory of WT amyloid formation, in particular elongation. But, once again, the mechanism was not clear. In chapter 3 it was investigated how CC48 inhibited WT elongation. Here, it was investigated whether the conformation, rather than a generic disulphide bridge constrain in this region, was

the likely cause of inhibition. This was done mutationally by keeping one end of the disulphide bridge constant at position 41 while changing the other end from position 48 through 52. A large difference in inhibition potential was observed depending on the where the second cystein was placed. This lead to the conclusion that a specific β-hairpin conformation rather than a generic constrain on this region was causing inhibition of WT elongation. Interestingly, the strongest inhibition observed was when the second cystein was at position 48, *i.e.*, CC48. Even though a specific β-hairpin conformation were likely causing inhibition, it was not sufficient to add the CC48 β-hairpin region alone (as a peptide). Unlike AS69, it was found that CC48 substoichiometrically inhibited WT elongation and, surprisingly, that inhibition became more efficient with increasing WT monomer concentrations. To explain these effects, modelling and global fitting was done by introducing ideas from reversible inhibition of enzymes into the amyloid field. From this modelling, it was found that CC48 outcompeted WT for binding to the fibril-end. Furthermore, the increasing inhibition efficiency with increasing monomer concentration could be explained by sequential binding of two additional WT monomers in a non-productive manner to fibril-ends that already had CC48 bound to them. Corroborating this model, it was found that linked heterodimeric constructs of CC48 and WT monomer were substantially more inhibitory at lower WT concentrations than CC48 was on its own. Furthermore, the heterodimers exhibited substantially lower WT monomer dependency of elongation inhibition than monomeric CC48. That WT monomers take part in inhibition is in strong contrast to their normal role as the substrate for the elongation reaction. This observation might thus allow for novel inhibition strategies *in vivo* that turns endogenous WT monomers away from being a part of the problem of amyloid formation (as substrate), and into part the solution as co-inhibitors.

Biasing α-synuclein towards adopting a β-hairpin by introducing disulphide bridges between the β-strands (as was done chapter 3) is not the only way to stabilise the β-hairpin. In chapter 4, the turn region was mutated to favour one of three β-turn types, all of whom was supposed to have more stabilising effects on β-hairpin formation than the WT turn sequence. When *de novo* aggregation was studied, only mutants of one of the β-turn types, namely β1, appeared to have slower aggregation kinetics than the WT. However, it could not be ruled out that the slower aggregation kinetics of β1 was a result of generally slower kinetics of adopting specific structures due to proline cis-trans isomerisation, rather than being due to β-hairpin formation. Surprisingly, all of the mutants for the two other β-turn types, namely β1' and β2', turned out to have faster aggregation kinetics than the WT. It was not clear why this was the case. To better understand if the amyloid firbils formed by the mutants had similarities to the WT fibrils, cross-elongation was performed where WT seeds were offered to mutant monomer, or mutant seeds were offered to WT monomers. Whenever one type of monomer was able to elongate a different type of seeds, elongation was always substantially slower than self elongation. Furthermore, offering WT seeds to the mutants revealed that only 1 out of 4 β1 mutants, 2 out of 5 β1' mutants, and 3 out of 4 β2' mutants could elongate WT seeds. Conversely, when mutant seeds were offered to WT monomers, an almost opposite pattern was seen. All of the β1, 1 out of 5 β1', and 1 out of 4 β2 mutants' seeds could be elongated by the WT. It should be noted that the seeds from the β1' and β2' mutants that could be elongated by WT, were not able to elongate WT seeds. Lastly, it was shown that the mutants that were not able to elongate WT seeds, did not function as strong inhibitors, which one might have thought they would keeping in mind the behaviour of CC48.

Going beyond α-synuclein, chapter 5 describes an attempt to locate amyloid associated and AS10-induced β-hairpin forming sequences in the human proteome. Towards establishing such a search pattern, it was found that neither multiple sequence alignments, nor direct secondary structure prediction of known AS10 targets revealed useful search patterns. Running the TANGO

algorithm on the known targets of AS10, did however reveal a useful search pattern where two stretches of TANGO positive residues were connected by a short stretch of TANGO negative residues. However, this pattern turned out to be ubiquitous in the human proteome, *i.e.*, > 26000 sequences were located. The downstream application of the located sequences was to be experimentally validated by showing binding to AS10, as well as having their amyloidogenicity assessed. This is not feasible to do for 26000 sequences. To make this more feasible, the search pattern was extended to include biophysical constrains including hydrophobicity, aromaticity, and number of glycine residues which should increase specificity. This reduced the number of located sequences substantially, however the number of hits was still > 2000, making a full validation of the located sequences unfeasible. However, picking a few matches randomly among this smaller set is perhaps more likely to yield amyloidogenic peptides that can bind to (and be inhibited by) AS10, than if the same was attempted using the larger set.

7

BIBLIOGRAPHY

[1] William Thomas Astbury, Sylvia Dickinson, and Kenneth Bailey. The X-ray interpretation of denaturation and the structure of the seed globulins. *Biochemical Journal*, 29(10):2351–2360.1, October 1935.

[2] Stanley B Prusiner, Michael P McKinley, Karen A Bowman, David C Bolton, Paul E Bendheim, Darlene F Groth, and George G Glenner. Scrapie prions aggregate to form amyloid-like birefringent rods. *Cell*, 35(2):349–358, 1983.

[3] C. L. Masters, G. Simms, N. A. Weinman, G. Multhaup, B. L. McDonald, and K. Beyreuther. Amyloid plaque core protein in Alzheimer disease and Down syndrome. *Proceedings of the National Academy of Sciences*, 82(12):4245–4249, June 1985.

[4] L. C. Serpell, J. Berriman, R. Jakes, M. Goedert, and R. A. Crowther. Fiber diffraction of synthetic alpha -synuclein filaments shows amyloid-like cross-beta conformation. *Proceedings of the National Academy of Sciences*, 97(9):4897–4902, April 2000.

[5] A Clark, C.E Lewis, A.C Willis, G.J.S Cooper, J.F Morris, K.B.M Reid, and R.C Turner. Islet amyloid formed from diabetes-associated peptide may be pathogenic in type-2 diabetes. *The Lancet*, 330(8553):231–234, August 1987.

[6] P. Westermark, C. Wernstedt, E. Wilander, D. W. Hayden, T. D. O'Brien, and K. H. Johnson. Amyloid fibrils in human insulinoma and islets of Langerhans of the diabetic cat are derived from a neuropeptide-like protein also present in normal islet cells. *Proceedings of the National Academy of Sciences*, 84(11):3881–3885, June 1987.

[7] Corino Andrade. A peculiar form of peripheral neuropathy: Familiar atypical generalized amyloidosis with special involvement of the peripheral nerves. *Brain*, 75(3):408–427, 1952.

[8] G. G. Glenner, W. Terry, M. Harada, C. Isersky, and D. Page. Amyloid Fibril Proteins: Proof of Homology with Immunoglobulin Light Chains by Sequence Analyses. *Science*, 172(3988):1150–1151, June 1971.

[9] S. K. Maji, M. H. Perrin, M. R. Sawaya, S. Jessberger, K. Vadodaria, R. A. Rissman, P. S. Singru, K. P. R. Nilsson, R. Simon, D. Schubert, D. Eisenberg, J. Rivier, P. Sawchenko, W. Vale, and R. Riek. Functional Amyloids As Natural Storage of Peptide Hormones in Pituitary Secretory Granules. *Science*, 325(5938):328–332, July 2009.

[10] M. R. Chapman. Role of Escherichia coli Curli Operons in Directing Amyloid Fiber Formation. *Science*, 295(5556):851–855, February 2002.

[11] Rudolf Virchow. Ueber eine im Gehirn und Rückenmark des Menschen aufgefundene Substanz mit der chemischen Reaction der Cellulose. *Archiv für Pathologische Anatomie und Physiologie und für Klinische Medicin*, 6(1):135–138, March 1854.

[12] J.B Cavanagh. Corpora-amylacea and the family of polyglucosan diseases. *Brain Research Reviews*, 29(2-3):265–295, April 1999.

[13] Rudolf Virchow. Nouvelles observations sur la substance animale analogue à la cellulose végétale. *CR Acad. Sci.(Paris)*, 37:860–861, 1853.

[14] Rudolf Virchow. Neue Beobachtungen über amyloide Degeneration. *Virchows Archiv*, 11(2):188–189, February 1857.

[15] N. Friedreich and A. Kekulé. Zur Amyloidfrage. *Archiv für Pathologische Anatomie und Physiologie und für Klinische Medicin*, 16(1-2):50–65, January 1859.

[16] R Heschl. Eine hübsche à vista-Reaktion auf amyloid degenerirte Gewebe. *Wien Med Wochenschr*, 25:713–715, 1875.

[17] Rudolf Jürgens. Eine neue Reaction auf Amyloidkörper. *Archiv für Pathologische Anatomie und Physiologie und für Klinische Medicin*, 65(2):189–196, November 1875.

[18] Hermann Bennhold. Eine spezifische Amyloidfärbung mit Kongorot. *Münchener medizinische Wochenschrift*, 69:1537–1538, 1922.

[19] Hermann Bennhold. Über die Ausscheidung intravenös einverleibten Kongorotes bei den verschiedensten Erkrankungen insbesondere bei Amyloidosis. *Dtsch. Arch. klin. Med*, 142:32, 1923.

[20] Arthur Bookman and Julius Rosenthal. The clinical value of intravenous injection of congo red in the diagnosis of amyloid disease. *The American Journal of the Medical Sciences*, 173(3):396–398, 1927.

[21] P Divry. Sur les proprietes optiques de 1'amyloide. *cr soc. Bilge Biol.*, 97:1808–1810, 1927.

[22] P Divry. De la nature de l'altération fibrillaire d'Alzheimer. *J. Belge. Neurol. Psych*, 34:197–201, 1934.

[23] Hans Peter Missmahl and Marga Hartwig. Polarisationsoptische Untersuchungen an der Amyloidsubstanz. *Virchows Archiv für Pathologische Anatomie und Physiologie und für Klinische Medizin*, 324(4):489–508, 1953.

[24] Alan S. Cohen and Evan Calkins. Electron Microscopic Observations on a Fibrous Component in Amyloid of Diverse Origins. *Nature*, 183(4669):1202–1203, April 1959.

[25] R. D. Terry, N. K. Gonatas, and M. Weiss. Ultrastructural studies in alzheimer's presenile dementia. *The American Journal of Pathology*, 44:269–297, February 1964.

[26] Philip E. Duffy and Virginia M. Tennyson. Phase and electron microscopic observations of lewy bodies and melanin granules in the subtantia nigra and lucs caeruleus in parkinson's disease. *Journal of Neuropathology and Experimental Neurology*, 24(3):398–414, July 1965.

[27] Tsuranobu Shirahama and Alan S. Cohen. High-resolution electron microscopic analysis of the amyloid fibril. *The Journal of Cell Biology*, 33(3):679–708, June 1967.

[28] E. D. Eanes and G. G. Glenner. X-ray diffraction studies on amyloid filaments. *Journal of Histochemistry & Cytochemistry*, 16(11):673–677, November 1968.

[29] L. Bonar, A. S. Cohen, and M. M. Skinner. Characterization of the Amyloid Fibril as a Cross-Protein. *Experimental Biology and Medicine*, 131(4):1373–1375, September 1969.

[30] D. Bolton, M. McKinley, and S. Prusiner. Identification of a protein that purifies with the scrapie prion. *Science*, 218(4579):1309–1311, December 1982.

[31] Bruno Oesch, David Westaway, Monika Wälchli, Michael P. McKinley, Stephen B.H. Kent, Ruedi Aebersold, Ronald A. Barry, Paul Tempst, David B. Teplow, Leroy E. Hood, Stanley B. Prusiner, and Charles Weissmann. A cellular gene encodes scrapie PrP 27-30 protein. *Cell*, 40(4):735–746, April 1985.

[32] S. B. Prusiner. Nobel Lecture: Prions. *Proceedings of the National Academy of Sciences*, 95(23):13363–13383, November 1998.

[33] Joseph T. Jarrett and Peter T. Lansbury. Amyloid fibril formation requires a chemically discriminating nucleation event: studies of an amyloidogenic sequence from the bacterial protein OsmB. *Biochemistry*, 31(49):12345–12352, December 1992.

[34] J. H. Come, P. E. Fraser, and P. T. Lansbury. A kinetic model for amyloid formation in the prion diseases: importance of seeding. *Proceedings of the National Academy of Sciences*, 90(13):5959–5963, July 1993.

[35] Wei-Feng Xue, Andrew L Hellewell, Walraj S Gosal, Steve W Homans, Eric W Hewitt, and Sheena E Radford. Fibril fragmentation enhances amyloid cytotoxicity. *J Biol Chem*, 284(49):34272–34282, Dec 2009.

[36] Jessica Meinhardt, Carsten Sachse, Peter Hortschansky, Nikolaus Grigorieff, and Marcus Fändrich. Aβ(1-40) Fibril Polymorphism Implies Diverse Interaction Patterns in Amyloid Fibrils. *Journal of Molecular Biology*, 386(3):869–877, February 2009.

[37] Jozef Adamcik, Jin-Mi Jung, Jérôme Flakowski, Paolo De Los Rios, Giovanni Dietler, and Raffaele Mezzenga. Understanding amyloid aggregation by statistical analysis of atomic force microscopy images. *Nature Nanotechnology*, 5(6):423–428, June 2010.

[38] Wei-Feng Xue and Sheena E Radford. An imaging and systems modeling approach to fibril breakage enables prediction of amyloid behavior. *Biophysical journal*, 105(12):2811–2819, 2013.

[39] Volodymyr V. Shvadchak, Kseniia Afitska, and Dmytro A. Yushchenko. Inhibition of α-Synuclein Amyloid Fibril Elongation by Blocking Fibril Ends. *Angewandte Chemie*, 130(20):5792–5796, May 2018.

[40] Christine Röder, Nicola Vettore, Lena N. Mangels, Lothar Gremer, Raimond B. G. Ravelli, Dieter Willbold, Wolfgang Hoyer, Alexander K. Buell, and Gunnar F. Schröder. Atomic structure of PI3-kinase SH3 amyloid fibrils by cryo-electron microscopy. *Nature Communications*, 10(1):3754, December 2019.

[41] Yevhenii A. Kyriukha, Kseniia Afitska, Andrii S. Kurochka, Shubhra Sachan, Maksym Galkin, Dmytro A. Yushchenko, and Volodymyr V. Shvadchak. α-Synuclein Dimers as Potent Inhibitors of Fibrillization. *Journal of Medicinal Chemistry*, 62(22):10342–10351, November 2019.

[42] Ricardo Guerrero-Ferreira, Nicholas MI Taylor, Daniel Mona, Philippe Ringler, Matthias E Lauer, Roland Riek, Markus Britschgi, and Henning Stahlberg. Cryo-EM structure of alpha-synuclein fibrils. *eLife*, 7:e36402, July 2018.

[43] C. B. Anfinsen. Principles that Govern the Folding of Protein Chains. *Science*, 181(4096):223–230, July 1973.

[44] Cyrus Levinthal. How to fold graciously. *Mossbauer spectroscopy in biological systems*, 67:22–24, 1969. Publisher: University of Illinois Press Urbana, IL.

[45] Ehud Gazit. The "correctly folded" state of proteins: is it a metastable state? *Angewandte Chemie International Edition*, 41(2):257–259, 2002. Publisher: Wiley Online Library.

[46] Andrew J. Baldwin, Tuomas P. J. Knowles, Gian Gaetano Tartaglia, Anthony W. Fitzpatrick, Glyn L. Devlin, Sarah Lucy Shammas, Christopher A. Waudby, Maria F. Mossuto, Sarah Meehan, Sally L. Gras, John Christodoulou, Spencer J. Anthony-Cahill, Paul D. Barker, Michele Vendruscolo, and Christopher M. Dobson. Metastability of Native Proteins and the Phenomenon of Amyloid Formation. *Journal of the American Chemical Society*, 133(36):14160–14163, September 2011.

[47] Tuomas P. J. Knowles, Michele Vendruscolo, and Christopher M. Dobson. The amyloid state and its association with protein misfolding diseases. *Nature Reviews Molecular Cell Biology*, 15(6):384–396, June 2014.

[48] Brian O'Nuallain, Shankaramma Shivaprasad, Indu Kheterpal, and Ronald Wetzel. Thermodynamics of Aβ(1-40) Amyloid Fibril Elongation †. *Biochemistry*, 44(38):12709–12718, September 2005.

[49] Angela D. Williams, Shankaramma Shivaprasad, and Ronald Wetzel. Alanine Scanning Mutagenesis of Aβ(1-40) Amyloid Fibril Stability. *Journal of Molecular Biology*, 357(4):1283–1294, April 2006.

[50] Christopher M. Dobson. Protein folding and misfolding. *Nature*, 426(6968):884–890, December 2003.

[51] Timo Eichner and Sheena E. Radford. A Diversity of Assembly Mechanisms of a Generic Amyloid Fold. *Molecular Cell*, 43(1):8–18, July 2011.

[52] Patrizia Polverino de Laureto, Niccolò Taddei, Erica Frare, Cristina Capanni, Silvia Costantini, Jesús Zurdo, Fabrizio Chiti, Christopher M. Dobson, and Angelo Fontana. Protein Aggregation and Amyloid Fibril Formation by an SH3 Domain Probed by Limited Proteolysis. *Journal of Molecular Biology*, 334(1):129–141, November 2003.

[53] Erica Frare, Maria F. Mossuto, Patrizia Polverino de Laureto, Mireille Dumoulin, Christopher M. Dobson, and Angelo Fontana. Identification of the Core Structure of Lysozyme Amyloid Fibrils by Proteolysis. *Journal of Molecular Biology*, 361(3):551–561, August 2006.

[54] Luc Bousset, Laura Pieri, Gemma Ruiz-Arlandis, Julia Gath, Poul Henning Jensen, Birgit Habenstein, Karine Madiona, Vincent Olieric, Anja Böckmann, Beat H. Meier, and Ronald Melki. Structural and functional characterization of two alpha-synuclein strains. *Nature Communications*, 4(1):2575, December 2013.

[55] Anton A. Nizhnikov, Alexander I. Alexandrov, Tatyana A. Ryzhova, Olga V. Mitkevich, Alexander A. Dergalev, Michael D. Ter-Avanesyan, and Alexey P. Galkin. Proteomic Screening for Amyloid Proteins. *PLoS ONE*, 9(12):e116003, December 2014.

[56] Sara Breid, Maria E. Bernis, Julius T. Babila, Maria C. Garza, Holger Wille, and Gültekin Tamgüney. Neuroinvasion of α-Synuclein Prionoids after Intraperitoneal and Intraglossal Inoculation. *Journal of Virology*, 90(20):9182–9193, October 2016.

[57] Andrew J Baldwin, Tuomas P J Knowles, Gian Gaetano Tartaglia, Anthony W Fitzpatrick, Glyn L Devlin, Sarah Lucy Shammas, Christopher A Waudby, Maria F Mossuto, Sarah Meehan, Sally L Gras, John Christodoulou, Spencer J Anthony-Cahill, Paul D Barker, Michele Vendruscolo, and Christopher M Dobson. Metastability of native proteins and the phenomenon of amyloid formation. *J Am Chem Soc*, 133(36):14160–14163, Sep 2011.

[58] Nicola Vettore and Alexander K. Buell. Thermodynamics of amyloid fibril formation from chemical depolymerization. *Physical Chemistry Chemical Physics*, 21(47):26184–26194, 2019.

[59] Sho Asakura, Michiki Kasai, and Fumio Oosawa. The effect of temperature on the equilibrium state of actin solutions. *Journal of Polymer Science*, 44(143):35–49, May 1960.

[60] Fumio Oosawa and Michiki Kasai. A theory of linear and helical aggregations of macromolecules. *Journal of Molecular Biology*, 4(1):10–21, January 1962.

[61] Michiki Kasai, Sho Asakura, and Fumio Oosawa. The cooperative nature of G-F transformation of actin. *Biochimica et Biophysica Acta*, 57(1):22–31, January 1962.

[62] Dahui Zhao and Jeffrey S. Moore. Nucleation–elongation: a mechanism for cooperative supramolecular polymerization. *Org. Biomol. Chem.*, 1(20):3471–3491, 2003.

[63] Peter A. Korevaar, Charley Schaefer, Tom F. A. de Greef, and E. W. Meijer. Controlling Chemical Self-Assembly by Solvent-Dependent Dynamics. *Journal of the American Chemical Society*, 134(32):13482–13491, August 2012.

[64] Ph Sa Vassar and CF Culling. Fluorescent stains, with special reference to amyloid and connective tissues. *Archives of pathology*, 68:487–498, 1959.

[65] SM Saeed and Gerald Fine. Thioflavin-T for amyloid detection. *American journal of clinical pathology*, 47(5):588–593, 1967. Publisher: Oxford University Press Oxford, UK.

[66] Hironobu Naiki, Keiichi Higuchi, Masanori Hosokawa, and Toshio Takeda. Fluorometric determination of amyloid fibrils in vitro using the fluorescent dye, thioflavine T. *Analytical Biochemistry*, 177(2):244–249, March 1989.

[67] Tadato Ban, Daizo Hamada, Kazuhiro Hasegawa, Hironobu Naiki, and Yuji Goto. Direct Observation of Amyloid Fibril Growth Monitored by Thioflavin T Fluorescence. *Journal of Biological Chemistry*, 278(19):16462–16465, May 2003.

[68] Harry LeVine. Thioflavine T interaction with amyloid β-sheet structures. *Amyloid*, 2(1):1–6, January 1995.

[69] Gade Malmos K, Blancas-Mejia LM, Weber B, Buchner J, Ramirez-Alvarado M, Naiki H, and Otzen D. Tht 101: a primer on the use of thioflavin t to investigate amyloid formation. *Amyloid*, 24(1):1–16, 2017.

[70] Alexander K. Buell, Jamie R. Blundell, Christopher M. Dobson, Mark E. Welland, Eugene M. Terentjev, and Tuomas P. J. Knowles. Frequency Factors in a Landscape Model of Filamentous Protein Aggregation. *Physical Review Letters*, 104(22):228101, June 2010.

[71] Alexander J. Dear, Georg Meisl, Thomas C. T. Michaels, Manuela R. Zimmermann, Sara Linse, and Tuomas P. J. Knowles. The catalytic nature of protein aggregation. *The Journal of Chemical Physics*, 152(4):045101, January 2020.

[72] Samuel I A Cohen, Michele Vendruscolo, Mark E Welland, Christopher M Dobson, Eugene M Terentjev, and Tuomas P J Knowles. Nucleated polymerization with secondary pathways. I. time evolution of the principal moments. *J Chem Phys*, 135(6):065105, Aug 2011.

[73] Georg Meisl, Julius B Kirkegaard, Paolo Arosio, Thomas C T Michaels, Michele Vendruscolo, Christopher M Dobson, Sara Linse, and Tuomas P J Knowles. Molecular mechanisms of protein aggregation from global fitting of kinetic models. *Nat Protoc*, 11(2):252–272, Feb 2016.

[74] Katsuzo Wakabayashi, Hirokazu Hotani, and Sho Asakura. Polymerization of salmonella flagellin in the presence of high concentrations of salts. *Biochimica et Biophysica Acta (BBA) - Protein Structure*, 175(1):195–203, February 1969.

[75] Maria Andreasen, Georg Meisl, Jonathan D. Taylor, Thomas C. T. Michaels, Aviad Levin, Daniel E. Otzen, Matthew R. Chapman, Christopher M. Dobson, Steve J. Matthews, and Tuomas P. J. Knowles. Physical Determinants of Amyloid Assembly in Biofilm Formation. *mBio*, 10(1):e02279–18, /mbio/10/1/mBio.02279–18.atom, January 2019.

[76] T. P. Knowles, C. A. Waudby, G. L. Devlin, S. I. Cohen, A. Aguzzi, M. Vendruscolo, E. M. Terentjev, M. E. Welland, and C. M. Dobson. An analytical solution to the kinetics of breakable filament assembly. *Science*, 326(5959):1533–1537, Dec 2009.

[77] Samuel I A Cohen, Sara Linse, Leila M Luheshi, Erik Hellstrand, Duncan A White, Luke Rajah, Daniel E Otzen, Michele Vendruscolo, Christopher M Dobson, and Tuomas P J Knowles. Proliferation of amyloid-β42 aggregates occurs through a secondary nucleation mechanism. *Proc Natl Acad Sci U S A*, 110(24):9758–9763, Jun 2013.

[78] Ricardo Gaspar, Georg Meisl, Alexander K Buell, Laurence Young, Clemens F Kaminski, Tuomas PJ Knowles, Emma Sparr, and Sara Linse. Secondary nucleation of monomers on fibril surface dominates α-synuclein aggregation and provides autocatalytic amyloid amplification. *Quarterly Reviews of Biophysics*, 50, 2017.

[79] Kejing Lao, Naichun Ji, Xiaohua Zhang, Wenwei Qiao, Zhishu Tang, and Xingchun Gou. Drug development for Alzheimer's disease: review. *Journal of Drug Targeting*, 27(2):164–173, February 2019.

[80] James Parkinson. An Essay on the Shaking Palsy. *The Journal of Neuropsychiatry and Clinical Neurosciences*, 14(2):223–236, 1817.

[81] Jean Martin Charcot and Alfred Vulpian. De la paralysie agitante. 8:765–767, 1861.

[82] Jean Martin Charcot and (George) (Sigerson). *Leçons sur les maladies du système nerveaux, faites à la Salpêtrière (English translation: Lectures on the diseases of the nervous system, delivered at La Salpêtrière)*. The New Sydenham Society, London, 1877.

[83] Jean Martin Charcot. *Leçons du mardi à la Salpêtrière : policlinique, 1888-1889*. Le Progrès médical; E. Lecrosnier et Babé, Paris, 2. edition, 1889.

[84] Jennifer G. Goldman and Christopher G. Goetz. History of Parkinson's disease. In *Handbook of Clinical Neurology*, volume 83, pages 107–128. Elsevier, 2007.

[85] Édouard Brissaud. Nature et pathogenie de la maladie de Parkinson (lecon 23). pages 488–501, 1895.

[86] Friederich Heinrich Lewy. Paralysis agitans. I. *Springer*, 1912.

[87] Michel Goedert, Maria Grazia Spillantini, Kelly Del Tredici, and Heiko Braak. 100 years of Lewy pathology. *Nature Reviews Neurology*, 9(1):13–24, January 2013.

[88] Constantin Tr{\textbackslash'e}tiakoff. *Contribution a l'etude de l'Anatomie pathologique du Locus Niger de Soemmering avec quelques deduction relatives a la pathogenie des troubles du tonus musculaire et de la maladie de Parkinson*. PhD Thesis, Theses de Paris, 1919.

[89] Rolf Hassler. Zur Pathologie der Paralysis agitans und des postenzephalitischen Parkinsonismus. 48:387–455, 1938.

[90] Nathan S. Kline and Alfred M. Stanley. Use of reserpine in a neuropsychiatric hospital. *Annals of the New York Academy of Sciences*, 61(1):85–91, April 1955.

[91] Parkhurst A. Shore, Alfred Pletscher, Edward G. Tomich, Arvid Carlsson, Ronald Kuntzman, and Bernard B. Brodie. Role of brain serotonin in reserpine action. *Annals of the New York Academy of Sciences*, 66(3):609–617, March 1957.

[92] Kathleen A. Montagu. Catechol Compounds in Rat Tissues and in Brains of Different Animals. *Nature*, 180(4579):244–245, August 1957.

[93] Arvid Carlsson, Margit Lindqvist, and Tor Magnusson. 3,4-Dihydroxyphenylalanine and 5-Hydroxytryptophan as Reserpine Antagonists. *Nature*, 180(4596):1200–1200, November 1957.

[94] A. Carlsson, M. Lindqvist, T. Magnusson, and B. Waldeck. On the Presence of 3-Hydroxytyramine in Brain. *Science*, 127(3296):471–471, February 1958.

[95] Å. Bertler and E. Rosengren. Occurrence and distribution of dopamine in brain and other tissues. *Experientia*, 15(1):10–11, January 1959.

[96] I. Sano, T. Gamo, Y. Kakimoto, K. Taniguchi, M. Takesada, and K. Nishinuma. Distribution of catechol compounds in human brain. *Biochimica et Biophysica Acta*, 32:586–587, January 1959.

[97] H Ehringer and O Hornykiewicz. Verteilung von Noradrenalin und Dopamin (3-Hydroxytyramin) im Gehirn des Menschen und ihr Verhalten bei Erkrankungen des extrapyramidalen Systems. *Klinische Wochenschrift*, 38(24):1236–1239, 1960.

[98] W. Birkmayer and O. Hornykiewicz. The L-3,4-dioxyphenylalanine (DOPA)-effect in Parkinson-akinesia. *Wiener Klinische Wochenschrift*, 73:787–788, November 1961.

[99] W. Birkmayer and O. Hornykiewicz. Der L-Dioxyphenylalanin (=L-DOPA)-Effekt beim Parkinson-Syndrom des Menschen: Zur Pathogenese und Behandlung der Parkinson-Akinese. *Archiv für Psychiatrie und Nervenkrankheiten Vereinigt mit Zeitschrift für die Gesamte Neurologie und Psychiatrie*, 203(5):560–574, 1962.

[100] George C. Cotzias, Melvin H. Van Woert, and Lewis M. Schiffer. Aromatic Amino Acids and Modification of Parkinsonism. *New England Journal of Medicine*, 276(7):374–379, February 1967.

[101] M. M. Hoehn and M. D. Yahr. Parkinsonism: onset, progression, and mortality. *Neurology*, 17(5):427–427, May 1967.

[102] J. Langston, P Ballard, J. Tetrud, and I Irwin. Chronic Parkinsonism in humans due to a product of meperidine-analog synthesis. *Science*, 219(4587):979–980, February 1983.

[103] R. S. Burns, C. C. Chiueh, S. P. Markey, M. H. Ebert, D. M. Jacobowitz, and I. J. Kopin. A primate model of parkinsonism: selective destruction of dopaminergic neurons in the pars compacta of the substantia nigra by N-methyl-4-phenyl-1,2,3,6-tetrahydropyridine. *Proceedings of the National Academy of Sciences*, 80(14):4546–4550, July 1983.

[104] Hsiao-Chun Cheng, Christina M. Ulane, and Robert E. Burke. Clinical progression in Parkinson disease and the neurobiology of axons. *Annals of Neurology*, 67(6):715–725, June 2010.

[105] H. Bernheimer, W. Birkmayer, O. Hornykiewicz, K. Jellinger, and F. Seitelberger. Brain dopamine and the syndromes of Parkinson and Huntington Clinical, morphological and neurochemical correlations. *Journal of the Neurological Sciences*, 20(4):415–455, December 1973.

[106] Julian M. Fearnley and Andrew J. Lees. Ageing and parkinson's disease: Substantia nigra regional selectivity. *Brain*, 114(5):2283–2301, 1991.

[107] William Dauer and Serge Przedborski. Parkinson's Disease. *Neuron*, 39(6):889–909, September 2003.

[108] J Jankovic. Parkinson's disease: clinical features and diagnosis. *Journal of Neurology, Neurosurgery & Psychiatry*, 79(4):368–376, 2008.

[109] Sigurlaug Sveinbjornsdottir. The clinical symptoms of Parkinson's disease. *Journal of Neurochemistry*, 139:318–324, October 2016.

[110] A J Hughes, S E Daniel, L Kilford, and A J Lees. Accuracy of clinical diagnosis of idiopathic Parkinson's disease: a clinico-pathological study of 100 cases. *Journal of Neurology, Neurosurgery & Psychiatry*, 55(3):181–184, March 1992.

[111] L J Findley, M A Gresty, and G M Halmagyi. Tremor, the cogwheel phenomenon and clonus in Parkinson's disease. *Journal of Neurology, Neurosurgery & Psychiatry*, 44(6):534–546, June 1981.

[112] SERL Fahn. Recent developments in Parkinson's disease. *Macmillan health care information*, 2:293–304, 1987.

[113] Bastiaan R. Bloem, Jeffrey M. Hausdorff, Jasper E. Visser, and Nir Giladi. Falls and freezing of gait in Parkinson's disease: A review of two interconnected, episodic phenomena. *Movement Disorders*, 19(8):871–884, August 2004.

[114] L M Allcock. Frequency of orthostatic hypotension in a community based cohort of patients with Parkinson's disease. *Journal of Neurology, Neurosurgery & Psychiatry*, 75(10):1470–1471, October 2004.

[115] L. L. Edwards, E. M. M. Quigley, and R. F. Pfeiffer. Gastrointestinal dysfunction in Parkinson's disease: Frequency and pathophysiology. *Neurology*, 42(4):726–726, April 1992.

[116] Raimundo Nonato Campos-Sousa, Elizabeth Quagliato, Benedito Borges da Silva, Reynaldo Mendes de Carvalho Jr., Suilane Coelho Ribeiro, and Daniel França Mendes de Carvalho. Urinary symptoms in Parkinson's disease: prevalence and associated factors. *Arquivos de Neuro-Psiquiatria*, 61(2B):359–363, June 2003.

[117] C H Hawkes, B C Shephard, and S E Daniel. Olfactory dysfunction in Parkinson's disease. *Journal of Neurology, Neurosurgery & Psychiatry*, 62(5):436–446, May 1997.

[118] Stewart A. Factor, Terence McAlarney, Juan R. Sanchez-Ramos, and William J. Weiner. Sleep disorders and sleep effect in Parkinson's disease. *Movement Disorders*, 5(4):280–285, 1990.

[119] Murat Emre. Dementia associated with Parkinson's disease. *The Lancet Neurology*, 2(4):229–237, April 2003.

[120] Lonneke ML de Lau and Monique MB Breteler. Epidemiology of Parkinson's disease. *The Lancet Neurology*, 5(6):525–535, June 2006.

[121] Tamara Pringsheim, Nathalie Jette, Alexandra Frolkis, and Thomas D.L. Steeves. The prevalence of Parkinson's disease: A systematic review and meta-analysis: PD PREVALENCE. *Movement Disorders*, 29(13):1583–1590, November 2014.

[122] Paul F Worth. How to treat Parkinson's disease in 2013. *Clinical Medicine*, 13(1):93–96, February 2013.

[123] Peter Burkhard, Paola Dominici, Carla Borri-Voltattorni, Johan N. Jansonius, and Vladimir N. Malashkevich. Structural insight into Parkinson's disease treatment from drug-inhibited DOPA decarboxylase. *Nature Structural Biology*, 8(11):963–967, November 2001.

[124] J. Eric Ahlskog and Manfred D. Muenter. Frequency of levodopa-related dyskinesias and motor fluctuations as estimated from the cumulative literature: Levodopa Motor Complication Frequency. *Movement Disorders*, 16(3):448–458, May 2001.

[125] Olivier Rascol, David J. Brooks, Amos D. Korczyn, Peter P. De Deyn, Carl E. Clarke, and Anthony E. Lang. A Five-Year Study of the Incidence of Dyskinesia in Patients with Early Parkinson's Disease Who Were Treated with Ropinirole or Levodopa. *New England Journal of Medicine*, 342(20):1484–1491, May 2000.

[126] Hubert H Fernandez and Jack J Chen. Monoamine Oxidase-B Inhibition in the Treatment of Parkinson's Disease. *Pharmacotherapy*, 27(12 Part 2):174S–185S, December 2007.

[127] Maria João Bonifácio, P. Nuno Palma, Luís Almeida, and Patrício Soares-da Silva. Catechol-O-methyltransferase and Its Inhibitors in Parkinson's Disease. *CNS Drug Reviews*, 13(3):352–379, September 2007.

[128] Günther Deuschl, Carmen Schade-Brittinger, Paul Krack, Jens Volkmann, Helmut Schäfer, Kai Bötzel, Christine Daniels, Angela Deutschländer, Ulrich Dillmann, Wilhelm Eisner, Doreen Gruber, Wolfgang Hamel, Jan Herzog, Rüdiger Hilker, Stephan Klebe, Manja Kloß, Jan Koy, Martin Krause, Andreas Kupsch, Delia Lorenz, Stefan Lorenzl, H. Maximilian Mehdorn, Jean Richard Moringlane, Wolfgang Oertel, Marcus O. Pinsker, Heinz Reichmann, Alexander Reuß, Gerd-Helge Schneider, Alfons Schnitzler, Ulrich Steude, Volker Sturm, Lars Timmermann, Volker Tronnier, Thomas Trottenberg, Lars Wojtecki, Elisabeth Wolf, Werner Poewe, and Jürgen Voges. A Randomized Trial of Deep-Brain Stimulation for Parkinson's Disease. *New England Journal of Medicine*, 355(9):896–908, August 2006.

[129] M. H. Polymeropoulos, C. Lavedan, E. Leroy, S. E. Ide, A. Dehejia, A. Dutra, B. Pike, H. Root, J. Rubenstein, R. Boyer, E. S. Stenroos, S. Chandrasekharappa, A. Athanassiadou, T. Papapetropoulos, W. G. Johnson, A. M. Lazzarini, R. C. Duvoisin, G. Di Iorio, L. I. Golbe, and R. L. Nussbaum. Mutation in the alpha-synuclein gene identified in families with Parkinson's disease. *Science (New York, N.Y.)*, 276(5321):2045–2047, June 1997.

[130] Rejko Krüger, Wilfried Kuhn, Thomas Müller, Dirk Woitalla, Manuel Graeber, Sigfried Kösel, Horst Przuntek, Jörg T. Epplen, Ludger Schols, and Olaf Riess. Ala30Pro mutation in the gene encoding α-synuclein in Parkinson's disease. *Nature Genetics*, 18(2):106–108, February 1998.

[131] Juan J. Zarranz, Javier Alegre, Juan C. Gómez-Esteban, Elena Lezcano, Raquel Ros, Israel Ampuero, Lídice Vidal, Janet Hoenicka, Olga Rodriguez, Begoña Atarés, Verónica Llorens, Estrella Gomez Tortosa, Teodoro del Ser, David G. Muñoz, and Justo G. de Yebenes. The new mutation, E46K, of α-synuclein causes parkinson and Lewy body dementia: New α-Synuclein Gene Mutation. *Annals of Neurology*, 55(2):164–173, February 2004.

[132] Suzanne Lesage, Mathieu Anheim, Franck Letournel, Luc Bousset, Aurélie Honoré, Nelly Rozas, Laura Pieri, Karine Madiona, Alexandra Dürr, Ronald Melki, Christophe Verny, Alexis Brice, and for the French Parkinson's Disease Genetics Study Group. G51D α-synuclein mutation causes a novel Parkinsonian-pyramidal syndrome: SNCA G51D in Parkinsonism. *Annals of Neurology*, 73(4):459–471, April 2013.

[133] Petra Pasanen, Liisa Myllykangas, Maija Siitonen, Anna Raunio, Seppo Kaakkola, Jukka Lyytinen, Pentti J. Tienari, Minna Pöyhönen, and Anders Paetau. A novel α-synuclein mutation A53E associated with atypical multiple system atrophy and Parkinson's disease-type pathology. *Neurobiology of Aging*, 35(9):2180.e1–2180.e5, September 2014.

[134] Dorota Hoffman-Zacharska, Dariusz Koziorowski, Owen A. Ross, Michał Milewski, Jarosław Poznański, Marta Jurek, Zbigniew K. Wszolek, Alexandra Soto-Ortolaza, Jarosław Sławek, Piotr Janik, Zygmunt Jamrozik, Anna Potulska-Chromik, Barbara Jasińska-Myga, Grzegorz Opala, Anna Krygowska-Wajs, Krzysztof Czyżewski, Dennis W. Dickson, Jerzy Bal, and Andrzej Friedman. Novel A18T and pA29S substitutions in α-synuclein may be associated with sporadic Parkinson's disease. *Parkinsonism & Related Disorders*, 19(11):1057–1060, November 2013.

[135] Silke Appel-Cresswell, Carles Vilarino-Guell, Mary Encarnacion, Holly Sherman, Irene Yu, Brinda Shah, David Weir, Christina Thompson, Chelsea Szu-Tu, Joanne Trinh, Jan O. Aasly, Alex Rajput, Ali H. Rajput, A. Jon Stoessl, and Matthew J. Farrer. Alpha-synuclein p.H50Q, a novel pathogenic mutation for Parkinson's disease: α- Synuclein p.H50q, A Novel Mutation For Pd. *Movement Disorders*, 28(6):811–813, June 2013.

[136] Shannon K. McDonnell, Daniel J. Schaid, Alexis Elbaz, Kari J. Strain, James H. Bower, J. Eric Ahlskog, Demetrius M. Maraganore, and Walter A. Rocca. Complex segregation analysis of

Parkinson's disease: The Mayo Clinic Family Study. *Annals of Neurology*, 59(5):788–795, May 2006.

[137] S. Lesage and A. Brice. Parkinson's disease: from monogenic forms to genetic susceptibility factors. *Human Molecular Genetics*, 18(R1):R48–R59, April 2009.

[138] C. Klein and A. Westenberger. Genetics of Parkinson's Disease. *Cold Spring Harbor Perspectives in Medicine*, 2(1):a008888–a008888, January 2012.

[139] Marie-Christine Chartier-Harlin, Jennifer Kachergus, Christophe Roumier, Vincent Mouroux, Xavier Douay, Sarah Lincoln, Clotilde Levecque, Lydie Larvor, Joris Andrieux, Mary Hulihan, Nawal Waucquier, Luc Defebvre, Philippe Amouyel, Matthew Farrer, and Alain Destée. Alpha-synuclein locus duplication as a cause of familial Parkinson's disease. *Lancet (London, England)*, 364(9440):1167–1169, October 2004.

[140] A. B. Singleton, M. Farrer, J. Johnson, A. Singleton, S. Hague, J. Kachergus, M. Hulihan, T. Peuralinna, A. Dutra, R. Nussbaum, S. Lincoln, A. Crawley, M. Hanson, D. Maraganore, C. Adler, M. R. Cookson, M. Muenter, M. Baptista, D. Miller, J. Blancato, J. Hardy, and K. Gwinn-Hardy. alpha-Synuclein locus triplication causes Parkinson's disease. *Science (New York, N.Y.)*, 302(5646):841, October 2003.

[141] M. G. Spillantini, M. L. Schmidt, V. M. Lee, J. Q. Trojanowski, R. Jakes, and M. Goedert. Alpha-synuclein in lewy bodies. *Nature*, 388(6645):839–840, Aug 1997.

[142] Irene Litvan, Kailash P. Bhatia, David J. Burn, Christopher G. Goetz, Anthony E. Lang, Ian McKeith, Niall Quinn, Kapil D. Sethi, Cliff Shults, and Gregor K. Wenning. SIC Task Force appraisal of clinical diagnostic criteria for parkinsonian disorders. *Movement Disorders*, 18(5):467–486, May 2003.

[143] W R Gibb and A J Lees. The relevance of the Lewy body to the pathogenesis of idiopathic Parkinson's disease. *Journal of Neurology, Neurosurgery & Psychiatry*, 51(6):745–752, June 1988.

[144] Dennis W. Dickson, Hiroshige Fujishiro, Anthony DelleDonne, Joshua Menke, Zeshan Ahmed, Kevin J. Klos, Keith A. Josephs, Roberta Frigerio, Melinda Burnett, Joseph E. Parisi, and J. Eric Ahlskog. Evidence that incidental Lewy body disease is pre-symptomatic Parkinson's disease. *Acta Neuropathologica*, 115(4):437–444, April 2008.

[145] M. G. Spillantini, R. A. Crowther, R. Jakes, M. Hasegawa, and M. Goedert. alpha-Synuclein in filamentous inclusions of Lewy bodies from Parkinson's disease and dementia with lewy bodies. *Proceedings of the National Academy of Sciences of the United States of America*, 95(11):6469–6473, May 1998.

[146] Sarah H. Shahmoradian, Amanda J. Lewis, Christel Genoud, Jürgen Hench, Tim E. Moors, Paula P. Navarro, Daniel Castaño-Díez, Gabriel Schweighauser, Alexandra Graff-Meyer, Kenneth N. Goldie, Rosmarie Sütterlin, Evelien Huisman, Angela Ingrassia, Yvonne de Gier, Annemieke J. M. Rozemuller, Jing Wang, Anne De Paepe, Johannes Erny, Andreas Staempfli, Joerg Hoernschemeyer, Frederik Großerüschkamp, Daniel Niedieker, Samir F. El-Mashtoly, Marialuisa Quadri, Wilfred F. J. Van IJcken, Vincenzo Bonifati, Klaus Gerwert, Bernd Bohrmann, Stephan Frank, Markus Britschgi, Henning Stahlberg, Wilma D. J. Van de Berg, and Matthias E. Lauer. Lewy pathology in Parkinson's disease consists of crowded organelles and lipid membranes. *Nature Neuroscience*, 22(7):1099–1109, July 2019.

[147] Benoit I. Giasson, Kunihiro Uryu, John Q. Trojanowski, and Virginia M.-Y Lee. Mutant and Wild Type Human α-Synucleins Assemble into Elongated Filaments with Distinct Morphologies in Vitro. *Journal of Biological Chemistry*, 274(12):7619–7622, March 1999.

[148] Parvez Alam, Luc Bousset, Ronald Melki, and Daniel E. Otzen. α-synuclein oligomers and fibrils: a spectrum of species, a spectrum of toxicities. *Journal of Neurochemistry*, 150(5):522–534, September 2019.

[149] B. Winner, R. Jappelli, S. K. Maji, P. A. Desplats, L. Boyer, S. Aigner, C. Hetzer, T. Loher, M. Vilar, S. Campioni, C. Tzitzilonis, A. Soragni, S. Jessberger, H. Mira, A. Consiglio, E. Pham, E. Masliah, F. H. Gage, and R. Riek. In vivo demonstration that -synuclein oligomers are toxic. *Proceedings of the National Academy of Sciences*, 108(10):4194–4199, March 2011.

[150] Giuliana Fusco, Serene W. Chen, Philip T. F. Williamson, Roberta Cascella, Michele Perni, James A. Jarvis, Cristina Cecchi, Michele Vendruscolo, Fabrizio Chiti, Nunilo Cremades, Liming Ying, Christopher M. Dobson, and Alfonso De Simone. Structural basis of membrane disruption and cellular toxicity by α-synuclein oligomers. *Science*, 358(6369):1440–1443, December 2017.

[151] Kevin W. Tipping, Patricija van Oosten-Hawle, Eric W. Hewitt, and Sheena E. Radford. Amyloid Fibres: Inert End-Stage Aggregates or Key Players in Disease? *Trends in Biochemical Sciences*, 40(12):719–727, December 2015.

[152] Jan Bieschke, Jenny Russ, Ralf P. Friedrich, Dagmar E. Ehrnhoefer, Heike Wobst, Katja Neugebauer, and Erich E. Wanker. EGCG remodels mature α-synuclein and amyloid-β fibrils and reduces cellular toxicity. *Proceedings of the National Academy of Sciences*, 107(17):7710–7715, April 2010.

[153] Patrick Flagmeier, Georg Meisl, Michele Vendruscolo, Tuomas P J Knowles, Christopher M Dobson, Alexander K Buell, and Céline Galvagnion. Mutations associated with familial parkinson's disease alter the initiation and amplification steps of α-synuclein aggregation. *Proceedings of the National Academy of Sciences of the United States of America*, 113:10328–10333, September 2016.

[154] Sanjay Kumar, Deepak Kumar Jangir, Roshan Kumar, Manisha Kumari, Neel Sarovar Bhavesh, and Tushar Kanti Maiti. Role of Sporadic Parkinson Disease Associated Mutations A18T and A29S in Enhanced α-Synuclein Fibrillation and Cytotoxicity. *ACS Chemical Neuroscience*, 9(2):230–240, February 2018.

[155] Viktoria Ruf, Georg Sebastian Nübling, Sophia Willikens, Song Shi, Felix Schmidt, Johannes Levin, Kai Bötzel, Frits Kamp, and Armin Giese. Different effects of alpha-Synuclein mutants on lipid binding and aggregation detected by single molecule fluorescence spectroscopy and ThT fluorescence-based measurements. *ACS Chemical Neuroscience*, January 2019.

[156] Heiko Braak, Kelly Del Tredici, Udo Rüb, Rob A.I de Vos, Ernst N.H Jansen Steur, and Eva Braak. Staging of brain pathology related to sporadic Parkinson's disease. *Neurobiology of Aging*, 24(2):197–211, March 2003.

[157] Kelvin C. Luk, Victoria M. Kehm, Bin Zhang, Patrick O'Brien, John Q. Trojanowski, and Virginia M.Y. Lee. Intracerebral inoculation of pathological α-synuclein initiates a rapidly progressive neurodegenerative α-synucleinopathy in mice. *The Journal of Experimental Medicine*, 209(5):975–986, May 2012.

[158] Laura A Volpicelli-Daley, Kelvin C Luk, and Virginia M-Y Lee. Addition of exogenous α-synuclein preformed fibrils to primary neuronal cultures to seed recruitment of endogenous α-synuclein to lewy body and lewy neurite-like aggregates. *Nature protocols*, 9:2135–2146, September 2014.

[159] Sangjune Kim, Seung-Hwan Kwon, Tae-In Kam, Nikhil Panicker, Senthilkumar S. Karuppagounder, Saebom Lee, Jun Hee Lee, Wonjoong Richard Kim, Minjee Kook, Catherine A.

Foss, Chentian Shen, Hojae Lee, Subhash Kulkarni, Pankaj J. Pasricha, Gabsang Lee, Martin G. Pomper, Valina L. Dawson, Ted M. Dawson, and Han Seok Ko. Transneuronal Propagation of Pathologic α-Synuclein from the Gut to the Brain Models Parkinson's Disease. *Neuron*, 103(4):627–641.e7, August 2019.

[160] H. Braak, U. Rüb, W. P. Gai, and K. Del Tredici. Idiopathic Parkinson's disease: possible routes by which vulnerable neuronal types may be subject to neuroinvasion by an unknown pathogen. *Journal of Neural Transmission*, 110(5):517–536, May 2003.

[161] Elisabeth Svensson, Erzsébet Horváth-Puhó, Reimar W. Thomsen, Jens Christian Djurhuus, Lars Pedersen, Per Borghammer, and Henrik Toft Sørensen. Vagotomy and subsequent risk of Parkinson's disease: Vagotomy and Risk of PD. *Annals of Neurology*, 78(4):522–529, October 2015.

[162] Bojing Liu, Fang Fang, Nancy L. Pedersen, Annika Tillander, Jonas F. Ludvigsson, Anders Ekbom, Per Svenningsson, Honglei Chen, and Karin Wirdefeldt. Vagotomy and Parkinson disease: A Swedish register–based matched-cohort study. *Neurology*, 88(21):1996–2002, May 2017.

[163] Stephanie Lohmann, Maria E. Bernis, Babila J. Tachu, Alexandra Ziemski, Jessica Grigoletto, and Gültekin Tamgüney. Oral and intravenous transmission of α-synuclein fibrils to mice. *Acta Neuropathologica*, 138(4):515–533, October 2019.

[164] A. N. Sacino, M. Brooks, M. A. Thomas, A. B. McKinney, S. Lee, R. W. Regenhardt, N. H. McGarvey, J. I. Ayers, L. Notterpek, D. R. Borchelt, T. E. Golde, and B. I. Giasson. Intramuscular injection of α-synuclein induces CNS -synuclein pathology and a rapid-onset motor phenotype in transgenic mice. *Proceedings of the National Academy of Sciences*, 111(29):10732–10737, July 2014.

[165] Graham Fairfoul, Lynne I. McGuire, Suvankar Pal, James W. Ironside, Juliane Neumann, Sharon Christie, Catherine Joachim, Margaret Esiri, Samuel G. Evetts, Michal Rolinski, Fahd Baig, Claudio Ruffmann, Richard Wade-Martins, Michele T. M. Hu, Laura Parkkinen, and Alison J. E. Green. Alpha-synuclein RT-QuIC in the CSF of patients with alpha-synucleinopathies. *Annals of Clinical and Translational Neurology*, 3(10):812–818, October 2016.

[166] Mohammad Shahnawaz, Takahiko Tokuda, Masaaki Waragai, Nicolas Mendez, Ryotaro Ishii, Claudia Trenkwalder, Brit Mollenhauer, and Claudio Soto. Development of a Biochemical Diagnosis of Parkinson Disease by Detection of α-Synuclein Misfolded Aggregates in Cerebrospinal Fluid. *JAMA Neurology*, 74(2):163, February 2017.

[167] L Maroteaux, Jt Campanelli, and Rh Scheller. Synuclein: a neuron-specific protein localized to the nucleus and presynaptic nerve terminal. *The Journal of Neuroscience*, 8(8):2804–2815, August 1988.

[168] Akihiko Iwai, Eliezer Masliah, Makoto Yoshimoto, Nianfeng Ge, Lisa Flanagan, HA Rohan De Silva, Agnes Kittel, and Tsunao Saitoh. The precursor protein of non-Aβ component of Alzheimer's disease amyloid is a presynaptic protein of the central nervous system. *Neuron*, 14(2):467–475, 1995.

[169] B. G. Wilhelm, S. Mandad, S. Truckenbrodt, K. Krohnert, C. Schafer, B. Rammner, S. J. Koo, G. A. Classen, M. Krauss, V. Haucke, H. Urlaub, and S. O. Rizzoli. Composition of isolated synaptic boutons reveals the amounts of vesicle trafficking proteins. *Science*, 344(6187):1023–1028, May 2014.

[170] Sreeganga Chandra, Gilbert Gallardo, Rafael Fernández-Chacón, Oliver M. Schlüter, and Thomas C. Südhof. α-Synuclein Cooperates with CSPα in Preventing Neurodegeneration. *Cell*, 123(3):383–396, November 2005.

[171] J. Burre, M. Sharma, T. Tsetsenis, V. Buchman, M. R. Etherton, and T. C. Sudhof. α-Synuclein Promotes SNARE-Complex Assembly in Vivo and in Vitro. *Science*, 329(5999):1663–1667, September 2010.

[172] W. Sean Davidson, Ana Jonas, David F. Clayton, and Julia M. George. Stabilization of α-Synuclein Secondary Structure upon Binding to Synthetic Membranes. *Journal of Biological Chemistry*, 273(16):9443–9449, April 1998.

[173] Sreeganga Chandra, Xiaocheng Chen, Josep Rizo, Reinhard Jahn, and Thomas C. Südhof. A Broken α-Helix in Folded α-Synuclein. *Journal of Biological Chemistry*, 278(17):15313–15318, April 2003.

[174] C. Galvagnion, A. K. Buell, G. Meisl, T. C. Michaels, M. Vendruscolo, T. P. Knowles, and C. M. Dobson. Lipid vesicles trigger α-synuclein aggregation by stimulating primary nucleation. *Nat. Chem. Biol.*, 11(3):229–234, Mar 2015.

[175] Elizabeth R. Middleton and Elizabeth Rhoades. Effects of Curvature and Composition on α-Synuclein Binding to Lipid Vesicles. *Biophysical Journal*, 99(7):2279–2288, October 2010.

[176] Jere P. Segrest, Hans De Loof, Jan G. Dohlman, Christie G. Brouillette, and G. M. Anantharamaiah. Amphipathic helix motif: Classes and properties. *Proteins: Structure, Function, and Genetics*, 8(2):103–117, 1990.

[177] JPea Segrest, MK Jones, H De Loof, CG Brouillette, YV Venkatachalapathi, and GM Anantharamaiah. The amphipathic helix in the exchangeable apolipoproteins: a review of secondary structure and function. *Journal of lipid research*, 33(2):141–166, 1992.

[178] David F. Clayton and Julia M. George. The synucleins: a family of proteins involved in synaptic function, plasticity, neurodegeneration and disease. *Trends in Neurosciences*, 21(6):249–254, June 1998.

[179] Natalie Golts, Heather Snyder, Mark Frasier, Catherine Theisler, Peter Choi, and Benjamin Wolozin. Magnesium Inhibits Spontaneous and Iron-induced Aggregation of α-Synuclein. *Journal of Biological Chemistry*, 277(18):16116–16123, May 2002.

[180] Andrés Binolfi, Rodolfo M. Rasia, Carlos W. Bertoncini, Marcelo Ceolin, Markus Zweckstetter, Christian Griesinger, Thomas M. Jovin, and Claudio O. Fernández. Interaction of α-Synuclein with Divalent Metal Ions Reveals Key Differences: A Link between Structure, Binding Specificity and Fibrillation Enhancement. *Journal of the American Chemical Society*, 128(30):9893–9901, August 2006.

[181] Janin Lautenschläger, Amberley D. Stephens, Giuliana Fusco, Florian Ströhl, Nathan Curry, Maria Zacharopoulou, Claire H. Michel, Romain Laine, Nadezhda Nespovitaya, Marcus Fantham, Dorothea Pinotsi, Wagner Zago, Paul Fraser, Anurag Tandon, Peter St George-Hyslop, Eric Rees, Jonathan J. Phillips, Alfonso De Simone, Clemens F. Kaminski, and Gabriele S. Kaminski Schierle. C-terminal calcium binding of α-synuclein modulates synaptic vesicle interaction. *Nature Communications*, 9(1):712, December 2018.

[182] Katherina Vamvaca, Michael J. Volles, and Peter T. Lansbury. The First N-terminal Amino Acids of α-Synuclein Are Essential for α-Helical Structure Formation In Vitro and Membrane Binding in Yeast. *Journal of Molecular Biology*, 389(2):413–424, June 2009.

[183] Hirotomo Miake, Hidehiro Mizusawa, Takeshi Iwatsubo, and Masato Hasegawa. Biochemical Characterization of the Core Structure of α-Synuclein Filaments. *Journal of Biological Chemistry*, 277(21):19213–19219, May 2002.

[184] M. Vilar, H.-T. Chou, T. Luhrs, S. K. Maji, D. Riek-Loher, R. Verel, G. Manning, H. Stahlberg, and R. Riek. The fold of α-synuclein fibrils. *Proceedings of the National Academy of Sciences*, 105(25):8637–8642, June 2008.

[185] K Uéda, H Fukushima, E Masliah, Y Xia, A Iwai, M Yoshimoto, D A Otero, J Kondo, Y Ihara, and T Saitoh. Molecular cloning of cDNA encoding an unrecognized component of amyloid in Alzheimer disease. *Proceedings of the National Academy of Sciences*, 90(23):11282–11286, December 1993.

[186] W. Li, N. West, E. Colla, O. Pletnikova, J. C. Troncoso, L. Marsh, T. M. Dawson, P. Jakala, T. Hartmann, D. L. Price, and M. K. Lee. Aggregation promoting C-terminal truncation of -synuclein is a normal cellular process and is enhanced by the familial Parkinson's disease-linked mutations. *Proceedings of the National Academy of Sciences*, 102(6):2162–2167, February 2005.

[187] Ian V. J. Murray, Benoit I. Giasson, Shawn M. Quinn, Vishwanath Koppaka, Paul H. Axelsen, Harry Ischiropoulos, John Q. Trojanowski, and Virginia M.-Y. Lee. Role of α-Synuclein Carboxy-Terminus on Fibril Formation in Vitro †. *Biochemistry*, 42(28):8530–8540, July 2003.

[188] Ingrid M. van der Wateren, Tuomas P. J. Knowles, Alexander K. Buell, Christopher M. Dobson, and Céline Galvagnion. C-terminal truncation of α-synuclein promotes amyloid fibril amplification at physiological pH. *Chemical Science*, 9(25):5506–5516, 2018.

[189] Paul H. Weinreb, Weiguo Zhen, Anna W. Poon, Kelly A. Conway, and Peter T. Lansbury. NACP, A Protein Implicated in Alzheimer's Disease and Learning, Is Natively Unfolded †. *Biochemistry*, 35(43):13709–13715, January 1996.

[190] Francois-Xavier Theillet, Andres Binolfi, Beata Bekei, Andrea Martorana, Honor May Rose, Marchel Stuiver, Silvia Verzini, Dorothea Lorenz, Marleen van Rossum, Daniella Goldfarb, and Philipp Selenko. Structural disorder of monomeric α-synuclein persists in mammalian cells. *Nature*, 530(7588):45–50, February 2016.

[191] W. Wang, I. Perovic, J. Chittuluru, A. Kaganovich, L. T. T. Nguyen, J. Liao, J. R. Auclair, D. Johnson, A. Landeru, A. K. Simorellis, S. Ju, M. R. Cookson, F. J. Asturias, J. N. Agar, B. N. Webb, C. Kang, D. Ringe, G. A. Petsko, T. C. Pochapsky, and Q. Q. Hoang. A soluble -synuclein construct forms a dynamic tetramer. *Proceedings of the National Academy of Sciences*, 108(43):17797–17802, October 2011.

[192] Tim Bartels, Joanna G. Choi, and Dennis J. Selkoe. α-Synuclein occurs physiologically as a helically folded tetramer that resists aggregation. *Nature*, 477(7362):107–110, September 2011.

[193] Andres Binolfi, Francois-Xavier Theillet, and Philipp Selenko. Bacterial in-cell NMR of human α-synuclein: a disordered monomer by nature? *Biochemical Society Transactions*, 40(5):950–954, October 2012.

[194] Bruno Fauvet, Martial K. Mbefo, Mohamed-Bilal Fares, Carole Desobry, Sarah Michael, Mustafa T. Ardah, Elpida Tsika, Philippe Coune, Michel Prudent, Niels Lion, David Eliezer, Darren J. Moore, Bernard Schneider, Patrick Aebischer, Omar M. El-Agnaf, Eliezer Masliah, and Hilal A. Lashuel. α-Synuclein in Central Nervous System and from Erythrocytes, Mammalian Cells, and *Escherichia coli* Exists Predominantly as Disordered Monomer. *Journal of Biological Chemistry*, 287(19):15345–15364, May 2012.

[195] Bruno Fauvet, Mohamed-Bilal Fares, Filsy Samuel, Igor Dikiy, Anurag Tandon, David Eliezer, and Hilal A. Lashuel. Characterization of Semisynthetic and Naturally N^{α} -Acetylated α-Synuclein *in Vitro* and in Intact Cells: Implications for aggregation and cellular properties of α-synuclein. *Journal of Biological Chemistry*, 287(34):28243–28262, August 2012.

[196] Jacqueline Burré, Sandro Vivona, Jiajie Diao, Manu Sharma, Axel T. Brunger, and Thomas C. Südhof. Properties of native brain α-synuclein. *Nature*, 498(7453):E4–E6, June 2013.

[197] José M. Souza, Benoit I. Giasson, Qiping Chen, Virginia M.-Y. Lee, and Harry Ischiropoulos. Dityrosine Cross-linking Promotes Formation of Stable α-Synuclein Polymers: Implicatin of nitrative and oxidative stress in the pathogenesis of neurodegenerative synucleinopathies. *Journal of Biological Chemistry*, 275(24):18344–18349, June 2000.

[198] Youssra K. Al-Hilaly, Luca Biasetti, Ben J. F. Blakeman, Saskia J. Pollack, Shahin Zibaee, Alaa Abdul-Sada, Julian R. Thorpe, Wei-Feng Xue, and Louise C. Serpell. The involvement of dityrosine crosslinking in α-synuclein assembly and deposition in Lewy Bodies in Parkinson's disease. *Scientific Reports*, 6(1):39171, December 2016.

[199] Michael M. Wördehoff, Hamed Shaykhalishahi, Luca Groß, Lothar Gremer, Matthias Stoldt, Alexander K. Buell, Dieter Willbold, and Wolfgang Hoyer. Opposed Effects of Dityrosine Formation in Soluble and Aggregated α-Synuclein on Fibril Growth. *Journal of Molecular Biology*, 429(20):3018–3030, October 2017.

[200] María Soledad Celej, Rabia Sarroukh, Erik Goormaghtigh, Gerardo D. Fidelio, Jean-Marie Ruysschaert, and Vincent Raussens. Toxic prefibrillar α-synuclein amyloid oligomers adopt a distinctive antiparallel β-sheet structure. *Biochemical Journal*, 443(3):719–726, May 2012.

[201] Nikolai Lorenzen, Søren Bang Nielsen, Alexander K Buell, Jørn Døvling Kaspersen, Paolo Arosio, Brian Stougaard Vad, Wojciech Paslawski, Gunna Christiansen, Zuzana Valnickova-Hansen, Maria Andreasen, Jan J Enghild, Jan Skov Pedersen, Christopher M Dobson, Tuomas P J Knowles, and Daniel Erik Otzen. The role of stable α-synuclein oligomers in the molecular events underlying amyloid formation. *J Am Chem Soc*, 136(10):3859–3868, Mar 2014.

[202] Serene W. Chen, Srdja Drakulic, Emma Deas, Myriam Ouberai, Francesco A. Aprile, Rocío Arranz, Samuel Ness, Cintia Roodveldt, Tim Guilliams, Erwin J. De-Genst, David Klenerman, Nicholas W. Wood, Tuomas P.J. Knowles, Carlos Alfonso, Germán Rivas, Andrey Y. Abramov, José María Valpuesta, Christopher M. Dobson, and Nunilo Cremades. Structural characterization of toxic oligomers that are kinetically trapped during α-synuclein fibril formation. *Proceedings of the National Academy of Sciences*, 112(16):E1994–E2003, April 2015.

[203] Manuel Wolff, Judith J Mittag, Therese W Herling, Erwin De Genst, Christopher M Dobson, Tuomas P J Knowles, Dieter Braun, and Alexander K Buell. Quantitative thermophoretic study of disease-related protein aggregates. *Sci Rep*, 6:22829, 2016.

[204] Dagmar E Ehrnhoefer, Jan Bieschke, Annett Boeddrich, Martin Herbst, Laura Masino, Rudi Lurz, Sabine Engemann, Annalisa Pastore, and Erich E Wanker. EGCG redirects amyloidogenic polypeptides into unstructured, off-pathway oligomers. *Nature Structural & Molecular Biology*, 15(6):558–566, June 2008.

[205] Dong-Pyo Hong, Anthony L. Fink, and Vladimir N. Uversky. Structural Characteristics of α-Synuclein Oligomers Stabilized by the Flavonoid Baicalein. *Journal of Molecular Biology*, 383(1):214–223, October 2008.

[206] Seung R. Paik, Hyun-Ju Shin, Ju-Hyun Lee, Chung-Soon Chang, and Jongsun Kim. Copper(II)-induced self-oligomerization of α-synuclein. *Biochemical Journal*, 340(3):821–828, June 1999.

[207] K. M. Danzer, D. Haasen, A. R. Karow, S. Moussaud, M. Habeck, A. Giese, H. Kretzschmar, B. Hengerer, and M. Kostka. Different Species of -Synuclein Oligomers Induce Calcium Influx and Seeding. *Journal of Neuroscience*, 27(34):9220–9232, August 2007.

[208] Min Zhu, Sudha Rajamani, Joanna Kaylor, Shubo Han, Feimeng Zhou, and Anthony L. Fink. The Flavonoid Baicalein Inhibits Fibrillation of α-Synuclein and Disaggregates Existing Fibrils. *Journal of Biological Chemistry*, 279(26):26846–26857, June 2004.

[209] Lise Giehm and Daniel E. Otzen. Strategies to increase the reproducibility of protein fibrillization in plate reader assays. *Analytical Biochemistry*, 400(2):270–281, May 2010.

[210] Jeremy Pronchik, Xianglan He, Jason T. Giurleo, and David S. Talaga. In Vitro Formation of Amyloid from α-Synuclein Is Dominated by Reactions at Hydrophobic Interfaces. *Journal of the American Chemical Society*, 132(28):9797–9803, July 2010.

[211] A. K. Buell, C. Galvagnion, R. Gaspar, E. Sparr, M. Vendruscolo, T. P. Knowles, S. Linse, and C. M. Dobson. Solution conditions determine the relative importance of nucleation and growth processes in α-synuclein aggregation. *Proc. Natl. Acad. Sci. U.S.A.*, 111(21):7671–7676, May 2014.

[212] Thibault Viennet, Michael M. Wördehoff, Boran Uluca, Chetan Poojari, Hamed Shaykhalishahi, Dieter Willbold, Birgit Strodel, Henrike Heise, Alexander K. Buell, Wolfgang Hoyer, and Manuel Etzkorn. Structural insights from lipid-bilayer nanodiscs link α-Synuclein membrane-binding modes to amyloid fibril formation. *Communications Biology*, 1(1):44, December 2018.

[213] Marcel Falke, Julian Victor, Michael M. Wördehoff, Alessia Peduzzo, Tao Zhang, Gunnar F. Schröder, Alexander K. Buell, Wolfgang Hoyer, and Manuel Etzkorn. α-Synuclein-derived lipoparticles in the study of α-Synuclein amyloid fibril formation. *Chemistry and Physics of Lipids*, 220:57–65, May 2019.

[214] Vladimir N. Uversky, Jie Li, and Anthony L. Fink. Evidence for a Partially Folded Intermediate in α-Synuclein Fibril Formation. *Journal of Biological Chemistry*, 276(14):10737–10744, April 2001.

[215] Wolfgang Hoyer, Thomas Antony, Dmitry Cherny, Gudrun Heim, Thomas M Jovin, and Vinod Subramaniam. Dependence of alpha-synuclein aggregate morphology on solution conditions. *J Mol Biol*, 322(2):383–393, Sep 2002.

[216] S. Campioni, G. Carret, S. Jordens, L. Nicoud, R. Mezzenga, and R. Riek. The presence of an air-water interface affects formation and elongation of α-Synuclein fibrils. *J. Am. Chem. Soc.*, 136(7):2866–2875, Feb 2014.

[217] Dhiman Ghosh, Shruti Sahay, Priyatosh Ranjan, Shimul Salot, Ganesh M. Mohite, Pradeep K. Singh, Saumya Dwivedi, Edmund Carvalho, Rinti Banerjee, Ashutosh Kumar, and Samir K. Maji. The Newly Discovered Parkinson's Disease Associated Finnish Mutation (A53E) Attenuates α-Synuclein Aggregation and Membrane Binding. *Biochemistry*, 53(41):6419–6421, October 2014.

[218] H. Heise, W. Hoyer, S. Becker, O. C. Andronesi, D. Riedel, and M. Baldus. Molecular-level secondary structure, polymorphism, and dynamics of full-length -synuclein fibrils studied by solid-state NMR. *Proceedings of the National Academy of Sciences*, 102(44):15871–15876, November 2005.

[219] Marcus D Tuttle, Gemma Comellas, Andrew J Nieuwkoop, Dustin J Covell, Deborah A Berthold, Kathryn D Kloepper, Joseph M Courtney, Jae K Kim, Alexander M Barclay, Amy Kendall, William Wan, Gerald Stubbs, Charles D Schwieters, Virginia M Y Lee, Julia M George, and Chad M Rienstra. Solid-state NMR structure of a pathogenic fibril of full-length human α-synuclein. *Nature Structural & Molecular Biology*, 23(5):409–415, May 2016.

[220] Yaowang Li, Chunyu Zhao, Feng Luo, Zhenying Liu, Xinrui Gui, Zhipu Luo, Xiang Zhang, Dan Li, Cong Liu, and Xueming Li. Amyloid fibril structure of α-synuclein determined by cryo-electron microscopy. *Cell Research*, 28(9):897–903, September 2018.

[221] Binsen Li, Peng Ge, Kevin A. Murray, Phorum Sheth, Meng Zhang, Gayatri Nair, Michael R. Sawaya, Woo Shik Shin, David R. Boyer, Shulin Ye, David S. Eisenberg, Z. Hong Zhou, and Lin

Jiang. Cryo-EM of full-length α-synuclein reveals fibril polymorphs with a common structural kernel. *Nature Communications*, 9(1):3609, December 2018.

[222] Ricardo Guerrero-Ferreira, Nicholas MI Taylor, Ana-Andreea Arteni, Pratibha Kumari, Daniel Mona, Philippe Ringler, Markus Britschgi, Matthias E Lauer, Ali Makky, Joeri Verasdonck, Roland Riek, Ronald Melki, Beat H Meier, Anja Böckmann, Luc Bousset, and Henning Stahlberg. Two new polymorphic structures of human full-length alpha-synuclein fibrils solved by cryo-electron microscopy. *eLife*, 8:e48907, December 2019.

[223] Manuel Schweighauser, Yang Shi, Airi Tarutani, Fuyuki Kametani, Alexey G. Murzin, Bernardino Ghetti, Tomoyasu Matsubara, Taisuke Tomita, Takashi Ando, Kazuko Hasegawa, Shigeo Murayama, Mari Yoshida, Masato Hasegawa, Sjors H. W. Scheres, and Michel Goedert. Structures of α-synuclein filaments from multiple system atrophy. *Nature*, May 2020.

[224] Karin Nord, Elin Gunneriusson, Jenny Ringdahl, Stefan Ståhl, Mathias Uhlén, and Per-Åke Nygren. Binding proteins selected from combinatorial libraries of an α-helical bacterial receptor domain. *Nature Biotechnology*, 15(8):772–777, August 1997.

[225] Caroline Grönwall, Andreas Jonsson, Sara Lindström, Elin Gunneriusson, Stefan Ståhl, and Nina Herne. Selection and characterization of Affibody ligands binding to Alzheimer amyloid β peptides. *Journal of Biotechnology*, 128(1):162–183, January 2007.

[226] Wolfgang Hoyer, Caroline Grönwall, Andreas Jonsson, Stefan Stahl, and Torleif Härd. Stabilization of a beta-hairpin in monomeric alzheimer's amyloid-beta peptide inhibits amyloid formation. *Proceedings of the National Academy of Sciences of the United States of America*, 105:5099–5104, April 2008.

[227] Wolfgang Hoyer and Torleif Härd. Interaction of alzheimer's a beta peptide with an engineered binding protein–thermodynamics and kinetics of coupled folding-binding. *Journal of molecular biology*, 378:398–411, April 2008.

[228] Leila M Luheshi, Wolfgang Hoyer, Teresa Pereira de Barros, Iris van Dijk Härd, Ann-Christin Brorsson, Bertil Macao, Cecilia Persson, Damian C Crowther, David A Lomas, Stefan Stahl, Christopher M Dobson, and Torleif Härd. Sequestration of the abeta peptide prevents toxicity and promotes degradation in vivo. *PLoS biology*, 8:e1000334, March 2010.

[229] E. A. Mirecka, H. Shaykhalishahi, A. Gauhar, S. Akgül, J. Lecher, D. Willbold, M. Stoldt, and W. Hoyer. Sequestration of a β-hairpin for control of α-synuclein aggregation. *Angew. Chem. Int. Ed. Engl.*, 53(16):4227–4230, Apr 2014.

[230] Clara S. R. Grüning, Ewa A. Mirecka, Antonia N. Klein, Eckhard Mandelkow, Dieter Willbold, Stephen F. Marino, Matthias Stoldt, and Wolfgang Hoyer. Alternative Conformations of the Tau Repeat Domain in Complex with an Engineered Binding Protein. *Journal of Biological Chemistry*, 289(33):23209–23218, August 2014.

[231] Ewa A. Mirecka, Sophie Feuerstein, Lothar Gremer, Gunnar F. Schröder, Matthias Stoldt, Dieter Willbold, and Wolfgang Hoyer. β-Hairpin of Islet Amyloid Polypeptide Bound to an Aggregation Inhibitor. *Scientific Reports*, 6(1):33474, December 2016.

[232] Santiago Esteban-Martín, Jordi Silvestre-Ryan, Carlos W. Bertoncini, and Xavier Salvatella. Identification of Fibril-Like Tertiary Contacts in Soluble Monomeric α-Synuclein. *Biophysical Journal*, 105(5):1192–1198, September 2013.

[233] Jing L. Guo, Dustin J. Covell, Joshua P. Daniels, Michiyo Iba, Anna Stieber, Bin Zhang, Dawn M. Riddle, Linda K. Kwong, Yan Xu, John Q. Trojanowski, and Virginia M.Y. Lee. Distinct α-Synuclein Strains Differentially Promote Tau Inclusions in Neurons. *Cell*, 154(1):103–117, July 2013.

[234] Hamed Shaykhalishahi, Aziz Gauhar, Michael M Wördehoff, Clara SR Grüning, Antonia N Klein, Oliver Bannach, Matthias Stoldt, Dieter Willbold, Torleif Härd, and Wolfgang Hoyer. Contact between the β1 and β2 segments of α-synuclein that inhibits amyloid formation. *Angewandte Chemie International Edition*, 54(30):8837–8840, 2015.

[235] Hamed Shaykhalishahi, Ewa A. Mirecka, Aziz Gauhar, Clara S. R. Grüning, Dieter Willbold, Torleif Härd, Matthias Stoldt, and Wolfgang Hoyer. A β-Hairpin-Binding Protein for Three Different Disease-Related Amyloidogenic Proteins. *ChemBioChem*, 16(3):411–414, February 2015.

[236] JA Obeso, M Stamelou, CG Goetz, W Poewe, AE Lang, D Weintraub, D Burn, GM Halliday, E Bezard, S Przedborski, et al. Past, present, and future of parkinson's disease: a special essay on the 200th anniversary of the shaking palsy. *Movement Disorders*, 32(9):1264–1310, 2017.

[237] Paula Desplats, He-Jin Lee, Eun-Jin Bae, Christina Patrick, Edward Rockenstein, Leslie Crews, Brian Spencer, Eliezer Masliah, and Seung-Jae Lee. Inclusion formation and neuronal cell death through neuron-to-neuron transmission of alpha-synuclein. *Proc Natl Acad Sci U S A*, 106(31):13010–13015, Aug 2009.

[238] K. A. Conway, J. D. Harper, and P. T. Lansbury. Accelerated in vitro fibril formation by a mutant alpha-synuclein linked to early-onset Parkinson disease. *Nat Med*, 4(11):1318–1320, Nov 1998.

[239] Masami Masuda, Nobuyuki Suzuki, Sayuri Taniguchi, Takayuki Oikawa, Takashi Nonaka, Takeshi Iwatsubo, Shin-ichi Hisanaga, Michel Goedert, and Masato Hasegawa. Small molecule inhibitors of α-synuclein filament assembly. *Biochemistry*, 45(19):6085–6094, May 2006.

[240] Jens Wagner, Sergey Ryazanov, Andrei Leonov, Johannes Levin, Song Shi, Felix Schmidt, Catharina Prix, Francisco Pan-Montojo, Uwe Bertsch, Gerda Mitteregger-Kretzschmar, Markus Geissen, Martin Eiden, Fabienne Leidel, Thomas Hirschberger, Andreas A Deeg, Julian J Krauth, Wolfgang Zinth, Paul Tavan, Jens Pilger, Markus Zweckstetter, Tobias Frank, Mathias Bähr, Jochen H Weishaupt, Manfred Uhr, Henning Urlaub, Ulrike Teichmann, Matthias Samwer, Kai Bötzel, Martin Groschup, Hans Kretzschmar, Christian Griesinger, and Armin Giese. Anle138b: a novel oligomer modulator for disease-modifying therapy of neurodegenerative diseases such as prion and parkinson's disease. *Acta neuropathologica*, 125:795–813, June 2013.

[241] Gergely Tóth, Shyra J Gardai, Wagner Zago, Carlos W Bertoncini, Nunilo Cremades, Susan L Roy, Mitali A Tambe, Jean-Christophe Rochet, Céline Galvagnion, Gaia Skibinski, Steven Finkbeiner, Michael Bova, Karin Regnstrom, San-San Chiou, Jennifer Johnston, Kari Callaway, John P Anderson, Michael F Jobling, Alexander K Buell, Ted A Yednock, Tuomas P J Knowles, Michele Vendruscolo, John Christodoulou, Christopher M Dobson, Dale Schenk, and Lisa McConlogue. Targeting the Intrinsically Disordered Structural Ensemble of α-Synuclein by Small Molecules as a Potential Therapeutic Strategy for Parkinson's Disease. *PloS one*, 9(2):e87133, February 2014.

[242] Wolfgang Wrasidlo, Igor F Tsigelny, Diana L Price, Garima Dutta, Edward Rockenstein, Thomas C Schwarz, Karin Ledolter, Douglas Bonhaus, Amy Paulino, Simona Eleuteri, et al. A de novo compound targeting α-synuclein improves deficits in models of parkinson's disease. *Brain*, 139(12):3217–3236, 2016.

[243] Michele Perni, Céline Galvagnion, Alexander Maltsev, Georg Meisl, Martin B D Müller, Pavan K Challa, Julius B Kirkegaard, Patrick Flagmeier, Samuel I A Cohen, Roberta Cascella, Serene W Chen, Ryan Limbocker, Pietro Sormanni, Gabriella T Heller, Francesco A Aprile, Nunilo Cremades, Cristina Cecchi, Fabrizio Chiti, Ellen A A Nollen, Tuomas P J Knowles, Michele Vendruscolo, Adriaan Bax, Michael Zasloff, and Christopher M Dobson. A natural

product inhibits the initiation of α-synuclein aggregation and suppresses its toxicity. *Proceedings of the National Academy of Sciences of the United States of America*, 114:E1009–E1017, February 2017.

[244] Martin Kurnik, Cagla Sahin, Camilla Bertel Andersen, Nikolai Lorenzen, Lise Giehm, Hossein Mohammad-Beigi, Christian Moestrup Jessen, Jan Skov Pedersen, Gunna Christiansen, Steen Vang Petersen, Roland Staal, Girija Krishnamurthy, Keith Pitts, Peter H Reinhart, Frans A A Mulder, Scot Mente, Warren D Hirst, and Daniel E Otzen. Potent α-synuclein aggregation inhibitors, identified by high-throughput screening, mainly target the monomeric state. *Cell chemical biology*, August 2018.

[245] Paul J Muchowski and Jennifer L Wacker. Modulation of neurodegeneration by molecular chaperones. *Nature reviews Neuroscience*, 6(1):11–22, January 2005.

[246] Björn H Falkenburger, Theodora Saridaki, and Elisabeth Dinter. Cellular models for parkinson's disease. *Journal of neurochemistry*, 139 Suppl 1:121–130, October 2016.

[247] Eun-Jin Bae, Na-Young Yang, Miyoung Song, Cheol Soon Lee, Jun Sung Lee, Byung Chul Jung, He-Jin Lee, Seokjoong Kim, Eliezer Masliah, Sergio Pablo Sardi, and Seung-Jae Lee. Glucocerebrosidase depletion enhances cell-to-cell transmission of α-synuclein. *Nature communications*, 5:4755, 2014.

[248] Felipe Opazo, Antje Krenz, Stephan Heermann, Jörg B Schulz, and Björn H Falkenburger. Accumulation and clearance of α-synuclein aggregates demonstrated by time-lapse imaging. *Journal of neurochemistry*, 106(2):529–540, July 2008.

[249] Damla Pinar Karpinar, Madhu Babu Gajula Balija, Sebastian Kügler, Felipe Opazo, Nasrollah Rezaei-Ghaleh, Nora Wender, Hai-Young Kim, Grit Taschenberger, Björn H Falkenburger, Henrike Heise, Ashutosh Kumar, Dietmar Riedel, Lars Fichtner, Aaron Voigt, Gerhard H Braus, Karin Giller, Stefan Becker, Alf Herzig, Marc Baldus, Herbert Jäckle, Stefan Eimer, Jörg B Schulz, Christian Griesinger, and Markus Zweckstetter. Pre-fibrillar alpha-synuclein variants with impaired beta-structure increase neurotoxicity in Parkinson's disease models. *The EMBO Journal*, 28(20):3256–3268, October 2009.

[250] Elisabeth Dinter, Theodora Saridaki, Markus Nippold, Sarah Plum, Leonie Diederichs, Daniel Komnig, Luisa Fensky, Caroline May, Katrin Marcus, Aaron Voigt, Jörg B Schulz, and Björn H Falkenburger. Rab7 induces clearance of α-synuclein aggregates. *Journal of neurochemistry*, 138(5):758–774, September 2016.

[251] Erin K Butler, Aaron Voigt, A Kathrin Lutz, Jane P Toegel, Ellen Gerhardt, Peter Karsten, Björn H Falkenburger, Andrea Reinartz, Konstanze F Winklhofer, and Jörg B Schulz. The Mitochondrial Chaperone Protein TRAP1 Mitigates α-Synuclein Toxicity. *PLoS genetics*, 8(2):e1002488, February 2012.

[252] Vibha Prasad, Yasmine Wasser, Friederike Hans, Anand Goswami, Istvan Katona, Tiago F Outeiro, Philipp J Kahle, Jörg B Schulz, and Aaron Voigt. Monitoring α-synuclein multimerization in vivo. *FASEB journal : official publication of the Federation of American Societies for Experimental Biology*, page fj201800148RRR, September 2018.

[253] Michael M Wördehoff, Oliver Bannach, Hamed Shaykhalishahi, Andreas Kulawik, Stephanie Schiefer, Dieter Willbold, Wolfgang Hoyer, and Eva Birkmann. Single fibril growth kinetics of α-synuclein. *J Mol Biol*, Feb 2015.

[254] Clara S. R. Grüning, Stefan Klinker, Martin Wolff, Mario Schneider, Küpra Toksöz, Antonia N. Klein, Luitgard Nagel-Steger, Dieter Willbold, and Wolfgang Hoyer. The off-rate of monomers dissociating from amyloid-β protofibrils. *J. Biol. Chem.*, 288:37104–37111, 2013.

[255] James WP Brown, Alexander K Buell, Thomas CT Michaels, Georg Meisl, Jacqueline Carozza, Patrick Flagmeier, Michele Vendruscolo, Tuomas PJ Knowles, Christopher M Dobson, and Céline Galvagnion. β-synuclein suppresses both the initiation and amplification steps of α-synuclein aggregation via competitive binding to surfaces. *Scientific Reports*, 6:36010, 2016.

[256] C N Pace, E J Hebert, K L Shaw, D Schell, V Both, D Krajcikova, J Sevcik, K S Wilson, Z Dauter, R W Hartley, and G R Grimsley. Conformational stability and thermodynamics of folding of ribonucleases sa, sa2 and sa3. *Journal of molecular biology*, 279:271–286, May 1998.

[257] Aziz Gauhar, Hamed Shaykhalishahi, Lothar Gremer, Ewa A Mirecka, and Wolfgang Hoyer. Impact of subunit linkages in an engineered homodimeric binding protein to α-synuclein. *Protein Engineering, Design & Selection*, 27(12):473–479, 2014.

[258] Marija Iljina, Liu Hong, Mathew H Horrocks, Marthe H Ludtmann, Minee L Choi, Craig D Hughes, Francesco S Ruggeri, Tim Guilliams, Alexander K Buell, Ji-Eun Lee, Sonia Gandhi, Steven F Lee, Clare E Bryant, Michele Vendruscolo, Tuomas P J Knowles, Christopher M Dobson, Erwin De Genst, and David Klenerman. Nanobodies raised against monomeric α-synuclein inhibit fibril formation and destabilize toxic oligomeric species. *BMC biology*, 15:57, Jul 2017.

[259] C. A. Waudby, T. P. Knowles, G. L. Devlin, J. N. Skepper, H. Ecroyd, J. A. Carver, M. E. Welland, J. Christodoulou, C. M. Dobson, and S. Meehan. The interaction of alphaB-crystallin with mature alpha-synuclein amyloid fibrils inhibits their elongation. *Biophys. J.*, 98(5):843–851, Mar 2010.

[260] Cecilia Månsson, Paolo Arosio, Rasha Hussein, Harm H Kampinga, Reem M Hashem, Wilbert C Boelens, Christopher M Dobson, Tuomas P J Knowles, Sara Linse, and Cecilia Emanuelsson. Interaction of the molecular chaperone dnajb6 with growing amyloid-beta 42 (aβ42) aggregates leads to sub-stoichiometric inhibition of amyloid formation. *The Journal of biological chemistry*, 289:31066–31076, November 2014.

[261] Rakez Kayed, Elizabeth Head, Jennifer L Thompson, Theresa M McIntire, Saskia C Milton, Carl W Cotman, and Charles G Glabe. Common structure of soluble amyloid oligomers implies common mechanism of pathogenesis. *Science*, 300(5618):486–489, Apr 2003.

[262] Céline Galvagnion, James W P Brown, Myriam M Ouberai, Patrick Flagmeier, Michele Vendruscolo, Alexander K Buell, Emma Sparr, and Christopher M Dobson. Chemical properties of lipids strongly affect the kinetics of the membrane-induced aggregation of α-synuclein. *Proceedings of the National Academy of Sciences of the United States of America*, 113:7065–7070, 06 2016.

[263] Dorothea Pinotsi, Alexander K Buell, Celine Galvagnion, Christopher M Dobson, Gabriele S Kaminski Schierle, and Clemens F Kaminski. Direct observation of heterogeneous amyloid fibril growth kinetics via two-color super-resolution microscopy. *Nano Lett*, 14(1):339–345, Jan 2014.

[264] Nadine S Rösener, Lothar Gremer, Elke Reinartz, Anna König, Oleksandr Brener, Henrike Heise, Wolfgang Hoyer, Philipp Neudecker, and Dieter Willbold. A d-enantiomeric peptide interferes with heteroassociation of amyloid-β oligomers and prion protein. *The Journal of biological chemistry*, 293:15748–15764, October 2018.

[265] Alexander K Buell, Christopher M Dobson, and Tuomas P J Knowles. The physical chemistry of the amyloid phenomenon: thermodynamics and kinetics of filamentous protein aggregation. *Essays Biochem*, 56(1):11–39, Aug 2014.

[266] Matthew G. Iadanza, Matthew P. Jackson, Eric W. Hewitt, Neil A. Ranson, and Sheena E. Radford. A new era for understanding amyloid structures and disease. *Nature Reviews Molecular Cell Biology*, 19(12):755–773, December 2018.

[267] Mattias Törnquist, Thomas C. T. Michaels, Kalyani Sanagavarapu, Xiaoting Yang, Georg Meisl, Samuel I. A. Cohen, Tuomas P. J. Knowles, and Sara Linse. Secondary nucleation in amyloid formation. *Chemical Communications*, 54(63):8667–8684, 2018.

[268] Alexander K. Buell. The growth of amyloid fibrils: rates and mechanisms. *Biochemical Journal*, 476(19):2677–2703, October 2019.

[269] Filip Hasecke, Tatiana Miti, Carlos Perez, Jeremy Barton, Daniel Schölzel, Lothar Gremer, Clara S. R. Grüning, Garrett Matthews, Georg Meisl, Tuomas P. J. Knowles, Dieter Willbold, Philipp Neudecker, Henrike Heise, Ghanim Ullah, Wolfgang Hoyer, and Martin Muschol. Origin of metastable oligomers and their effects on amyloid fibril self-assembly. *Chemical Science*, 9(27):5937–5948, 2018.

[270] Paolo Arosio, Michele Vendruscolo, Christopher M. Dobson, and Tuomas P.J. Knowles. Chemical kinetics for drug discovery to combat protein aggregation diseases. *Trends in Pharmacological Sciences*, 35(3):127–135, March 2014.

[271] Tom Scheidt, Urszula Łapińska, Janet R. Kumita, Daniel R. Whiten, David Klenerman, Mark R. Wilson, Samuel I. A. Cohen, Sara Linse, Michele Vendruscolo, Christopher M. Dobson, Tuomas P. J. Knowles, and Paolo Arosio. Secondary nucleation and elongation occur at different sites on Alzheimer's amyloid-β aggregates. *Science Advances*, 5(4):eaau3112, April 2019.

[272] Katazyna Milto, Akvile Botyriute, and Vytautas Smirnovas. Amyloid-Like Fibril Elongation Follows Michaelis-Menten Kinetics. *PLoS ONE*, 8(7):e68684, July 2013.

[273] Pietro Sormanni, Francesco A. Aprile, and Michele Vendruscolo. Rational design of antibodies targeting specific epitopes within intrinsically disordered proteins. *Proceedings of the National Academy of Sciences*, 112(32):9902–9907, August 2015.

[274] Smriti Sangwan, Shruti Sahay, Kevin A Murray, Sophie Morgan, Elizabeth L Guenther, Lin Jiang, Christopher K Williams, Harry V Vinters, Michel Goedert, and David S Eisenberg. Inhibition of synucleinopathic seeding by rationally designed inhibitors. *eLife*, 9:e46775, January 2020.

[275] Emil Dandanell Agerschou, Patrick Flagmeier, Theodora Saridaki, Céline Galvagnion, Daniel Komnig, Laetitia Heid, Vibha Prasad, Hamed Shaykhalishahi, Dieter Willbold, Christopher M Dobson, Aaron Voigt, Bjoern Falkenburger, Wolfgang Hoyer, and Alexander K Buell. An engineered monomer binding-protein for α-synuclein efficiently inhibits the proliferation of amyloid fibrils. *eLife*, 8:e46112, August 2019.

[276] Ciaran P. A. Doherty, Sabine M. Ulamec, Roberto Maya-Martinez, Sarah C. Good, Jemma Makepeace, G. Nasir Khan, Patricija van Oosten-Hawle, Sheena E. Radford, and David J. Brockwell. A short motif in the N-terminal region of α-synuclein is critical for both aggregation and function. *Nature Structural & Molecular Biology*, 27(3):249–259, March 2020.

[277] Xiaodan Ni, Ryan P. McGlinchey, Jiansen Jiang, and Jennifer C. Lee. Structural Insights into α-Synuclein Fibril Polymorphism: Effects of Parkinson's Disease-Related C-Terminal Truncations. *Journal of Molecular Biology*, 431(19):3913–3919, September 2019.

[278] Clara M. Santiveri, Esther León, Manuel Rico, and M. Angeles Jiménez. Context-Dependence of the Contribution of Disulfide Bonds to β-Hairpin Stability. *Chemistry - A European Journal*, 14(2):488–499, January 2008.

[279] E. Gail Hutchinson, Richard B. Sessions, Janet M. Thornton, and Derek N. Woolfson. Determinants of strand register in antiparallel β-sheets of proteins. *Protein Science*, 7(11):2287–2300, November 1998.

[280] K. Gunasekaran, C. Ramakrishnan, and P. Balaram. Beta-hairpins in proteins revisited: lessons for de novo design. *Protein Engineering Design and Selection*, 10(10):1131–1141, October 1997.

[281] M. Angeles Jiménez. Design of Monomeric Water-Soluble β-Hairpin and β-Sheet Peptides. In *Protein Design*, volume 1216, pages 15–52. Springer New York, New York, NY, 2014. Series Title: Methods in Molecular Biology.

[282] A. G. Cochran, N. J. Skelton, and M. A. Starovasnik. Tryptophan zippers: Stable, monomeric β-hairpins. *Proceedings of the National Academy of Sciences*, 98(10):5578–5583, May 2001.

[283] Hang Yu, Wei Han, Wen Ma, and Klaus Schulten. Transient β -hairpin formation in α -synuclein monomer revealed by coarse-grained molecular dynamics simulation. *The Journal of Chemical Physics*, 143(24):243142, December 2015.

[284] Li-Mei Yan, Marianna Tatarek-Nossol, Aleksandra Velkova, Athanasios Kazantzis, and Aphrodite Kapurniotu. Design of a mimic of nonamyloidogenic and bioactive human islet amyloid polypeptide (IAPP) as nanomolar affinity inhibitor of IAPP cytotoxic fibrillogenesis. *Proceedings of the National Academy of Sciences*, 103(7):2046–2051, February 2006.

[285] Valentina Armiento, Anna Spanopoulou, and Aphrodite Kapurniotu. Peptide-Based Molecular Strategies To Interfere with Protein Misfolding, Aggregation, and Cell Degeneration. *Angewandte Chemie International Edition*, 59(9):3372–3384, February 2020.

[286] Kseniia Afitska, Anastasiia Priss, Dmytro A. Yushchenko, and Volodymyr V. Shvadchak. Structural Optimization of Inhibitors of α-Synuclein Fibril Growth: Affinity to the Fibril End as a Crucial Factor. *Journal of Molecular Biology*, 432(4):967–977, February 2020.

[287] Wolfgang Hoyer, Dmitry Cherny, Vinod Subramaniam, and Thomas M. Jovin. Rapid Self-assembly of α-Synuclein Observed by In Situ Atomic Force Microscopy. *Journal of Molecular Biology*, 340(1):127–139, June 2004.

[288] Tadato Ban, Masaru Hoshino, Satoshi Takahashi, Daizo Hamada, Kazuhiro Hasegawa, Hironobu Naiki, and Yuji Goto. Direct Observation of Aβ Amyloid Fibril Growth and Inhibition. *Journal of Molecular Biology*, 344(3):757–767, November 2004.

[289] M. S. Z. Kellermayer, A. Karsai, M. Benke, K. Soos, and B. Penke. Stepwise dynamics of epitaxially growing single amyloid fibrils. *Proceedings of the National Academy of Sciences*, 105(1):141–144, January 2008.

[290] Jesper Ferkinghoff-Borg, Jesper Fonslet, Christian Beyschau Andersen, Sandeep Krishna, Simone Pigolotti, Hisashi Yagi, Yuji Goto, Daniel Otzen, and Mogens H. Jensen. Stop-and-go kinetics in amyloid fibrillation. *Physical Review E*, 82(1):010901, July 2010.

[291] Mike Sleutel, Imke Van den Broeck, Nani Van Gerven, Cécile Feuillie, Wim Jonckheere, Claire Valotteau, Yves F Dufrêne, and Han Remaut. Nucleation and growth of a bacterial functional amyloid at single-fiber resolution. *Nature Chemical Biology*, 13(8):902–908, August 2017.

[292] Hannes M. Beyer, Patrick Gonschorek, Sophia L. Samodelov, Matthias Meier, Wilfried Weber, and Matias D. Zurbriggen. AQUA Cloning: A Versatile and Simple Enzyme-Free Cloning Approach. *PLOS ONE*, 10(9):e0137652, September 2015.

[293] Matthew Johnson, Arthur T. Coulton, Michael A. Geeves, and Daniel P. Mulvihill. Targeted Amino-Terminal Acetylation of Recombinant Proteins in E. coli. *PLoS ONE*, 5(12):e15801, December 2010.

[294] M. Grey, S. Linse, H. Nilsson, P. Brundin, and E. Sparr. Membrane interaction of α-synuclein in different aggregation states. *J Parkinsons Dis*, 1(4):359–371, 2011.

[295] T. Scheibel, J. Bloom, and S. L. Lindquist. The elongation of yeast prion fibers involves separable steps of association and conversion. *Proceedings of the National Academy of Sciences*, 101(8):2287–2292, February 2004.

[296] William P. Esler, Evelyn R. Stimson, Joan M. Jennings, Harry V. Vinters, Joseph R. Ghilardi, Jonathan P. Lee, Patrick W. Mantyh, and John E. Maggio. Alzheimer's Disease Amyloid Propagation by a Template-Dependent Dock-Lock Mechanism. *Biochemistry*, 39(21):6288–6295, May 2000.

[297] Alejandro G. Marangoni. *Enzyme Kinetics*. John Wiley & Sons, Inc., Hoboken, NJ, USA, November 2002.

[298] George D. Rose, Lila M. Glerasch, and John A. Smith. Turns in Peptides and Proteins. In *Advances in Protein Chemistry*, volume 37, pages 1–109. Elsevier, 1985.

[299] E. Gail Hutchinson and Janet M. Thornton. A revised set of potentials for β-turn formation in proteins. *Protein Science*, 3(12):2207–2216, December 1994.

[300] B. L. Sibanda and J. M. Thornton. β-Hairpin families in globular proteins. *Nature*, 316(6024):170–174, July 1985.

[301] David Pantoja-Uceda, Clara M. Santiveri, and M. Angeles Jiménez. *De novo* Design of Monomeric β-Hairpin and β-Sheet Peptides. In *Protein Design*, volume 340, pages 27–52. Humana Press, New Jersey, June 2006.

[302] John P. Anderson, Donald E. Walker, Jason M. Goldstein, Rian de Laat, Kelly Banducci, Russell J. Caccavello, Robin Barbour, Jiping Huang, Kristin Kling, Michael Lee, Linnea Diep, Pamela S. Keim, Xiaofeng Shen, Tim Chataway, Michael G. Schlossmacher, Peter Seubert, Dale Schenk, Sukanto Sinha, Wei Ping Gai, and Tamie J. Chilcote. Phosphorylation of Ser-129 Is the Dominant Pathological Modification of α-Synuclein in Familial and Sporadic Lewy Body Disease. *Journal of Biological Chemistry*, 281(40):29739–29752, October 2006.

[303] William J. Wedemeyer, Ervin Welker, and Harold A. Scheraga. Proline Cis-Trans Isomerization and Protein Folding. *Biochemistry*, 41(50):14637–14644, December 2002.

[304] Frederic Rousseau, Luis Serrano, and Joost W.H. Schymkowitz. How Evolutionary Pressure Against Protein Aggregation Shaped Chaperone Specificity. *Journal of Molecular Biology*, 355(5):1037–1047, February 2006.

[305] Elodie Monsellier and Fabrizio Chiti. Prevention of amyloid-like aggregation as a driving force of protein evolution. *EMBO reports*, 8(8):737–742, August 2007.

[306] Janelle Nunan and David H Small. Regulation of APP cleavage by α-, β- and γ-secretases. *FEBS Letters*, 483(1):6–10, October 2000.

[307] Fabian Sievers, Andreas Wilm, David Dineen, Toby J Gibson, Kevin Karplus, Weizhong Li, Rodrigo Lopez, Hamish McWilliam, Michael Remmert, Johannes Söding, Julie D Thompson, and Desmond G Higgins. Fast, scalable generation of high-quality protein multiple sequence alignments using Clustal Omega. *Molecular Systems Biology*, 7(1):539, January 2011.

[308] Timo Lassmann, Oliver Frings, and Erik L. L. Sonnhammer. Kalign2: high-performance multiple alignment of protein and nucleotide sequences allowing external features. *Nucleic Acids Research*, 37(3):858–865, February 2009.

[309] Cédric Notredame, Desmond G Higgins, and Jaap Heringa. T-coffee: a novel method for fast and accurate multiple sequence alignment 1 1Edited by J. Thornton. *Journal of Molecular Biology*, 302(1):205–217, September 2000.

[310] David T Jones. Protein secondary structure prediction based on position-specific scoring matrices 1 1Edited by G. Von Heijne. *Journal of Molecular Biology*, 292(2):195–202, September 1999.

[311] Daniel W A Buchan and David T Jones. The PSIPRED Protein Analysis Workbench: 20 years on. *Nucleic Acids Research*, 47(W1):W402–W407, July 2019.

[312] Ana-Maria Fernandez-Escamilla, Frederic Rousseau, Joost Schymkowitz, and Luis Serrano. Prediction of sequence-dependent and mutational effects on the aggregation of peptides and proteins. *Nature Biotechnology*, 22(10):1302–1306, September 2004.

[313] R. Prabakaran, Dhruv Goel, Sandeep Kumar, and M. Michael Gromiha. Aggregation prone regions in human proteome: Insights from large-scale data analyses: Aggregation Studies on Human Proteome. *Proteins: Structure, Function, and Bioinformatics*, 85(6):1099–1118, June 2017.

[314] Charles J. Bowerman, Derek M. Ryan, David A. Nissan, and Bradley L. Nilsson. The effect of increasing hydrophobicity on the self-assembly of amphipathic β-sheet peptides. *Molecular BioSystems*, 5(9):1058, 2009.

[315] F. Timur Senguen, Naomi R. Lee, Xianfeng Gu, Derek M. Ryan, Todd M. Doran, Elizabeth A. Anderson, and Bradley L. Nilsson. Probing aromatic, hydrophobic, and steric effects on the self-assembly of an amyloid-β fragment peptide. *Mol. BioSyst.*, 7(2):486–496, 2011.

[316] Karen E. Marshall, Kyle L. Morris, Deborah Charlton, Nicola O'Reilly, Laurence Lewis, Helen Walden, and Louise C. Serpell. Hydrophobic, Aromatic, and Electrostatic Interactions Play a Central Role in Amyloid Fibril Formation and Stability. *Biochemistry*, 50(12):2061–2071, March 2011.